UNIVERSIDADE DE LISBOA

INSTITUTO SUPERIOR TÉCNICO

DESIGN, TESTING AND MODELLING OF FAÇADE INTEGRATED PHOTOVOLTAIC SYSTEMS

Karol Bot

Supervisor: **Doctor Laura Elena Aelenei**

Co-Supervisors: **Doctor Carlos Augusto Santos Silva**
Doctor Maria da Glória de Almeida Gomes

Thesis approved in public session to obtain the PhD Degree in Sustainable Energy Systems

Jury final classification: Pass with Distinction

2020

UNIVERSIDADE DE LISBOA

INSTITUTO SUPERIOR TÉCNICO

DESIGN, TESTING AND MODELLING OF FAÇADE INTEGRATED PHOTOVOLTAIC SYSTEMS

Karol Bot

Supervisor: Doctor Laura Elena Aelenei

Co-Supervisors: Doctor Carlos Augusto Santos Silva
Doctor Maria da Glória de Almeida Gomes

Thesis approved in public session to obtain the PhD Degree in Sustainable Energy Systems

Jury final classification: Pass with Distinction

Jury

Chairperson: Doctor Paulo Manuel Cadete Ferrão, Instituto Superior Técnico, Universidade de Lisboa

Members of the Committee:

Doctor Maria Manuela de Oliveira Guedes de Almeida, Escola de Engenharia, Universidade do Minho

Doctor Helder José Perdigão Gonçalves, Laboratório Nacional de Energia e Geologia

Doctor Luís Filipe Moreira Mendes, Instituto Superior Técnico, Universidade de Lisboa

Doctor Carlos Augusto Santos Silva, Instituto Superior Técnico, Universidade de Lisboa

2020

Acknowledgements

The development of this PhD would not have been possible without the financial support received from the Foundation of Science and Technology, through the infra-structural research fellowship grant “Projeto de Infraestruturas de Investigação Científica, “NZEB_LAB - Infraestrutura de Investigação da Integração dos Sistemas Solares em Edifícios” (Refª. LISBOA-01-0145-FEDER-022075). Also, I am grateful to LNEG and Instituto Superior Técnico and MIT Portugal Program for hosting me as a PhD candidate.

I am very grateful to my supervisor Laura Aelenei, for having accepted to supervise my work, for all her patience, extensive dedication and daily support to contribute to my formation as a professional, to make me more innovative, structured and to be better understood in academic community. I would also like to acknowledge Professor Hélder Gonçalves, the coordinator of the NZEB_LAB Project, for giving the opportunity to work in LNEG during my PhD.

I am also very grateful to my supervisors Carlos Augusto Santos Silva and Maria da Glória de Almeida Gomes, for having accepted to supervise my work and for all the support during the course. Their support was fundamental during this journey.

Finally, to my family, for making this journey possible through all the support I received from them. To my husband, also for all his help, crucial support, understanding and patience during all this period.

Resumo

O presente trabalho incide sobre sistemas integrados de energia solar (BI-SES), nomeadamente sistemas térmicos fotovoltaicos integrados (BIPVT) em edifícios. Nos últimos anos tem havido um interesse crescente, do ponto de vista de engenharia e arquitetura, no desenvolvimento estratégico de fachadas de edifícios para atender aos requisitos atuais de eficiência energética e sustentabilidade. Este estudo tem como objetivo desenvolver novas soluções de fachadas com a integração de sistemas de energia solar, avaliar o seu desempenho, experimental e numericamente e, através de uma análise paramétrica baseada em modelos validados, melhorar o design do sistema. O caso de estudo está localizado no edifício Solar XXI do Laboratório Nacional de Energia e Geologia em Lisboa, Portugal. Consiste em uma sala de teste com um sistema BIPVT instalado que foi posteriormente testado com os novos protótipos P1a (módulo fotovoltaico com módulo de isolamento interno) e P1b (módulo fotovoltaico com módulo de tanque interno de água) com um complexo sistema de automação.

Foi desenvolvida uma extensa campanha experimental com o registo e análise de diferentes parâmetros climáticos exteriores e ambientais da sala de teste e dos elementos BI-SES, tendo sido também realizada a caracterização térmica dos elementos. Este estudo foi complementado com uma análise numérica que consistiu, numa primeira fase, na simulação dinâmica de fluidos computacional (usando o ANSYS Fluent) para a análise de elementos BI-SES e, numa segunda fase, na simulação energética da integração de elementos BI-SES na sala de teste (usando o EnergyPlus). Foi realizada uma análise paramétrica com 82 cenários, variando parâmetros como a posição do dispositivo de proteção da janela, o número de painéis fotovoltaicos no sistema, a espessura da camada de ar, as trocas de ar entre os sistemas BI-SES e a sala e os seus modos de operação.

As principais conclusões do estudo indicam que o BI-SES (BIPVT) existente e o novo protótipo em suas duas versões, têm potencial para aumentar a sustentabilidade do edifício, reduzindo as necessidades de energia para aquecimento e arrefecimento. No entanto, a sua operação precisa de ser adaptada a outros sistemas existentes na zona térmica, como os dispositivos de sombreamento, tendo o modo automático de operação, com pontos de ajuste operacionais inteligentes, provado ser o mais adequado.

Abstract

The present work focuses on integrated solar energy systems (BI-SES), namely integrated photovoltaic thermal systems (BIPVT) in buildings. In recent years there has been a growing interest, from the point of view of engineering and architecture, in the strategic development of building facades to meet current requirements for energy efficiency and sustainability. This study aims to develop new façade solutions with the integration of solar energy systems, evaluate their performance, experimentally and numerically and, through a parametric analysis based on validated models, to improve the system design. The case study is located in the Solar XXI building of the National Energy and Geology Laboratory in Lisbon, Portugal. It consists of a test room with a BIPVT system installed that was later tested with the new prototypes P1a (photovoltaic module with internal insulation module) and P1b (photovoltaic module with internal water tank module) with a complex automation system.

An extensive experimental campaign was developed with the registration and analysis of different external and environmental climatic parameters of the test room and the BI-SES elements, and the thermal characterization of the elements was also carried out. This study was complemented with a numerical analysis that consisted, in a first phase, in the dynamic simulation of computational fluids (using ANSYS Fluent) for the analysis of BI-SES elements and, in a second phase, in the energy simulation of the integration of BI-SES elements. SES in the test room (using EnergyPlus). A parametric analysis was performed with 82 scenarios, varying parameters such as the position of the window protection device, the number of photovoltaic panels in the system, the thickness of the air layer, the air exchanges between the BI-SES systems and the room and their modes of operation.

The main conclusions of the study indicate that the existing BI-SES (BIPVT) and the new prototype in its two versions, have the potential to increase the sustainability of the building, reducing the energy needs for heating and cooling. However, its operation needs to be adapted to other existing systems in the thermal zone, such as shading devices, having the automatic mode of operation, with intelligent operational set points, proved to be the most suitable.

Palavras-chave

BI-SES (sistemas integrados de energia solar em edifícios), BIPVT (sistemas térmicos fotovoltaicos integrados em edifícios), Simulação dinâmica de fluidos computacional, Simulação energética de edifícios, Campanha experimental

Keywords

BI-SES (Building Integrated Solar Energy Systems), BIPVT (Building Integrated Photovoltaic Thermal Systems), Computational Fluid Dynamics, Building energy simulation, Experimental campaign

Index

Index of figures

Index of tables

Nomenclature

U	Objective function
x	Independent variables
G_i	Equality constraints function
H_i	Inequality constraints function
Nu	Nusselt number
Q_{pv}	PV module heat flux (conduction) (W/m^2)
k	Thermal conductivity (W/(m.K))
T	Temperature (ºC)
l	Thickness (m)
Gr	Grashof
g	Gravity acceleration ($m.s^2$)
β	Coefficient of thermal expansion
Re	Reynolds number
ρ	Density (kg/m^3)
Vl	Fluid velocity (m/s)
Deq	Equivalent diameter (m^2)
μ	Viscous forces ($kg \cdot m^{-1} \cdot s^{-1}$)
Pr	Prandtl number
h	Convective heat transfer coefficient ($W/(m^2.K)$)

v	Kinematic viscosity ($kg \cdot m^{-1} \cdot s^{-1}$)
α_l	Thermal diffusity (m^2/s)
Ra	Rayleigh number (dimensionless)
H	Height
$H*$	Dimensionless height
ys	Sensor's height (m)
H	Total system height (m)
$\theta\ exp$	Dimensionless temperature
T_y	Sensor's temperature (ºC)
T_{amb}	Ambient temperature (outdoors) (ºC)
T_{pv}	PV interior module temperature (ºC)
T_{pv-t}	PV interior module temperature at the top height of the panel (ºC)
T_{pv-m}	PV interior module temperature at the middle height of the panel (ºC)
T_{pv-b}	PV interior module temperature at the bottom height of the panel (ºC)
T_i	Indoor temperature (temperature of the room) (ºC)
T_{comf}	Comfort temperature (ºC)
T_{comf}^{min}	Comfort temperature - minimum (ºC)
T_{comf}^{max}	Comfort temperature - maximum (ºC)
T_{ac}^{a}	Average temperature of the air cavity (ºC)
T_{ac}	Temperature of the air cavity (ºC)
T_{ac-i}	Temperature of the air cavity in the inlet height (ºC)

T_{ac-m} Temperature of the air cavity in the middle height (ºC)

T_{ac-o} Temperature of the air cavity in the outlet height (ºC)

ΔT Temperature gradient (ºC)

T_{inl} Inlet temperature (ºC)

T_{out} Outlet temperature (ºC)

T_{bf} Backflow temperature (ºC)

T_{wlse} Interior wall exterior surface temperature (ºC)

T_{wlsi} Interior wall interior surface temperature (ºC)

T_{ise} Insulation module exterior surface temperature (ºC)

T_{isi} Insulation module interior surface temperature (ºC)

T_{wse} Water tank exterior surface temperature (ºC)

T_{wsi} Water tank interior surface temperature (ºC)

T_w Water temperature (ºC)

G_V Incident solar radiation in the vertical surface of the BIPVT/Prototype façade (W/m^2)

G_h Global horizontal solar radiation (W/m^2)

G_d Diffuse horizontal solar radiation (W/m^2)

G_D Direct normal solar radiation (W/m^2)

η_t Thermal efficiency

η_{tot} Total efficiency

Q_{int} Heat flux of solid component (conduction) (W/m^2)

Q_v Convective heat flux (W/m^2)

A	Area (m^2)
η_e	Electrical efficiency
P	Nominal power (W)
T_{NOCT}	PV module normal operation condition temperature (ºC)
$R.F.$	Register failures
y_t	Predicted value during the period t
$\hat{y}_t$	Measured value during the period t
$\bar{y}$	Measured average value during the period
n	number of samples

Abbreviations

BI-SES	Building Integrated Solar Energy Systems
LNEG	Laboratório Nacional de Energia e Geologia
NZEB	Net Zero Energy Building
PV	Photovoltaic
EMS	Energy Management Systems
EPBD	Energy Performance in Buildings Directive
HVAC	Heating Ventilation and Air Conditioning
ASHRAE	American Society of Heating, Refrigerating and Air-Conditioning Engineers
RQ	research questions
O	objectives
EMS	Energy Management System
BIPVT	Building Integrated Photovoltaic Thermal systems
P1a	Prototype with interior module of EPS
P1b	Prototype with interior module of water tank
IT	Information Technology
AI	Artificial Intelligence
ANN	Artificial Neural Networks
BPS	Building Performance Simulation
EPS	Expanded polystyrene foam

Chapter 1. Introduction

Chapter 1 introduces the topics of design, modelling and optimisation of Building Integrated Solar Energy Systems (BI-SES) for the building façades. This chapter presents the context of the investigation, the scope of the project under which the thesis was developed, objectives and the motivation of the thesis. Finally, it presents an outline of the document.

In a brief overview, this thesis is inserted in the current context that the building sector is facing concerning the requirements to improve the building's energy performance while reducing the energy demand. The thesis aims to contribute to increasing the energy performance of buildings by proposing a new design of BI-SES that uses renewable energy and improves thermal performance, and by studying the existing system. The proposition of the new design is preceded by a literature review concerning published studies of new BI-SES designs as well as other pertinent topics, and proceeded by an experimental and numerical assessment of the systems' performance, with emphasis on the thermal behaviour.

1.1. Context

The energy use in buildings in the EU and US represents around 40% of final energy demand (Junker et al. 2018), and are therefore one of the most significant contributors to the increase of greenhouse gas emissions and the global warming effect. To maintain a minimum level of comfort for the occupants, it is required, in general, significant use of energy to operate the systems. The maintenance of minimum indoor comfort plays a significant role in the occupants' health, working efficiency and overall satisfaction, and therefore shall not be neglected. For this reason, there has been an increasing pressure to conciliate the improvement of occupant's comfort with the reduction of greenhouse gas emissions caused by the systems that provide comfort. However, achieving indoor building comfort with improved energy efficiency is still a challenge (Shaikh et al. 2016).

In general, the maximization of comfort is a conflicting objective with the minimization of energy use, which makes energy management in building a complex problem. An energy management system (EMS) that can control the comfort variables taking into consideration the multiple parameters together with the exterior climate conditions and the normative and policy requirements highlights the need to develop further energy management systems that are sustainable, flexible and resilient. Nowadays, the design of buildings must be adequately prepared to meet the building occupants' energy needs, and to include the local supply of at least part of the energy uses. The need for correct design applies both to new buildings and to older buildings that must be rehabilitated to achieve the requirements. The main parameters that influence indoor comfort are the architecture characteristics and construction materials, the behaviour of the occupants, the internal thermal loads, and the management strategies regarding the lighting, equipment, systems, and fenestration surfaces (Shaikh et al. 2016). The comfort variables that are possible to manage, as temperature and illuminance, are usually controlled by active energy systems. However, passive strategies may also be very useful in buildings, especially in façade integrated solar energy systems, the focus of the present thesis.

The investigation of innovative energy systems integrated into buildings and also conciliating active and passive strategies to EMS improvement are essential to achieve occupants' comfort using minimal energy use. The innovative systems are so-called because they present new methods or advances in technology or applications. Integrated solar systems associated with automation algorithms and a passive component may increase and ensure the energy efficiency without jeopardising the occupant comfort. In this context, the solar energy systems integrated into the façades typically promote the better performance of multiple physical domains simultaneously, having the capacity to (Ghasempourabadi et al. 2016; Loonen et al. 2017): i) significantly diminish the energy demand; ii) improve the level of indoor environmental quality; iii) impact on the match between on-site harvested renewable energy generation and use.

The operation of solar systems integrated with the façades has intrinsic time-varying performance, and the conventional metrics may provide potentially misleading information due to the dynamics of the system. For this reason, more accurate evaluation of the parameters that characterise these systems may be obtained by employing element and whole-building performance indicators, such as efficiency, total primary energy needs and comfort metrics (Loonen et al. 2017). This evaluation can be done through building performance simulations or extensive experimental analysis and calculations, which allow making informed decisions

regarding optimal performance, energy savings, occupant comfort, environmental and economic aspects. While extensive experimental campaigns can be very time-consuming and expensive, building performance simulation is an alternative (or complement) that can be used for prototyping and exploration of parametric analysis based on virtual testing.

Concerning the scope of the thesis, detailed analysis of the performance indicators of integrated solar energy systems in buildings allows, principally, to compare cost-effective measures and determine the adequate EMS schemes. The analysis of the systems assesses what might be named "passive testing" or "active testing" (Lamberts, Ghisi, and Papst 2000). The expression "passive testing" alludes to the utilization of information gathered during a regular activity/operation of the structure, with no intercession to expand the scope of operation features carried out during a specific period. Conversely, “active testing” entails the utilization of indicated control arrangement to observe and analyse the response to an almost all-inclusive scope of operation features, or a specific unique arrangement of features.

Within this context, the work developed in the framework of this thesis and the project NZEB_LAB allowed the creation of tested and validated innovative advanced solar systems integrated to façades. The present thesis is integrated into the Project NZEB_LAB "Research Infrastructure on Integration of Solar Energy Systems in Buildings". The Project NZEB_LAB is being developed in the National Laboratory for Energy and Geology (LNEG), Unit of Renewable Energies and Systems, since February 2017. The project focuses on Net Zero Energy Buildings (NZEB) performance research, involving building energy efficiency, renewable energy systems integration, construction and materials, efficient use and interaction with the urban grid. The NZEB concept may be defined as a building that over a year is neutral (i.e., it delivers as much energy to the supply grids as it uses from the grids) when energy efficiency measures are successfully combined with energy renewable sources. Accordingly, the net-zero-energy performance may be achieved as a result of executing two fundamental steps: first, reduce building energy demand and second, generate electricity or other energy carriers to obtain enough credits to achieve the desired energy balance (L. Aelenei et al. 2016; Garde et al. 2017; Gonçalves, Aelenei, and Rodrigues 2012).

Through the research developed by the Project NZEB_LAB, it is aimed to develop and promote optimal guidelines for achieving NZEB widespread adoption at the national level by 2020, while optimising the NZEBs energy design and operation concepts suited to the Portuguese climatic conditions and construction practices, in association with industrial partners. The work

plan proposed for the present thesis focuses on the development, testing and analysis of new BI-SES.

1.2. Motivation

The development of this work is motivated mainly by the notable potential of development of new BI-SES for façades. The potential for development is driven mostly by the new directives aiming to lead the construction sector to construct and rehabilitate buildings aiming to meet zero (or nearly zero) energy balance (through high-performance materials, systems and techniques), as the new Energy Performance in Building Directive (EPBD) (Hamdy, Hasan, and Siren 2013). The performance of a building refers to the capacity to attend the established functional and non-functional requirements during its lifetime, considering the design characteristics and exposure conditions. Each part of the building construction or system may have different criteria of performance, attending to a specific normative or technical requirement. The energy performance of a building, more specifically, is defined as the amount of energy consumed or estimated to meet the needs associated with a standard pattern of use (European Parliament 2010).

To attend the building's energy demand, different sources of energy are available, from the pollutant fossil fuels to renewable energies. Often, to achieve nearly zero-energy status, renewable energy is used in the building context, and an example is the use of BIPVT systems. In summary, according to the European Parliament (2010), nearly zero energy buildings are so-called due to the almost null energy needs from the grid, being the demand covered by renewable energy resources from nearby or on-site, having the building also very high energy performance. The assessment of the energy balances in a building, to achieve nearly zero or net-zero energy use, is influenced by different factors and may have different interpretations. According to Marszal et al. (2010), there are diverse renewable energy options for generation on-site and off-site, from the purchase of green energy supply from off-site producers to the on-site generation in which transport of sources is not necessary, as solar and wind energy integrated with the building (Marszal et al. 2010). The methods of metric of the energy balance

between the demand and the supply also vary according to different interpretations, taking into consideration the balancing period, primary energy used, CO2 conversion factors, connections to the infrastructure, requirements for energy efficiency, indoor comfort, building-grid interaction, among others. The balance period may vary from the operation year to the total period of utilisation of the life cycle of the building, according to the different approaches.

Two principal types of balance are identified by Sartori, Napolitano and Voss (2012). The first is the import/export balance, focusing on the energy flows between the building and the grid. The second is the load/generation balance, focusing on the quantities disregarding their interplay (Sartori, Napolitano, and Voss 2012). The authors highlight the importance of the balances but reinforce that the path to success is the prioritisation of the energy efficiency of the building and its systems.

Under the Energy Performance in Building Directive (European Parliament 2018; Hermelink et al. 2012), for the European Union, the metric of balance is the primary energy supplied (considering the renewable and non-renewable part) and the minimum building-related demands (heating, cooling, ventilation, domestic heating water and lighting). To meet the minimum requirements of zero or nearly zero amount of energy, the use of renewable energy and also strategies adapted to the local climate to achieve indoor comfort should be considered.

The relationship between the thermal comfort of the building occupants and energy use is hugely significant. According to Antoniadou and Papadopoulos (2017), the last decade was marked by the exponential interest of the researchers in indoor comfort assessment of buildings, linked not only with the human needs but also with a series of European Directives and International Standards – as the call for nearly zero energy buildings (Antoniadou and Papadopoulos 2017). This new focus on nearly zero energy buildings was preceded by many detailed and prominent studies on HVAC systems and construction materials, from 1970 to 1990. Nowadays, the need is not only to increase the use of highly efficient passive and active systems as solar photovoltaic energy systems integrated to façades but also to reduce the embodied energy of the construction materials and complexity of the systems. It demonstrates that the new approaches must be integrated and pertinent to the buildings lifetime, having focus not only on one element efficiency but also on how the building's occupant may impact its response or operation, and the climate surrounding the building.

There is a strong focus on the relationship between the thermal comfort parameters of the

building's occupants, building characteristics and its systems, and the environment in which it is located – and this relationship must also be exploited to the BI-SES impact on buildings. Thermal comfort is defined as "that condition of mind, which expresses satisfaction with the thermal environment" (Taleghani et al. 2013). Different indexes and characterization parameters of thermal comfort may be used to assess the condition of the human body concerning the thermal comfort, including allowances for temperature, humidity, air velocity, and others. Current norms, for example, ISO 7730 (Olesen and Parsons 2002) and ASHRAE 55 (De Dear and Brager 2002), have their methodologies based on adaptive models and heat balance models (from simplified to sophisticated approaches). Hensen and Lamberts (2012) provide a detailed description of these assessments. The thermal comfort related variables and parameters may be extensively assessed through the use of computational energy simulations (Hensen and Lamberts 2012), in a broader form than the purely experimental assessment once allows easy and fast variation of the parameters in order to provide prompt basis for decisions making.

Once innovative BI-SES systems are, essentially, new systems under consideration to future industry escalation, it is exceptionally essential to develop extensive experimental campaigns, not only to have realistic values of the performance within the time, but also to be used to complement the further simulations that will serve to optimise the design of the systems. The qualitative short and long-term behaviour of weather and indoor environmental data must also be described in detail, and short-interval environmental data is required to drive the calculations of the interaction building/environment, once determine the boundaries of the system. Short-term weather data collection and storage have evolved along with the computer capabilities and information revolution of the last four decades. However, many of the most recent studies had as basis very general climate behaviour (as direct use of a weather file with a characteristic year or a short period registered, for example). Nowadays, this situation is improving as technology lowers the cost and increases the sophistication of data observation, management, and modelling (Hensen and Lamberts, 2012), and is possible to obtain data not only from the practical representation of this information in hourly weather files and typical weather years but also to develop singular weather files for model validation with experimental campaigns.

The nature of the modelling process defines the parameters/features required (temperature, solar radiation, and others) while the time constants and objective of modelling suggests the appropriate observation interval. For example, large building structural components generally have relatively long-time constants (hours) concerning the heat transfer, making the hourly

approach more suitable. However, many building elements respond much more quickly (Hensen and Lamberts, 2012), as is the case of BIPVT systems. With solar systems integrated to façades, the resolution of the calculations must be increased, because the processes usually are non-linear and dependent on particular weather conditions. The present thesis is also motivated by this aspect, once aims not only to propose a new element design but also extensively test its behaviour.

The very dynamic behaviour of BI-SES shall not be seen as an obstacle to their implementation on a building's façade. Indeed, it shall be considered that these elements may complement the performance of common building constructive elements that have an intrinsic slower response to weather variations. If corrected designed and operated, the BI-SES may provide, by these means, more flexibility to the building energy systems operation. There is a vast potential for the integration of solar energy in façades – not only to produce electricity but also to recover heat. Solar energy technology integrated to façades are strongly related to adaptive techniques, once solar energy may be used with many different purposes, like heating, cooling and energy conversion.

1.3. Objectives

The work developed in the framework of this thesis and the project NZEB_LAB allowed the creation of tested and validated innovative advanced solar systems integrated to façades, aiming to both generate energy and reduce demand for heating and cooling of the building in an integrated approach.

In this research, the following main research questions are approached:

RQ1 Which new innovative advanced solar systems integrated to façades are being proposed, in terms of design, intelligence and automation?

RQ2 How can this thesis assess the performance of the BI-SES under study, based on experimental and numerical approach? Based on the RQ1, how can this thesis contribute, in

terms of innovation, with the design of a new prototype?

RQ3 How can the operation modes of the BI-SES (tested through simulation and experimental testing), contribute to improving the synergies between the indoor environment and the climate in which it is inserted?

Taking into consideration the impacts of the building sector on energy use and the usual non-renewable sources of energy, the design of innovative solar systems integrated with façades is an urgent need. It is a demanding concern that must be addressed in order to achieve sustainable and nearly zero energy buildings. From the past decades to date, efforts have been made in order to contribute to the development of this sector. However, investments in innovation are still needed, as is stated by researches during the last two decades (Chwieduk, 2003; Maurer, Cappel and Kuhn, 2015).

The most important factors to consider are the design and integration of the systems on the architectural aesthetic, the integration of the system in the building use and energy demand pattern and accordance to the climate in which it is inserted — also, the optimisation and Energy Management Systems (EMS) regarding the occupant's comfort and economic needs. The decision making for the implementation of the BI-SES systems must be based on a robust technical and economic analysis to evaluate the feasibility and cost-benefit of its implementation.

Despite not approaching the proposed new BI-SES by the economic point of view, this thesis focuses on the technical aspects and aims to contribute to this sense. It is essential to highlight, however, that issues might be found regarding innovative systems that are in the prototyping stage, once the costs are usually higher than systems in industrial production and commercialisation stage. In the scope of the investigation line of the reduction of energy use, generation of renewable energy, an increase of resilience and flexibility of the energy systems in buildings, the research presented by this thesis is pertinent and aim to contribute to the sustainable development of the building's sector.

The present thesis sets out the following objectives, motivated by what has been presented so far regarding the design, experimental and numerical analysis of the new application of solar energy systems integrated with building façade:

O1 To propose the design of new concepts for solar energy systems as a solution for new

buildings and retrofits;

O2 To develop a detailed numerical and experimental investigation of new solar energy innovative systems to access its performance and thermal behaviour;

O3 To develop a parametric analysis based on validated models of the BI-SES and room, in order to improve the system smart operation and design, to respond in real-time to the energy and comfort needs of the adjacent space where integrated;

O4 To contribute to the technology transfer and dissemination of the results obtained, to accelerate the implementation of new sustainable energy systems.

1.4. Summary of the methodology

After the development of the introduction in which the context of the thesis is presented, the literature review was conducted. The literature review was carried out through refined filtering, based on the topics of interest: Integrated thermal systems, integrated photovoltaic systems, integrated photovoltaic thermal systems. The objective was to identify, among the sample of selected works, the type of system studied, whether the analysis was experimental or numerical, which simulation tool was used, parametric analysis variables and determined efficiency for the systems. This identification served as a basis for example for the methodologies to be adopted.

As presented in the previous sub-section, the literature review was followed by the case study chapter. Within the scope of this thesis, the case study is addressed at the systems level (which are the existing BIPVT and new prototype), and at the level of its integration with the adjacent thermal zone, which is the test room. These elements are the subject of a brief description here. The test room in question was chosen as a case study because it is a laboratory designed to integrate facade prototypes and serves as a controlled environment while it is occupied - thus translating into a “living lab”. This test cell is in the Solar XXI building, in Lisbon, which was conceived as a low energy demand building with integration of renewable energy generation to achieve the NZEB concept. In total, this building has 19 BIPVT systems installed on the south façade, in addition to other renewable energy systems. The test room is a room in controlled

conditions, with a floor area of 16.70 m^2 and a glass area of 2.82 m^2. It is occupied by one person, and other heating / cooling systems were not used during the entire monitored period, as well as the window and door are kept closed at all times, with the exception of the occupant entering and leaving the room.

The BIPVT system in this room consists of four photovoltaic modules, with 12.7% electrical efficiency and 160 Wp each. There is a fixed thickness of the air cavity of 16 centimetres and the system is operated manually. The inlet is located at the bottom and the outlet at the top. It has three temperature sensors and two heat flow sensors. The manual mode of operation is divided into heating mode and cooling mode. The heating mode is operational during the winter, in which it allows air to circulate between the air cavity and the adjacent thermal zone during the day and is closed at night. The cooling mode allows external circulation during the day and night, to cool the photovoltaic modules and increase the electrical efficiency of the system in the summer.

The new prototype was developed with the aim of creating other comparative solutions with the existing BIPVT system. The development of a new prototype aims not only to address the need for intelligent and more adaptive solutions for the façades, but also to test whether operations in manual and automatic mode make sense for the context in which they are inserted - especially for buildings of service where its manual operation depends on the occupant's awareness of operation. The occupant itself tends to perceive when he needs the heat recovery provided by such systems, but does not have the same perception of operation when the environment is comfortable and the objective is to increase electrical efficiency by cooling the modules, for example.

The case study description is followed by the experimental analysis, that is also fundamental to validate de computational model developed in Chapter 5. The experimental analysis of each segment monitored the following parameters, in terms of the object of study: The climate - the ambient temperature and the components of solar radiation, The test room - the ambient temperature, occupation, blind positioning, functioning of the existing bipvt openings and fenestration opening, O BIPVT - system temperatures and heat flow with manual measurement of air speed. The prototype - parameters similar to BIPVT, with the addition of the water temperature. The main results of the experimental analysis were the relationship between variables, efficiencies and dimensionless analysis. The experimental configuration was described in the thesis in terms of observable variable, sensor brand / model, measurement

range and precision. In addition, sensor location schemes have been described.

The numerical analysis, the last component of the thesis, aims to identify the different energy vectors and to characterise the energy uses, to include, among other aspects, the survey of the characteristics of the surroundings and the systems techniques, the characterisation of the utilisation profiles and the quantification, monitoring and dynamic simulation of the energy uses. This step is firmly based on computational resources and experimental campaign, aiming to test scenarios that were not possible to test through the experimental approach. The objective of numerical modeling is to analyze the element and obtain a detailed profile of the system's cross section, and then analyze the integration of the systems with the test room, in order to assess the impact that the different configurations of the systems have on the energy needs for heating and cooling this thermal zone. It starts with the analysis of BIPVT through the use of ANSYS Fluent, in simulation in steady state, to obtain the outlines of temperature, air speed and turbulence. The BIPVT analysis used a uniform mesh, a mesh size of 0.005m, and the analysis of the prototype P1a and P1b used a mesh size of 0.002, chosen due to the computational capacities to process the mesh given the geometry area. Then, a dynamic simulation is performed using the EnergyPlus software, including model validation and parametric analysis. The parametric analysis study five groups of scenarios, considering the systems' air gap thickness, zone mixing air flow, number of PV panels (system height), comfort setpoint of operation, and window blind position (in order to reduce the uncertainty caused by the direct solar gains through the window).

After the development of case study characterization and performance analysis through the use of experimental and numerical methods, the conclusions are drawn as well as the recommendations for future works.

1.5. Thesis organization

The present document is segmented in six chapters. Chapter 1 is the introduction to the topic, in which the context, motivation and objectives are presented. Also, the present subsection of text organisation reflects the structure of the document. Chapter 2 describes the background information, in which both primary theoretical literature are revised and new literature that

contain the state of the art researches and methods being studied by different authors.

Chapter 3 presents the case study developed in this thesis – existing systems and the newly developed prototypes integrated into the façade of the test room in the Solar XXI Building, located in Lisbon, Portugal. Chapter 4 refers to the experimental analysis, in which the climatic conditions, test rooms and its systems are monitored and analysed. It is developed to provide a reliable characterisation of the thermal behaviour of the test room and its systems.

Chapter 5 refers to the numerical analysis of the building and its systems and new prototypes of solar energy systems integrated to the façades of the test rooms, from design to numerical and experimental analysis. This chapter also presents the validation of the engineering models of the prototypes, room and BIPVT system. Chapter 6 presents the conclusions of the work, highlighting the main findings, contributions, and suggestions of future works.

Chapter 2. Building Integrated Solar Energy Systems (BI-SES)

To appraise the state of the art regarding the topic of this thesis, it is pertinent to review some crucial topics related to the façade elements and the innovation they have been suffering in the last years. These topics cover the latest propositions, to the date of this thesis publication, for advanced BI-SES in terms of design and optimisation process, and energy performance assessment. The following subsections discuss these topics considering the central concepts, technologies and methods, and the main developments to date.

The building façade has a crucial role in acting as the interface between the environment and the indoor ambient. It has a significant impact not only on the occupant's comfort but also on building energy demands and the aesthetics of the building. Commonly, designing a building façade takes into consideration several factors, as the climatic conditions and surrounding buildings, indoor and spatial characteristics, needs of the building occupants regarding comfort and costs, and others. Factors as solar heat gains, orientation, and solar distribution must be considered when designing façades. For both transparent/translucid and opaque façades elements, heat gain and loss must be optimised, with the enhancement of ventilation and air movement, and others crucial factors (Halawa et al. 2018).

From an engineering and architecture perspective, in the last years, there has been a growing focus on the strategic development of building façades, it is, to contribute to meet the requirements of the high-performance regulations while being sustainable and aesthetically pleasant. This strategic development brings new experiments, innovative systems and technology to be integrated into the formal functions of the envelope (Formentini and Lenci 2018). The characterization of the façade solutions is made through the direct assessment of their physical characteristics (thickness, thermal conductivity and others), or through the use of calculations using the former ones (thermal resistance, U-value and others). As so, most often, the usual façade elements are characterized regarding its U-value, or thermal resistance, specific heat, density, conductivity and thicknesses. However, solar systems integrated into façade elements must also be characterized by additional parameters, such as efficiency in cooling and heating periods. The façade elements may improve the energy flexibility of the building, by the adequation of the constructive elements thermal performance to climate and building usage profile, also by being adaptive or automated to adapt to the different boundary conditions.

Given this context and the flexibility that façade elements can offer in the design process, innovative façade elements based on solar energy systems can introduce significant benefits in reducing the building energy demand (Pomponi et al. 2016). Based on this context, state of the art concerning the innovative solar systems integrated into façades is reviewed in this section.

The source of information used for the development of the subsection describing the solar thermal, solar photovoltaic and hybrid systems is the Clarivate Analytics Web-of-Science. Fig. 1 presents in detail the survey method and rationale used for the systematic review. In summary, the eligibility criteria and study selection are based on the accordance of the published material within the search terms, period, the relevance of the field to this thesis, keywords and abstract pertinent to the objectives, and consideration through the screening of appropriate content throughout the text. Thus, Fig. 1 also presents the results in terms of the number of publications filtered through the adopted survey methodology. The data items, summary measures and report characteristics are based on the study details (reference), study characteristics (study type and technology type), extension of analysis, among others.

In the survey step previous to the detailed consideration of the title and abstract pertinent to the objective of the study (resulting in 115 articles), the results obtained by the source of information were segmented concerning the year of publication (Fig. 2), journal of publication (Fig. 3) and country of submission (Fig. 4).

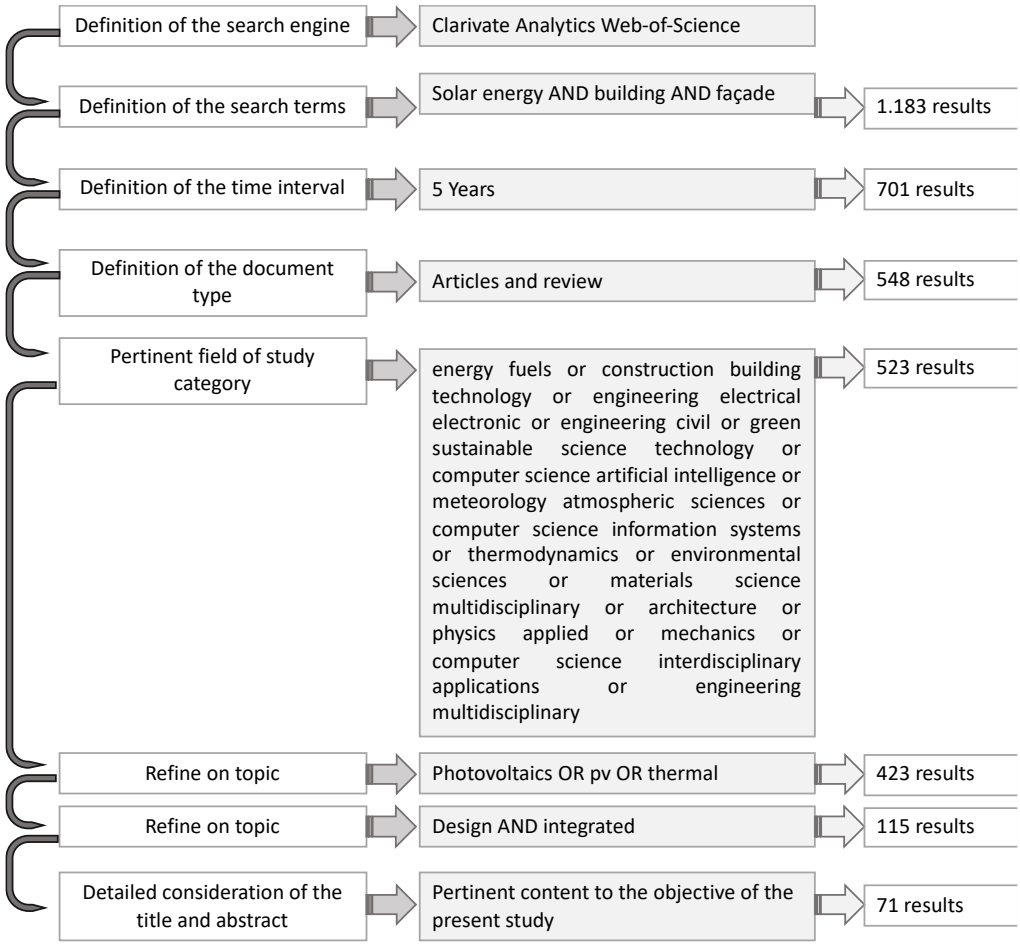

Fig. 1. State of the art survey method and results for the state of the art review.

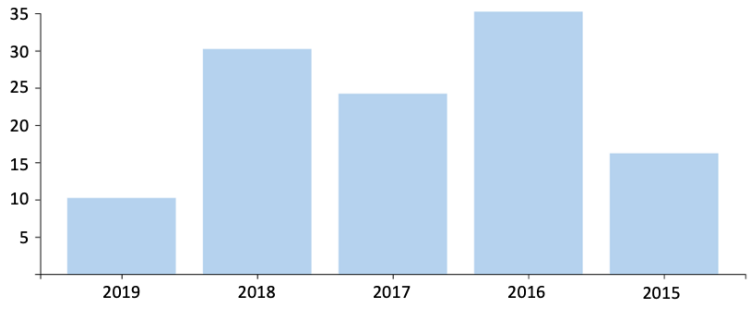

Fig. 2. Segmentation by year of publication.

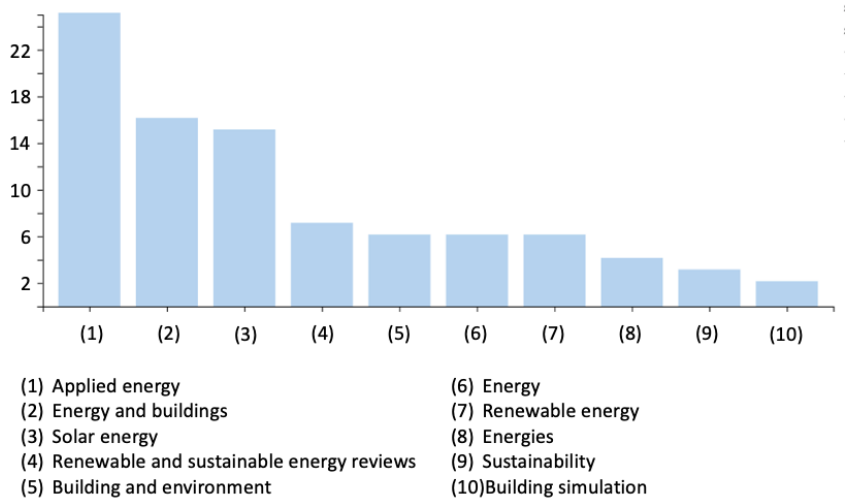

Fig. 3. Segmentation by the journal of publication.

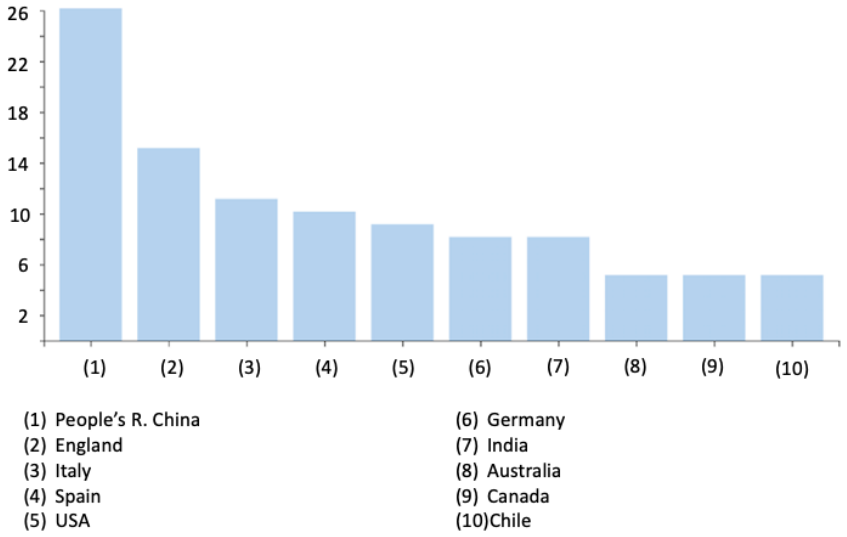

Fig. 4. Segmentation by country of submission.

2.1. Integrated solar thermal systems

A sample of 16 scientific articles was considered as representative innovative solar thermal systems pertinent to the scope of the thesis, among the 71 articles reviewed concerning the state of the art of BI-SES. A brief summary of the most pertinent is presented here, followed by a

table with a summary of the studies.

As a first introduction to the topic, some recent review articles are able to provide an overall panorama on the technology and the suitability of the building integrated solar thermal system assessed considering many different aspects. In Maurer, Cappel and Kuhn (2017), a review is done on the most important contributions of recent years of building-integrated solar thermal systems, in terms of systems being designed, results being achieved in terms of thermal characterization, and simple models to evaluate the systems – being this publication an interesting compilation of studies to have an overall view of the current technology status for building integration. More specific and inserted in the scope of this thesis, examples of reviews of thermal systems aiming to reduce nominal energy needs of the building may be founding in Prieto et al. (2018) and in Valladares-Rendon, Schmid and Lo (2017). An example is in Prieto et al. (2018), in which there is a detailed review concerning the possibilities of use of solar cooling integrated façades, by exploring their feasibility concerning orientation, efficiency, and climate in which it is used. In their particular study, it is concluded that warm-dry climates and east/west orientations are the best situations for solar cooling façade applications, reaching a theoretical solar fraction of 100% (Prieto et al. 2018). In Valladares-Rendon, Schmid and Lo (2017), is developed a review of shading thermal solutions to decrease direct solar gains and improve energy savings, balanced with visual comfort. This publication emphasizes the importance of employing the solar thermal elements with more than one purpose in a single element, reinforcing that solar façade elements shall not have a static purpose.

Also considering well constituted review studies, in O'Hegarty, Kinnane and McCormack (2016), the authors review and analysed solar thermal façades in terms of the type, technology used, and the materials that constitute it. Daily efficiency models are presented, based on a combination of analysis methods, constituting a good data resource for comparison among technologies. Lamnatou et al. (2015) present a critical review of the simulation methods and usage of building-integrated solar thermal systems. Not only thermal, but other types of BI solar configurations such as photovoltaic and hybrid systems are covered.

Considering more specific studies, namely on the using of building integrated solar thermal system as a shading device, in Velasco et al. (2017), a Venetian blind double-skin façade with the integrated solar thermal collector is analysed through CFD software. The authors emphasize that the system would promote energy efficiency by means of avoiding direct solar gains while being aesthetically pleasant. Also, in Sun et al. (2016), the authors present a façade system with

parallel transparent plastic slats sandwiched between glass panes to form a parallel slat transparent insulation material to reduce coupled convective and radiative heat transfer inside the air cavity of the panes of a double glazed window. It contributes to increasing the thermal resistance, without constraining the daylight access to the point of visual comfort reduction. In Li, Qu and Peng (2016), the work focuses on the innovation of building-integrated solar thermal shading system, to reduce the energy demand and improve the daylight levels through modelling and simulations.

The design of new and innovative prototypes is a prominent part of the recent publications, showing that different research groups are looking for BI-SES thermal solutions around the world. In Buonomano et al. (2018), the design and the thermodynamic analysis of a new prototype of a flat-plate water-based solar thermal collector are developed, with the aim to integrate the system in building façades. The innovation is based on the use of inexpensive materials and simplified design, aiming to reduce the production and installation costs to improve market penetration. The applications are the production of hot water for domestic uses and space thermal comfort. This study contrast with the tendency in academia of developing expensive prototypes, as it aims to reach buildings in a faster manner by implications and technology transfer. As in the previously mentioned work, in Agathokleous et al. (2019), it is also possible to find a flat-plate based thermal collector to be integrated into building façade envelopes but based on using air as the fluid. The authors also focused on the use of cost-effective materials and simple design solutions. They develop an energy dynamic simulation model and economic performance analyses and conclude that the system payback would be close to six years.

The integration of incorporated storage system in thermal prototypes are also to note. In Garnier, Muneer and Currie (2018), a novel incorporated solar collector with storage for water heaters was created, followed by a praiseworthy CFD investigation. The proposed project is composed by a heating component to give household independence through the high-temperature water system and considers the coordination of the system and the rooftop configuration, enabling the system unit to be inserted inside an auxiliary protected material board framework. Another example is in Resch-Fauster et al. (2018), in which the proposition focuses on an integrated solar thermal collector and latent heat storage modules. The overheating protection supplied by this system has high efficiency of the optimized configuration, calculated in function of other thermophysical characteristics. This study also reinforces the modularity that the BI-SES systems are adopting in recent years. In Ibanez-Puy

et al. (2018), a ventilated active thermoelectric envelope component is studied. It focuses on a modular active ventilated façade prototype with a thermoelectric system, to be installed in the building envelope and provide a high comfort level. The system integrates a passive design strategy through the ventilation and an active strategy through the use of an active thermoelectric solution. This study is an example of coupling passive and active techniques to improve the overall system performance.

Also considering the integration of thermal storage in the developed systems, in Guarino et al. (2017), the authors study the performance of a building-integrated thermal storage system, with the aim to improve the energy performances of the system in a cold climate. In Navarro et al. (2016), it is presented a novel system of phase change material (PCM) inside the structural horizontal building component. The structural element was a composed concrete element with macro-encapsulated PCM located into 14 channels, coupled to a solar air collector to melt and induce the phase change. The technique presented by these authors may be considered more intrusive once are coupled with hard materials of civil construction (concrete), that must per si present a reliable structural performance throughout the whole building lifetime. In Hengstberger et al. (2016), a solution is presented by also using PCM embedded into the absorber insulation which buffers the heat during the day and releases it in the night. A parametric analysis is developed with the use of a dynamic simulation tool to find the best melting temperature of a thin layer of PCM at different positions.

More complex systems are also under analysis in the last years, as in Shen et al. (2016), the authors introduce an innovative compact solar thin film with an interiorly extruded pin-fin flow channel that is convenient for the building integration. A simulation model was used, and a prototype of the solar thin film was fabricated, to test the system under different controlled conditions. The methodology presented by this work is pertinent to the thesis, once discuss the process of designing and testing.

The simulation of these systems is assessed in different spheres, and the CFD analysis is one of the most used. In He et al. (2016), an innovative tile-shaped dual-function solar collector is analysed for water heating. The study is developed by using CFD software and aims not only to provide optimal designs but also meet good aesthetics. In Giovanardi et al. (2015), a modular unglazed solar thermal façade system was developed to aid the installation of active solar façades, with particular focus on the renovation of existing buildings. In He et al. (2015), the authors investigate the loop-heat-pipe water heating performance of an innovative heat pump

assisted solar, using both theoretical and experimental methods.

Table 1 presents the complete list and classification of the solar thermal systems reviewed in this work, considering the system type, existence/non-existence of experimental and numerical analysis, existence/non-existence of parametrical analysis and details, reached efficiency of the system under study. The nomenclature (N.S.) stands for “not stated”, meaning that the feature was not mentioned in the article.

The results obtained show, concerning the solar thermal systems, that there is not a specific trend concerning the systems under study in the most recent publications – with exception of the use of PCM or storage systems in a considerable number of the sample. However, the focus can be given to the integration between passive and active techniques, and to the modularity and multiple purposes of the same element. The technologies vary from innovative system design to innovative methods of operation or material combination. Also, the thermal efficiency (η_t) of the systems is in most case, not directly assessed. In the studies using dynamic simulation, most parts of them assessed the impact of the systems in thermal behaviour through the calculation of nominal energy needs for heating and cooling of the thermal zone, based on determined setpoints. Others use computational fluid dynamics analysis to have a detailed profile of the thermal behaviour of the systems given the specified boundary conditions and evaluate the systems in terms of temperatures (mostly based on the outlet-inlet differences). Parametric analysis is not always done in the reviewed studies, but in the studies that develop this component, the geometry, inlet velocity and inlet temperature (T_{inl}) are the most used variables of variation.

Table 1. Summary of the studies – solar thermal systems.

Reference	System type	Experimental analysis	Numerical analysis	Simulation tool or technique	Parametric analysis	Thermal efficiency	Electrical efficiency	Total efficiency
(Buonomano et al., 2018)	Water solar flat-plate solar thermal collector	x	x	Matlab	active and passive analysis	N.S.	N.S.	0.16 - 0.46
(Agathokleous et al., 2019)	Flat-plate solar thermal air collector	x	x	Matlab	active and passive analysis	N.S.	N.S.	N.S.
(Garnier, Muneer and Currie, 2018)	Integrated collector storage solar water heaters		x	CFD software	aspect ratio	N.S.	N.S.	N.S.
(Resch-Fauster et al., 2018)	Integrated solar thermal collector and latent heat storage panels	x	x	N.S.		N.S.	N.S.	N.S.
(Ibanez-Puy et al., 2018)	Ventilated active thermoelectric envelope	x		N.S.		N.S.	N.S.	N.S.
(Velasco et al., 2017)	Venetian blind collector		x	CFD software		N.S.	N.S.	N.S.
(Guarino et al., 2017)	PCM thermal storage	x	x	EnergyPlus		N.S.	N.S.	N.S.
(Navarro et al., 2016)	Active slab with PCM coupled to a solar air collector	x		N.S.		N.S.	N.S.	N.S.
(Sun et al., 2016)	Double glazing façade system with PS-TIM		x	CFD software	cell aspect ratios	N.S.	N.S.	N.S.
(Hengstberger et al., 2016)	Solar thermal collectors with PCM	x	x	CFD software		N.S.	N.S.	N.S.
(Shen et al., 2016)	Solar thermal façade with an interiorly extruded pin-fin flow channel	x	x	N.S.		0.63	N.S.	N.S.
(Li, Qu and Peng, 2016)	Building-integrated solar thermal shading		x	EnergyPlus		N.S.	N.S.	N.S.
(He et al., 2016)	Dual-function solar collectors with and without tile-shaped covers and water heating		x	CFD software	inlet water temperature, flow rate, weather	0.73	N.S.	N.S.
(Giovanardi et al., 2015)	Modular unglazed solar thermal element		x	N.S.	building typology, system geometry and characteristics	N.S.	N.S.	N.S.
(He et al., 2015)	Heat pump assisted solar façade loop-heat-pipe	x	x	N.S.		N.S.	N.S.	N.S.
(Li, Dai and Wang, 2015)	Solar thermal curtain wall	x	x	N.S.		0.56	N.S.	N.S.

2.2. Integrated photovoltaic systems

A sample of 37 scientific articles was considered as presenting innovative solar photovoltaic systems (working only with the photovoltaic effect), among the 71 articles reviewed concerning the state of the art of BI-SES. A brief summary of the most pertinent is presented here, followed by a table with a summary of the studies. Concerning the review studies, some studies extensively present the technology and state of the art. In Shukla, Sudhakar and Baredar (2016), an extensive review is presented concerning the design of Building Integrated Photovoltaic (BIPV) systems. It focuses on the development of the technology, classification of cells and products, and industry/research opportunities. Another study, develop by Tripathy, Sadhu and Panda (2016), presents a review of the state-of-the-art of the PV products for building different components of envelopes, their properties and accordance with international standards.

The BIPV systems are being used not only in new buildings but also in retrofit of older buildings to achieve more sustainability, being the studies in this area broadly pertinent. The methodological approach to assess these systems vary between studies. In Aguacil, Lufkin and Rey (2019), the work aims to provide a methodology to contribute to the decision-making process concerning the use of BIPV in the urban renewal process. It considers the surface types and trade-offs between self-consumption and self-sufficiency. It is a straightforward approach that aims to facilitate the analysis of suitability concerning different factors. A very pertinent content may be found in Biyik et al. (2017), once the authors reviewed the BIPV and BIPVT possible uses in terms of types, supply, generation power, performance characterization, and approaches of analysis. They identify two crucial research areas concerning this subject: i) increase on system efficiency utilizing ventilation while reducing the modules temperature ii) use of thin-film applicable for integration in buildings. This study is an excellent source to assess the comparison between BIPV and BIPVT (further explored in the next sub-section). In Shukla, Sudhakar and Baredar (2017), the study also presents a comprehensive review of the BIPV commercial solutions and their characteristics and a comparison of international testing and operation standards and instructions. The authors focus on BIPV solutions for different façade elements.

The impact of the building architecture in the use of BIPV systems are also being assessed. In Chen, Yang and Peng (2019), it is explored the impact of archetypes and confounding factors in the optimisation of the design of the BIPV systems. They focus specifically on high-rise

buildings with BIPV façades, making use of data-driven models incorporating qualitative and quantitative analysis. It intends to facilitate the analysis by defining typical types of façades in which the buildings are inserted. The impact of module temperature is also object of study, and pertinent to this thesis. In Agathokleous and Kalogirou (2018), the authors study a naturally ventilated BIPV system, and the assessment is based on experimental thermal analysis. This study is particularly attractive to the thesis, and further results obtained by the authors are presented in Table 2. In Agathokleous et al. (2019), the authors continued the previous work by presenting a simulation-based thermal analysis of the same system. In Wang et al. (2017), a ventilated PV double-skin façade and a PV insulating glass unit are studied through comparative experiments, to evaluate the solar heat gain and U-value of the systems. In Cipriano et al. (2016), the focus was on a PV ventilated component, and the use of a data-driven approach to iteratively identify the unknown parameters, determine their impact in the simulation outputs and ultimately, to assess the deviations of the computational outputs against the measured data.

Other studies using simulation tools and experimental campaigns are also presented in the literature, to develop a parametric analysis considering different parameters of the system. In Peng et al. (2016), the authors used EnergyPlus (the same software that is used in the scope of the whole-building simulation in this thesis) and developed a whole-year energy performance evaluation and saving potential of a ventilated photovoltaic double-skin façade in a cool-summer Mediterranean climate zone, a study that is pertinent to the thesis scope. The work developed a sensitivity analysis over the numerical model, considering different air gap width and operation models of the ventilation. In Pantic et al. (2016), they present a theory-based and experimental investigation of electricity generation potential concerning different orientations of the modules in the façade elements.

The PV modules are also integrated in buildings with the purpose of providing shading and by this mean reducing the direct solar gains in buildings. In Asfour (2018), the study focuses on the association of the PV modules in shading devices, and the study is oriented to hot climates. They also develop a parametric simulation to evaluate the potential of different designs. In Luo et al. (2018), PV-blind embedded double skin façade is studied by coupling thermal-electrical-optical models. The aim was to evaluate and optimize the system by using ray-tracing, radiosity and net radiation methods, as well as other usual thermal models for buildings. In Tablada et al. (2018), the authors also study the use of PV coupled to shading devices for farming plants growing application – focusing on windows and balconies. In (Cheng et al. 2019), the study

derived a new metric for assessing the daylight quality by comparing different coverage ratios of the PV cell and window-wall-ratios. They also compared different orientations and assessed the net electricity use of the building. In Karthick et al. (2018), they investigated semi-transparent building integrated photovoltaic modules on façades, focusing on different coverage ratios. In Zhang, Lu and Peng (2017), the authors also investigate the potential savings generated by the use of PV associated to shading elements, developing a parametric analysis concerning tilt angles and orientation of the system.

BIPV systems were also studied as a window component. In Connelly et al. (2016), the idea of semi-transparent BIPV with concentrator is additionally investigated. They propose a "smart window" framework comprising a thermotropic layer with integrated PV modules. The authors propose a system that naturally reacts to climatic conditions and analyse the power generation, natural light availability and heat transfer from the system to the building structure, through parametric analysis of different solar energy ratios incident on the PV. In Wang et al. (2016), they evaluated the energy performance of an a-Si semi-transparent PV insulating glass unit via numerical simulation and experimental tests. Considering the measured optical and electrical features of the PV, an integrated model was made to simulate the energy performance of the system under analysis. In Favoino et al. (2016), they propose a novel simulation framework for the performance evaluation of a responsive structure, based on envelope advances in terms of the switchable photochromatic coating. The analysis is done by incorporating building energy simulation and lighting simulation, and varying parameters as the climate in which it is inserted.

Also considering windows, in Wu et al. (2016), a novel static concentrating PV system, reasonable for use in windows or coating exteriors, has been proposed. The proposed concentrating PV system is lightweight, with minimal economic effort and ready to produce power. Moreover, this system consequently reacts to atmospheric conditions by changing the parity of power created by the PV with the measure of sunlight-based light and heat allowed through it into the structure. It also offers the possibility to control the energy utilization in the building. In Liu et al. (2016), they improved the structure of a commonplace semi-transparent PV module and investigated the utilization of three sorts of high-reflectivity heat protection movies to frame the BIPV. Hence, the creators broke down the impact of the system structures on the optical, heat, and control time execution of the semi-transparent PV module and how much the execution improved.

Semi-transparent PV cells are also a trend in recent studies. In Qiu, Yang and Zhang (2019),

they investigate mergers of vacuum glazing and BIPV integration and analyse its capacity to reduce the energy needs of the buildings. In Huang et al. (2018), they also present a detailed investigation of the thermal and power efficiencies of a similar novel system, and combined design improvement of photovoltaic envelope solutions. In Sun et al. (2018), they combine optical, electrical and energy models to assess the integration of semi-transparent photovoltaic in commercial buildings. The publication assesses the effect of window design on the energy needs of the building. In Tak et al. (2017), the authors structured a semi-transparent sun-powered cell window, in which the transparency can be changed by modifying its temperature and dissolvable vapour pressure. Further details may be seen in the reference, in which a modelling test with the proposed system was led to look at the impacts on energy utilization, power generation, and inhabitant comfort. The outcomes demonstrate that the proposed window has a significant potential to generate electrical energy.

In the last years, the use of concentration systems in BIPV systems were also focus of publications. In Sornek, Filipowicz and Jasek (2018), a Fresnel lens is used to increase the efficiency of BIPV systems. The analysis of the system is made both employing dynamic simulations and experimental campaigns, in which they improved the general productivity of the building integrated photovoltaic systems by the use of a Fresnel lens. During the tests, the efficiency of the photovoltaic module increased by about 7% (reaching an η_e of 22%). In Bunthof et al. (2016), they build up the examination dependent on three Concentrator Photovoltaic (CPV) systems arrangements that take into account the development of semi-straightforward structure veneer components. The systems likewise are a Fresnel focal point based concentrator and a novel level planar optic concentrator. In Correia et al. (2016), Luminescent Solar Concentrators are displayed as being financially savvy parts effectively incorporated in PV that can improve and advance the integration between PV components and building structures, with considerable potential outcomes for energy generation in façades, while improving urban aesthetics. In Sabry (2016), a range of prismatic total interior reflection low concentration PV façades with different head angles has been evaluated, dependent on the location and characteristics of surrounding areas of the building. Every veneer design is mimicked by ray-tracing procedure, and its presentation is examined against sensible direct sun-based radiation information in two clear sky days representing the summer and winter of the area under study. Ray-tracing recreations uncovered that the majority of the chosen arrangements could gather the vast majority of the direct solar radiation in summer.

In Kang, Cho and Lee (2015), they developed a light-catching system that can be connected to BI-SES based on the PV use, which naturally promotes light exposure during the entire year. The structure is streamlined as for the precise scope of the occurrence light by breaking the underlying symmetry. The authors show the viability of the designed light-catching structure for different occurrence point ranges by means of exhaustive reproduction studies and trial results utilizing organic photovoltaic elements. In Hofer et al. (2016), they present a modelling framework, coupling parametric 3D with high-resolution electrical modelling of the shading devices composed by thin-film PV modules, to re-enact electric energy of geometrically complex PV applications. The proposed modelling framework can foresee with high spatial-transient resolution the shading positioning and adapt it, over each PV modules, being critical to improving the electricity generation through the adequate positioning of the modules and also contributing to the control of direct solar gains in the building.

BIPV systems are being particularly used in the façades of research institutions, in which they are object of case studies. In Palacios-Jaimes et al. (2017), a plan to transforming a university building into NZEB is presented, and it demonstrates that BIPV system may provide the power needs and lessen the structure's energy use in a financially savvy way. The investigation emphatically centres around the life cycle assessment, surveying the net emissions of CO_2 and the harms caused in a near setting with traditional power sources. In Yang (2015), they identify the technical barriers and risks related to the utilization of BIPV in different stages of the building life-cycle, together with the proposal of potential arrangements. When a straightforward answer could not be proposed, suggestions for future innovative work are made. The proposed approach incorporates assessment of past productions and gathering of criticism from the business experts.

Table 2 presents the complete list and classification of the solar photovoltaic systems reviewed in this work, considering the system type, existence/non-existence of experimental and numerical analysis, existence/non-existence of parametrical analysis and details, reached efficiency of the system under study.

The results of this sub-section show a considerable amount of studies being made concerning BI-SES based on photovoltaic technology. Three main design trends were identified based on this review: i) improvement of standard BIPV configurations through smart ventilation; ii) use of photovoltaic technology integrated into building façades as shading devices, and iii) use of concentrators in the PV systems integrated into building façades and rooftop. As in the previous

category, many studies do not approach the systems in direct terms of efficiency (in this case, η_e). They are approached in terms of nominal energy needs, energy balances (demand and on-site supply), and temperatures of the system. Also, a parametric analysis is mostly done by varying parameters as orientation, cell coverage ratio, air gap width, ventilation rates, and geometries.

Table 2. Summary of the studies – solar photovoltaic systems.

Reference	System type	Experimental analysis	Numerical analysis	Simulation tool or technique	Parametric analysis	Thermal efficiency	Electrical efficiency	Total efficiency
(Aguacil, Lufkin and Rey, 2019)	BIPV	x	x	BIM	Archetype, energy cost	c	0.17	N.S.
(Chen, Yang and Peng, 2019)	BIPV		x	EnergyPlus, je+, R, GenOpt	Archetype, confounding fators	N.S.	0.06 - 0.15	N.S.
(Cheng et al., 2018)	STPV	x	x	Daysim, EnergyPlus	Coverage ration, Orientation, WWR	N.S.	N.S.	N.S.
(Qiu, Yang and Zhang, 2019)	Vacuum PV insulated glass unit	x	x	EnergyPlus, Berkeley	System types, orientation	N.S.	N.S.	N.S.
(Asfour, 2018)	BIPV as shading device		x	DesignBuilder, EnergyPlus	Design configuration	N.S.	N.S.	N.S.
(Sun et al., 2018)	Integrated semi-transparent cadmium telluride PV glazing		x	EnergyPlus, Radiance		N.S.	N.S.	N.S.
(Huang et al., 2018)	Vacuum PV insulated glass unit		x	EnergyPlus, GA	Different curtain walls	N.S.	N.S.	N.S.
(Luo, Zhang, Liu, Su, et al., 2018)	PV-blind integrated glazing	x	x		Position, cell efficiency, airflow	N.S.	N.S.	N.S.
(Tablada et al., 2018)	PV (PV) modules as shading devices integrated with farming planters	x	x		Configuration	N.S.	N.S.	N.S.
(Sornek, Filipowicz and Jasek, 2018)	BIPV with Fresnel lens	x	x	TRNSYS		N.S.	0.22	N.S.
(Agathokleous and Kalogirou, 2018)	Ventilated BIPV	x				N.S.	N.S.	N.S.
(Agathokleous and Kalogirou, 2018)	Ventilated BIPV		x	CFD software		N.S.	N.S.	N.S.
(Karthick et al., 2018)	Semi-transparent building-integrated PV	x	x		Orientation, characteristic	N.S.	N.S.	N.S.
(Zhang, Lu and Peng, 2017)	Polar PV shadings		x	EnergyPlus	tilt angles	N.S.	N.S.	N.S.
(Tak et al., 2017)	Changeable Organic Semi-Transparent Solar Cell Window		x			N.S.	N.S.	N.S.
(Wang et al., 2017)	PV double-skin façade and PV insulating glass	x	x	EnergyPlus		N.S.	0.05 - 0.07	N.S.
(Palacios-Jaimes et al., 2017)	BIPV					N.S.	N.S.	N.S.

(Bunthof et al., 2016)	Concentrator solar PV	x				N.S.	0.24	N.S.
(Connelly et al., 2016)	Reflective membrane for a novel Building Integrated Concentrating PV	x	x		Membrane compositions	N.S.	N.S.	N.S.
(Wang et al., 2016)	Semi-transparent PV insulating glass	x	x	EnergyPlus	Air gap depth, rear side glass	N.S.	N.S.	N.S.
(Favoino et al., 2016)	Photovoltachromic switchable glazing	x	x	EnergyPlus	Climate	N.S.	N.S.	N.S.
(Correia et al., 2016)	Luminescent solar concentrators	x				N.S.	N.S.	N.S.
(Wu et al., 2016)	Smart solar concentrators for BIPV		x			N.S.	N.S.	N.S.
(Sabry, 2016)	Prismatic total interior reflection low concentration PV			Ray tracing technique	Head angles	N.S.	N.S.	N.S.
(Cipriano et al., 2016)	Natural ventilated PV		x		Detection of characteristic features	N.S.	N.S.	N.S.
(Hofer et al., 2016)	Dynamic PV shading modules		x		methodology development	N.S.	N.S.	N.S.
(Peng et al., 2016)	Semi-transparent PV double-skin façade		x	EnergyPlus	Air gap width, ventilation	N.S.	N.S.	N.S.
(Pantic et al., 2016)	BIPV	x	x		Orientation	N.S.	N.S.	N.S.
(Liu et al., 2016)	Semitransparent BIPV with high-reflective heat insulation	x	x			N.S.	0.8	N.S.
(Kang, Cho and Lee, 2015)	Asymmetrically textured structure for efficient light trapping in building-integrated organic PVs	x	x			N.S.	N.S.	N.S.

2.3. (Building) Integrated Hybrid systems

In comparison with solar thermal collectors and photovoltaic systems, the integrated hybrid systems employ both technologies in the same system, generating both thermal energy and electricity. A sample of 18 scientific articles was considered as presenting coupled innovative solar photovoltaic and thermal systems, among the 71 articles reviewed concerning the state of the art of BI-SES. A brief summary of the most pertinent is presented here, followed by a table with a summary of the studies.

In Lee et al. (2017), an extensive review is presented on PV/T systems, being of particular interest to works concerning the design of innovative energy façade elements, due to the novelty of the systems presented. The study reviews the structure guidelines and working instruments of the PV/T façade systems, execution, control procedures and building applications. They highlight the use of electrochromic coating as the most used smart coating for thermal applications in PV systems and also highlight that concerning PV shading, the external shading is the most utilized due to its low initial costs. The authors also state that algae growth façades and folding façades (complex geometry) shading systems are as yet rising solutions, with high initial investment costs and requiring professional installers. They are, indeed, a promising arrangement because of their multi-purpose capabilities. Dynamic shading systems were found to spare 12% to 50% of the structure cooling power utilization. In Lai and Hokoi (2015), a survey of a significant number of shading systems on the main façades facing south or north (depending on the hemisphere, referred as sun-oriented façades) is presented, considering studies that have been published after 2010, segmenting the study in opaque and translucid elements.

In a most recent study of Lai and Hokoi (2017), the state of the art sun oriented control systems for façades are introduced, with a comparative assessment of sun-powered control systems and with guidelines for the improvement of new ones. It incorporates multifunctional frameworks and modelling with BIPV and thermal energy generation. In complement, in Debbarma, Sudhakar and Baredar (2017), the authors survey the BIPV and BIPVT advancements, and energy and exergy examination of BIPV and BIPVT systems are likewise discussed. This work reviews the ongoing advancements of innovation around the world. In Agathokleous and Kalogirou (2016), the work presents state of the art on the thermal analysis of double skin façades with BIPV in terms of the published studies carried out on these systems. In Zhang et

al. (2015), an in-depth review of the recently emerging active building-integrated solar thermal/PV technologies is also provided. The authors elaborate on the concept, parameters of classification and assessment, among other topics.

In Nagy et al. (2016), they propose modular adaptive solar façade, in order to couple the element with the very dynamic environment surrounding the building boundaries. The energy behaviour and aesthetic expression of the façade can be managed to employ high spatio-temporal resolution responses. The design process and operational plan are described, along with simulation results of the thermal behaviour and power production/consumption. In Peng et al. (2015), the authors elaborate on the energy performance of a ventilated photovoltaic façade under varied ventilation modes and controlling modes, for different climacteric conditions, aiming to improve the energy conversion efficiency.

In Chialastri and Isaacson (2017), a prototype of a BIPVT was constructed, based on the thermal and electrical energy, aiming to achieve visual comfort and shading control through the system application. In this article, the prototype was evaluated under various conditions to characterize its performance. In Dehra (2017), they present a study on energy evaluation of a photovoltaic wall with the use of either natural convection incited or fan-helped ventilation system. The vertical photovoltaic sun-oriented wall was introduced on the façade of a pre-assembled outside test-room. The prototype development was manufactured with two economically accessible photovoltaic modules, an air cavity and an insulated back layer.

In Smyth et al. (2019), the authors propose a modular hybrid photovoltaic/solar thermal façade technology that uses an Integrated collector storage solar technology. In light of a patented solar thermal diode concept and shaped into a flat modular profile incorporating PV cells/module, the proposed system aims to heat the indoor environment, provide hot water and also generate electricity. In Luo et al. (2018), the authors proposed an arrangement of a building integrated photovoltaic thermoelectric wall solution. It is examined by a numerical model of comprising of a PV framework and thermoelectric brilliant wall element. The thermal and electrical components of the system under cooling prevailing atmospheres was numerically researched utilizing iterative system model. The presentation of the system is optimized by a near investigation with a traditional solid wall.

In Barman et al. (2018), the study investigates the outcomes of a solar transparent photovoltaic window, focusing on angles of incidence, thermal gains using direct solar gains and energy

generation. In Ahmed-Dahmane, Malek and Zitoun (2018), the proposed BIPVT system prototype is composed of air collectors connected to an air handling unit to manage the airflow. The solution works based on two applications, namely for heating and cooling needs.

In Gaur and Tiwari, (2015), a BIPVT system is analysed. There is a focus on the improvement of the articulation between electrical and thermal efficiencies, and heat transfer through the structure. These articulations between thermal and electrical efficiencies are substantially crucial for various climatic conditions and diverse façade BI-SES designs. The system modules have been intensely studied for their energy, exergy and operational attributes with and without associated air pipe. In Buonomano et al. (2016), a BIPVT system has been analysed for residential applications, assessing active and passive operational applications. In Oh et al. (2018), they built up an incorporated model for evaluating the techno-financial execution of the BIPVT on façades, with an emphasis on energy demand and supply.

Table 3 presents the complete list and classification of the hybrid solar systems reviewed in this work, considering the system type, existence/non-existence of experimental and numerical analysis, existence/non-existence of parametrical analysis and details, reached efficiency of the system under study.

The hybrid systems presented by the sample of publications reviewed in the scope of this work are, mainly, façade elements of BIPVT walls, in which the principal analysis is made through numerical simulation via a finite element of CFD analysis. Also, as in the previous sub-sections, many of the studies do not present the results in terms of system efficiency, and parametric analysis is developed in nearly half of them. The parameters under analysis in the parametric analysis are ventilation modes and air velocity, geometry (duct width, for example) and glazing type.

Table 3. Summary of the studies – hybrid systems.

Reference	System type	Experimental analysis	Numerical analysis	Simulation tool or technique	Parametric analysis	Thermal efficiency	Electrical efficiency	Total efficiency
(Smyth et al., 2019)	Hybrid Photovoltaic/Solar Thermal (HyPV/T) Façade	x	x		Glazing type	0.65	0.08-0.23	N.S.
(Oh et al., 2018)	distributed solar generation system		x	Finite element		N.S.	N.S.	N.S.
(Barman et al., 2018)	window integrated CdTe based semi-transparent photovoltaic module	x	x			N.S.	N.S.	N.S.
(Luo, Zhang, Liu, Wu, et al., 2018)	solar photovoltaic thermoelectric radiant wall system	x	x	steady-state analysis		N.S.	N.S.	N.S.
(Lee et al., 2017)	Building Integrated Photovoltaic and Wind Turbine System		x	CFD software		N.S.	N.S.	N.S.
(Lai and Hokoi, 2017)	ventilated BIPV curtain walls	x	x		Channel width, flows	N.S.	N.S.	N.S.
(Chialastri and Isaacson, 2017)	BIPVT solar air collector	x	x			0.31	0.07	N.S.
(Dehra, 2017)	Photovoltaic solar wall	x	x			N.S.	N.S.	0.31 - 0.37
(Buonomano et al., 2016)	BIPVT			TRNSYS	Building-plant	N.S.	N.S.	N.S.
(Nagy et al., 2016)	The Adaptive Solar Façade	x	x			N.S.	N.S.	N.S.
(Gaur and Tiwari, 2015)	thin film BIOPVT systems		x			N.S.	N.S.	N.S.
(Peng et al., 2015)	semi-transparent photovoltaic façade	x	x		Ventilation modes	N.S.	N.S.	N.S.
(Ahmed-Dahmane, Malek and Zitoun, 2018)	BIPVT system with two applications controlled by an air handling unit	x	x			N.S.	N.S.	N.S.

2.4. Design of BI-SES

The BI-SES design process is also relevant to this thesis. In the built stock context, there is usually more than one parameter that must be optimised at the same time, and this must be considered since the design stage. The fundamental approach is to minimise the loads while maximising the occupant's comfort.

Hence it is essential to identify the key parameters that significantly impact the system energy use and efficiency. Entire buildings are broad, multi-scale, multi-material, with exceptionally unique analysis approach frameworks with wide assortments of influences. When addressing the design, applications and control of BI-SES and its relationship with the building itself, it becomes very complex to create functional systems that are adaptable and generally relevant to the improvement of energy performance; once there must be a trade-off between factors as life-cycle assessment and real improvement it brings to the energy demand reduction (Borggaard et al. 2009).

In the preliminary project stage, one of the most critical factors is to design the façade building elements regarding the geometry and materials of the elements. In a later stage, the control of the building devices is critical to energy performance. In Jaluria (2007), the different steps in the design and optimisation of thermal systems are presented in detail. In Fig. 5, it is possible to see the flow of work – from physical process proposition to the communication of the design - specified by the author.

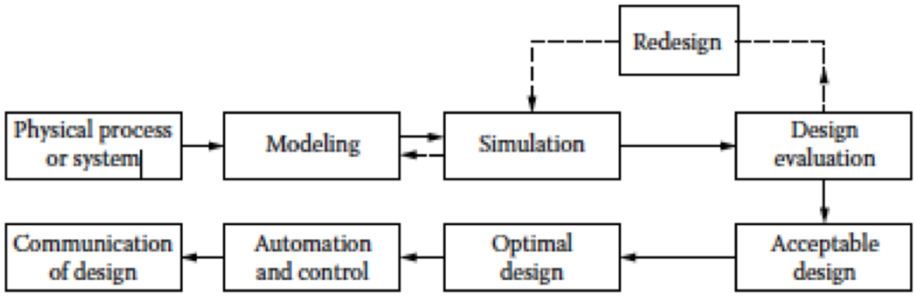

Fig. 5. Work flow in the design and optimisation of thermal system. Source: (Jaluria 2007).

The optimization – which in the strict sense is the determination of the maximum or minimum of an objective function (U) under certain constraints - of the building energy performance can

be defined and implemented in a variety of ways. According to Abu Bakar et al. (2015), considering the building context, it is essential to have different parameters optimized at the same time – emphasizing the multi-objective optimisation. Usually, there is no single worldwide arrangement. The influential idea in characterizing an ideal point is that of Pareto optimality, which states that when optimizing a multi-objective problem, a solution is considered to be optimal (or Pareto optimal) if it is not possible to improve it in one of the objectives without compromising the performance of the other objective.

One of the most important techniques used to solve multi-objective optimisation in whole-building energy simulation is, indeed, the genetic algorithms. An extensive review of genetic algorithms may be found in Goldberg and Holland (1988). Genetic algorithms are global optimisation techniques. In Jaluria (2007), there is an extensive step-by-step explanation of the optimisation processes in thermal systems. The optimisation process starts with the definition of the U (objective) to be maximised or minimised, with a certain number of x (variables impacting the objective results - design variables/conditions). May be expressed as presented in Eq. 1, in which U_{opt} represents the optimal value of U, and where the x's represent the design variables and operating conditions. Eq. 2 represents the equality constraints of the system (G_i), while Eq. 3 represents the inequality constraints of the system (H_i).

$$U = U\,(x_1, x_2, x_3, \dots, x_n) \rightarrow U_{opt} \qquad \text{Eq. (1)}$$

$$G_i(x_1, x_2, x_3, \dots, x_j) = 0, \ \text{for } j = 1, 2, 3, \dots, m \qquad \text{Eq. (2)}$$

$$H_i(x_1, x_2, x_3, \dots, x_n) \leq \text{or} \geq C_i, \ \text{for } i = 1, 2, 3, \dots, l \qquad \text{Eq. (3)}$$

The constraints arise due to the inherent limitations on the ranges of the physical variables and conservation principles, particularly those related to mass, momentum and energy. There are equality and inequality constraints. Equality constraints represent fixed parameters that are required to meet, whereas the inequality constraints indicate the maximum or minimum value

of a function (with upper or lower limits). The operating conditions also need to be specified. In summary, the steps of formulation of the problem are (Jaluria 2007): i) determination of the design variables; ii) selection and definition of the U; iii) determination of the equality constraints; iv) determination of the inequality constraints; v) choose an algorithm/method to solve the problem.

Energy management is the set of activities that contribute to saving energy in organizations (Silva and Carreira 2014). Energy management activities are organized according to an Energy Management Program that describes the activities and is usually supported by IT systems known as Energy Management Systems (EMS). Several authors point to a framework that clearly distinguishes different classes of activities: data acquisition and storage, data processing and analysis, reporting, control, diagnosis and optimisation. The data acquisition, storage, analysis and reporting describe the activities related to the collection and processing of data from different types of sensors, like meters or weather stations. This data can be used to monitor and evaluate the operation of the building and identify mismatches between the models in order to calibrate them or identify energy efficiency actions. The objective of the control, diagnosis and optimisation of the energy management system is to satisfy the inhabitant's normal solace while diminishing energy utilization concerning the energy generated during the operation of the building. Energy management system requires the definition of functions that evaluate indoor comfort parameters (grouped in numerous classes and the most critical are temperature, humidity, indoor air quality and lighting levels), occupants choices and electricity control.

The BI-SES automated systems must comply with the occupants' preferences (through setpoint definition), and adequate the operation to comply both with the energy requirements and occupants preferences (Neves and Silva 2014; Vega, Santamaria, and Rivas 2015). The automated systems applied to buildings go beyond the empiric rule-based systems that have proven its robustness in the past decades but do not have the required flexibility to handle new energy management processes like using artificial intelligence models to forecast and optimize energy use or exchange information with the occupants. In Vega, Santamaria and Rivas (2015), it is presented, in a recent work, the trend for the incorporation of domotics concept associated with smart homes, that alludes to the automation and control of energy use brought together or potentially remote way, controlled by cutting edge metering foundation of the electric system with a shrewd meter

The intelligence of an EMS is related to the coordination level, that minimizes human

intervention and improves energy efficiency. Thus, in Intelligent Buildings, the electromechanical devices used to control the environmental conditions are the same type of systems used in conventional EMS systems. Devices such as luminaries, window blinds or HVAC (heating, ventilation and air conditioning) systems, are still attached to a traditional power network but are also connected to a digital networked to exchange messages with each other through a management platform. All these systems maintain large quantities of data, and as buildings become increasingly managed digitally, more data will be generated and managed.

Considering what was presented in the previous paragraphs, it is possible to conclude that there has been much enthusiasm for the field of energy, where energy proficiency tasks have developed from applying conventional practices (assemble and-overlook venture) to influential works on including innovations. It is pivotal to actualize the enhancement of the framework activity through administration procedures thinking about elements as exactness, affectability, speed, reproducibility, convenience and level of detail, accessibility of information, nature of the yield and phase of the venture (Abu Bakar et al. 2015).

According to Shaikh *et al.* (2016), the aims of the building management system for energy and comfort are (i) comfort requirements in achieving a high comfort index (for thermal, visual, air quality, humidity and various plug loads, occupant's preferences, their behaviour, occupancy pattern and adaptive comfort needs) and; (ii) Integration of the building comfort conditions with energy and cost-saving strategies. In Vega, Santamaria and Rivas (2015), is presented an extensive review of the last 15 years' researches related to the energy management in buildings, considering the grid, domotics, protocols, intelligent monitoring and prospective evolution. According to Shaikh et al. (2014), energy system control is commonly incorporated and coordinated with equipment and programming systems.

In Ascione et al. (2015), the simulation of the automated control in real-time of the BI-SES is done by coupling MATLAB and EnergyPlus to implement a genetic algorithm optimization. In Shaikh et al. (2016), there is also a contribution of a framework to achieve indoor building comfort with improved energy efficiency, through the use of the multi-objective genetic algorithm and hybrid multi-objective genetic algorithm. Thus, in Beaudin and Zareipour (2015), another comparative analysis of the building energy management systems is presented, focusing on modelling approaches and impact on operations outcomes.

The intelligent optimisation and control strategies in buildings have been reported by many

scientific works (Evins 2013). Dounis and Caraiscos (2009) presented advanced control schemes, whereas Nguyen and Aiello (2013) discussed energy-intelligent buildings based on occupant's activity, and Sadineni, Madala and Boehm (2011) discussed the passive design and energy-efficient designs. Banos et al. (2011) covered the optimisation of renewable and sustainable energy, whereas Wang et al. (2009) reviewed the field of multi-criteria decision analysis as a powerful tool for the decision making process.

2.5. Energy performance assessment of BI-SES and its impact on buildings

The BI-SES façade propositions must be evaluated both in terms of element energy performance and in terms of its impact on the energy performance of the building/thermal zone in which it is inserted. According to Platzer, Simmler and Bryn (2005), a broad range of performance indicators may be useful to characterize the performance of façade elements. Three main groups may be used to characterize them: building performance indicators (BPI), component performance indicators (CPI) and building performance criteria (BPC). In Platzer, Simmler and Bryn (2005), detailed consideration is given to them. Examples are heating and cooling energy needs, lighting consumption, among others. As façade elements may influence somewhat different energy use patterns and indicators, it is difficult to stick to useful energy. The CPIs are portrayed by being especially an amount straightforwardly associated with the item without considering the utilization of the item. For the most part, the CPI is a number dependent on physical estimations, explicit to item, which portray a particular execution identified with energy transport or capacity. Instances of CPIs are the U-values, visual transmittance, productivity, among others. The last one, BPCs, are execution related parameters which are not a marker for energy utilization, yet by and by impact the energy execution of the segment. They portray the solace for the client, that ought to be kept in an ideal range.

2.5.1. Features of characterization

Generally, in most of the studies reviewed in the previous sections, the characterization of the systems was made through the use of BPIs or CPIs, by means of energy needs analysis to reach thermal comfort or by the analysis of the system efficiency. However, dimensionless numbers may also characterise the heat transfer properties of the flowing medium and the mode of the flow, as presented by Kusuda and Ta (1977) and Aelenei (2006), and so provide insights over the thermal performance of the façade system.

The Nusselt number (Nu) refers to the actual heat transfer coefficient in the relation of that of still air over a given characteristic length (Eq. 4). It refers to the ratio of the actual flow of the heat occurring between a surface and the adjacent fluid and the heat flow occurring if the heat transfer was purely by conduction. It is also referred to as a dimensionless temperature gradient in the boundary layer surrounding the solid surface. When the air is standing still the Nu will be equal to 1. If the air movements increase either due to temperature differences or to external forces, the Nu will also increase. In the scope of this thesis, the Nu calculation will be done for the prototypes.

$$\mathrm{Nu} = \frac{\mathrm{q}}{\mathrm{k} \cdot \frac{\Delta \mathrm{T}}{\mathrm{l}}} \qquad \text{Eq. (4)}$$

The Grashof number (Gr) (Eq. 5) is used as criteria for fluid movements due to natural convection. It refers to the relation between the buoyancy forces and viscous forces (μ).

$$\mathrm{Gr} = \frac{\mathrm{g} \cdot \beta \cdot \Delta \mathrm{T} \cdot \mathrm{l}^3}{\mathrm{v}^2} \qquad \text{Eq. (5)}$$

The Prandtl number (Pr) is characterized by being the ratio between the momentum diffusivity (also referred to as kinematic viscosity (v)) and the thermal diffusivity, presented by the Eq. 6.

$$\mathrm{Pr} = \frac{\nu}{\alpha_l} = \frac{\mu\, c_p}{k} \qquad \text{Eq. (6)}$$

The Rayleigh number (Ra) (Eq. 7) refers to the phenomenon of heat transfer in a fluid and has importance to the phenomena of conduction and convection.

$$\mathrm{Ra} = \frac{g\, \beta\, \Delta T\, l^3}{\nu \propto} \qquad \text{Eq. (7)}$$

Moreover, dimensionless thermal behaviour through a ventilated façade element may be based on the relationship between dimensionless height (Eq. 8) and temperature (Eq. 9), as will be further developed in the experimental analysis. The dimensionless height represents the ration relationship between the sensor's height and the total air duct system height. The dimensionless temperature defines a ratio between the temperature gradient existent between the air cavity temperature at a determined height of the system (sensor's height) and ambient temperature, and the gradient existent between the room temperature and ambient temperature.

$$H* = \frac{ys}{H} \qquad \text{Eq. (8)}$$

$$\theta\, \mathrm{exp} = \frac{Ty - Tamb}{Ti - Tamb} \qquad \text{Eq. (9)}$$

The calculation of the η_t (Eq.10) and η_e (Eq.11) are presented below. The global efficiency is characterized in this work by being the sum of thermal and electrical efficiencies, as was adopted in previous studies elaborated by LNEG, to generate comparable values.

$$\eta_t = \frac{Q_{int} + Q_v}{G_V \times A} \qquad \text{Eq. (10)}$$

$$\eta_e = \frac{P}{G_V \text{ x } A} \text{ x } (1 - \beta c \text{ x } (T_{mpc} - T_{NOCT}) \quad \text{Eq. (11)}$$

The improvement in energy efficiency is one of the most crucial aims of European policies to address energy security and climate change. Significant steps have been taken towards the improvement of energy efficiency, more specifically concerning the appliances and construction sector (Burman, Mumovic, and Kimpian 2014). According to Burman, Mumovic and Kimpian (2014), as the technology and business processes change along the time, the assessment of a building's performance must also change and improve correspondently. Buildings must quickly respond to the demand effectively according to the supply availability and impacting factors, supporting a high level of adaptively (Burman, Mumovic, and Kimpian 2014).

The European Directive 2002/91/EC (European Comission 2002) that came into force in 2003 and the recast of the EPBD, Directive 2010/31/EU (European Comission 2010) (dated from 2010), and the present Directive 2018/844 (European Parliament 2018) from 2018, defines the majority of policies and regulations adopted by the EU Member States to increase the energy performance of buildings. The Directive requires that all State members should adopt a prescribed regulation for a methodology to assess energy performance at least concerning heating, hot water, cooling, ventilation and lighting in usual conditions. The plans of each country should also emphasise and ensure the increase of the NZEBs, assuring quality and improving precision and making the energy performance evaluation more robust. According to Hensen and Lamberts (2012), three approaches can be used to evaluate the performance of a building or its elements. These methods are: i) experimental; ii) theoretical (analytical); iii) computational (numerical).

2.5.2. Experimental assessment

By means of experimental analysis, it is possible to observe and register real parameters and characteristics of the systems/elements in the study that will conduct to the evaluation of the

heat transfer through the façade components. The experimental approach has the capability of producing the most realistic answers for many flow problems, in overall terms. In this method of evaluation, equipment is needed, and scaling problems may be faced, as well as measurements difficulties and failures of register. Operational costs are also existent, but are not evaluated in the scope of this work.

The experimental models are developed using empirical relations, over the measurement of input and output signals of the system with the consideration of the system's response (Harish and Kumar 2016). Experimental models do not hand over any information about the system behaviour except the measured parameter – but can also be used by soft computing data-driven models (black box and grey box methods) and validation. According to Krarti (2016), it is essential to develop a descriptive sheet for the building envelope, including accurate information concerning construction materials, dimensions, and the characteristics of building envelope assemblies.

In European Commission (2000), there is an extensive review for the energy assessment through experimental analysis. According to this document, "for measuring and estimating the required parameters, it is necessary to use accurate and full data for a long-time period. In reality, however, full data is seldom available. Additionally, existing measuring instrumentation is not well maintained and/or calibrated, resulting in poor trustworthiness. During the measuring activity, it should be ensured that the measured system is under the thermodynamic equilibrium, indicated by the stability of the instrument readings.

2.5.3. Numerical assessment

To implement the assessment methodologies, most countries opted for the use of a whole-building simulation through the means of energy modelling software developed according to the defined methodology to determine the energy performance. Energy modelling is one of the most accurate and cost-effective methods to calculate energy performance through the fundamentals related to physical properties. Besides, to assess the energy performance, there are critical operation conditions that must be set up and considered – as interior gains, systems

usage power and schedule. The energy performance reflects the state of the building or system component, considering the main parameters of characterization (Burman, Mumovic, and Kimpian 2014). In the theoretical approach, there is a considerable number of simplifications and assumptions in order to make the problem tractable. This approach is useful in preliminary design work, with reasonable answers in a minimum amount of time. However, its application is restricted to simple geometry and physics, usually linear problems. Examples of the assessment of thermal load estimation through the analytical approach may be found in Ogunsola and Song (2015), in which the formulation, analytical solution and validation is assessed for a thermal network in simplified mode.

In the computational approach, the assumptions are limited, and a computer with high performance is used to solve the governing equations in a dynamic approach. There is no restriction to linearity, and dynamic behaviour in time may be assessed for complex physics. On the other hand, there may exist truncation errors, boundary condition problems and high computational costs. In the following subsection, the computational methods will be further explored, once is a central component of the present thesis. Most of the studies on heating and cooling loads calculations for buildings are firmly based on computational simulations, due to the challenges imposed by the many aspects involved in whole building modelling. The computational tools for simulation are developed with the purpose of facilitating the analysis and the evaluation of the design regarding the energy, thermal, acoustic, lighting components, among others.

Most numerical methods assess the envelope of a building by interpreting them as discrete capacitances and resistances. This can be seen most distinctly in the derivation of the finite volume method. A broad number of sub-models may compose a complex heat balance model, e.g. different exterior convection models, different transient conduction models, and different interior radiation models. In Georgescu and Mezić (2015), it is possible to find a systematic approach to the division of the regions inside a building, through the use of a Kooperman operator to decompose the time-series output into spatial models, with the aim of identifying frameworks for the creation of simplified energy models.

Primarily, a numerical model is a mathematical description of the energy behaviour of a system. Three main blocks compose the modelling structure: input variables, output variables and the system itself. According to Harish and Kumar (2016), one of the three blocks will be determined in the process of modelling, according to the available and suitable information. The availability

of data and characteristics of the modelling process classifies the energy models as white-box, black-box or grey-box models. In general terms, according to Wang and Srinivasan (2015), in the white-box model, the physical principles are used to calculate thermal dynamics and energy behaviour for each building component or on the whole building level, with known logic of the system (known interior relationships and physics of the system). It is necessary to note that the availability of the whole input physical data of the systems needed for the development of the models may be a crucial limitation of white-box models. The black-box method approaches energy usage without knowing the interior system/building relationships, as they are based only on the system output and input. Grey-box method is a mixture of both white-box and black-box, intending to eliminate some of the limitations of each technique.

2.5.3.1. White-box methods

White-box methods are especially relevant in the ambit of this thesis, once is the main simulation method used, once allow to evaluate the impact of the variation of physical characteristics of the systems and obtain the desired output concerning its impact on the energy consumption. The white-box methods are also known as engineering, physical-based and analytical methods. Engineering methods use physical laws to determine the dynamic energy behaviour thermal, being possible to asses both the whole building and sub-level components, appropriately developed over the past fifty years (Zhao and Magoulès 2012). The white-box methods may be segmented in two categories: i) comprehensive method and; ii) the simplified method.

The comprehensive techniques use complex physical functions or thermal dynamics to accurately calculate the energy demand for all components, based on building's and environmental data. Despite reporting very accurate characterization of the thermal performance, the drawback is the level of expertise needed to develop this model and the time required to elaborate it. The level of accuracy is proportional to the precision of the input and capabilities of the engineer, and the variations of the results may be significant (Zhao and Magoulès 2012). Given precise data input and model development, white-box models have

good prediction accuracy for a broad range of operating conditions. The parameters involved are vast, and in some cases a reduced-order model is needed to reduce complexity of the model (Killian and Kozek 2016).

In most buildings, the plan data differ from the used materials, and the inability to access them may lead to the wrong parametrization. Each building is singular in terms of input parameters and its values, and so the white-box models may not be the most useful to model predictive control applications (Killian and Kozek 2016). Elaborated details on the comprehensive tools that work with the prediction of energy use though white-box models may be found in (Crawley et al. 2008). Another possible classification for the white-box models is presented by Foucquier et al. (2013). According to the authors, the engineering methods may be segmented into three sub-categories, with gradual increase of details needed: i) the multizone technique (considers the space as a homogeneous volume where all states variables are uniform); ii) the zonal method (divides each room into several cells) and; iii) the CFD method (describes each zone in several control volumes). While the input information can be easily extractable from the projects of a new building, in existing buildings the challenge increases.

In conclusion, it is better to use more detailed models for the sake of reliability and precision of simulation result, if enough time and knowledge are available. Overall, the lack of knowledge or unavailability of the necessary input parameters to many buildings will lead to a low accurate simulation. In these circumstances, the black-box models suit the purpose of predicting the energy demand having into consideration historical data on energy use and other factors. Despite not being used in the scope of this thesis, black-box and grey-box methods are also introduced, in order to generate a consistent comparison between numerical evaluation methods. This thesis will use the white-box modelling approach, due to the objective of the work, availability of accurate and detailed data and time.

2.5.3.2. Black-box methods

Black-box models, also known as data-driven models, are created by estimating the critical data inputs and outputs of the system and fitting a linear or non-linear numerical function to surmised

the activity of the structure (Killian and Kozek 2016). The statistical-based/computational intelligence models more noticeable contrast with physical techniques is the fact that the first does not require any knowledge on the physical parameters of the system itself. No heat transfer conditions or geometrical parameters are required to start the model. These models depend on the implementation of a function deduced from samples of training information depicting the energy behaviour of a particular system. Accordingly, these techniques are very much adjusted when the physical highlights of the considered structure are not known (Foucquier et al. 2013). These techniques are powerful because they do not need much information concerning the structure geometry or the itemized physical phenomena to conclude a precise prediction model of energy behaviour. Conversely, they depend on measures and in such situations where it is hard to gather information, it can turn into the main problem (Foucquier et al. 2013).

In Foucquier et al. (2013), the black-box models are categorized depicting the method utilized in the field of the system energy prediction through artificial intelligence: the multiple linear regression, the ANN, and the support vector machine. They contend that the unwavering quality of these strategies is profoundly reliant on the quality and measure of accessible information, just like the physical methodologies subject to the intricacy of the underlying model. It is dubious about developing a qualitative and comparative analysis of the various techniques devised in this field since the performances will depend on the training data used as input. Contrasted with physical methodologies, these require fewer data about the structure and may show up as increasingly agreeable to convey. Physical techniques are progressively advantageous in extensions, where the translation of natural wonders is wanted. In Mosavi et al. (2019), an extensive audit of AI techniques for energy assessment is displayed. It explores the best in the class of the AI models utilized in the prediction of energy behaviour alongside deep scientific categorization of models and applications. A comprehensive examination of the publication advances to an appraisal and execution assessment of these models and their application, and talk of the noteworthy difficulties and open doors for future research.

In Wang and Srinivasan (2017), the authors differentiate the capabilities of different artificial intelligence-based building energy use predictions, comparing single and ensemble prediction models. Examples are multiple linear regression, ANN, and support vector regression, and ensemble prediction method that, by combining multiple single AI-based prediction models improves the prediction accuracy manifold. It elaborated on the principles, advantages and limitation of each accessed method.

In Killian and Kozek (2016), the points of interest and weaknesses of the black-box specific techniques are discussed, alongside an itemized survey of the basics. One of the main advantages of these models is the limited number of parameters, and also the complexity of the model structure is low, making them a suitable choice for model predictive control. Drawbacks stem the way that most settings do not have physical importance. In this way, they are not interpretable for structure operators. According to Zhao and Magoulès (2012), these techniques are not complex to be developed but also have critical drawbacks, weighting according to the objective of the simulation: inaccuracy and lack of flexibility. ANNs and SVMs are suitable at solving non-linear problems, making them applicable to forecasting energy demand in building stock. On the other hand, sufficient historical data is needed.

2.5.3.3. Grey-box methods

According to Foucquier et al. (2013), the last classification of strategies considered is the mixture of the previously described approaches, which depend on both physical models to reproduce building thermal balances and AI systems to advance info parameters. A blend of white-box and black-box models gives the grey box approach. Even though the inward structure of the framework elements is not entirely known, the essential framework elements and the general model structure is given. This model does, be that as it may, have a few unknown free parameters which can be evaluated utilizing framework distinguishing proof (Killian and Kozek 2016). Hybrid methodologies show up as a best in class in recent years. They can be considered as a great trade-off among physical and AI-based techniques and loosen up their disadvantages by consolidating them. Grey-box techniques might be acknowledged in circumstances where a physical model is accessible, yet is fragmented or does not offer enough subtleties, and this way must be adjusted as well as finished. When managing existing structures, where it usually is testing to reconstruct a point by physical point model, such methodologies could be of extraordinary assistance (Foucquier et al. 2013).

According to Li and Zhang (2018), the emerging grey-system theory provides a convenience surrogate solution to short-term energy demand prediction. This system illustrates that a part of

the data within the system are known, while the other part of the data is unknown, and each parameter of the system is within a relationship of uncertainty. Many systems could be studied as a grey system because there is always a degree of uncertainties involved. The data that can be read from a system may still be uncertain and insufficient due to interior and external noise of the operation of concern. In the presence of a relatively small amount of building information and an insufficient source of data, it shows to be suitable to solve some uncertainty problems.

Table 4 presents a summary of the methods and a brief of their main techniques. It is essential to highlight that there are, however, challenges in the building performance simulation processes that must be mentioned. With more complex systems, as adaptive façades, simulation can be more complicated than performance prediction of traditional façades, because existing simulation tools were not initially developed for this purpose, and are adapting along the time (Loonen et al. 2017). Thus, time-varying properties must be considered when they exist, and modelling of dynamic operation must reflect real-world use of the devices and services. In Martinaitis et al. (2015), an elaborate analysis of the effect of occupancy profiles on the energy performance is developed, accessing applicability of the default BPS software profiles. Loonen et al. (2017) present an extensive review of the requirements and limitations of the software used for performance assessment and simulation. In general, they do not have friendly interfaces, and some must be adapted to transient routines and control algorithms. Moreover, the authors mentioned the control strategies that are intrinsic, extrinsic or hard-coded. Also, design performance evaluation of complex BI-SES in an envelope could require the need for calculating metrics that may not be directly available as outputs of the simulation tool.

Individually, for the assessment of energy performance of low-energy buildings, Cho et al. (2011) summarise the technical background and the development of new features to evaluate, test and validate the building processes. Thus, in Deng, Wang and Dai (2014), there is a literature-research on the NZEB evaluation, with extensive look through the definitions, methods, tools and indicators, and life cycle assessment.

Considering the content presented by Table 4, and in the scope of this work, as previously states the white-box models will be used, once the objective of this thesis is to provide a detailed thermal profile of the BI-SES under study, and plenty of data is available due to the extensive experimental campaigns developed and knowledge of the systems and room usage patterns. Next chapter presents the description of the case study.

Table 4. Summary of the methods/techniques. Adapted from: (Foucquier et al. 2013).

Method	Technique	The specificity of each technique	Application	Building geometry	Training data	Physical interpretation	Advantages	Drawbacks
White-box models (Detailed/simplified engineering)	CFD method	One cell = a control volume; Local state variables	Contaminant distribution; indoor air quality; segmented temperatures, velocity and turbulence fields; HVAC systems	Detailed geometry description and constructive solutions	No training data is required	Results can be interpreted in physical terms	Detailed description of the fluid flows occurring inside the building; Large volume zones.	Huge computation time; Complexity of the model implementation; Requirements of a detailed description of the flow field in subjacent surfaces of the fluid/solid.
	Zonal method	One cell = a division of a room; Local state variables	Indoor thermal comfort; Artificial and natural ventilation; HVAC; Building physics behaviour	Detailed geometry description and constructive solutions	No training data is required	Results can be interpreted in physical terms	Spatial and time distribution of local state variables (temperature, concentration, pressure, airflow) in a large volume.	Large computational time; Requirements of a detailed description of the flow field and flow profiles.
	Nodal method	One cell = a room; Uniform state variables	Determination of the total energy use/the average of the indoor temperature/cooling or heat load; Time evolution of the global energy use/the space-averaged indoor temperature	Detailed geometry description and constructive solutions	No training data is required	Results can be interpreted in physical terms	Multiple zone buildings; Reasonable computation time; Easier implementation.	Difficulty in studying large volume systems; Unable to study local effects as the heat of pollutant sources.

Black-box models (Statistical/Artificial Intelligence models)	Conditional demand analysis/ Regression techniques (MLR)	Starting hypothesis; linear relation between variables and the output	Forecasting of the energy use; Evolution of the energy demand	Detailed description of the geometry is not required	A large amount of training data collected over an exhaustive period is required	There are several difficulties to interpret results in physical terms	Regression function describing the system	A large amount of training data/Non-collinearity between data
	Artificial Neural Networks	No starting hypothesis but huge "black box" which prevents from physical interpretations	Prediction of energy use and energy uses	Detailed description of the geometry is not required	A large amount of training data collected over an exhaustive period is required	There are several difficulties to interpret results in physical terms	A huge training faculty	A large amount of thorough and representative data; No physical interpretation
	Support Vector Regression	Starting hypothesis: kernel function imposed by the user	Forecasting of energy use or temperature	Detailed description of the geometry is not required	A large amount of training data collected over an exhaustive period is required	There are several difficulties to interpret results in physical terms	A reasonable amount of training data with mainly vector data; Minimization problem based on the SEM	Determination of the kernel function; Difficulty to adjust parameters C and Ɛ
	Ensemble prediction method	Combine multiple hypotheses to form a better hypothesis	Prediction of energy use and energy uses	Detailed description of the geometry is not required	A large amount of training data collected over an exhaustive period is required	There are several difficulties to interpret results in physical terms	Improve robustness of a single model, reduce variance	Computationally expensive, the complexity of implementation and interpretation
Grey-box models (Hybrid models)	Usually coupling of different methods	Couple engineering methods with computational intelligence	Prediction of energy use and energy uses, as well as more detailed parameters	A rough description of the building geometry is enough	A small amount of training data collected over a short period is required	Results can be interpreted in physical terms	May overcome the limitations of both white and black-box methods used.	Huge computation time; Complexity of the model implementation and input data

Chapter 3. Case study

Following the pertinent literature review, this chapter aims to describe the elements and features of the case study building and particularly the BI-SES systems in the façade of the Solar XXI, at the National Laboratory for Energy and Geology (LNEG), Lisbon, Portugal. It focuses on the description of the characteristics of the climate, the building, the existing systems, and new prototype.

3.1. Location and climate

The case study is located in Lisbon, Portugal, in the Solar XXI building (38º46'21.74" N; 9º10'35.54" W) from the National Laboratory for Energy and Geology. In Miranda *et al.* (2002), it is described that the continental Portuguese territory (between latitudes 37º and 42ºN) is located in the transitional region between the subtropical anticyclone and the subpolar depression zones. Lisbon has a subtropical-Mediterranean climate, with the Atlantic Ocean wind reaching the rain but maintaining moderate temperatures. The climate is also influenced by the orography and the effect of the Atlantic Ocean, with the continentality climate affecting around 220 km of the regions furthest from the Ocean. The Portuguese climatic zones are described in Diário da República n.º 234/2013 (2013) (Fig.6), and the summary of the territory division is presented in Fig. 6 (a) winter and (b) summer. According to the same reference, Lisbon is classified as I1 (winter climatic zone) and V2 (summer climatic zone). The average solar energy incident in a south-oriented vertical surface, in the I1 winter climatic zone and heating season, is 108 (kWh/m^2). The same surface, in the V2 summer climatic zone and cooling season, has an average incident solar energy of 380 (kWh/m^2).

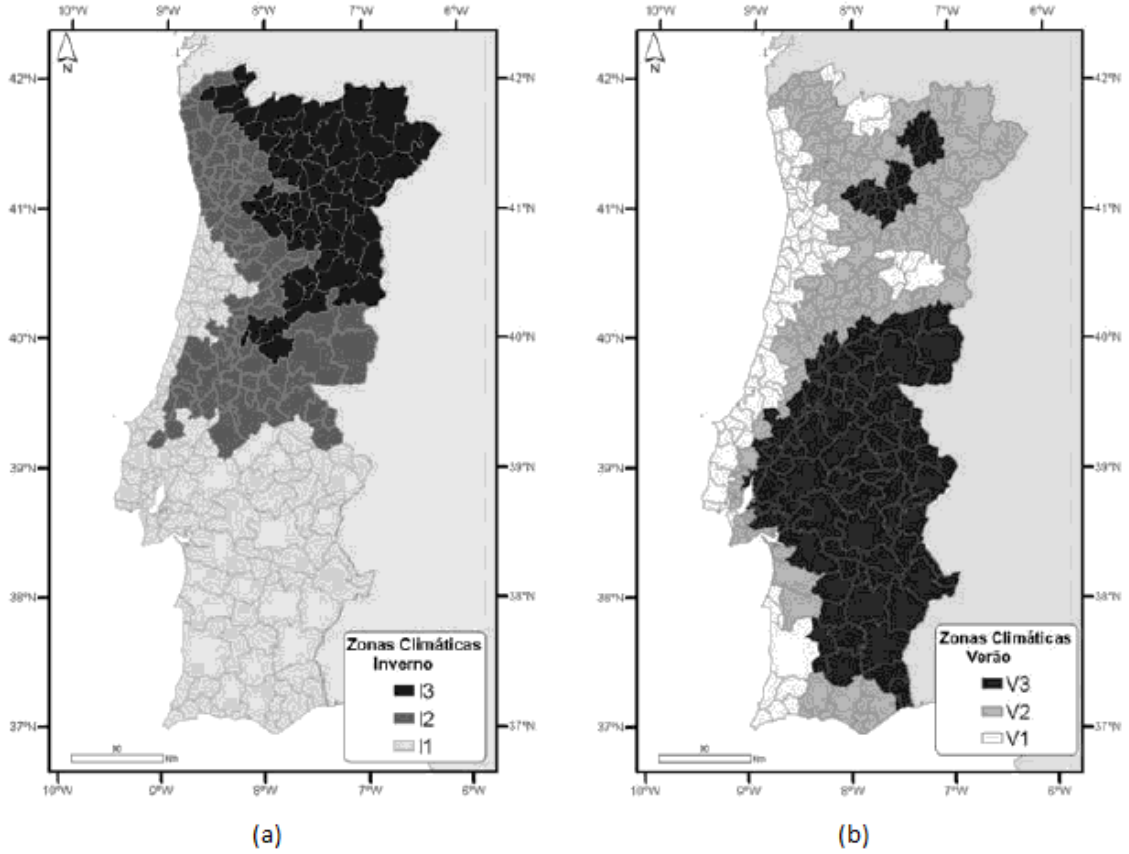

Fig. 6. Portuguese climatic zones, (a) winter and (b) summer.

3.2. Building characteristics

The present sub-section is constituted by the description of the building in the conditions previous to the installation of the new prototypes under study. The physical characteristics of the buildings, in the scope of this research, is composed by the description of the envelope of the test room (exterior and interior walls, floor, ceiling, roof and fenestration surfaces) considering the thermal characteristics of the elements. Also, other parameters as interior gains and air infiltration are described. The HVAC description accounts to the consideration of previously installed equipment for heating, ventilation and air conditioning, in case of existence in the test room focus of this thesis. The output of this section will be the data to be used to describe the building in the numerical modelling assessment.

Solar XXI building (Fig. 7) was designed as a low energy demand building that integrates renewable energy into the main façade and roof. The building integrates solutions and strategies aiming to reduce cooling loads using passive strategies and solutions, namely external solar shading, natural ventilation and passive cooling by means of 32 buried pipes that act exchanging heat in the soil (as is possible to see in Fig. 8). The buried pipes are not used in the scope of this thesis. For the heating period, the solution and strategies integrated by Solar XXI building are the optimized envelopes externally insulated, direct solar gain through south-oriented main façade of the building. Moreover, the main façade is composed by building integrated photovoltaic thermal systems (BIPVT), that aim not only to generate electrical energy but also act as a natural heat recovery system. These systems are integrated into all main façade and consist of 76 photovoltaic multi-crystalline silicon modules and have an area of about 96 m^2 and 12 kW peak power installed. Productivity is about 1004 kWh/kW. The geometry and functionality of the BIPVT system will be further described in the next sub-sections.

Fig. 7. Solar XXI Building and location of monitored test rooms.

Two test rooms are prepared in the Solar XXI building to test BI-SES, energy flexibility, intelligent management of system-to-building interaction and occupant behaviour. A rectangle signs the test rooms mentioned test rooms in the main façade, in Fig. 7. Specifically, one of the test rooms is the object of study in the present thesis (NZEB_LAB 1), since there is a complex system of automation and monitoring.

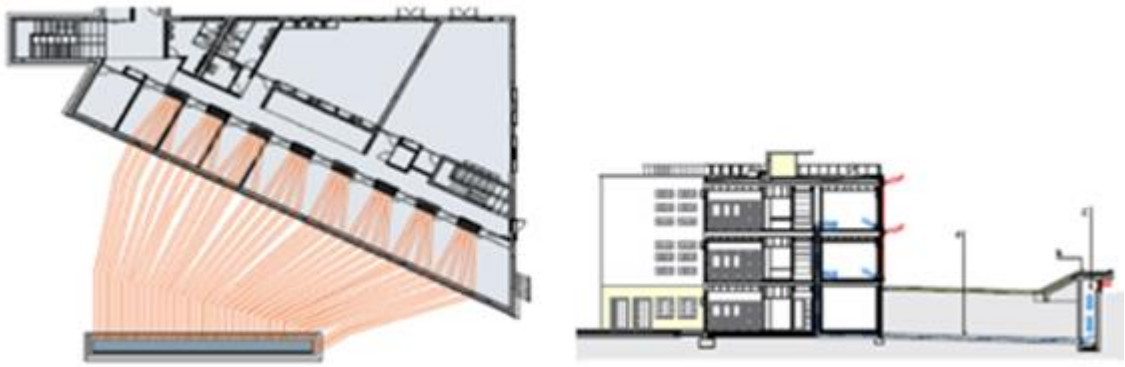

Fig. 8. Buried pipes passive cooling system.

The geometry of the test rooms is presented in Fig. 9-a top view and Fig. 9-b cross-section of the BIPVT system. The test room under analysis in the present work (NZEB_LAB 1) has a floor area of 16,70 m^2. The exterior wall has a gross area of 3,97m^2, with a glazing area of 2,82m^2 (considering only the available glazing area in the test rooms). The lateral walls (West and East oriented) are adjacent to other rooms with similar thermal behaviour. The interior wall that opposes the exterior wall (North oriented) is adjacent to the corridor of the building. All of the test room surfaces are subjected to heat losses and gains. However, the interior walls are in contact with thermal zones with similar thermal behaviour; the reason why the heat gains are not accentuated, and these surfaces are considered adiabatic during numerical analysis in Chapter 5. The ceiling of the room is also adjacent to a thermal zone with similar thermal behaviour and is also considered adiabatic in numerical analysis, as well as the floor, once there is also a floor underneath the test rooms (a thermal zone with similar temperatures).

The building will be segmented into thermal zones, to describe it in terms of the specific room used with the purpose of energy simulations. The concept of he thermal zones for modelling purposes is detailed explained in Diário da República n.º 159/2013 (2013) - the thermal zones are considered the space or set of spaces that can be considered together due to their similarities in terms of user profile, lighting and equipment, mechanical ventilation and air conditioning system and, as for air-conditioned spaces. Due to the similarities in terms of solar exposure conditions, small commercial buildings and services with a useful floor area of up to 250 m^2 can be considered to have only one thermal zone, according to Diário da República n.º 159/2013 (2013). However, in the scope of this study, the test room used for testing is considered as a thermal zone, to obtain accurate and detailed results on the building energy simulations considering the test of the prototype (further described in the next sections). The concept of

thermal zone introduces the boundary conditions, envelope and interior gains assumed for further modelling and simulation. Building thermal behaviour and the related energy use are defined by a complex interaction of heat gains, losses and storage in building materials and finishing. Fig. 9-b presents the cross-section of the thermal zone cell used as a case study for this work. Fig. 9-c presents a picture of the interior of the test room.

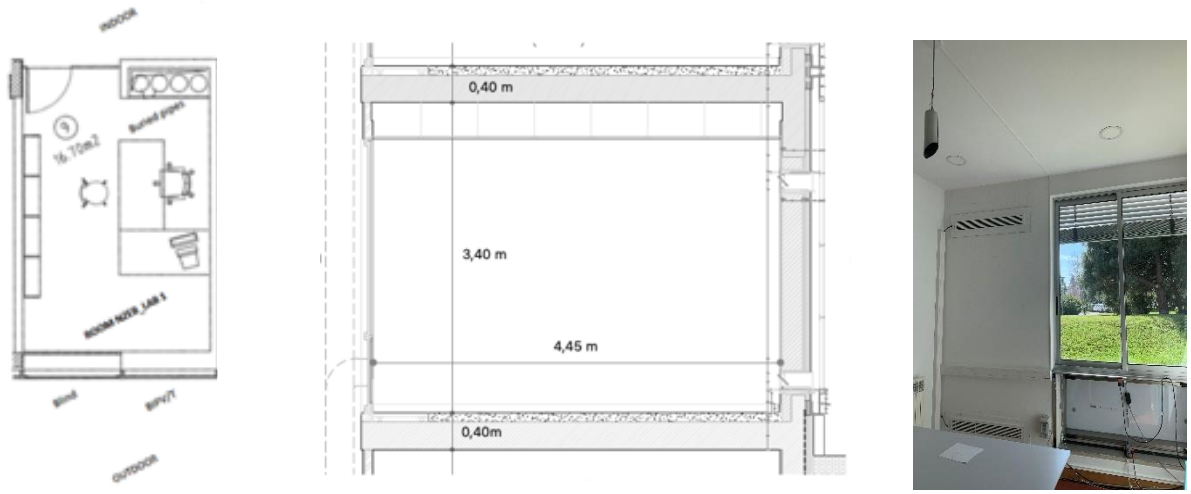

(a) (b) (c)

Fig. 9. (a) Test room top view; (b) cross-section view; (c) picture of the test room and BIPVT system.

A significant heat flux source is the direct heat gain, which originates from solar radiation transmitted through the transparent components of the building skin such as windows and skylights. Another main contributor to the heat balance of a building is the heat flow through the opaque building envelope. These transmission losses or gains can mainly be described by the physical process of conductive heat transfer through the materials, although the heat exchange at the inner and outer surfaces and within voids and cavities is based on the principles of convection and radiation. These fundamental principles will not be further described once they are common knowledge in the field. However, further details may be found in (Kusuda and Ta 1977). Also, Verbeke and Audenaert (2018) describe further the main components of heat fluxes in buildings.

The constructive elements of the envelope that separates the indoor from the outdoor are described in Table 5, in terms of element, material, thickness, conductivity, density and specific heat of the element. According to Verbeke and Audenaert (2018), many energy performance

rating schemes and code standards set specific requirements to the thermal resistance (R-value) or thermal transmittance (U-value) of building components.

Table 5. Characteristics of the test rooms envelope components.

Opaque elements	***Elements***	***Thickness (m)***	***Conductivity (W/(m.K))***	***Density (kg/m³)***	***Specific heat (J/(kg.K)***
Exterior walls	*Traditional plaster*	0.030	1.300	1900	1000
	EPS	0.060	0.040	1000	1400
	Masonry	0.220	0.420	1000	790
	Traditional plaster	0.020	1.300	1900	1000
Interior walls	*Traditional plaster*	0.010	1.300	1900	1000
	EPS	0.060	0.040	1000	1400
	Masonry	0.110	0.410	1455	790
	Traditional plaster	0.010	1.300	1900	1000
	Concrete	0.300	2.000	2350	1000
	Shaping layer	0.100	0.700	1300	1000
	Linoleum	0.003	0.170	1200	1000
Roof/Ceiling	*Linoleum*	0.003	0.170	1200	1000
	Cam forma	0.100	0.700	1300	1000
	Concrete	0.300	2.000	2350	1000
	Air cavity	Thickness of 0,05m with standard air properties			
	Pladour	0.130	0.250	900	820
BIPVT system	*(Described in detail in Table 5)*				
Translucid elements	***Parameter***				***Value***
Double Glazing surface (window)	Optical data type				Spectral average
	Thickness (m)				0,014
	Solar transmittance at normal incidence				0,75
	Front side solar reflectance at normal incidence				0,17
	Back side solar reflectance at normal incidence				0,17
	Visible transmittance at normal incidence				0,82
	Front side visible reflectance at normal incidence				0,15
	Back side visible reflectance at normal incidence				0,15
	Infrared transmitted at normal incidence				0,05
	Front side infrared hemispherical emissivity				0,84
	Back side infrared hemispherical emissivity				0,84
	Conductivity (W/(m.K))				0,268
	Dirt correction factor for solar and visible transmittance				1
	Solar diffusing				No
	Young´s module (Pa)				-
	Poisson's ratio				-

These performance indicators related to the one-dimensional steady-state thermal conduction of building envelope components such as walls, roofs and floors. R-values and U-values are simplified representations of the heat transfer of a building envelope component, as these indicators do not factor in any dynamic behaviour. The glazing system is described further in terms of its thermal and optical properties.

The accurate description of the building envelope and the previously presented specific climatic conditions are crucial for the success of the energy analysis. As described by Verbeke and Audenaert (2018), many of the boundary conditions inducing these heat fluxes are not constant over time. Weather conditions such as outside air temperature and solar irradiance are continually fluctuating. In most cases, the building operation also imposes fluctuating interior heat loads. While solar radiation and convective heat flows vary simultaneously with the fluctuation of the outdoor boundary conditions, the conductive heat flows through the building skin will display a time lag compared to the external excitation.

Heat gains through glazing or from interior activities will raise the indoor temperature, and the interior temperature fluctuations will affect the net conduction, ventilation and radiative heat flow to and from a room. Some of the heat entering the material will be absorbed and stored inside the construction assembly, and therefore the temperature of these materials will slightly rise.

3.3. Test room interior gains

A significant heat flux consists of heat generated (interior gains) or extracted interiorly due to building operations. These thermal loads stem from heat losses from various sources such as artificial lighting, office equipment and metabolic heat gains from building occupants. The interior gains through lighting, occupation and various equipment are often significant elements in the thermal balance of the zones. The use of scheduling is described by a fraction of peak usage for each time interval. The occupancy component is described not only based on the number of occupants but also the usual metabolic rate existent for the performed activities (activity levels), radiant fraction, and on the comfort level expectations according to the season of the years. The heat gains from lighting, in particular, may be broken down between the visible portion and the thermal portion (DoE 2010). Details on the occupant behaviour for whole-building energy simulations may be found in Hoes *et al.* (2009). The output of this section will be the data to be used to describe the interior gains of the building in the numerical modelling process. Table 6, Table 7 and Table 8 describe the interior gains of the building due to occupation, lighting and equipment, respectively.

Table 6. Characteristics of the test room occupation patterns.

Interior gain	***Parameter***	***Value***
People	*Number of people calculation method*	People
	Number of people	1
	Fraction radiant	0.5
	Activity level	120
	Clothing insulation calculation method	1 – 0.5

Table 7. Characteristics of the test room lighting.

Interior gain	***Parameter***	***Value***
Lighting	*Design level calculation method* *Lighting level (W)* *Watts per zone floor area (W/m^2)* *Watts per person (W/person)* *Return air fraction* *Fraction radiant* *Fraction visible* *Fraction replaceable* *End-use subcategory*	*No lighting was used during the testing period and numerical assessment, due to the daylight availability.*

Table 8. Characteristics of the test room equipment.

Interior gain	***Parameter***	***Heating system***	***Data acquisition system***	***Computer***
Equipment	*Design level (W)*	Design level	Design level	Design level
	Watts per zone floor area (W/m^2)	1989	*100*	*150*
	Fraction latent	0.3	0.3	0.3
	Fraction radiant	0.7	0.7	0.2
	Fraction lost		0	0.5
	End-use subcategory	General	General	General

Thus, air infiltration will introduce outside air by ventilation and infiltration through the building façade and will be responsible for other components of the heat flux process in buildings. In case the temperature of the outside air differs from the indoor air temperature, heat flux is associated with this air movement. It is referred to as convective heat gains or heat losses. In any case, determining the real air infiltration in a room is a complicated process, because any gap present in the envelope can be an inlet or outlet of the air, and the air infiltration can have different values in each segment of the gap area. The air movement, however, will be punctually

determined through the experimental campaign in the next chapter.

3.4. Building existing systems

The dynamic scenario described in the previous sections highlights the importance of describing not only the characteristics of the building envelope but also the characteristics of the pre-existing systems, in order to provide the most extensive information possible for further analysis. In the case study test room, the existing systems are the BIPVT installed in the façade, the blind system over the glazing surface and the buried pipes. These pre-existing systems will be presented in detail in the next sub-sections.

3.4.1. Building Integrated Photovoltaic Thermal system (BIPVT)

3.4.1.1. Characteristics

The BIPVT systems with heat recovery aim to increase the outlet temperature (T_{out}) compared to the inlet temperature (T_{inl}) of the system, having as source air the air volume from the test room. It is composed of a PV area per BIPVT system of 5,25 m^2 (four modules), with vent opening areas (inlet at the bottom and outlet at the top of the system) of 0,186 m^2 each for the interior, and other two with same area for the exterior (allowing circulation between air cavity and the exterior in order to cool the PV panels). Between the interior wall and the PV modules, there is an air cavity of 0,16 m of thickness. Moreover, it is important to mention the properties of the air considered to be flowing or stationary in the air cavity. It is considered to have a density (ρ) of 1,213 kg/m^3, specific heat of 1006,7 J/kg.K, thermal conductivity (k) of 0,02544 W/(m.K) and viscosity of 1,79 x 10^{-5} kg/m.s (Ansys 2018). The BIPVT PV modules

efficiency is 12,7% with 160 W peak (bp solar 2003), and these values are used for further calculations. Table 9 presents the thermal characteristics of the constructive elements of the BIPVT systems, being the "exterior wall" the wall that separates the test room from the air cavity between wall and photovoltaic panels.

Table 9. Characteristics of the BIPVT constructive elements.

Constructive element	***Components***	***Thickness (m)***	***Conductivity (W/(m.K))***	***Density (kg/m^3)***	***Specific heat (J/(kg.K)***
Photovoltaic panel	*Opaque glazing*	0.003	1.800	2330	677
	Air cavity	*0,16cm of thickness, standard thermal properties*			
Exterior wall	*Traditional plaster*	0.030	1.300	1900	1000
	EPS	0.060	0.040	1000	1400
	Masonry	0.220	0.420	1000	790
	Traditional plaster	0.020	1.300	1900	1000

Fig. 10 presents the details of the geometry of the BIPVT systems, as well as the pictures of the exterior and interior view of the system. The BIPVT thermal behaviour is registered by temperature and heat flux sensors. There is a total of three temperature sensors, located at the bottom (inlet), at the middle of the air cavity and the top (outlet). The temperature sensors location is signed with a blue circle, whereas the heat flux sensors are signed as a red square. The temperature sensors located in the inlet and outlet openings are located 0,08 m from the inferior surface of the opening. The heat flux sensor used in the scope of the thesis is the one located in the wall, and its height is approximately 0,88 m above the inlet opening, in the same height as the air cavity temperature sensor. The dimensions of the air duct are also shown in the picture.

3.4.1.2. Operation mode

The BIPVT system is composed by four vents (one at the bottom and one at the top at the indoor component and outdoor component) as was previously described, that allow either interior circulation to heat the room or external circulation to cool the PV panels. The vents are operated either manually according to the occupant wishes or automatic, according to a control logic for

the automation process.

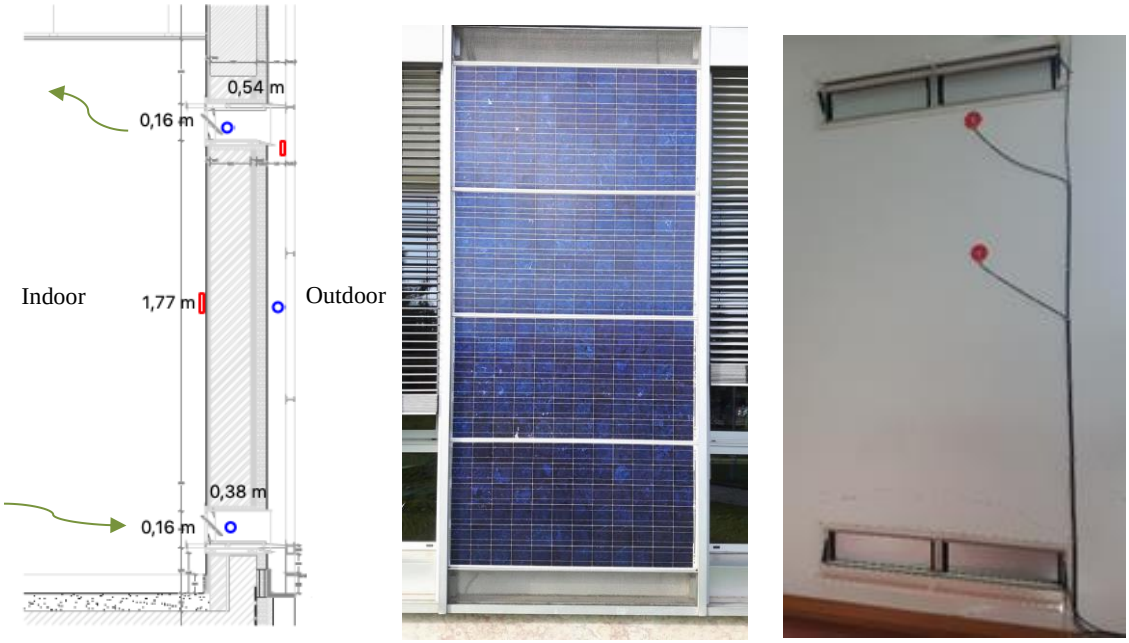

(a) *(b)* *(c)*

Fig. 10. (a) Cross-section of the BIPVT system and sensors location; (b) exterior view of the system; (c) interior view of the system.

Figure 11 presents the operation scheme of the BIPVT system, considering a manual operation. The manual operation was segmented in two: heating more and cooling mode. The heating mode refers to the wintertime – at night all the vents are closed, and during the day the interior vents are opened. The cooling mode refers to the summertime, in which the interior vents are closed, and exterior vents are opened both during night and day.

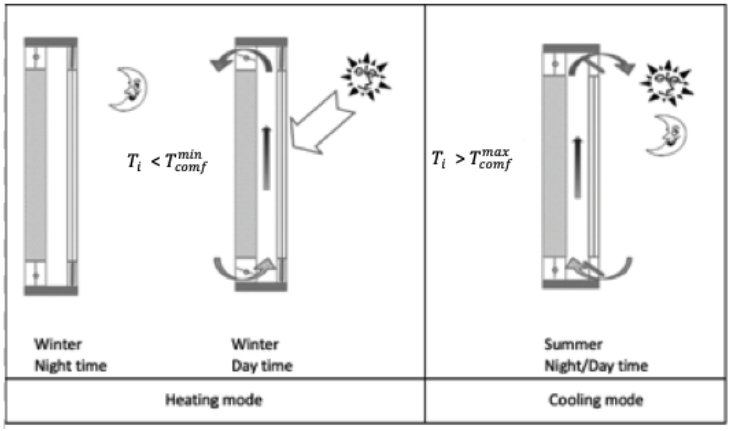

Fig. 11. Manual operation scheme. Source: (L. E. Aelenei 2016)

The heat balance of the BIPVT system is presented in a scheme in Fig. 12. It considers the solar gains, conductive and convective heat fluxes throughout the module. The heat transfer through radiation within the system was ignored in this scheme.

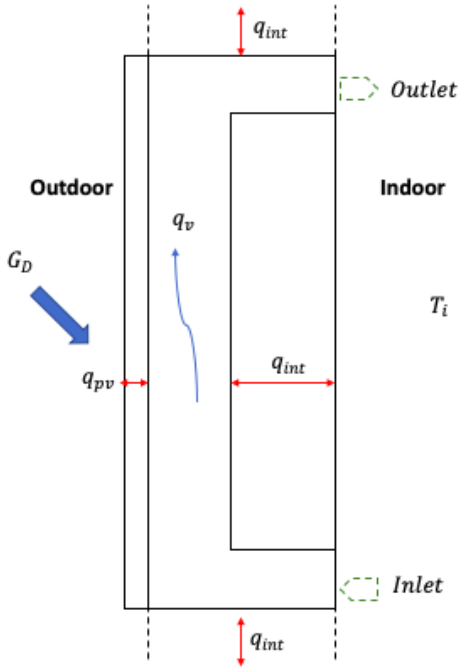

Fig. 12. BIPVT heat balance scheme.

The proposed control logic process for the automatic operation scheme is presented in Fig. 13. It takes into consideration a maximum temperature of comfort (T_{comf}^{max}) and a minimum temperature of comfort (T_{comf}^{min}) (in which between the occupant is considered comfortable – comfort range temperature (T_{comf})), indoor temperature (T_i) and air cavity temperature (T_{ac}). The temperatures considered for the operation may be changed according to the occupant's preferences, in terms of setpoint definition for the smart operation of the system. However, during the development of this work, the T_{comf} range assumed are between 18 ºC and 25 ºC, being 18 ºC the T_{comf}^{min} and 25 ºC the T_{comf}^{max}. The average of the air cavity temperature (T_{ac}^{a}) do also interfere with the operation of the vents, as is possible to see in the scheme. It is important to highlight here that the temperatures considered for the air cavity considering the experimental values obtained refers to a punctual value translating the temperature in the sensor's location, whereas the average temperature accounts with all the sensors located within the air cavity

(vertical duct, inlet and outlet).

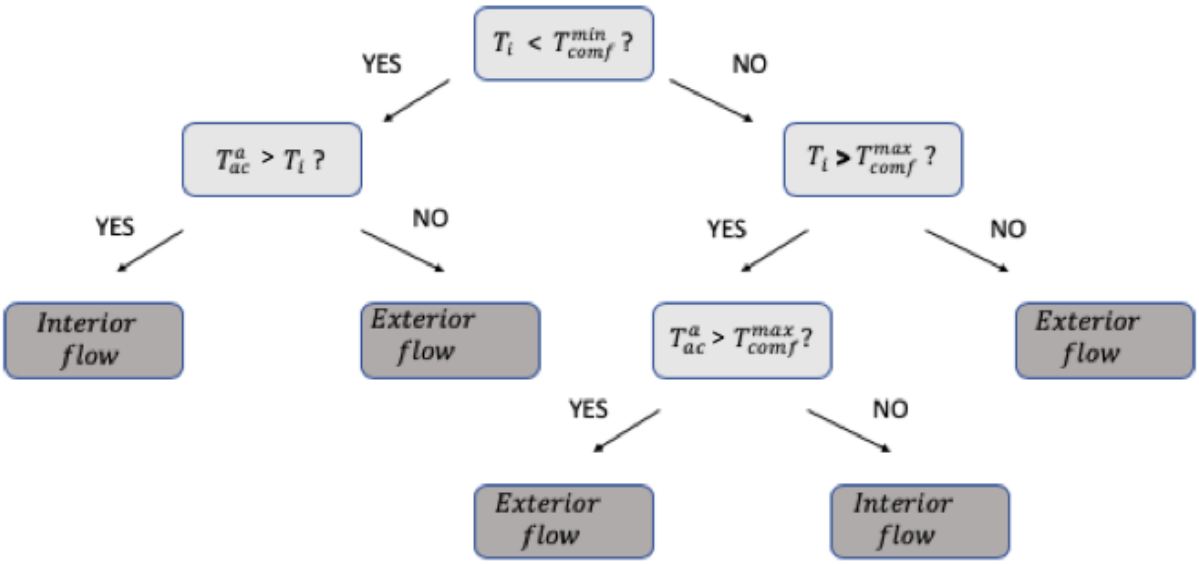

Fig. 13. Control logic for the automation process of the BIPVT system.

3.4.2. Window blinds

The blind system existent in the test room covers all the glazing part of the window. The blind installed in the test room has an automation system that allows the user to control the slat angle and opening of the system. In the current context, the blind system tend to be quite useful, even when manually operated. Studies show that the correlation between control behaviour and the environmental variables involved with the thermal and visual comfort tend to be extremely dynamic (H. Shen et al. 2015). For this reason, during the experimental and numerical analysis of this thesis, the blind system was in a static position and manual control, to avoid adding more uncertainty in the test room thermal analysis. Fig. 14 presents the detailed geometry of the blind system.

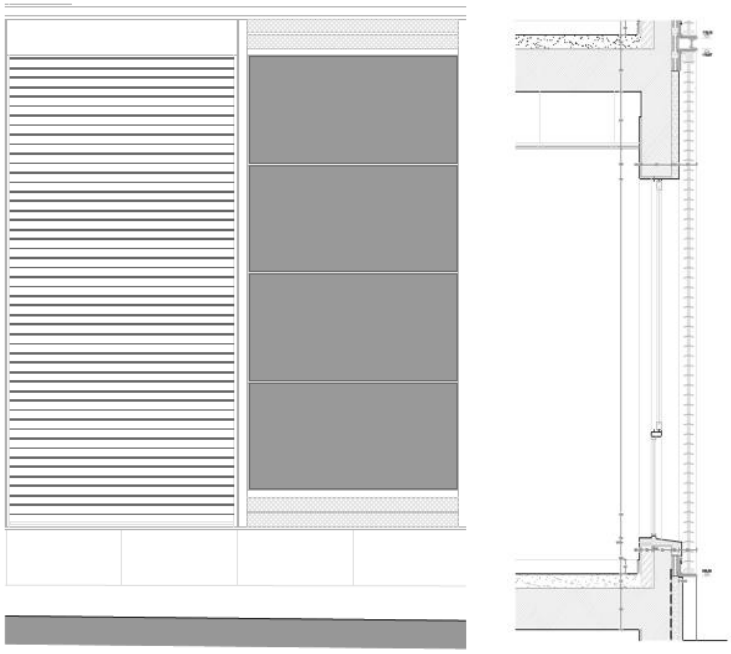

(a) *(b)*

Fig. 14. Geometry of the blind system in (a) front-view and (b) cross-section.

Pertinent details are presented in Table 10. More details on the description of the parameters may be found in DoE (2010). The values adopted for the thermal and visible characteristics of the blinds are the standard values assumed for a blind with medium reflectivity material, and values are according to DoE (2010).

Table 10. Characteristics of the blind materials.

System	***Parameter***	***Value***
Blind	*Slat orientation*	Horizontal
	Slat width (m)	*0.06*
	Slat separation (m)	0.01875
	Slat thickness (m)	0.001
	Slat angle (deg)	90
	Slat conductivity (W/(m.K))	0.9
	Slat beam solar transmittance	0
	Front side slat beam solar reflectance	0.5
	Back side slat beam solar reflectance	0.5
	Slat diffuse solar transmittance	0
	Front side slat diffuse solar reflectance	0.5
	Back side slat diffuse reflectance	0.5
	Slat beam visible transmittance	0
	Front side slat beam visible reflectance	0.5
	Back side slat beam visible reflectance	0.5
	Slat diffuse visible transmittance	0
	Front side slat diffuse visible transmittance	0.5
	Back side slat diffuse visible transmittance	0.5

Slat infrared hemispherical transmittance	0
Front side slat infrared hemispherical emissivity	0.9
Back side slat infrared hemispherical emissivity	0.9
Blind to glass distance (m)	0.05
Blind top opening multiplier	0.5
Blind bottom opening multiplier	0.5
Blind left side opening multiplier	0.5
Blind right side opening multiplier	0.5
Minimum slat angle (deg)	3
Maximum slat angle (deg)	175

3.4.3. Buried pipes

The use of the soil as inertial mass for the thermal conditioning of buildings by contact is an old practice. However, its use as a heat exchanger through buried pipes, for natural ventilation of buildings is relatively recent, starting to be implemented in the last decades. The practice consists of burying ducts at usual depths between 0.5 m and 1.5 m - with extensions and diameters varying according to each particular case. The air circulates from the outside to the interior of the surroundings, through the action of the external wind and of natural convection. In summer, soil temperature values are lower than the outdoor air temperature. At low depth, the soil temperature does not show many variations along the year. Through the system of buried pipes, it is possible to promote natural ventilation and decrease the temperature variations inside the building. This type of system is used to interconnect the interior of the building to the ground and exterior air inlet. The properties of the pipes' material, the surface area of the pipe in contact with the ground and the amount of circulating air are factors that relate to the efficiency of the system.

Fig. 15 presents details on the geometry of the buried pipe. Despite being represented in this subsection, the operation of the buried pipes system does not object to studying in the scope of this thesis, neither in experimental nor numerical analysis. The buried pipes systems were not activated in the test room during the experimental campaigns and will not be further discussed.

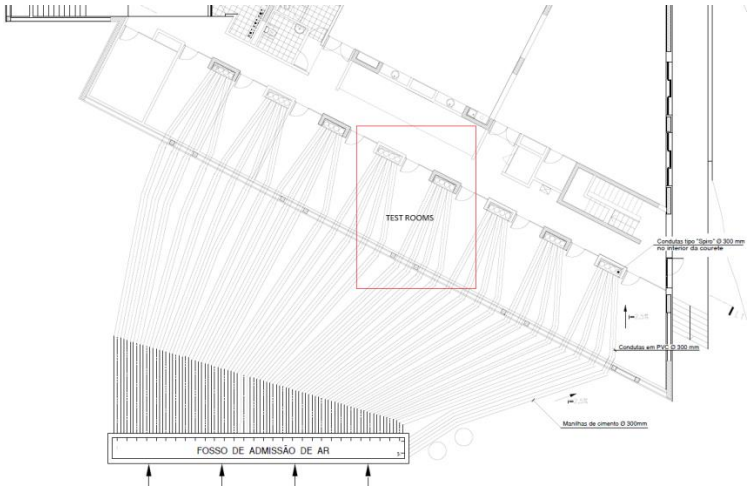

Fig. 15. Geometry of the buried pipes system.

3.5. Previous studies based on Solar XXI building

Besides the existing systems described, other systems were developed in previous studies concerning the Solar XXI building along the years. In (Pereira, 2015), a prototype was developed in a test room, consisting of an outer module composed by a PV panel, and air cavity and an inner layer of PCM material. This prototype was experimentally and numerically analysed. The results obtained showed that the maximum η_t of 15,8% in the winter and negative efficiencies in the summer, while the η_e achieved is 8,4% in the winter and 4,2% in the summer. Detailed information may be found in (R. J. Pereira 2015).

In (Ventura 2014), an automated prototype composed of a PV panel, and air cavity and a PCM board inner layer was developed. In this study, different operation modes were implemented and tested. The maximum η_t obtained was 35%, while η_e was near 10%. More details may be found in (Ventura 2014). In (Mendes 2011), the BIPVT system from the Solar XXI building is thermally described based on an experimental campaign.

3.6. New BIPVT prototype

3.6.1. Prototype characteristics

The design of the new BIPVT prototype is based on the use of engineering concepts, methods and techniques in order to provide a solution that contributes to meet the needs identified in the whole-building energy analysis. A very detailed description of the design method of thermal systems may be found in Jaluria (2007). The interest lies in designing, producing and testing new elements that will improve the energy conditions of the building, by conjugating elements present on the market and new configurations and operation. In this section, the formulation of the design problem and objectives are specified, along with requirements and technical specifications. Moreover, after the production of the proposed prototypes, tests are presented in further sections in terms of experimental campaign and numerical modelling.

The new prototype was developed with the aim of creating other comparative solutions with the existing BIPVT system in the Solar XXI Building. The development of a new prototype aims not only to address the need for intelligent and more adaptive solutions for the façades, but also to test whether operations in manual and automatic mode make sense for the context in which they are inserted - mainly in the case of buildings of service where its manual operation depends on the occupant's awareness of operation. The occupant itself tends to perceive when he needs the heat recovery provided by such systems but does not have the same perception of operation when the environment is comfortable and the objective is to increase electrical efficiency by cooling the modules, for example. example.

Therefore, the prototype developed by the NZEB_LAB project and presented in this thesis is composed of a metallic frame, photovoltaic module, with electrical efficiency of 15%, 120 Wp and an effective area of 0,96 m^2, inverter and any other accessories that may be needed, It has an air cavity and a solid internal modular component, being possible to intercalate between an EPS module (Referred to as P1a) for thermal insulation and a water tank module for thermal storage (Referred to as P1b). There are four vents (two facing outwards and two facing inwards), which can be operated manually or automatically (through the establishment of set points) through an HMI.

There are snap rails that should ideally be proportionate to flexible positioning of the interior module to allow future changes in air cavity thickness (depending on future results of component design optimisation processes). On the inner sides of the frame, there should be experimental cable troughs and their insulation caps to isolate the box from possible marginal air infiltration.

Due attention should also be paid to the insulation provided by the vents when closed and water tank insulation since when closed they should avoid unwanted airflow between the surrounding spaces and the air cavity and the tank may have unwanted water infiltration – as well as to avoid evaporation of the water to avoid losses of volume and unwanted in air humidity. Inside these openings or in the air cavity duct, fans can be installed to ensure forced airflow at times when ventilation is required, when the flow generated by natural ventilation is not sufficient, operated by the occupant of the room.

To complement, Table 11 presents the constructive solution composition of the prototype in its two versions (P1a – EPS thermal insulation and P1b – water tank), regarding the most critical simulation parameters, as seen in previous sections. The material layers are presented considering the direction from the outside to the inside of the building. The concept of the prototype is presented in Fig. 16.

Table 11. Constructive elements of the prototype.

Constructive element	***Components***	***Thickness (m)***	***Conductivity (W/(m.K))***	***Density (kg/m^3)***	***Specific heat (J/(kg.K)***
Prototype P1a	*PV module (Opaque glazing)*	*0.003*	*1.800*	*2330*	*677*
	Air layer	*0.10*	*Thermal resistance in accordance with thickness*		
	EPS - Thermal insulation	*0.070*	*0.040*	*1000*	*1400*
Prototype P1b	*PV module (Opaque glazing)*	*0.003*	*1.800*	*2300*	*677*
	Air layer	*0.1*	*Thermal resistance in accordance to thickness*		
	Tank material	*0.01*	*0.19*	*1390*	*840*
	Water	*0.08*	*0.606*	*1000*	*4182*
	Tank material	*0.01*	*0.01*	*1390*	*840*

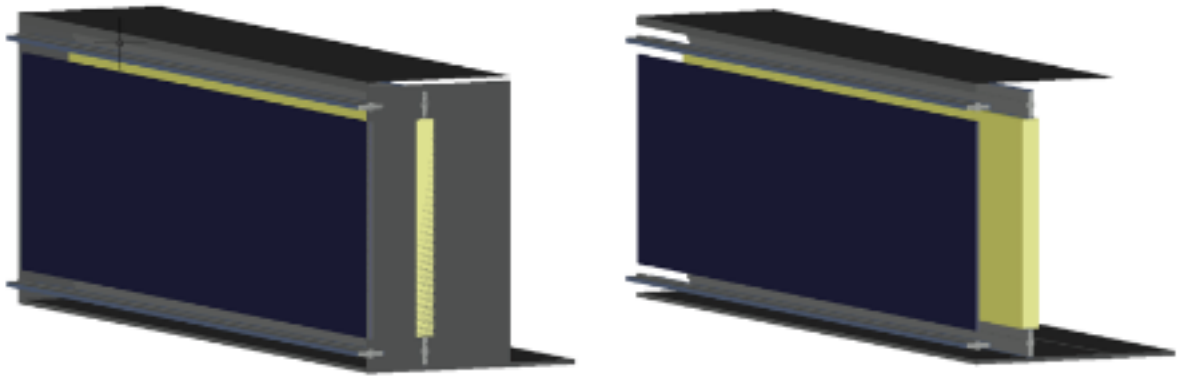

Fig. 16. Prototype concept in 3D.

The dimensions of the outter frame are presented in Fig. 17. They correspond to the available area and to the thickness between the interior face of the wall and the exterior face of the BIPVT system (54,7cm thickness /depth) and the available glazing area to be removed and substituted by the prototype (and 71,5cm height (interior) and 78,8cm height (exterior) per 173,5cm of width). The difference between the interior and exterior height is due to a small slope presented in the outer part of the frame, inserted during the manufacturing process. This slope was made for two reasons: i) to adequate the frame to market PV module size, and ii) to promote the drainage in case of any rainwater infiltration through the exterior vents.

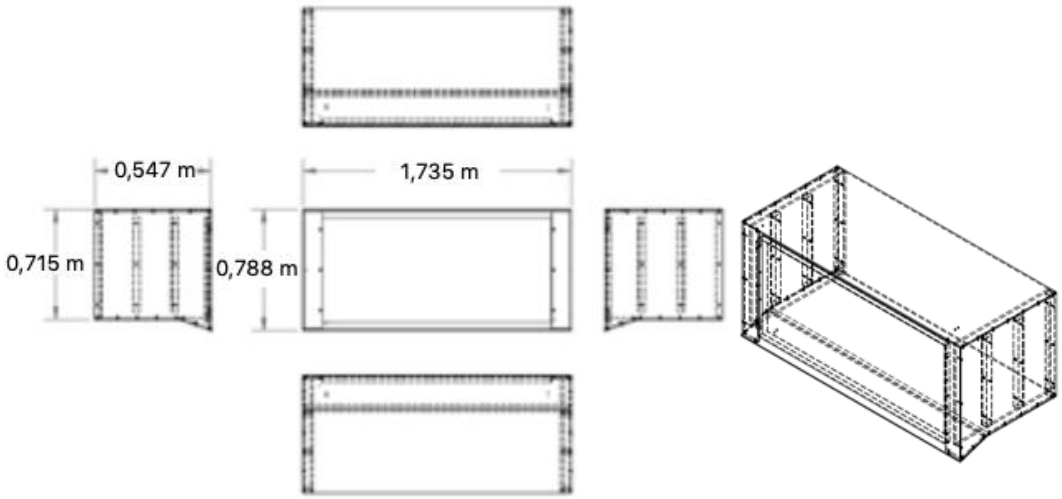

(a) (b)

Fig. 17. Metal frame of the prototypes – (a) dimensions in mm – and (b) ensembled frame.

Fig. 18 presents the cross-section of the prototype, with the detail of the interior modular part. The inlet and outlet vents have near 0.07m of height. Metal interior support frames have approximately 0.038m at the top and the same at the bottom, with 0.5 m for the interior module height.

After the process of engineering design, the prototypes were manufactured and installed in the test rooms, under the scope of the NZEB_LAB Infrastructure Project, from the National Laboratory for Energy and Geology. Fig. 19 presents: a) the front view of the Prototype; b) back view of the Prototype; c) water tank module; and d) . EPS insulation module.

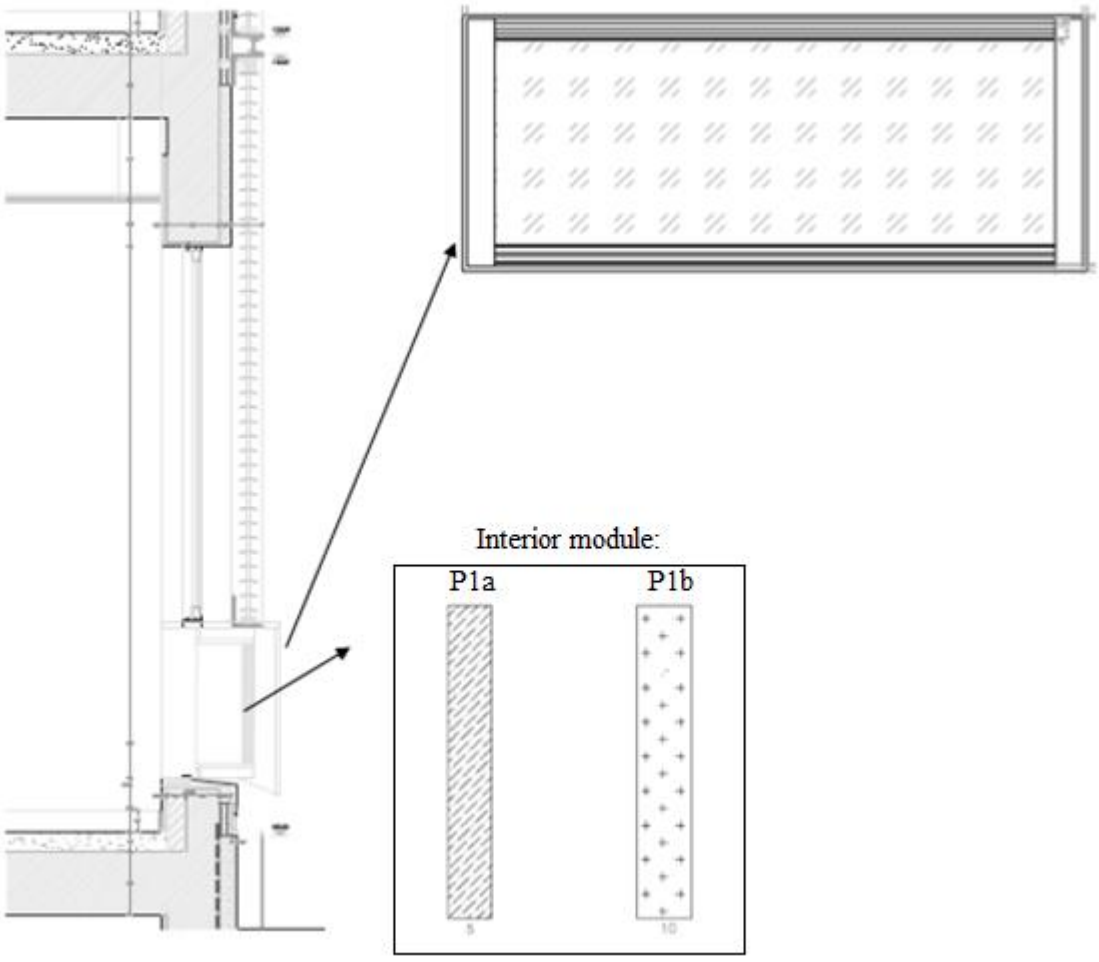

Fig. 18. Cross-section of the Prototypes.

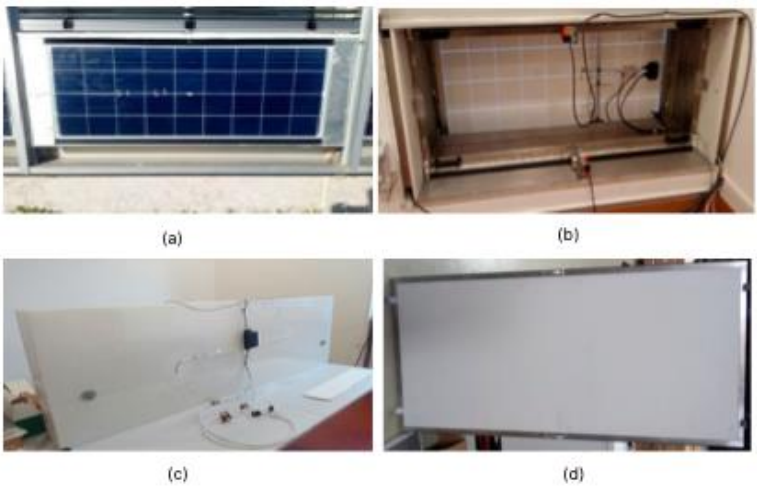

Fig. 19. a) Front view of the Prototype; b) Interior view of the Prototype (without interior module); c) Water tank interior module; d) EPS interior module.

3.6.3. Operation mode and automation

As in the BIPVT system previously described, the setups of operation are also variable according to the occupant's desire. For the testing presented in the next chapter in the scope of this thesis, the same setpoints were used. Also, in similarity to the BIPVT system previously described, the prototype has four vents (bottom and upon the exterior surface and bottom and upon the interior surface), and also three fans located at an equal distance one from another at the top of the air duct. The prototype vents are operated either manually according to the occupant wishes or automatic, according to a control logic for the automation process. The manual operation follows as was presented in Fig.14.

The automatic operation is based on the sensors installed on the prototype. The actuators responsible for the vents' movement are from Belimo, model LM24A-F, with a rotation time of 150s/90º. According to the testing conditions of the prototype, the test phase will be selected on a human-machine interface (HMI) touch screen. The prototypes will have structural configurations that will allow the air cavities to assume suggested thicknesses between 5 cm and 10 cm, this thickness is controlled by the positioning of the interior solution a) or b). The air flows between the outside, the air cavity and the interior of the thermal zone (through the automated or manual operation vents) should ideally be controlled according to the zone temperatures and a T_{comf} band stipulated by as well as in the function of a temperature gradient

between the air duct and outside temperatures also stipulated by the user. Fig. 20 presents the data acquisition system of the prototype and the HMI screen.

(a) (b) (c)

Fig. 20. a) Data acquisition system with HMI; b) main menu of the HMI; c) screen of vents operation.

Fig. 21 presents the control logic used to automatically operate the prototypes, in which C1 and C2 stand for exterior vents and C3 and C4 for interior vents (bottom and top, respectively). In this scheme, T_i stands for Room temp in the sensor's location, T_{comf}^{min} and T_{comf}^{max} for the lower and upper T_{comf} limits, respectively. T_{amb} refers to the exterior temperature in the sensor's location, and T_{ac}^{a} the T_{ac} in the sensor's location. This nomenclature is used here, being in terms different from the nomenclature adopted for the rest of the work, due to the variables names implemented in the algorithm of operation and control panel present in the HMI. They are, however, referred in the content of this paragraph. After the characterization of the case study BI-SES elements and test room, this work proceeds with the experimental analysis.

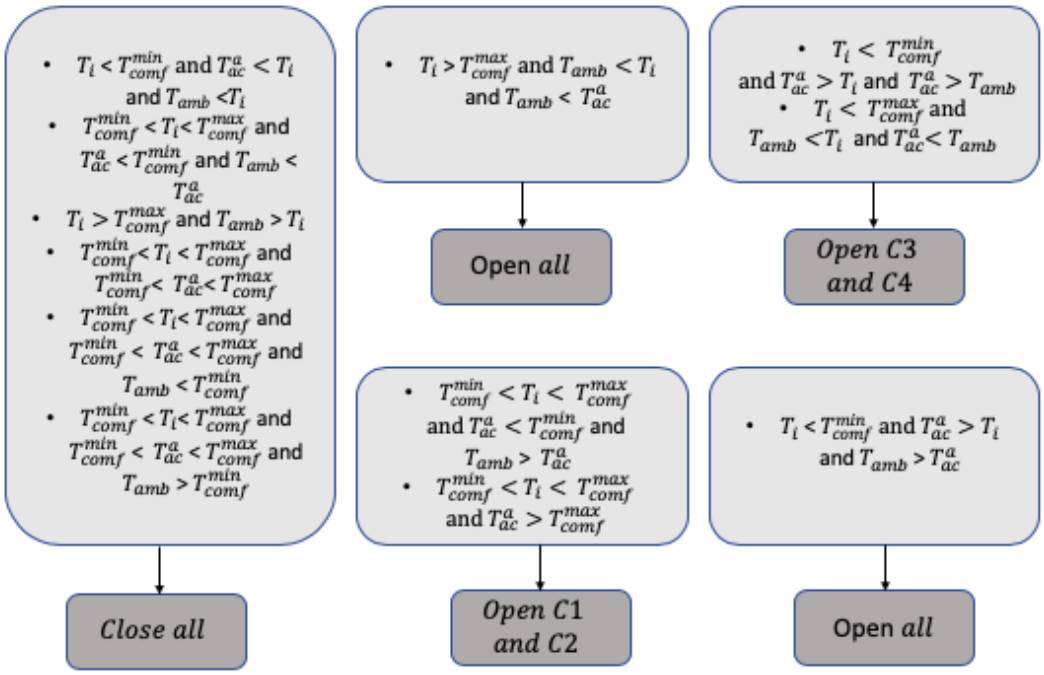

Fig. 21. Control logic in automatic mode.

Chapter 4. Experimental analysis

The experimental part of the investigation intends to obtain the measured values that correspond to real-situation of the variable/component under study given the boundary conditions existent in the moment. Furthermore, the part based on performance calculation will have these obtained real-situation values as inputs to the equations. This Chapter focuses on the climatic characterization, and performance characterization of the BI-SES system, through an extensive campaign developed during the year of 2018 and 2019.

The experimental analysis also includes the room usage pattern and temperature to establish the boundary conditions and interior gains for further analysis. The experimental approach allows the performance characterisation for the boundary conditions and element thermal behaviour registered during the period of the experimental campaign.

It is also crucial to validate the mathematical/simulation models. In addition, it is necessary to highlight that the experimental campaign results also reflect the uncertainty associated with the BI-SES systems measured in real testing conditions, once there are a large number of variables interfering with each other, and it is complicated and sometimes impossible to isolate the correlations between few variables in the systems.

4.1. Experimental setup

The experimental setup describes the conditions of the experimental analysis developed. It is based on the definition of the observable variables, sensors description and positioning, description of data acquisition definitions and periods of register. The observable variables are generically presented in Fig. 22, and are valid to the configurations of the BIPVT systems including the prototype (varying the variable designation according to the system),

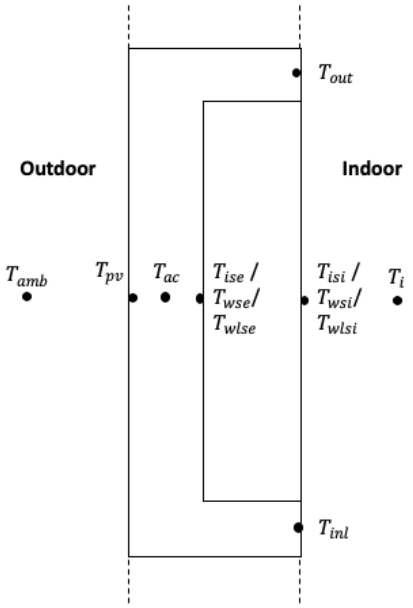

Fig. 22. Variables of the system.

The experimental approach is segmented in three main aspects: outdoor testing (weather), systems testing and indoor testing, under the most stable and controlled conditions possible. The system testing allows the thermal characterization of the systems based on the measured data. The results are shown in terms of yearly analysis and terms of short periods or daily analysis. The yearly analysis presents the values concerning the whole period of experimental evaluation. The shorter periods correspond to a winter month and a representative summer month, and the daily analysis presents the data concerning a clear sky day of each system period of analysis (which characteristic of T_{amb} and G_D vary according to each period).

A detailed description of the location and type of the sensors of the BIPVT were presented in Chapter 3. The prototype (a and b) has an elaborate experimental setup, composed of many sensors for different purposes, connected to a human-machine interface (HMI) in which the control algorithm is implemented. Fig. 23 presents, using coloured points, the sensor's location and function.

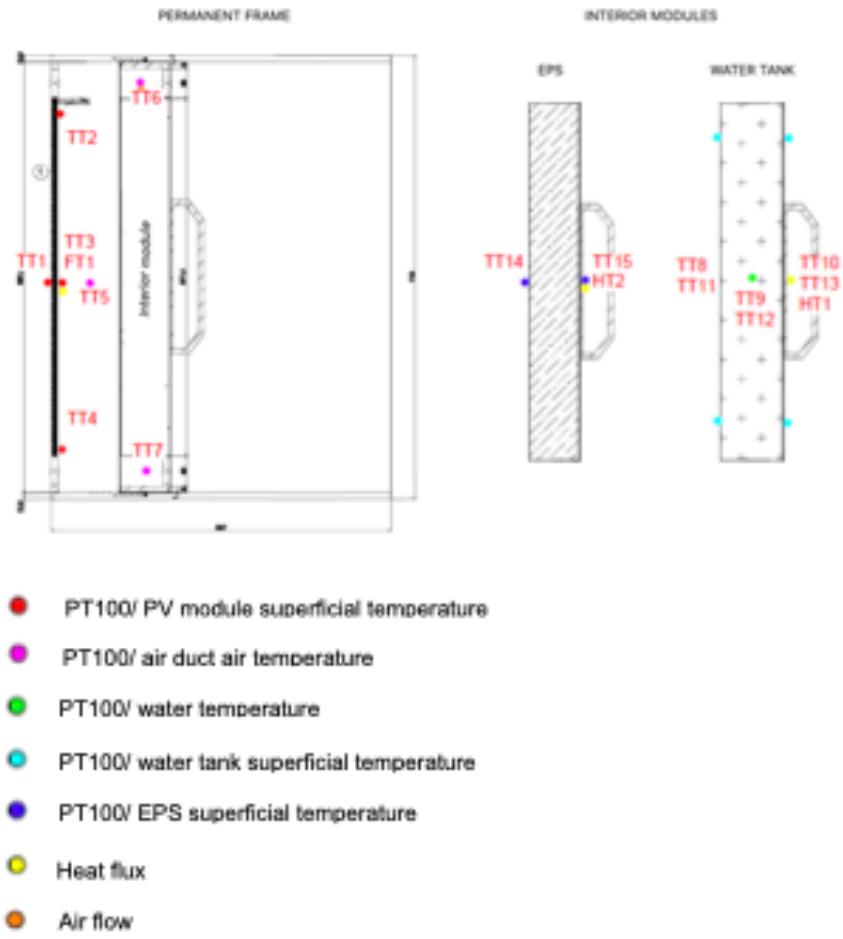

Fig. 23. Sensor location in the permanent and mobile parts.

The detailed description of sensors, in terms of observable variable, brand/model, range of measurements and accuracy are shown in Table 12. Table 12 segments them under consideration system under analysis (climatic conditions, BIPVT and prototype). The sensors that measure voltage (TS1) and current (TC1) of the PV module are not used in the scope of this work, however, are installed in the prototypes.

The experimental evaluation concerning the weather data ranges from January/2018 to June/2019 with an average of 37 registers per hour (time step of 2-3 minutes between registers). It is important to highlight that there are two values of G_D being registered: i) one of them is from the LNEG weather station – and is the one that provide the results presented in the weather experimental analysis; ii) the second is from the façade of the test room, presenting the values correspondent to the ones used to calculate the efficiencies and co-relation between variables in the systems' results.

Table 12. Detailed description of the sensors.

Sensor	*Observable variable*	*Brand/Model*	*Range*	*Accuracy*
		Climatic conditions		
	Outdoor temperature	PT100	-70 to 500 ºC	0,03 – 0,07
	Global horizontal radiation	Kipp & Zonen / CM6B 951765	200 to 4000 nm	< 0.2 %
	Direct normal radiation (weather station)	Kipp & Zonen / CHP1 100434	200 to 4000 nm	< 0.2 %
	Direct normal radiation (wall of test room)	Kipp & Zonen / CHP1 100434	200 to 4000 nm	< 0.2 %
	Diffuse horizontal radiation	Kipp & Zonen / CM6B 983431	200 to 4000 nm	< 0.2 %
		BIPVT		
	Air cavity temperature	Omega / PT100	-70 to 500 ºC	0,03 – 0,07
	PV module temperature	Omega / PT100	-70 to 500 ºC	0,03 – 0,07
	Conductive heat flux	Hukseflux HFP01	-2000 to +2000 W/m².	60 x 10^{-6} V/(W/m²)
	Anemometer	Testo 425	0 m/s to 20 m/s	0.01 m/s
		Prototype (a and b)		
TT1	Exterior superficial temperature of the PV module	Omega / SA2F-RTD-3-100-A-10M	-50 ºC to 200 ºC	0,03 – 0,07
TT2	Interior superficial temperature of the PV module (upper)	Omega / SA2F-RTD-3-100-A-10M	-50 ºC to 200 ºC	0,03 – 0,07
TT3	Interior superficial temperature of the PV module (middle)	Omega / SA2F-RTD-3-100-A-10M	-50 ºC to 200 ºC	0,03 – 0,07
TT4	Interior superficial temperature of the PV module (bottom)	Omega / SA2F-RTD-3-100-A-10M	-50 ºC to 200 ºC	0,03 – 0,07
TT5	Air temperature in the air duct	Omega / PR-10-2-M45-100-ST	-200 ºC to 600 ºC	0,03 – 0,07
TT6	Air temperature in the air duct outlet	Omega / PR-10-2-M45-100-ST	-200 ºC to 600 ºC	0,03 – 0,07
TT7	Air temperature in the air duct inlet	Omega / PR-10-2-M45-100-ST	-200 ºC to 600 ºC	0,03 – 0,07
TT8	Exterior superficial temperature of the water tank	Omega / SA2F-RTD-3-100-A-10M	-50 ºC to 200 ºC	0,03 – 0,07
TT9	Water temperature	Omega / PR-10-2-M45-100-ST	-200 ºC to 600 ºC	0,03 – 0,07
TT10	Interior superficial temperature of the water tank	Omega / SA2F-RTD-3-100-A-10M	-50 ºC to 200 ºC	0,03 – 0,07
TT11	Exterior superficial temperature of the water tank	Omega / SA2F-RTD-3-100-A-10M	-50 ºC to 200 ºC	0,03 – 0,07
TT12	Water temperature	Omega / PR-10-2-M45-100-ST	-200 ºC to 600 ºC	0,03 – 0,07
TT13	Interior superficial temperature of the water tank	Omega / SA2F-RTD-3-100-A-10M	-50 ºC to 200 ºC	0,03 – 0,07
TT14	Exterior superficial temperature of the EPS	Omega / SA2F-RTD-3-100-A-10M	-50 ºC to 200 ºC	0,03 – 0,07
TT15	Interior superficial temperature of the EPS	Omega / SA2F-RTD-3-100-A-10M	-50 ºC to 200 ºC	0,03 – 0,07
TT16	Room temperature	RS Pro / 376-1477 e 813-878	-10 ºC to 40 ºC	0,2°C
TT17	Ambient temperature	RS Pro / 376-1477 e 813-878	-10 ºC to 40 ºC	0,2°C
HT1	Heat flux on the interior surface of the water tank	GreenTEG AG / gSKIN-XP 26 9C	-150 to 150 kW/m^2	0,02
HT2	Heat flux on the interior surface of the EPS	GreenTEG AG/ gSKIN-XP 26 9C	-150 to 150 kW/m^2	0,02
FT1	Anemometer	Sensor Data/ SDFT 35.10.1.1.5	0 m/s to 10 m/s	
TS1	Voltage of the PV module	Not given	Not given	Not given
TC1	Current of the PV module	Not given	Not given	Not given

The BIPVT system experimental evaluation ranged from January/2018 to the beginning of January/2019. The prototypes were monitored from February to June/2019. Table 13 presents the register periods explored in the experimental analysis. The weather data and indoor data are collected on a continuous basis. It is possible to see that the BIPVT is the system with the longest time of analysis, allowing a more accurate thermal characterization during the whole year. The prototype has reduced time of experimental analysis, due to the timeline of the manufacturing of the same in the scope of the NZEB_LAB project.

Table 13. Register periods for each observed element.

Campaign	***2018***												***2019***					
	1	***2***	***3***	***4***	***5***	***6***	***7***	***8***	***9***	***10***	***11***	***12***	***1***	***2***	***3***	***4***	***5***	***6***
Weather data	✓	✓	✓	✓	✓	✓	✓	✓	✓	✓	✓	✓	✓	✓	✓	✓	✓	✓
Room temperature	✓	✓	✓	✓	✓	✓	✓	✓	✓	✓	✓	✓	✓	✓	✓	✓	✓	✓
BIPVT system	✓	✓	✓	✓	✓	✓	✓	✓	✓	✓	✓	✓	✓	✓				
Prototype P1a														✓	✓			
Prototype P1b															✓	✓	✓	

4.2. Climatic conditions characterization

The weather data was collected from the LNEG weather station and also from sensors installed next to the test rooms, to capture the most accurate values to validate the computational models and control algorithms correctly. The collected data are the parameters of T_{amb} , G_h , G_d and G_D. The output of this phase will be the data record to be used both for the control algorithms and for the development of the weather files to be used in computational modelling. More in-depth information on the use of weather data experimental campaigns to create weather files may be found in (Hensen and Lamberts, 2012). In more detail, the weather data was collected for the whole year of 2018 and the first semester of 2019.

During the year of 2018, there were near 8328 valid hours registered, with 432 missing hours of register due to register failures or maintenance of the equipment. The major register failures (represented in the graphs with the "R.F." nomenclature) concerning weather data of 2018 were in March and April (failure in data logger), May (failure in equipment), July and August (external calibration of the equipment), and December (energy power break). Concerning the

weather data of 2019, the registers failures were in March and April (energy power break), and May (substitution of the equipment). Minor fail on the data acquisition may also be noted, namely in situations when the T_{amb} suddenly hits 0 ºC in the graphs (meaning no register is being made during those consecutive timesteps).

The results obtained for the T_{amb} are presented in Fig. 24, in terms of frequency of occurrence. The annual temperatures are most concentrated between 10 ºC and 21 ºC but still accounts by many hours above 21 ºC, whereas fewer hours bellow 10 ºC. The T_{amb} also hits extreme peaks of near 45 ºC. Moreover, G_h and T_{amb} are presented in Fig. 25. Between June/2018 and October/2018, the temperatures were within this interval during a considerable number of hours. The annual temperatures hit a peak in August (44,03 ºC), and its lowest in February (2,95 ºC). The average yearly temperature was 16,43 ºC. Fig. 26 presents the values of G_D, and Fig. 27 presents the values of G_d.

The G_h hit the highest values between July and August. However, due to system maintenance, there is a lack of registers in some days of these months (as previously mentioned). In January and February, the highest radiation value is near 600W/m^2. The BIPVT system has better production of heat/electricity when the G_D is incident directly on the south-oriented façade. During the winter, the solar angle propitiates this production, once the sun is lower in the sky than in the summer.

Overall, the year of 2018 was a year with high-temperature peaks during a few days of the summer period. The low temperatures (below a considered T_{comf} of 25 ºC) have significant occurrence, showing that there is plenty of hours during the year in which BI-SES elements would be useful for heating the space while reducing the consumption of energy through the use of other equipment for the same purpose. Fig. 28 presents in detail the fluctuations of weather variables during February and June of 2018. It is possible to note that during the winter month, the T_{amb} presents more significant fluctuations during the day.

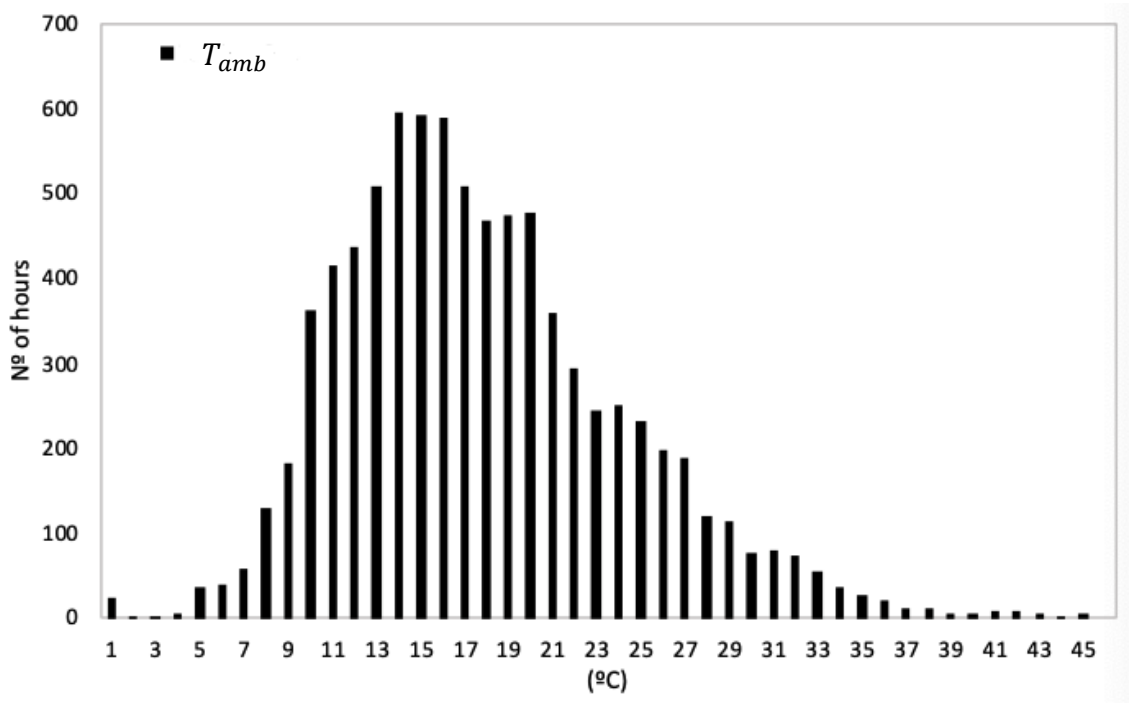

Fig. 24. T_{amb} frequency - 2018.

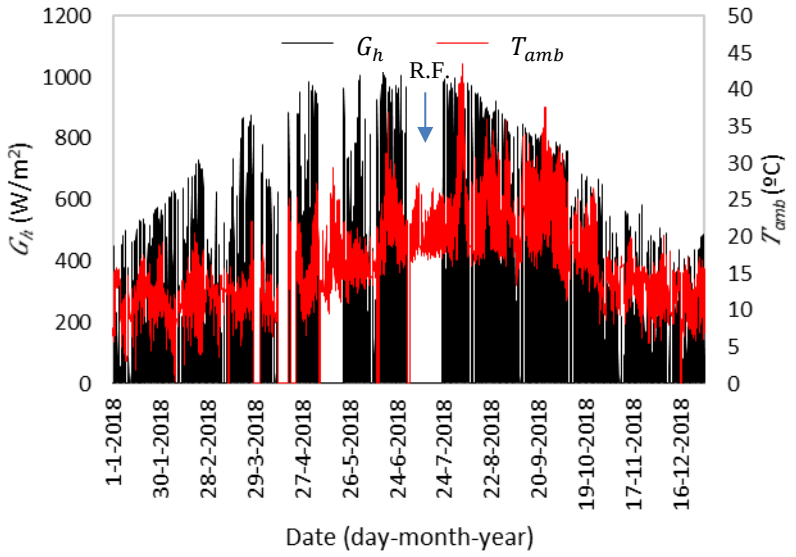

Fig. 25. T_i and G_h - 2018

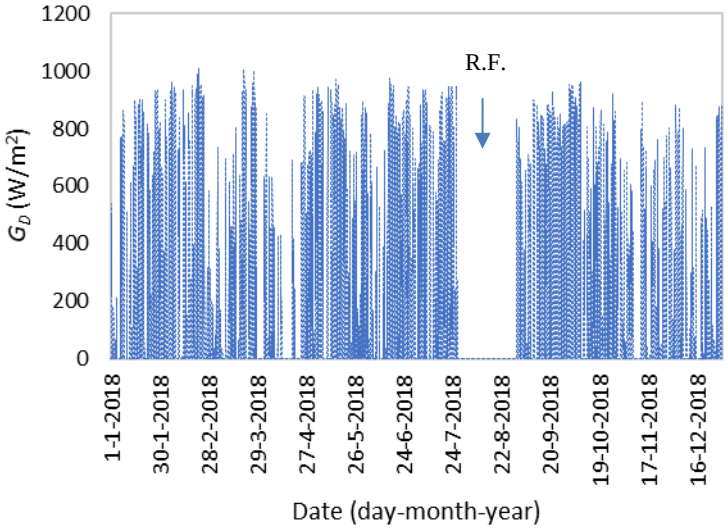

Fig. 26. G_D – 2018.

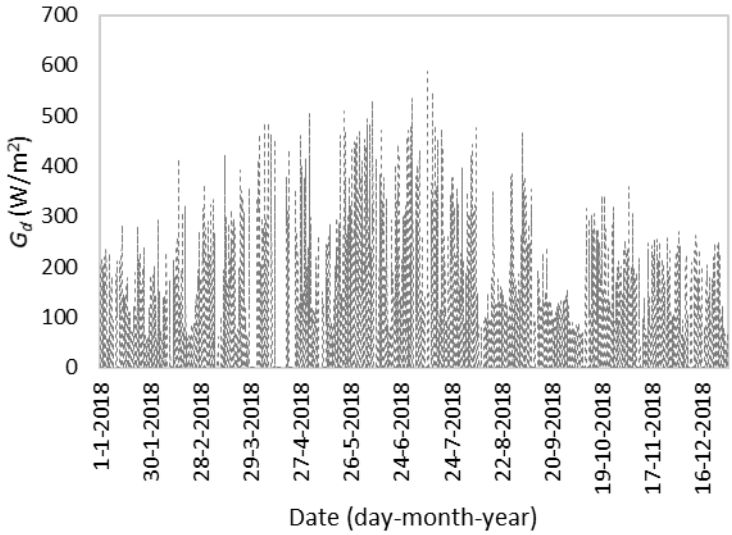

Fig. 27. G_d – 2018.

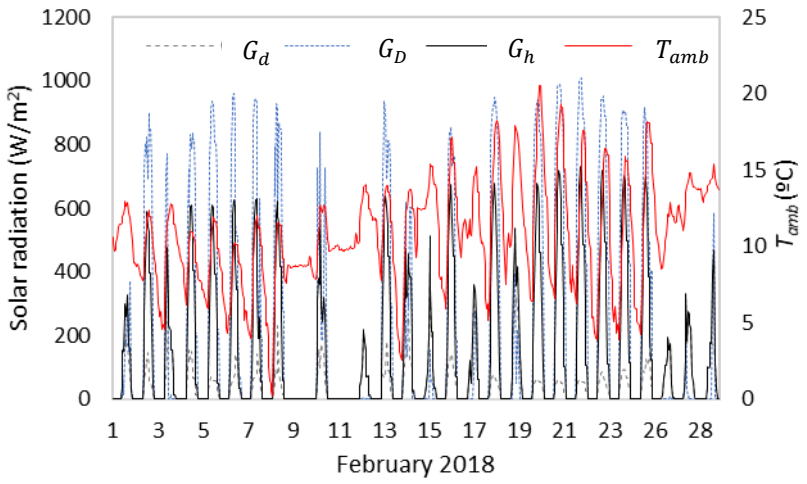

(a)

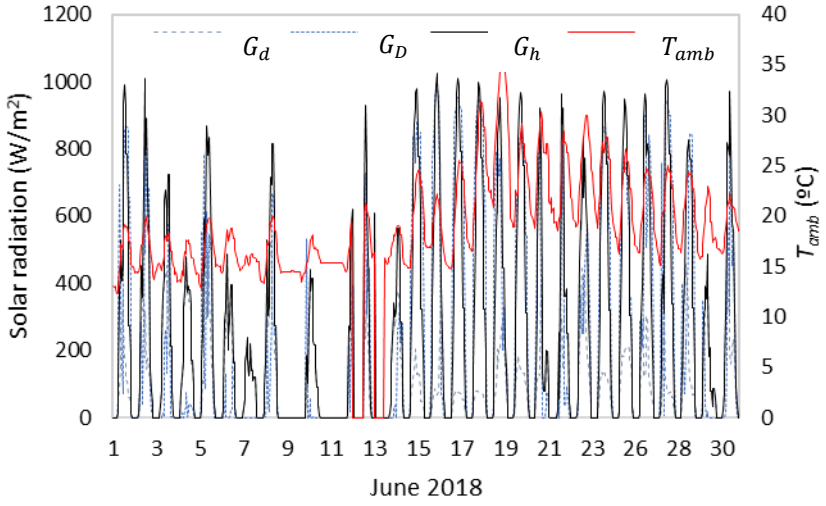

(b)

Fig. 28. Weather data details (G_h, G_d, G_D and T_{amb}) of (a) February and (b) June of 2018.

For the year of 2019, Fig. 29, G_h and T_{amb} data concerning the first semester of the year. Fig. 30 presents the results for G_D and Fig. 31 presents the results for G_d. During the registered period, the T_{amb} hits its minimum of nearly 0 ºC in the first quarter of January and first quarter of February, while the maximum was registered in the third quarter of May and first quarter of June (nearly 35 ºC). It is necessary to note that the maximum values registered do not mean the maximum for the whole summer since the experimental campaigns stopped (in the scope of this thesis) at the end of June/2019. The register faults may be noticed in the periods in which

the temperature hits 0 ºC unexpectedly. During the first semester of 2019, minor register failures occurred in the data acquisition, also being possible to note in the graphs when the T_{amb} hits 0 ºC. During the year of 2019, in contrast with 2018, no major register failures happened during the period under analysis. Fig. 32 presents the results for the fluctuations of February and June of 2019.

After presenting the results for the climate conditions experimental analysis, the results for the room temperature and usage profile, BIPVT and BI-SES prototypes will be presented.

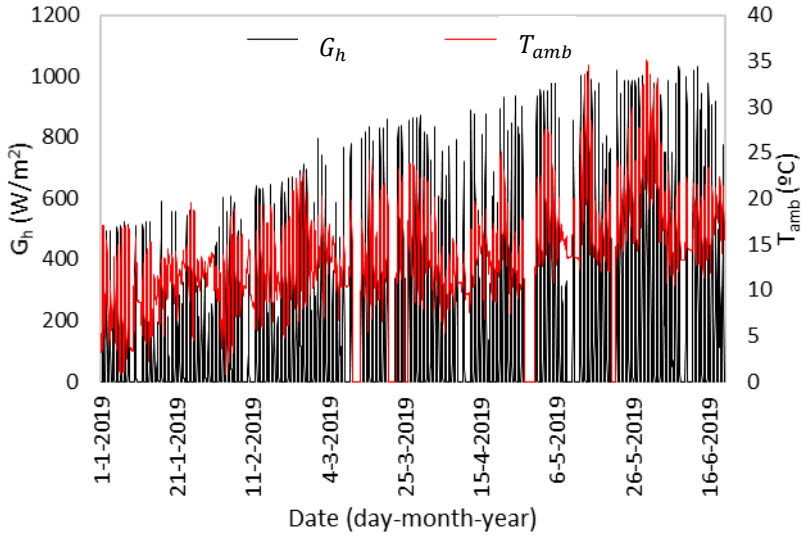

Fig. 29. T_i and G_h - first semester of 2019.

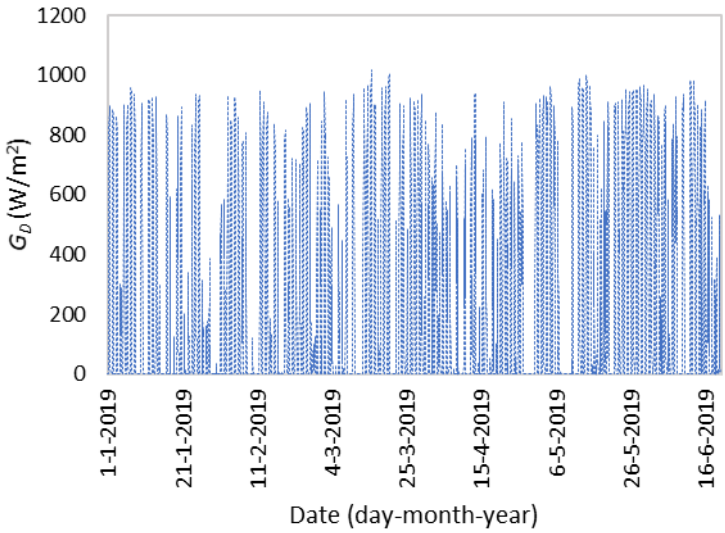

Fig. 30. G_D – first semester of 2019.

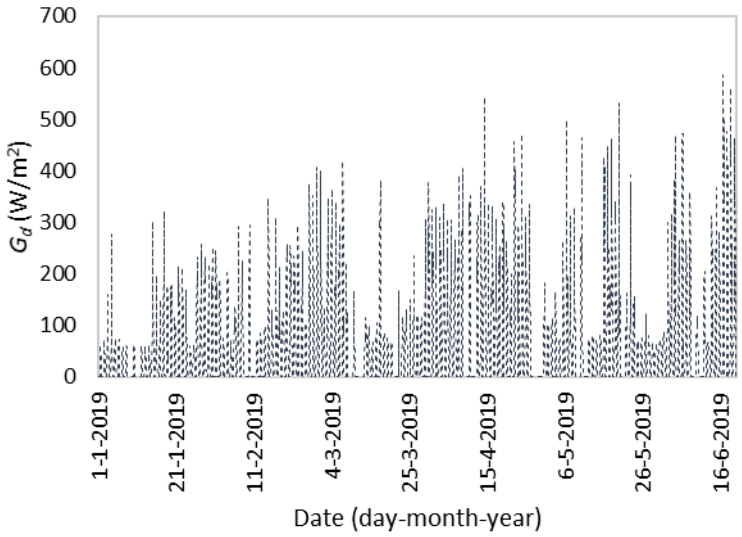

Fig. 31. G_d – first semester of 2019.

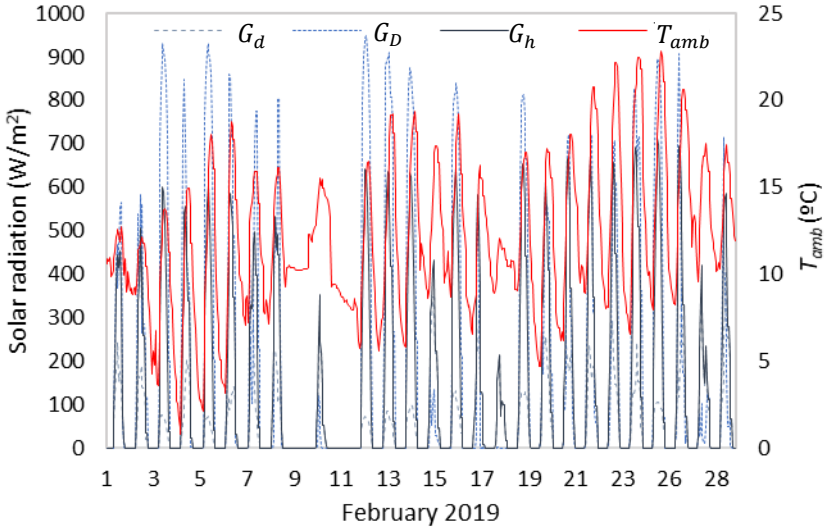

(a)

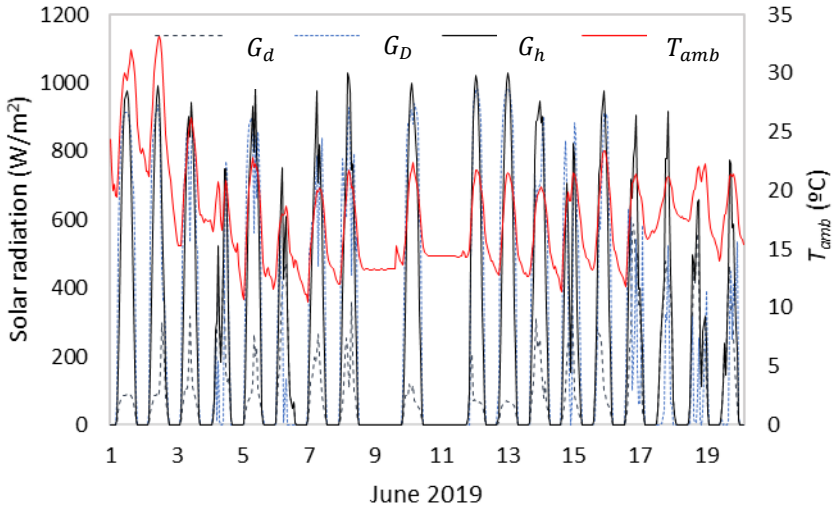

(b)

Fig. 32. Weather data – First semester of 2019: T_{amb} and G_h, G_D and G_d.

4.2. Room temperature and usage profile

The indoor temperature (T_i) and usage profile was also evaluated for the different testing periods of the BI-SES under study. For the year of 2018, the T_i is fully presented to have a picture of whole year temperature fluctuations. The entire year is shown in Fig. 33, and specific periods of summer and winter are presented in Fig. 34. Due to the passive solutions integrated into the design of the Solar XXI building, that is already a net-zero energy building, and it is possible to see that the most of annual hours are within the comfort zone, having the most critical periods in January/2018 and February/2018 due to energy needs for heating, and in August/2018 and September/2018 due to energy needs for cooling. These data (whole year of 2018 and beginning of 2019) are used for the BIPVT analysis, however the yearly room temperature profile may be exploited for the prototype's suitability analysis. From the yearly data and considering that both BIPVT and prototype are used mainly for heating purposes, from January to May the temperatures achieve values below the minimum comfort temperatures, in which the systems could be used, as well as from the middle of October to the December.

Fig. 35 presents the T_i that surrounded the prototype P1a during the manual operation mode campaign, while Fig. 36 presents the T_i during the automatic operation mode campaign. It is necessary to note that during the experimental campaign in automatic mode, the data acquisition

timestep was reduced on March 19th, leading to a more significant representation of the date in the presented graph in Fig. 30. Fig. 37 shows the T_i during the automatic operation of P1b, while Fig. 38 presents the T_i during the manual operation of P1b.

The registered T_i are mostly within the comfort band of temperature and is possible to see that the lower temperatures (that happen at night when the room is not receiving solar gains and is losing heat to the exterior) increase over the progression of the figures (that begin in February 2019 and end in April 2019). There are also some minor register failures, namely in Fig. 37 in which the temperature suddenly hits 0 ºC in a brief moment and then the registers came back to normal. During the considered period for the prototypes, only on a few occasions, the temperature exceeded the maximum comfort temperature.

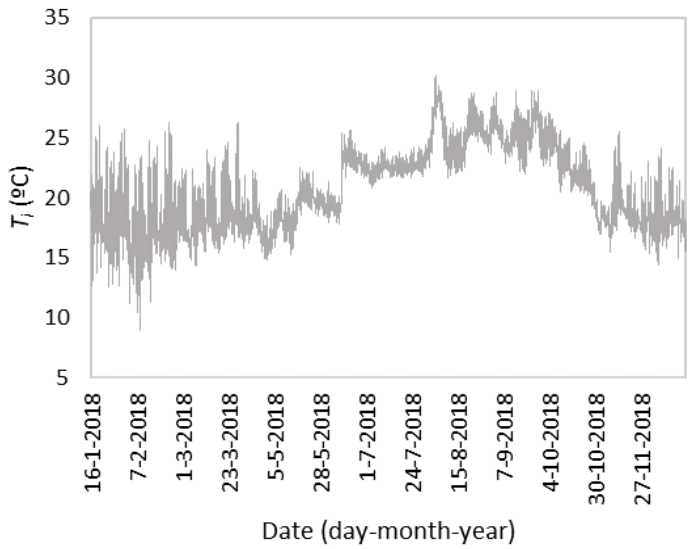

Fig. 33. T_i– 22-01-2018 to 12-01-2019.

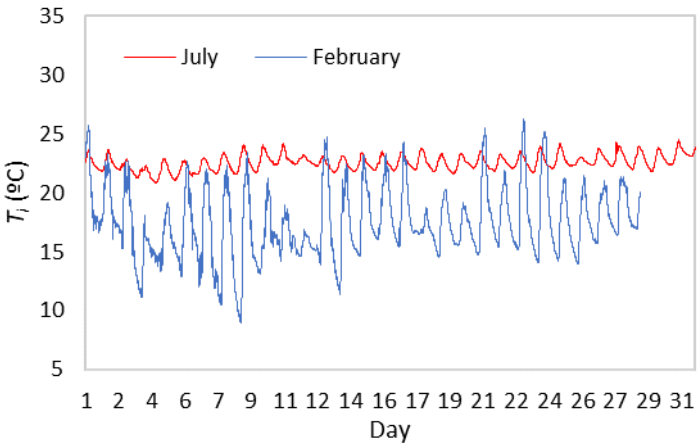

Fig. 34. T_i details of the February and July of 2018.

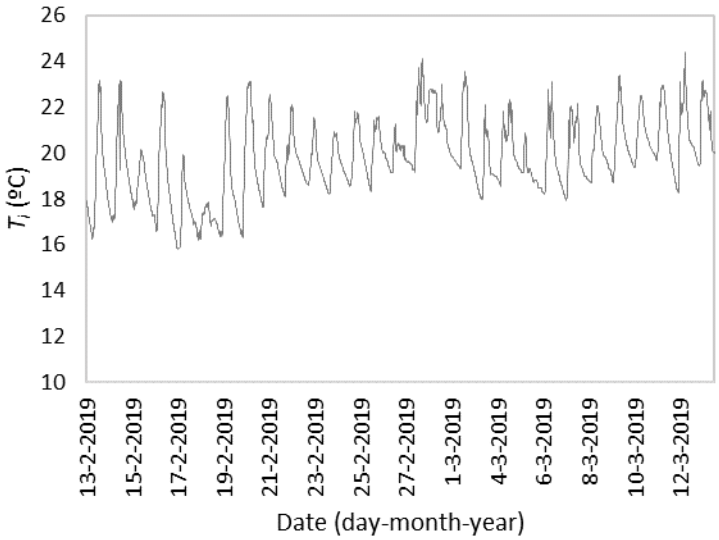

Fig. 35. T_i (13-02-2019 to 13-03-2019), P1a in manual mode.

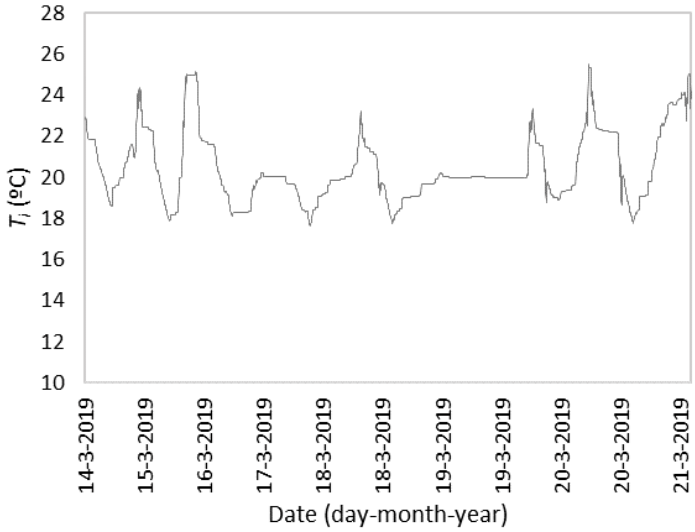

Fig. 36. T_i (14-03-2019 to 21-03-2019).

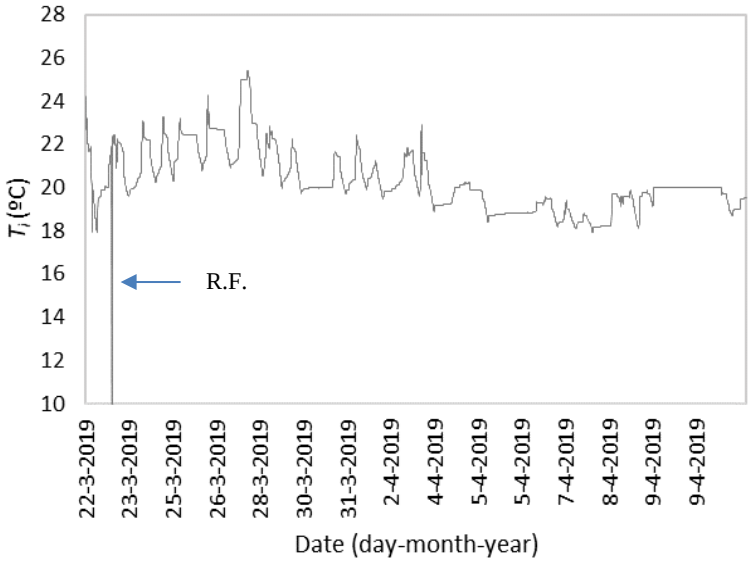

Fig. 37. T_i (22-03-2019 to 09-04-2019).

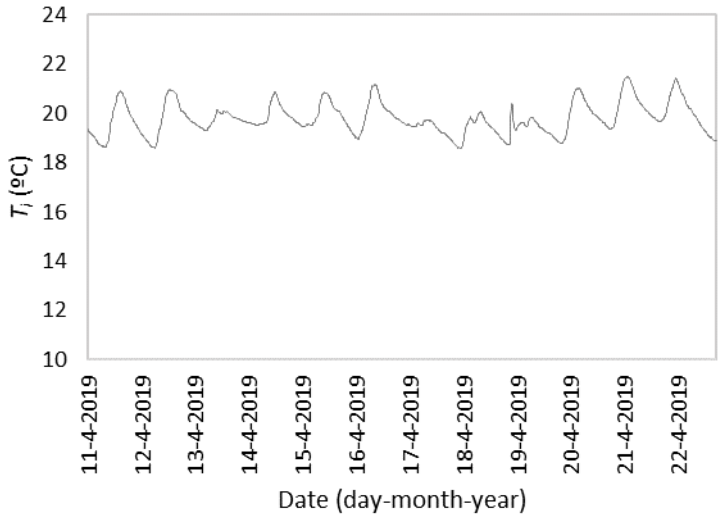

Fig. 38. T_i (11-04-2019 to 22-04-2019).

Table 14 represents the usage profile of the room for the beginning of 2018 and the monitored period of the prototypes of 2019. This profile (part corresponding to 2018) is used further to the validation of the numerical model, scheduling for the internal gains and also thermal loads determination. The usage profile was monitored in terms of date, time interval, the number of occupants, equipment/appliances being used, status of the light, condition of the BIPVT openings, window and door openings, blind position, heating system and buried pipes usage. For most of the year, on a global basis, the room is occupied by one person, being occupied by two only in brief meetings or maintenance of the monitoring systems. One desktop is used continuously, for data acquisition and work, and frequently one notebook. The window is kept closed all the time, while the door is just opened when the occupant is entering and leaving the room.

The heating system is turned on a few occasions, and the buried pipes are always off. Most of the systems, as buried pipes and heating system, as well as the window and door opening, had their operation avoided, to reduce the uncertainty of the results due to many heat gain and losses and air change that the room would be submitted to. Buried pipes and lighting were off during the whole period.

Table 14. Usage register of the room.

Date	***Time interval***	***Nº occup.***	***Equip.***	***Prototype openings***				***BIPVT openings***				***Window***	***Door***	***Blind***	***Heating***
				1	***2***	***3***	***4***	***1***	***2***	***3***	***4***				
22/01/2018 to 28/01/2018	00:00 – 23:59	0	1 dk									closed	closed	closed - 90º slat a.	Off
15/02/2018 to 22/02/2018	00:00 – 08:00	0	1 dk									closed	closed	closed - 90º slat a.	Off
	08:00 – 12:00	1	1 dk									closed	closed	closed - 90º slat a.	Off
	12:00 – 13:00	0	1 dk									closed	closed	closed - 90º slat a.	Off
	13:00 – 18:00	1	1 dk									closed	closed	closed - 90º slat a.	Off
	18:00 – 23:59	0	1 dk									closed	closed	closed - 90º slat a.	Off
04-02-2019	14:50 - 16:40	2	1 dk + 1 nb			x	x	x		x	x	closed	open	closed - 90º slat a.	Off
05-02-2019	10:00 - 15:00	2	1 dk			x	x	x		x	x	closed	closed	closed - 90º slat a.	Off
11-02-2019	11:00 - 18:00	1	1 dk + 1 nb					x		x	x	closed	closed	closed - 90º slat a.	Off
12-02-2019	09:25 - 17:00	1	1 dk + 1 nb			x	x	x		x	x	closed	closed	closed - 90º slat a.	Off
13-02-2019	08:45 - 12:00	1	1 dk + 1 nb			x	x	x		x	x	closed	closed	closed - 90º slat a.	Off
28-02-2019	07:45 - 16:00	1	1 dk + 1 nb					x		x	x	closed	closed	50% open - 90º slat a.	Off
06-03-2019	09:35 - 17:00	1	1 dk + 1 nb					x		x	x	closed	closed	closed - 45º slat a.	On
07-03-2019	09:15 - 12-:20	1	1 dk + 1 nb					x	x	x	x	closed	closed	closed - 45º slat a.	Off
	12:20 - 14:05	1	1 dk + 1 nb	x	x	x	x	x	x	x	x	closed	closed	closed - 45º slat a.	Off
	14:05 - 15:05	1	1 dk + 1 nb	x	x							closed	closed	closed - 45º slat a.	Off
	15:05 - 16:25	1	1 dk + 1 nb			x	x					closed	closed	closed - 45º slat a.	Off
	16:25 - 17:30	1	1 dk + 1 nb									closed	closed	closed - 45º slat a.	Off

08-03-2019	08:30 - 14:00	1	1 dk + 1 nb		x x x x	closed	closed	closed - 45º slat a.	Off
13-03-2019	09:00 - 11:40	1	1 dk + 1 nb			closed	closed	closed - 45º slat a.	Off
	11:40 - 16:55	1	1 dk + 1 nb	x x		closed	closed	closed - 45º slat a.	Off
14-03-2019	09:00 - 13:00	1	1 dk + 1 nb			closed	closed	closed - 45º slat a.	Off
	13:30 - 17:00	1	1 dk + 1 nb	automatic		closed	closed	closed - 45º slat a.	Off
19-03-2019	09:00 - 16:35	1	1 dk + 1 nb	automatic		closed	closed	closed - 45º slat a.	On
25-03-2019	07:50 - 17:00	1	1 dk + 1 nb	automatic		closed	closed	closed - 45º slat a.	Off

dk – desktop ; nb - notebook

4.3. Experimental analysis of BIPVT

The pre-existent BIPVT system, studied in this work, is the BIPVT element with the most extensive period analysed in the experimental campaign in the scope of this thesis, once was an already existent system installed in the Solar XXI building façade, with fully installed monitoring equipment and acquisition system. The BIPVT system is analysed in terms of system registered/measured temperatures and conductive heat flux, with thermal and η_e being calculated based on these results.

4.3.1. BIPVT – PV module temperature

A PV module exposed to the solar radiation has its temperature usually above the ambient temperature, being dependent on the solar radiation intensity, ambient temperature, and wind velocity, as well as the technology and structure used to compose this module. In the scope of this thesis, factors as wind velocity and impact of technology, material and structure are not analysed. Complementary analysis of the impact of different factors on the PV module temperature may be found in Kaplani and Kaplanis (2014). In Schwingshackl *et al.* (2013) there is a framework presented in how the wind effect may be included in the PV module temperature, and is significantly useful for studies in which the PV module temperature are derived from calculations. This sub-section aims to evaluate purely the PV module temperature by directly measuring the temperature in its interior surface, that is the surface direct in contact with the adjacent air cavity, as well as to use the obtained values for further theoretical calculation of the PV module electrical efficiency.

The yearly obtained values for the T_{pv} (Fig. 39), and in detail, the temperature fluctuations in February and July (Fig. 40), shows a considerable superficial temperature amplitude in the PV module, concerning its inner surface. Overall, during the year of 2018, the maximum temperatures can overcome 60 ºC, while the minimums can be as low as 0 ºC. It shows that the PV module, as is known, is a significant source of heat to interior air cavities when is exposed to direct solar radiation, to transfer heat to the room through convection and work as a heat recovery system. The high temperatures may, however, decrease the electrical efficiency of the photovoltaic generation – despite the present study focusing mainly on the potential of the

systems to reduce the nominal energy needs for heating to achieve comfort of the occupants of the adjacent thermal zone, for which the high temperatures of the PV module achieve the purpose.

In a short amount of time as a day, the temperatures show variations from near 60 ºC to near 5 ºC, showing the effect of the direct solar radiation in heating the module. It is possible to note that the peaks in colder months are higher than the peaks in warmer months, despite warmer months present lower temperature amplitude during the day. It is due to the solar angle in relation to the south façade.

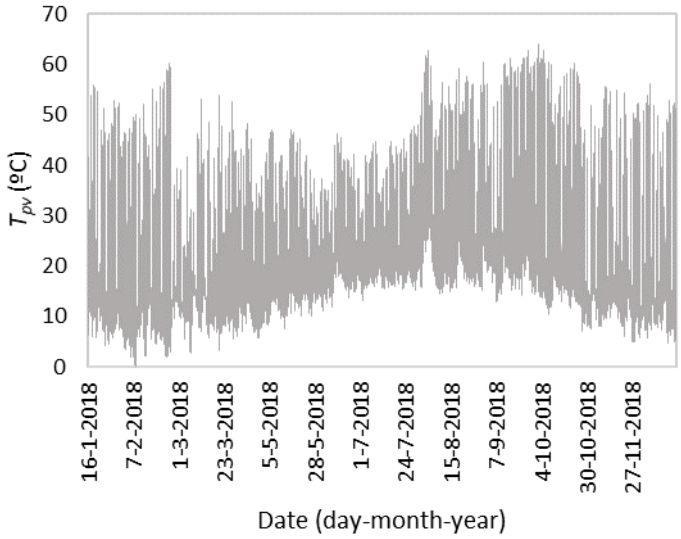

Fig. 39. (BIPVT) T_{pv} for the year of 2018 and first days of 2019.

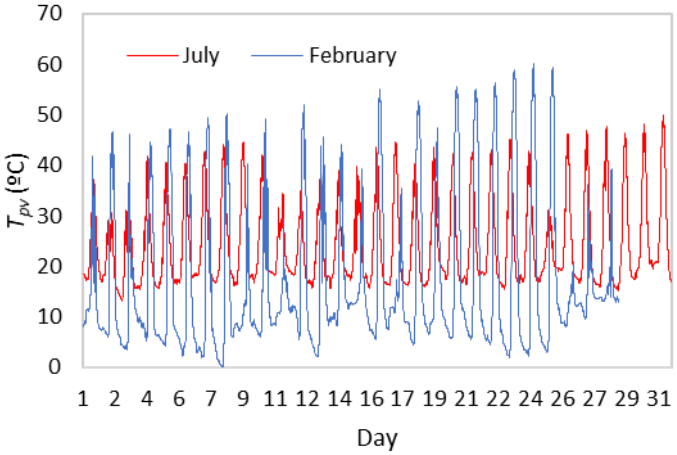

Fig. 40. (BIPVT) PV module data details of the February and July of 2018.

From the experimental values of PV module temperature, it is possible to conclude that the obtained values are higher than the ambient temperature during the sun exposition hours, being this an excellent passive source of heat to the adjacent air cavity, in which the circulating air will heat the adjacent thermal zone. The variation on the PV module temperature, as in February (Fig. 40), is very abrupt – having in about one third of the daily hours the temperature over 30ºC (as an example). However, to serve as a heat source, it is enough that the panel hits a higher temperature than the air cavity temperature. The PV module temperature profile, in BIPVT systems, seems to be adequate to the operation of the heat recovery system in usual working hours, as was the case of Solar XXI Building. In other hand, during the warmer months (having July as an example in Fig. 40), it is adequate to allow external air circulation, avoiding the overheat of the air cavity and increasing the electrical efficiency of the system by the reduction on the PV module temperature, once the system will not be operating to heating the test room.

4.3.2. BIPVT – air cavity temperature

As previously mentioned, the PV module temperature directly affects the air cavity temperature, once is the main source of heat during the sun exposure hours. In this context, this work follows by analysing the air cavity temperature. It considers the air cavity temperature for the BIPVT system as a punctual temperature obtained for half-height of the air cavity, due to the availability of only one sensor. However, it is important to highlight that the temperature within the air cavity is not homogeneous – and to complement the study in terms of sensor availability limitations, it is possible to see in the CFD analysis further presented the temperature contour of the system, aiming to demonstrate the temperature gradient both in horizontal and vertical directions. The temperatures of inlet and outlet are located at the bottom and the top of the system, as is further presented as a gradient value. The air cavity temperature is impacted not only by the PV module temperature, but also by the interior wall temperature (boundary between the system and the thermal zone), by the possible openings or leakage surfaces that allow the air mixing between the air from outdoor and/or air from indoors, and by the thermal bridges existent in the system.

Given these considerations, the experimental results of the temperature of the BIPVT air cavity

are shown in Fig. 41 and Fig. 42. During the year of 2018, the maximum air temperatures inside the air cavity (middle height of the system) are near 35 ºC, while the minimum air temperatures hit 1,47 ºC. The amplitude of the temperatures is lower during June/2018 and July/2018, with an increased minimum temperature when compared to the winter months. In August/2018 the T_{ac} hits its maximum registered, with 56,57 ºC. The annual average temperature of the air cavity is 19,13 ºC.

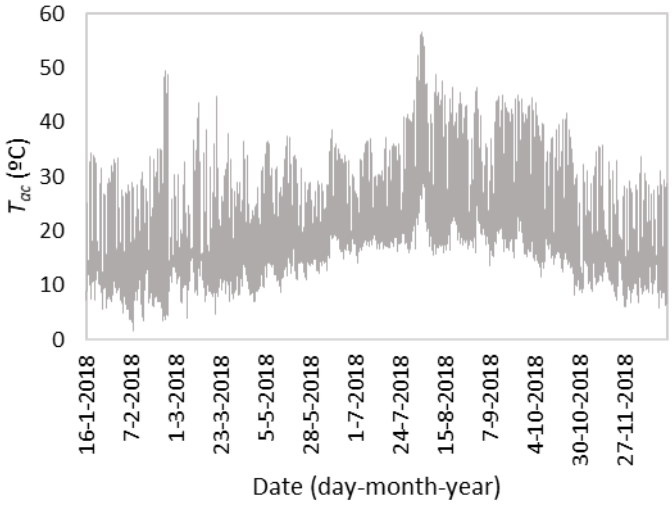

Fig. 41. (BIPVT) T_{ac}: a) Year of 2018.

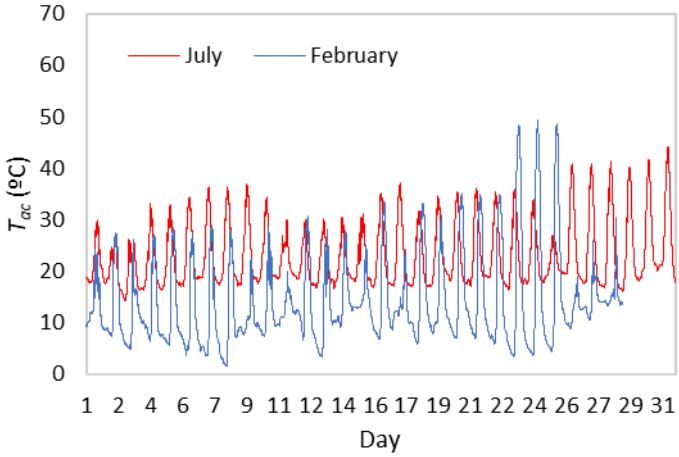

Fig. 42. (BIPVT) T_{ac} details of the February and July of 2018.

There are considerable daily fluctuations on the BIPVT T_{ac}, due to the thermal resistance of the PV module that separates this air cavity from the outdoors. The detail is presented in Fig 42, where it is possible to see that during the summer the daily BIPVT T_{ac} amplitude is lower than in the winter, also reflecting in smaller differences between the inlet temperature (T_{inl}) and outlet temperature (T_{out}) (presented in the next sub-section), which is also influenced by the

room temperature and would be later reflected in efficiency reduction, since the efficiency calculation formula is based on the temperature gradient. During the month of February, during all the registered days the T_{ac} was, for the hours with higher sun exposure, higher than the minimum established comfort temperature, meaning that the system would be useful for heating the adjacent thermal zone and contributing to raising its temperature by the convection generated due to the temperature gradient within the air cavity. The obtained results for the air cavity temperature are similar to other BIPVT system prototype previously evaluated the Solar XXI façade (L. Aelenei, Pereira, and Gonçalves 2013) from previous years, despite this thesis presenting a significant improvement in terms of data set size, being more representative in terms of periods of analysis.

4.3.3. BIPVT – temperature gradient

As previously mentioned, being the PV module temperature is the main source of heat to the air cavity, within the air cavity a temperature gradient is generated due to convection. This temperature gradient (ΔT) refers to the temperature difference between the inlet and the outlet of the BIPVT system at a given moment, and is responsible for the convective heat flux generated by the system when calculating its further thermal efficiency.

In Fig. 43, the ΔT between the outlet and inlet registers of the temperature sensors is calculated and shown. During the winter months, the ΔT is more elevated due to the lower T_i in comparison to summer months, and to the higher values of G_D due to the solar angle in winter. For the monitored period, these values could reach 14 ºC in some peaks, although in general, they reached near 6 ºC. Despite being a low temperature gradient value, 6ºC is enough for the system to actuate as a heat recovery source if the thermal zone temperature is lower than the air cavity temperature.

In the summertime, the ΔT assume values as low as 1 ºC, being possible to see even a few periods in which the T_{inl} are higher than the T_{out}. As is possible to see in the detail of (Fig. 44), the amplitude is higher during February in an order varying from 4 ºC to 13 ºC. This factor will also be reflected in the thermal performance of the system under real-condition testing.

As expected, during most part of the year the T_{out} is higher than T_{inl}. The ΔT in a system

impacts as well in the airflow velocity, once the heat source will generate a vertical upwards air flow within the air cavity due to buoyancy forces resulting from density differences due to temperature variations.

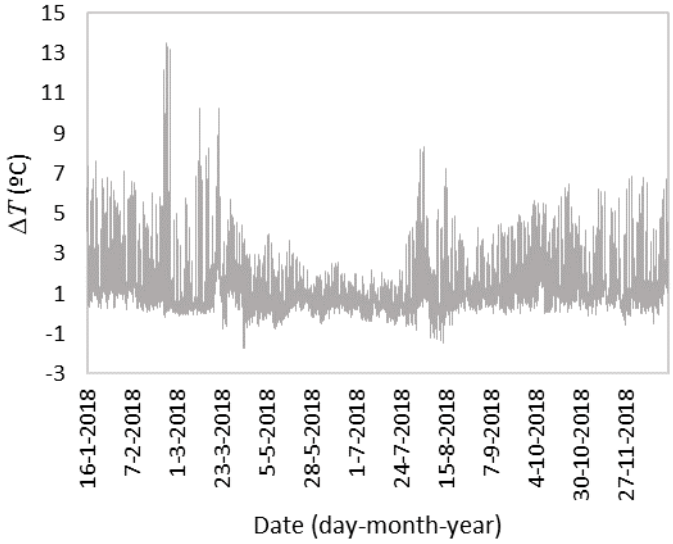

Fig. 43. (BIPVT) ΔT (outlet-inlet) temperatures (2018).

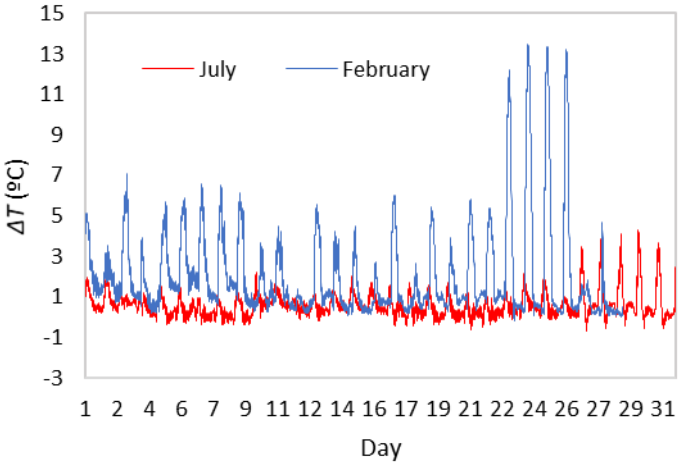

Fig. 44. (BIPVT) ΔT (outlet-inlet) data for February and July, 2018.

4.3.4. BIPVT – the relationship between physical quantities

The relationship between the measured variables is also important to highlight. The relationship explored in the scope of this work, for the BIPVT system, is the relationship between T_{ac} and T_{pv}. It is recognized that the T_{ac} is not dependent only of T_{pv}, having the T_{amb} and T_i also

impact on the temperature of the air cavity. However, as this is a BI-SES under analysis, the T_{pv} results mainly of the solar radiation exposition, and the PV module is the major heat source of the system under operating hours. For this reason, this relationship is here assessed.

Fig. 45 shows the results for the relationship between the annual T_{ac} and T_{pv} in a scatter plot. As it is possible to see, there is a positive correlation. As the T_{pv} increases, the number of possible values for the T_{ac} do also increase, meaning that for a certain T_{pv}, a broader range of T_{ac} values exist. The lower the T_{pv}, more concentrated are the possible values for the T_{ac}. In some cases, the T_{ac} can be slightly higher than the T_{pv}, due to the thermal gains in the room, thermal inertia of the interior wall and possible position of the vents. The best-fit line that represents this relationship (and that are further presented for the prototypes in the next sub-sections) is characterized as being the approximation of this relationship (T_{pv} and T_{ac}) demonstrated by the graph equation.

In order to make this relationship more specific according to the season (as Fig. 45 presented the values for the whole year), the same relationship is explored containing only the data for February 2018 (Fig. 46-a and Fig. 46-b) and for July 2018 (Fig. 47-a and Fig 47-b), with detail for the temperatures fluctuations. Similar behaviour was found for the winter month (Fig. 46-a), while a very concentrated behaviour was obtained for the summer month (Fig. 46-b).

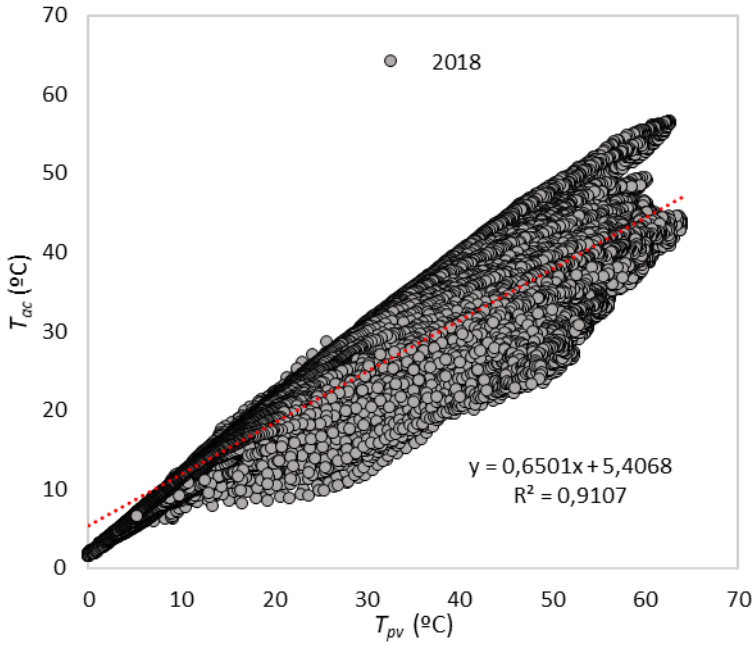

Fig. 45. (BIPVT) Relationship between air cavity and T_{pv} for the entire year of 2018.

The R^2 value refers to the goodness of fit and is a fraction between 0,0 and 1,0. The higher the

R^2 value, the more accurate the prediction of the relationship may be considered. It is necessary to recognize, however, that the R^2 has its limitations, once cannot be used to determine is there is any kind of bias in the acquired data under analyse. In the scope of this study, it only aims to provide preliminary insights over the relationship. Considering the data presented in Fig. 46 and Fig. 47, it demonstrated that the relationship is broader during winter (with less confidence), while is more straightforward during the summer (with more confidence), increasing the predictability accuracy. The night periods have considerable impacts over the results of the best-fit line, once during the night the temperature is very similar to the air cavity temperature, and as so may be considered a bias in the relationship results, once the hours in which the PV module is cool due to the lack of solar availability are almost half of the day.

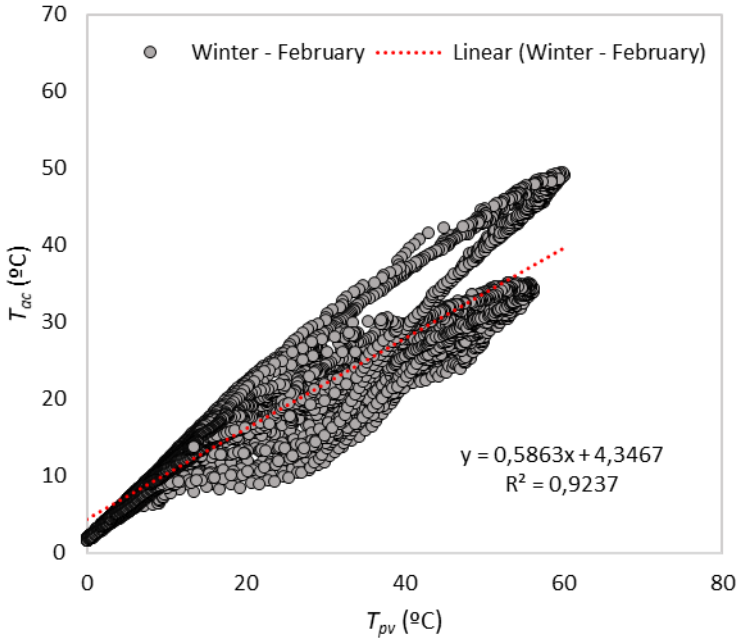

(a)

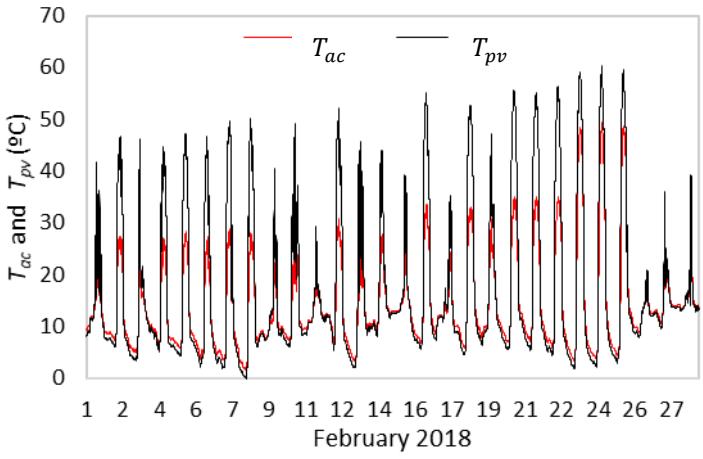

(b)

Fig. 46. (BIPVT) a) Relationship between air cavity and T_{pv} for winter time; and b) comparison between temperatures.

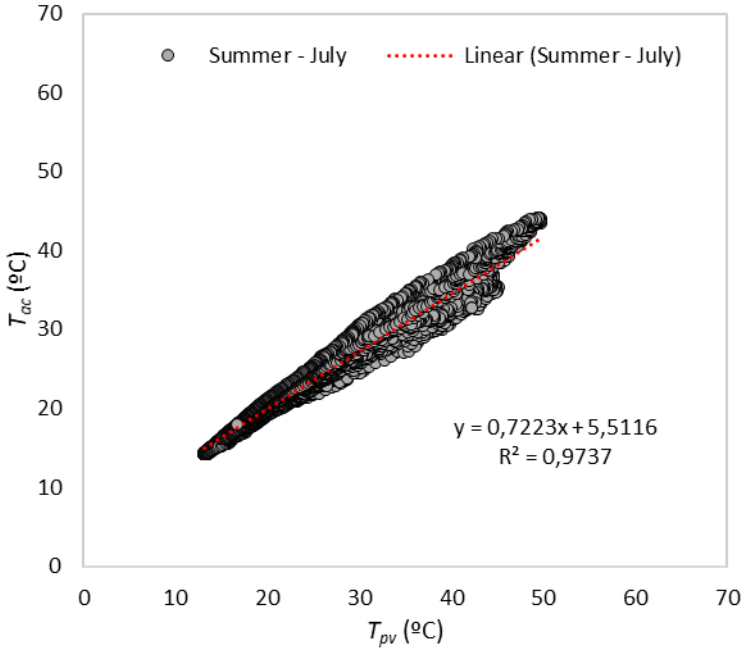

(a)

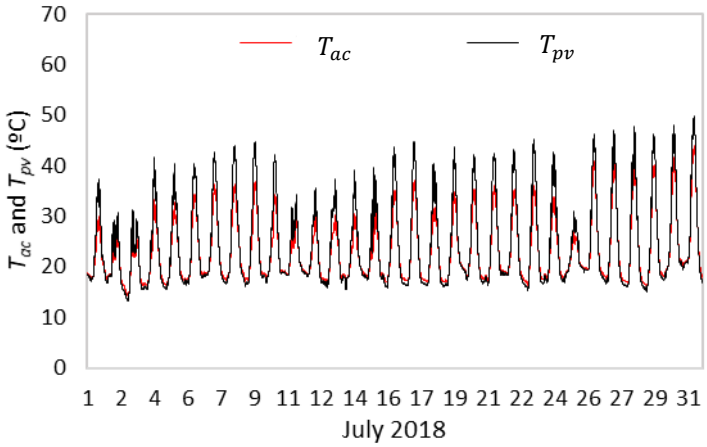

(b)

Fig. 47. (BIPVT) a) Relationship between air cavity and T_{pv} for summer time; and b) comparison between temperatures.

Considering the different temperature sensors present inside the system (air cavity, PV module, inlet, outlet) and outdoors, there are outlier temperatures, superior to what is considered the statistical maximum of the year under the register. During the year, 50% of the T_{ac} are between 13 ºC and 24 ºC, while 50% of annual T_{pv} are between 14 ºC and 28 ºC. Annual temperatures of the outlet are slightly higher than the inlet, confirming that the existent q_v alongside the air. The difference between outlet and T_{inl} will also reflect on the η_t of the system. As a conclusion for this relationship, despite being clearly related, it is unconvinced to treat temperature of air

cavity as a single-valued function of PV module temperature, because the performance of BIPVT system is affected by many other factors. The relationship between the variables could be improved by creating a broader set of variables (as adding ambient temperature as well), and also the co-relation analysis would be benefited to associate delay periods to each measured variable, as a couple of hours to days before the period in question.

4.3.5. BIPVT – daily analysis

This sub-section presents the detail of a daily analysis, considering a winter day in which it is pertinent to the operation of the BIPVT system, and good sun-exposure weather conditions. The daily analysis of the registered values and calculations for the heat recovery BIPVT system is done considering the day of January 11th, 2019. The interior vents of the system were opened at 10:45h and closed at 15:15h. Fig. 48 presents the registered values for the 24h of the day. It is possible to see the effect of the opening of the vents on the temperature of the air cavity, being responsible for a decrease of nearly 9 ºC at the moments that followed 10:45h (from 40 ºC to 31 ºC).

The PV module hit approximately 55 ºC, slightly decreasing the temperature parabola with the opening of the vents. The system temperature achieved a difference of almost 20 ºC from the T_{amb}, due to the solar gains on the PV modules, the thermal inertia of the interior wall and T_i. It is also possible to note the excellent insulation of the interior wall when analysing the values from the heat flux sensor, which slightly vary from 5 W/m^2 to 48W/m^2. On the other hand, the heat flux through the PV module achieved values of 210W/m^2 at noon. During the vents opening hours, it is possible to see the detailed profile in Fig. 49. The registered air velocity in the inlet, for the period under investigation, was 0,01m/s (manual measurement with anemometer sensor, punctually during few minutes in the operation hours). It is essential to highlight that the air velocity in the inlet, for the BIPVT system, was not measured on a constant basis due to the lack of a permanent sensor, and intrinsically vary during the day and the period of the year – due to many factors impacting on the air movement.

Due to the thermal inertia, it is possible to see that the system still slightly increases the temperature even with the decrease of the G. The T_{out} is lower than the T_{ac} in the order of 2 ºC, due to the air mixing in the outlet, between the system air at a given temperature and the room

air at another given temperature. Also, a difference of almost 10 ºC was registered between the T_{out} and T_{inl}. The energy performance and efficiencies will be discussed in another section.

Few minutes before the opening of the system, there is an abrupt reduction on the heat flux through the PV module, meaning that the direction of the flux shifted. This value is mostly impacted by solar radiation exposure and increase on the air cavity temperature, which is higher than the ambient temperature. Besides the measured variables presented here and the impact of the vents opening on the system thermal behaviour, other variables that are not under control and monitoring may be impacting the system, as the wind speed.

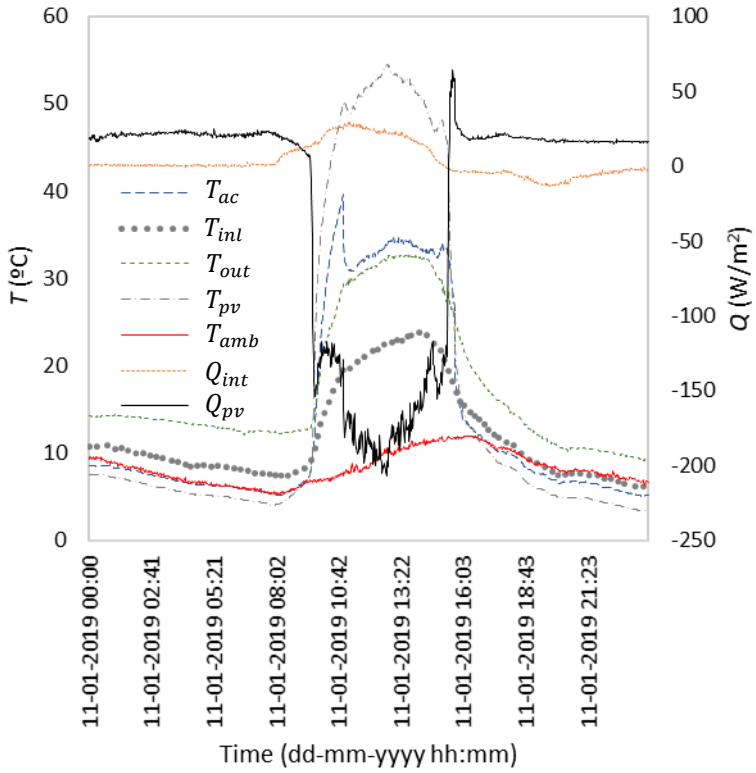

Fig. 48. (BIPVT) Daily behaviour of the system under manual operation, opened at 10:45h and closed at 15:15h.

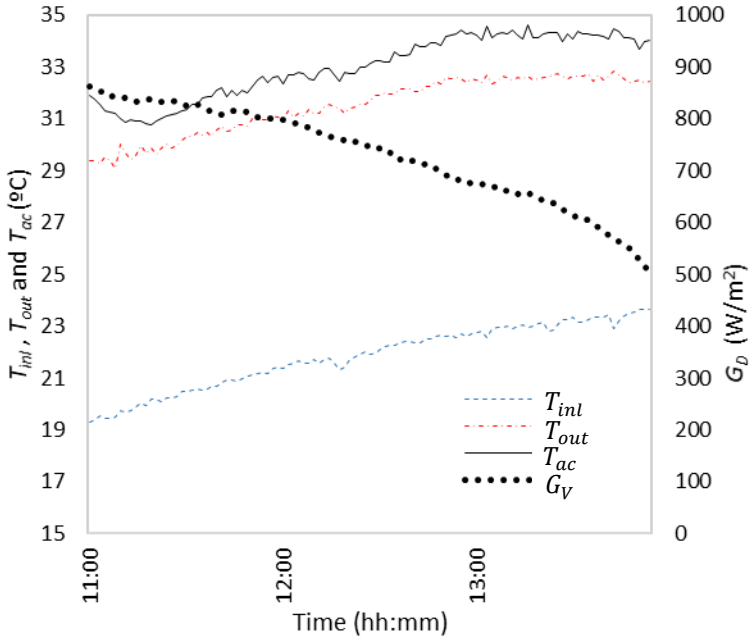

Fig. 49. (BIPVT) Detailed profile during the opening hours.

4.4. Experimental analysis of BIPVT Prototype (a, b)

Following the study of the pre-existing system, this section presents the experimental analysis of the new BIPVT prototypes. The results for the experimental analysis concerning the new prototype designed are discussed in this sub-section, for each parameter under study in the measurement campaign. The prototype P1a is constituted by the interior module made of EPS, while P1b is formed by the interior module made of a water tank. The testing was performed both in manual and automatic mode of vents controlling for both interior modules. The manual mode and automatic modes were previously presented in the case study description. For the Prototype P1a, the manual mode was tested first, from 13/02/2019 to 13/03/2019. The period of testing in automatic mode followed the period in manual mode, namely from 14/03/2019 to 21/03/2019.

In this day (21/03/2019), the EPS interior module was changed by the water tank interior module (so called here Prototype P1b) that was tested first in automatic mode (from 22/03/2019 to 09/04/2019) and then in manual mode (from 11/04/2019 to 23/04/2019). The climatic conditions for all the periods are the ones presented for the first semester of 2019, in the first sub-section of this chapter (weather data), and for this reason, will not be repeated here. It is valid to highlight that, due to the tightness of the water tank in the aluminium frame and also

the weight of it, and the water tank was slightly more away from the PV surface (near 1 cm more than the P1a during its experimental campaign).

4.4.1 Prototype (a, b) PV module temperature

The results for the T_{pv} are measured in the three sensors' height, aiming to provide a more broad evaluation than in the previously presented BIPVT system, in which only one sensor was available to represent this variable. As was possible to see in previous studies, thermographic analysis confirm that there are variations of temperature in different points of a same PV module submitted to same solar exposure conditions, having the middle height of the system usually higher temperatures (Bazilian, Kamalanathan, and Prasad 2002; Tsanakas, Ha, and Buerhop 2016).

The results for the P1a are shown in Fig. 50, for the manual operation mode. It is possible to see that the middle height of the PV module is the section that reaches higher temperatures, in accordance with other results obtained in the literature (Bazilian, Kamalanathan, and Prasad 2002; Tsanakas, Ha, and Buerhop 2016), when compared to the bottom and top heights, despite having similar values. During the cold periods of the modules, namely at night, there are no considerable differences concerning the temperature in different heights of the module (that may be inferior to 1 ºC), while during the day the differences may reach values near 10-20 ºC). This difference is more noticeable, however, in Fig. 51 for the automatic mode of operation of P1a, due to the lower period under the register and larger scale in the X-axis, does not mean that the gradient of the air temperatures in different heights is higher.

Similar behaviour may be observed for the P1b in both automatic (Fig. 52) and manual (Fig. 53) modes. In Fig. 51 and Fig. 52, it is possible to see a modification in the sampling rate of the measures, being responsible for a more extensive day period in the X-axis. In the automatic mode of both interior modules (P1a and P1b), it is possible to see that the differences between middle and top/bottom are higher because in the inlet and outlet the air is mixing more consistent with the room air at a given temperature, is also responsible for extracting heat of the PV surface in the given heights.

This PV module temperature results for the prototypes are similar with the BIPVT results for the same variable under analysis, and for the same period of the year.

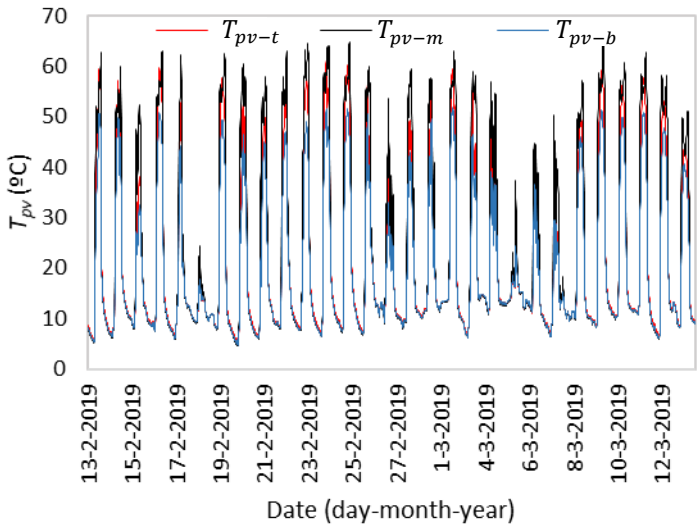

Fig. 50. (P1a) T_{pv} in manual mode.

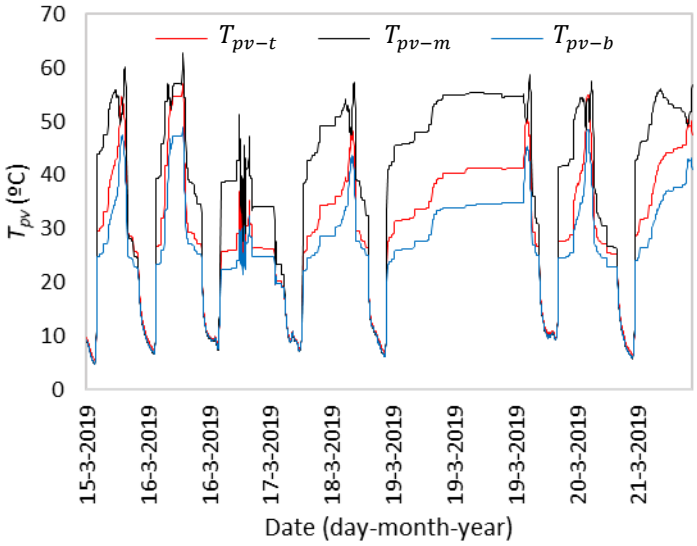

Fig. 51. (P1a) T_{pv} in automatic mode.

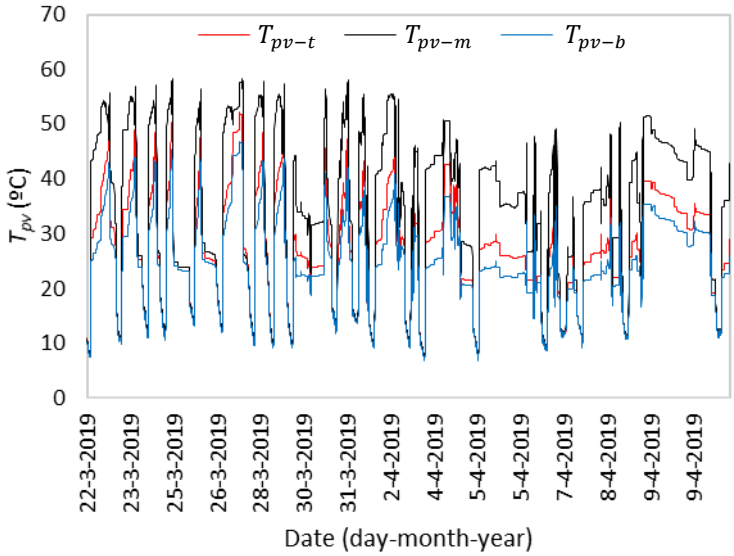

Fig. 52. (P1b) T_{pv} in automatic mode.

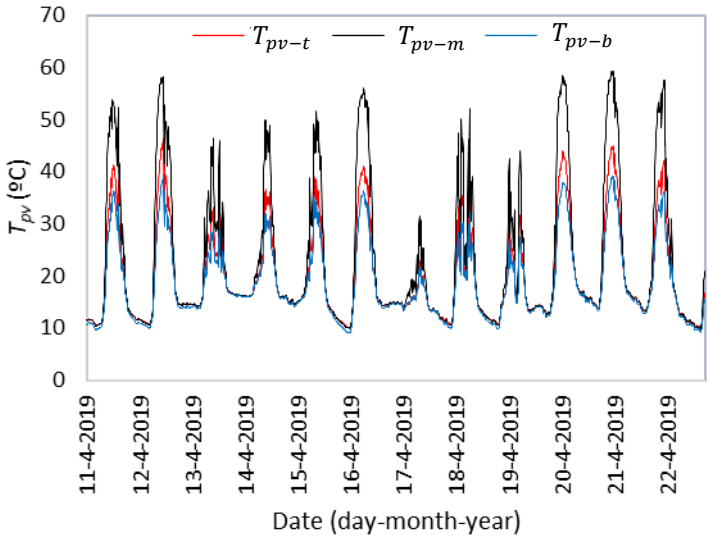

Fig. 53. (P1b) T_{pv} in manual mode.

4.4.2 Prototype (a, b) air cavity temperature

Following the same presentation of variables as presented in the BIPVT results, this sub-section presents the air cavity temperature for the Prototype. The T_{ac} obtained results shown presented in Fig. 54 and Fig. 55 for the manual mode of operation and automatic mode of operation, respectively, for P1a. It is possible to see that the temperature is higher in the middle of the air cavity duct, followed by the outlet and then T_{inl} of the air. These results are similar to the superficial temperatures of the PV module, once the PV module is the primary source of heat.

As so, the temperature stratification inside the air cavity is significant during the day, in which the PV module works as a heat source due to its high temperature. In the outlet height, the air cavity temperature is very similar to the temperature in the middle of the system height, being slightly lower. It is due to the PV module temperature different between middle height and top, and a couple of possible reasons that are not monitored or under control: i) the existence of thermal bridges in the vents that are separating the air cavity from the indoor and outdoor; ii) opening of the vents; iii) infiltration through the vents that causes air mixing/backflows.

The T_{ac} hit maximums between 47 ºC and 50 ºC at its maximum and near 7º as its minimum during the registered period. During the night period, the temperature in the middle of the air cavity is inferior to the inlet and T_{out}, due to the sensor being closer to the PV module while the inlet and outlet sensors are closer to the room. In the automatic mode, the behaviour in terms

of temperature segmentation is similar. However, the maximum temperatures were reduced, with only one peak near 45 ºC, also due to the increased interaction with the room air at a different temperature due to the more constant opening of the vents. At night, the temperatures are similar between the periods of manual and automatic operation modes.

The results for the automatic mode of P1b are shown in Fig. 56, while the manual mode is presented in Fig. 57. In contrast with what is observed for the P1a, it was observed in the P1b results that the air temperature in the outlet was higher than in the middle height of the air duct, during almost all the period. Although a direct comparison is not possible due to the differences in the weather and room experimental results due to the campaigns not happening at the same day/time, one of the possible reasons may be attributed to the thermal characteristics of the interior module. . It is necessary to highlight that no direct comparison is possible in this point, once the operational conditions of the room vary as well as the outdoor climate. The operation modes were not tested under precisely same conditions.

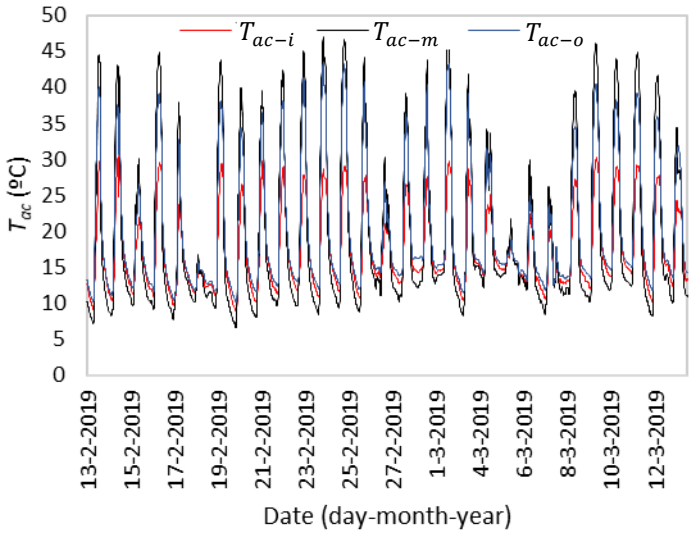

Fig. 54. (P1a) T_{ac} in manual mode.

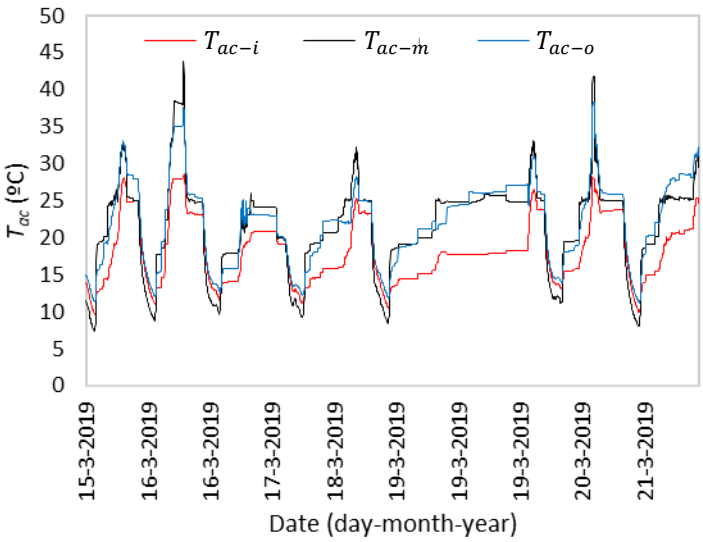

Fig. 55. (P1a) T_{ac} in automatic mode.

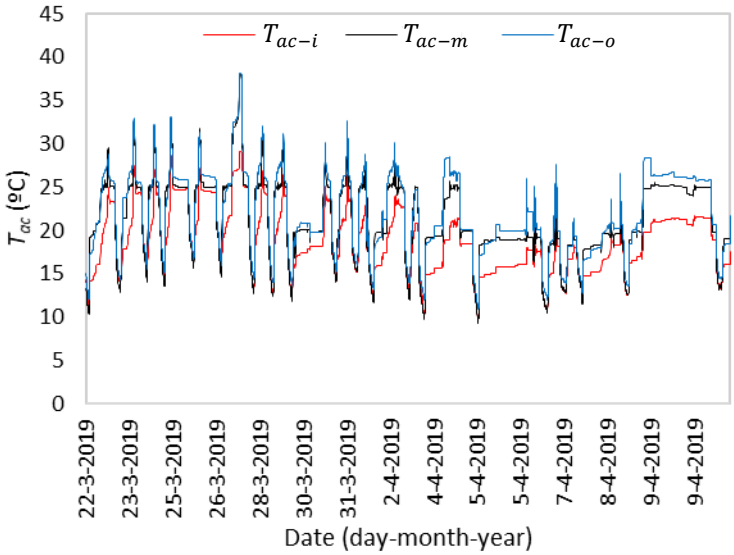

Fig. 56. (P1b) T_{ac} in automatic mode.

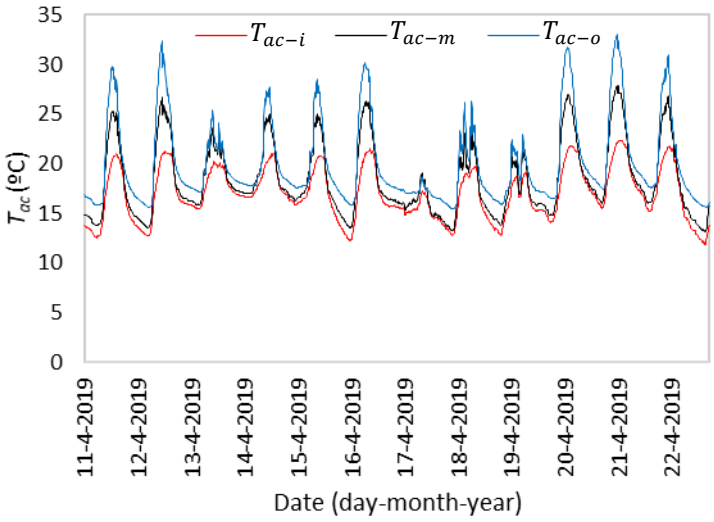

Fig. 57. (P1b) T_{ac} in manual mode.

4.4.3. Prototype (b) water tank temperature

The use of the water element in the prototype aims to serve as a thermal energy storage, due to the thermal properties of the water in storing heat and elevated thermal inertia. This section presents the results for the temperatures of the exterior and interior wall of the water tank, and the water inside the tank.

The results are shown in Fig. 58 and Fig. 59, for the automatic and manual operation of P1b (prototype with water tank as an internal module), respectively. In the day 23/04/2019, the temperature sensor presented two register faults, as is possible to see in Fig. 59, but the faults does not affect the overall data registered.

The temperatures of the exterior and interior surfaces of the water tank are higher than the water temperature during the day (nearly 2 ºC to 5 ºC), in which there is a source of heat from the air cavity. In contrast, during the night, the temperatures of the water and interior surface are higher (nearly 2 ºC) than the exterior surface, demonstrating the capability of the tank to work as a storage module.

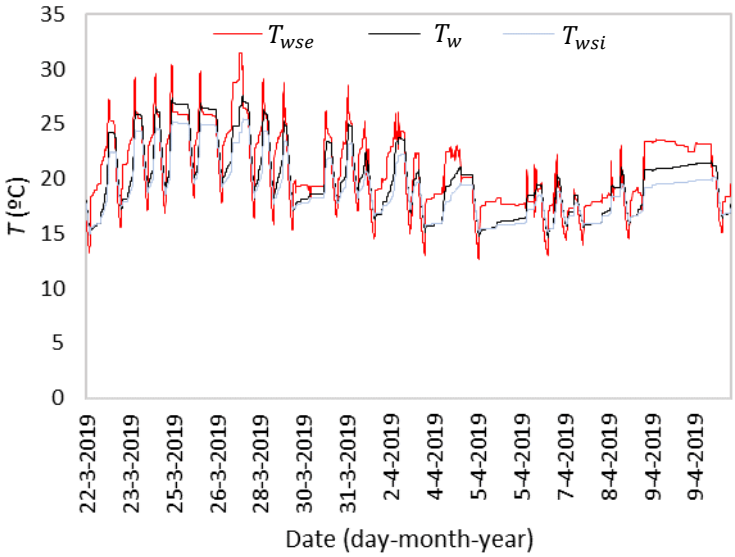

Fig. 58. (P1b) Water tank temperatures in automatic mode.

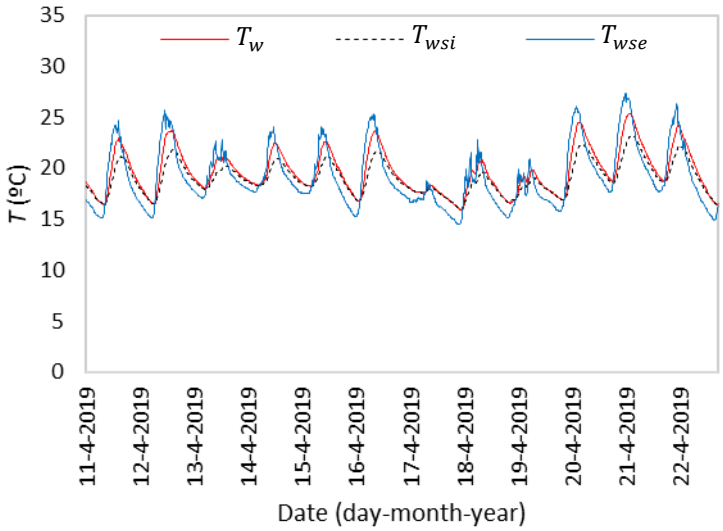

Fig. 59. (P2a) Water tank temperatures in manual mode.

4.4.4. Prototype (a, b) airflow velocity

The airflow velocity (m/s) in the outlet of the air cavity for the P1a in manual and automatic operation modes, respectively, are shown in Fig. 60 and Fig. 61. A minor register fault happened in P1a during a manual operation mode, as is possible to see in the graph. Fig. 62 and Fig. 63 shows the results for the P1b in automatic and manual operation modes, respectively. It

is to note that the anemometer is located in the outlet of the system, and there is no anemometer in the inlet. The obtained values are, however, noise and do not represent the proper values actually existent in the system in the experimental campaign periods. It happened because the airflow velocity within the system was extremely low, and did not achieve the minimum value within the measurement scale of the equipment.

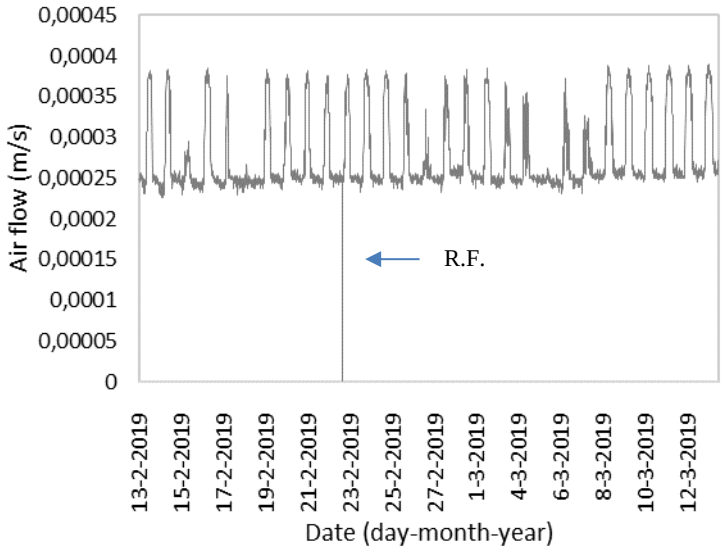

Fig. 60. (P1a) Outlet airflow velocity in manual mode.

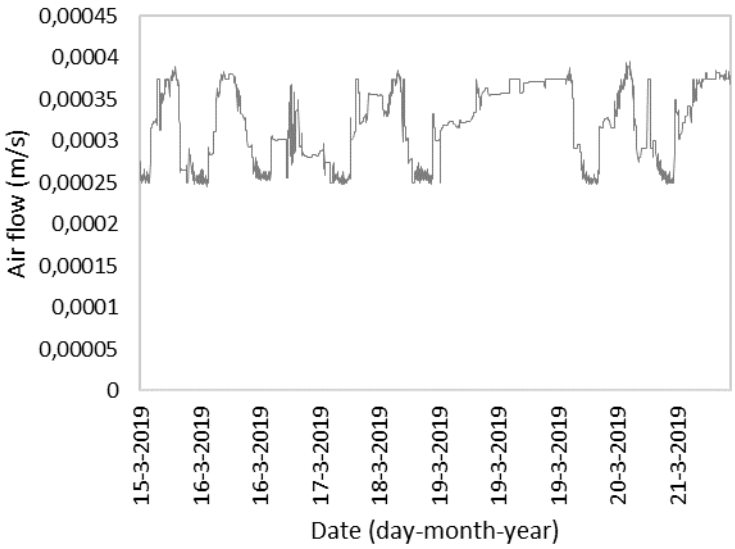

Fig. 61. (P1a) Outlet airflow velocity in automatic mode.

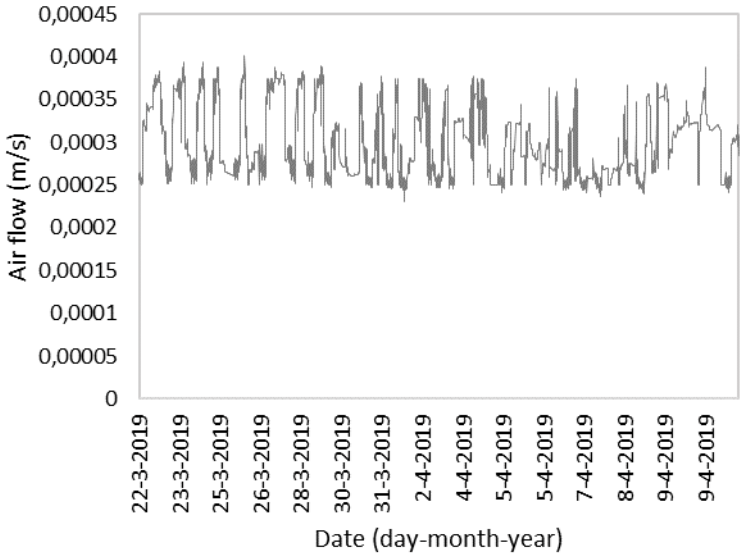

Fig. 62. (P1b) Outlet airflow velocity in automatic mode.

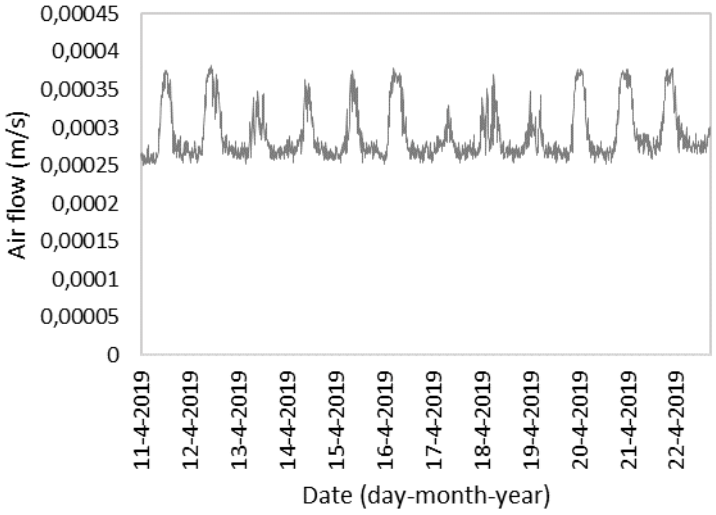

Fig. 63. (P1b) Outlet airflow velocity in manual mode.

4.4.5 Prototype (a, b) conductive heat flow

The interior element of the system act as a barrier between the air cavity and the adjacent thermal zone, in order to insulate and allow the air to circulate from the inlet to the outlet. However, it also transfer heat through conduction, and the results concerning this variable are presented in this sub-section.

The observed conductive heat flux through the interior EPS module (P1a) is shown in Fig. 64

and Fig. 65, for manual and automatic operational modes, respectively. By the results, it is possible to note that the flux happened, during the mentioned experimental periods, from the air cavity to the room, and did not happen, during the observed period, in the opposite direction (from room to air cavity).

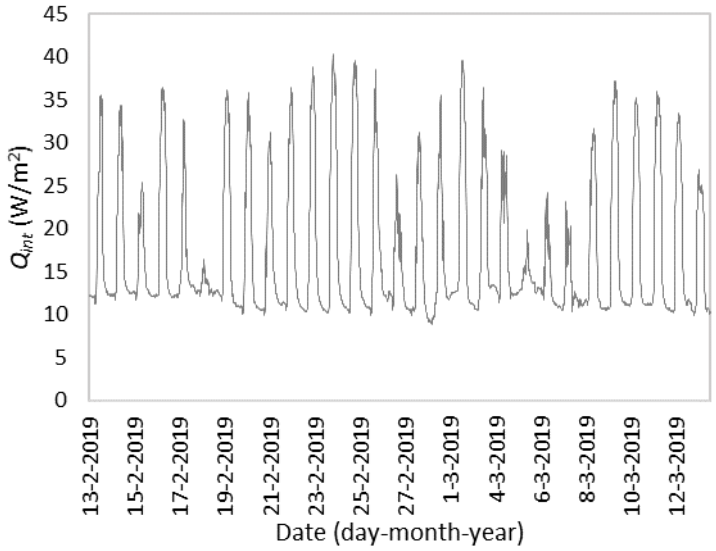

Fig. 64. (P1a) EPS heat flux in manual mode.

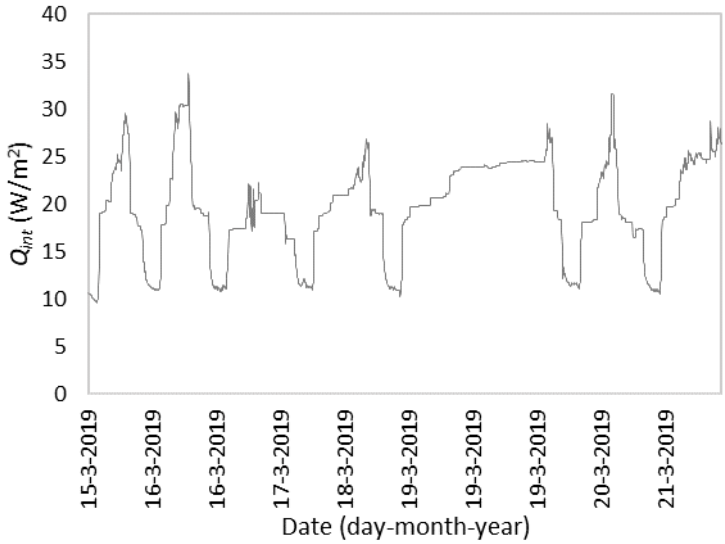

Fig. 65. (P1a) EPS heat flux in automatic mode.

The heat flux results for the water tank were made through calculation, once the sensor presented errors in operation due to bad installation of the same. The calculation considered the temperatures in both sides (interior and exterior) of the water tank and the properties of the materials. Fig. 66 presents the results for the automatic operation mode, and Fig. 67 for the manual operation mode. Contrary to what was observed in the EPS model, in which the flux

occurred only in one direction, in the water tank there were situations in which the flux inverted the direction, from the room to the air cavity. These periods happen at night when the primary heat source (PV module) decrease its temperature.

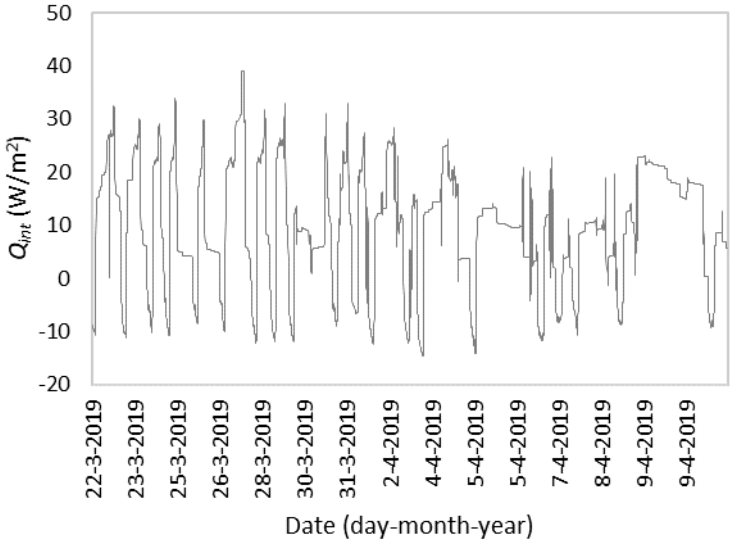

Fig. 66. (P1b) water tank heat flux in automatic mode.

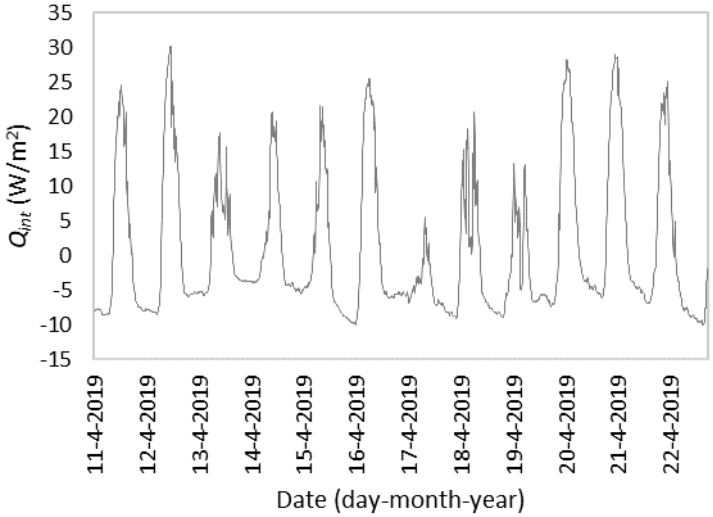

Fig. 67. (P1b) water tank heat flux in manual mode.

4.4.6. Prototype (a, b) operation of the vents

One of the most fundamental aspects of the prototype design was the automated function. The

automation of the prototypes was reflected in the operation of the vents that allowed the air circulation throughout the openings, for different purposes according to the temperature setting of the system, room and outdoors, as was presented in the scheme of Fig. 21. The analysis of the vents opposition and moment of operation is essential to determine the behaviour of the system and which objective the algorithm was operating to meet at a given point. The operation of the vents was also obtained through the data acquisition system, and in the following graph, the opening positions were represented by binaries, being 0 corresponding to closed and 1 corresponding to open.

In the scope of this work, in which the general aim was to improve the thermal comfort of the occupants of the test room, the exterior vents were not opened in the manually operated testing periods. It is to notice that, in many cases, the usual occupants of the buildings do not have enough time or awareness to operate a BI-SES in each moment manually it is needed. The occupants can sensorially feel thermal discomfort and operate the prototype in order to feel the room – but hardly will operate it in the reverse way, when the room does not need it, but the exterior opening would be useful to cooling the PV modules in order to increase the η_e of the system. In the scope of laboratory testing, it is viable but complicated to implement in the case of future market dissemination. It is common sense that the occupants visualize smart buildings and energy building components as independent systems. In other words, the occupants aim to have a smart operation that does not require the system to be directly (and time-consuming) operated by them. The feeling of systems' modernity in building terms includes a more sustainable and comfortable building, as well as less time consuming to be operated.

The operation happened when the room occupant judged relevant to operate the system due to observable environmental conditions. During the P1a testing period, only the interior vents were opened, in three distinct periods, while the vents facing the outdoor were always closed.

In contrast with the manual operation previously presented, the operation of the vents in the automatic mode of P1a is presented in Fig. 68. The vents were operating, in automatic mode, not only to benefit the indoor heating but also to cooling the PV module during the times when it was pertinent given the setpoints determined. In general, by the observation of the operation of the vent in automatic mode, it is possible to conclude that there is a very complicated dynamic scenario of vents operation, accounting with several periods in which the vents were opened and closed during the whole testing period in automatic mode. Same behaviour was observed for the prototype P1b.

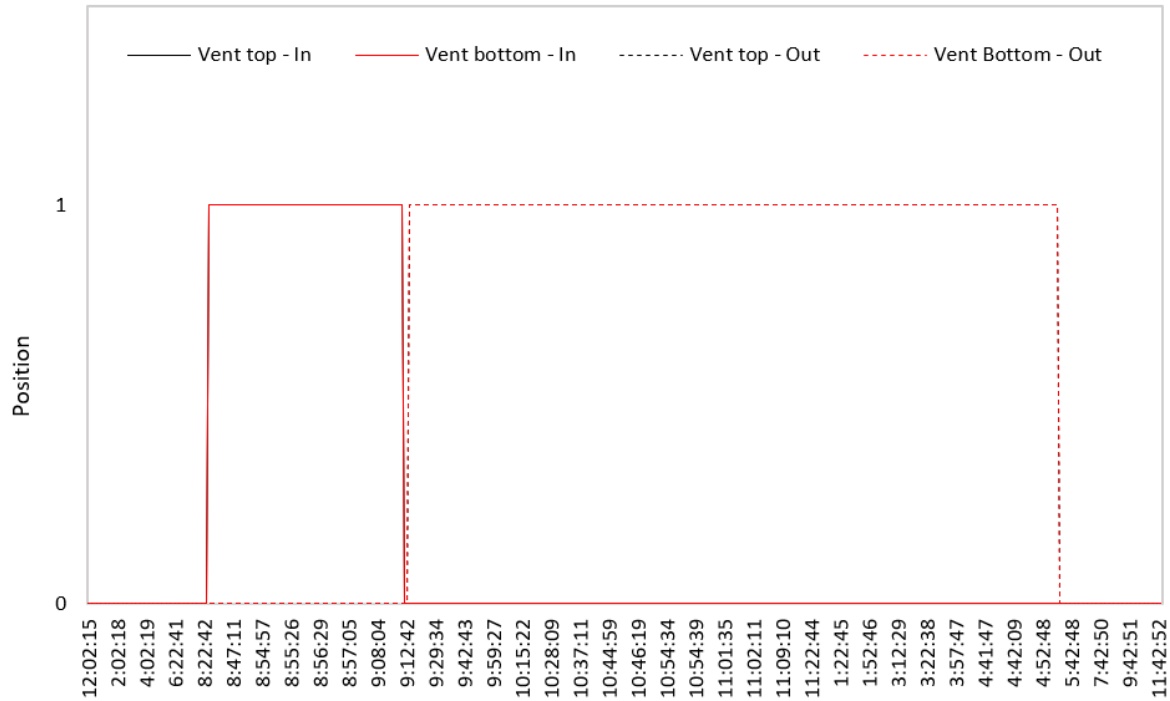

Fig. 68. (P1a) Vents opening in automatic mode (21/03).

4.4.7. Prototype (a, b)– the relationship between physical quantities

Considering the new prototype system, the relationship between the different variables in appreciation (T_{ac} and T_{pv}) are also studied, as in the BIPVT system and for the same reasons.

Fig. 69 presents the relationship between the T_{ac} and T_{pv}, for P1a in manual operation mode. At lower T_{pv}, there is no considerable variations in the T_{ac} (recorded values are more concentrated). By the time the T_{pv} increases, in similarity to the BIPVT behaviour previously presented, the number of possible values for the T_{ac} do also increase (the concentration in lower). In this case, no considerable value for the T_{ac} was higher than the T_{pv}, except in shallow temperatures of the night periods. The linear line that represents the relationship is characterized as being the approximation demonstrated by the graph equation. Details concerning the data of the temperature profile fluctuations that generated this graph are presented in Fig. 70. For the automatic operation mode, the same results are presented in Fig. 71 and Fig 72, is to note that the number of registers is lower.

Although having a smaller number of data samples (nearly one month of registers) than in the

BIPVT system, the P1a in manual mode presented an elevated value for the R^2 of the best-fit line. For the automatic mode, the number of registers is even smaller (a week), reflecting in the reduced R^2 of the best-fit line. A larger number of samples in the data set of the automatic period could provide a more reliable approximation. The differences between manual and automatic may lay on the fact that the automatic operation is much more active during the day than in manual operation mode, contributing to keeping the T_{ac} nearly 10ºC lower (in the peak temperature hours) than in the manual mode, while the T_{pv} is similar in both operation modes.

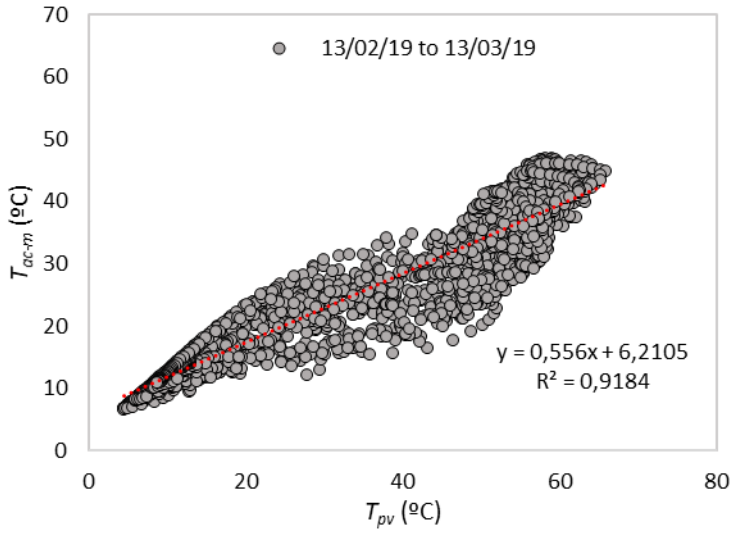

Fig. 69. (P1a) Relationship between $T_{ac}$and T_{pv} for the manual operation period.

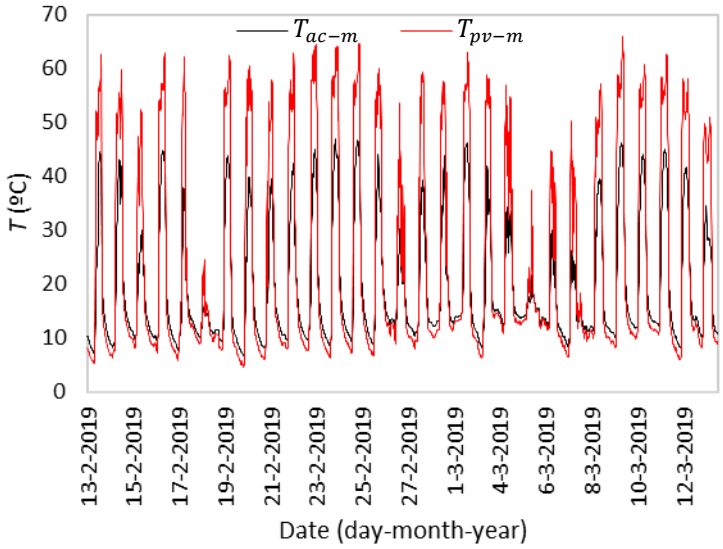

Fig. 70. (P1a) T_{ac} and T_{pv} for the manual operation period.

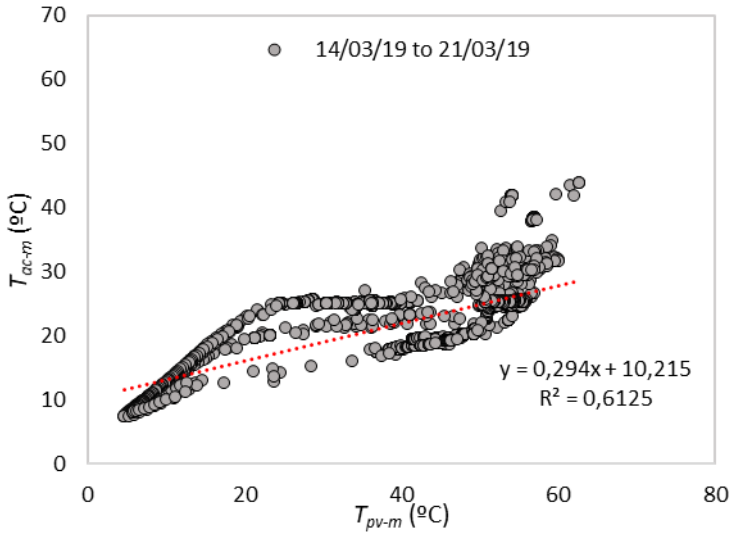

Fig. 71. (P1a) Relationship between T_{ac} and T_{pv} for the automatic operation period.

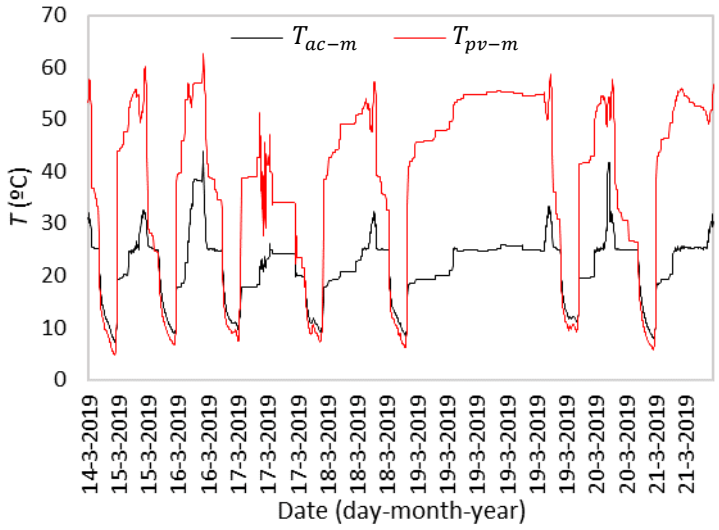

Fig. 72. (P1a) T_{ac} and T_{pv} for the automatic operation period.

Considering the P1b, the results are shown for automatic operation mode in Fig. 73, and temperature details in Fig. 74. The results for the manual operation mode are shown in Fig. 75, and the temperature details in Fig. 76. Despite not being directly comparable once the boundary conditions are not the same for the two testing periods concerning P1a and P1b, it is possible to see that the R^2 values for the P1b are smaller than for P1a, both for the manual and automatic periods. It is possible to notice a decrease in R^2 with the reduction in the number of samples of data in the scatter plot, as one of the possible causes of the decrease in the best-fit line accuracy.

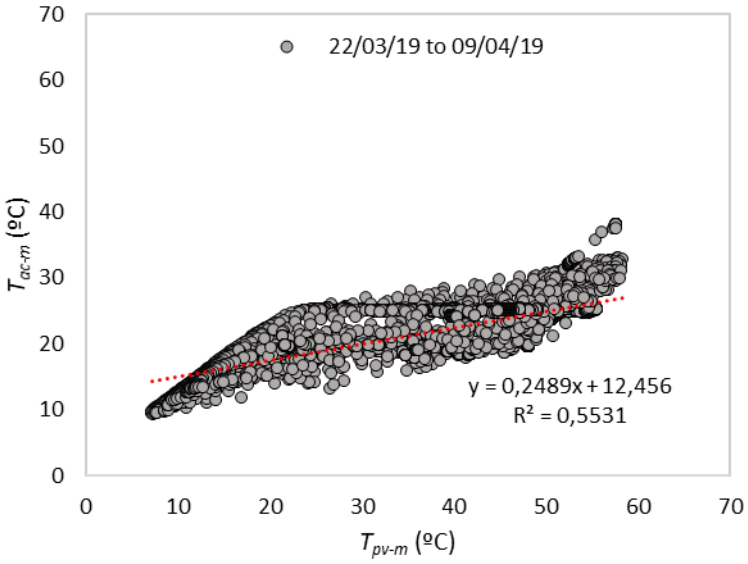

Fig. 73. (P1b) Relationship between air cavity and T_{pv} for the automatic operation period.

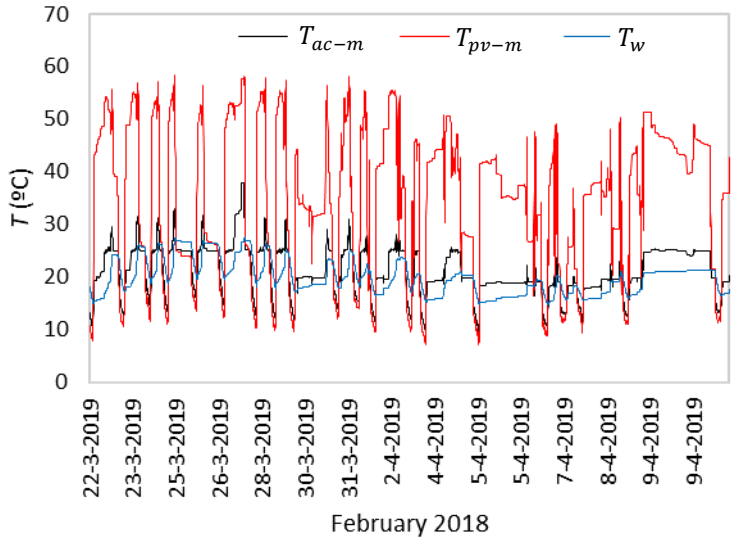

Fig. 74. (P1b) Air temperature and T_{pv} for the automatic operation period.

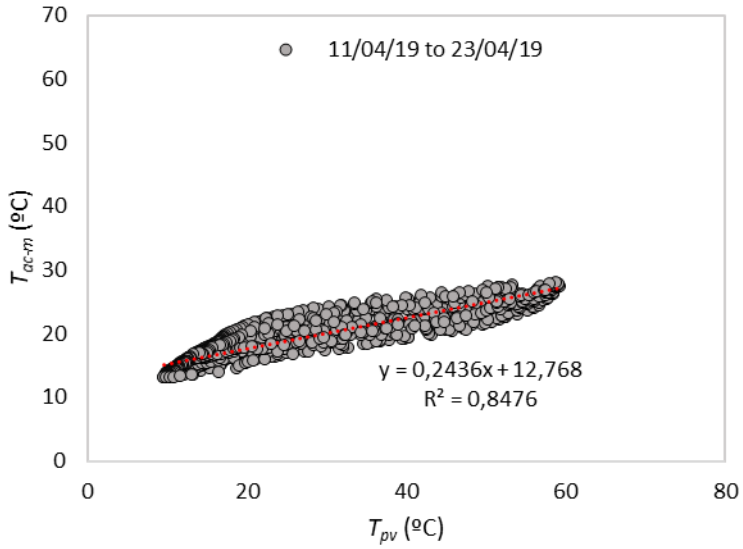

Fig. 75. (P1b) Relationship between air cavity and T_{pv} for the manual operation period.

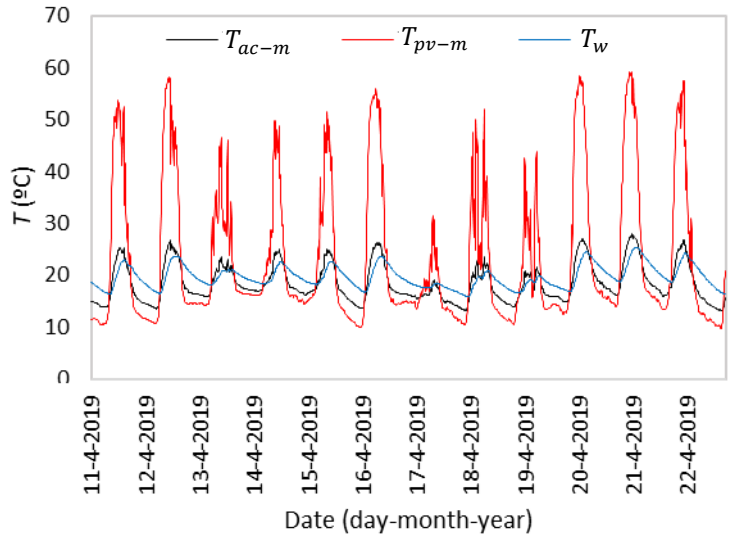

Fig. 76. (P2a) Air temperature, T_{pv} and water temperature for the manual operation period.

4.4.8. Prototype (a, b)– daily analysis

The results concerning the daily behaviour of the system during 24h for both operation modes manual and automatic are presented next. Fig. 77 and Fig. 78 present a daily behaviour of the system for the prototype P1a in manual and automatic operation mode, respectively. A register failure (R.F.) may be noticed in the data acquisition of the Q_{int} in Fig. 78, however was after the operation hours of the prototype, not compromising, as so, the calculation of the efficiencies

of the system.

During the P1a experimental campaign, both for manual and automatic modes, the T_{amb} reached nearly 30 ºC at noon, and the T_{pv-m} varied between 50 ºC and 60 ºC during the working hours. The T_{ac-m} of the P1a in automatic mode, however, assumed values very similar to the T_{amb}, indicating that most probably the prototype achieved conditions to open its exterior vents as well during some periods of the day. In this case, the ΔT was much higher in the manual operation mode than in automatic operation mode, what is going to impact as well in the calculated thermal efficiency of the system.

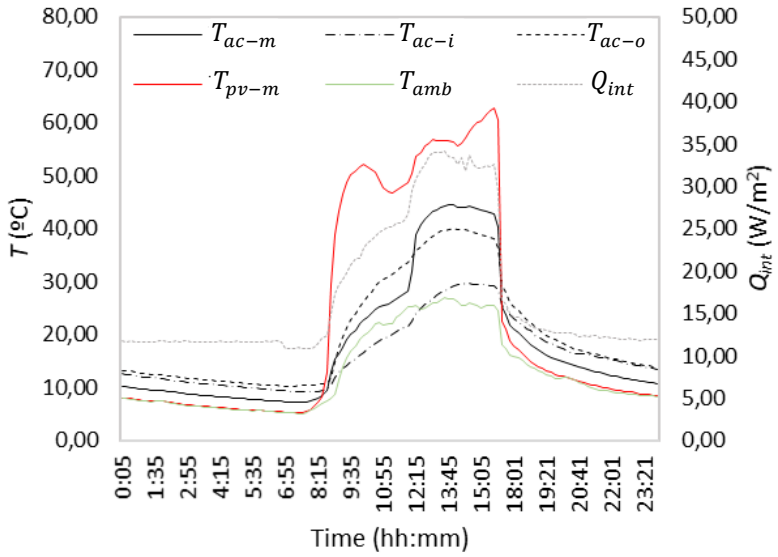

Fig. 77. (P1a) Daily behaviour of the system under manual operation (February 13th, 2019).

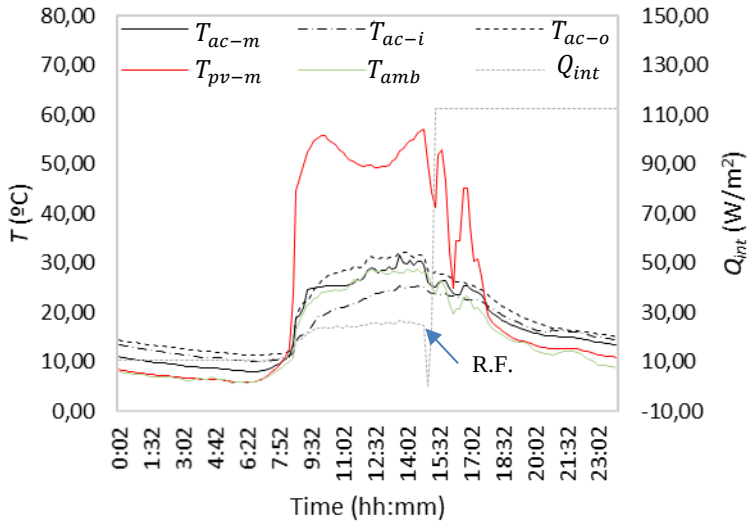

Fig. 78. (P1a) Daily behaviour of the system under automatic operation (March 21st, 2019).

Fig. 79 and Fig. 80 present a daily behaviour for the prototype P1b in automatic and manual operation mode, respectively. The T_{amb} for the P1b in automatic mode was considerably lower than in previous developed experimental campaign for the P1a (nearly 10ºC during the day, with a peak at 9:23 h). The T_{pv-m}, however, also achieve high values during the day, as a result of the incident solar radiation. In the manual mode, the variation in the T_{pv-m} was much higher and highest value was nearly 45 ºC. It was reflected, as well, in the T_{ac-m} , that in some moments of the day was nearly 20 ºC higher than the T_{amb}.

In the manual mode, the T_{pv-m} was nearly 20 ºC lower than in the automatic mode, possibly due to presence of clouds during some hours of the day and reduction of the solar radiation exposure. The same happened with the T_{amb} in manual mode of the P1b, in which the maximum value was nearly 20 ºC. The ΔT within the system was also lower.

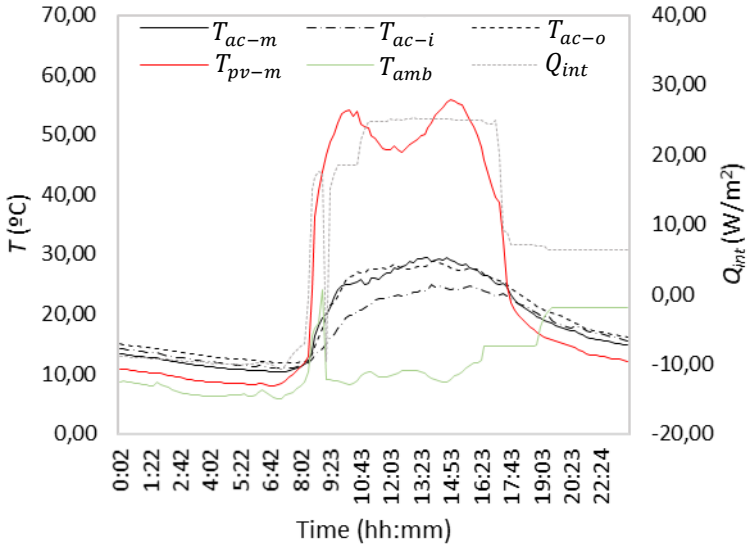

Fig. 79. (P1b) Daily behaviour of the system under automatic operation (March 22nd, 2019).

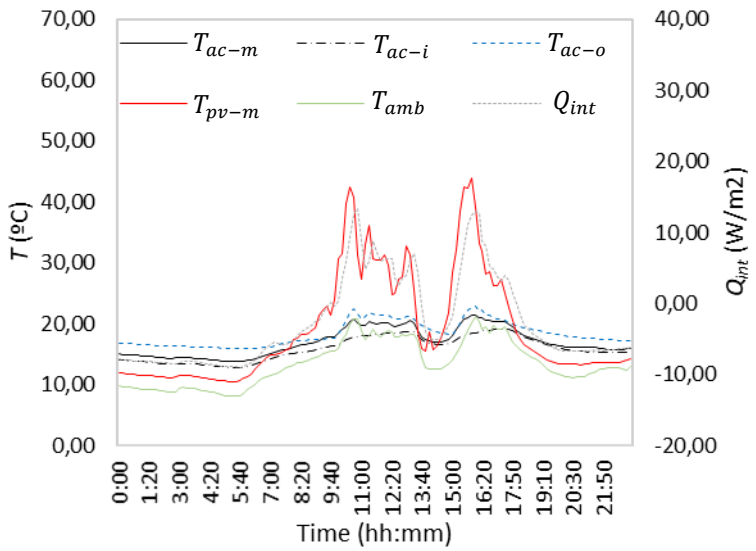

Fig. 80. (P1b) Daily behaviour of the system under manual operation, April 19th, 2019.

4.5. Energy performance and efficiencies

Considering the obtained results so far, it was possible to conclude that the T_{pv} reach values as high as in the BIPVT system, although the BIPVT system had a single sensor, and as was possible to see by the results obtained for the prototype that there is a considerable gradient of temperature in different heights of the panel. For the P1a, both in manual and automatic modes, the temperature in the middle of the air cavity was higher than in the inlet and outlet, and the losses for the room through conduction in the interior module were low. For the P1b, both in manual and automatic modes, the temperature in the outlet was for most of the measured period, higher than in the middle of the air cavity height. Concerning the operation of the vents, the automatic vent operation is much more dynamic (and despite this factor not being considered in the scope of this work, shall consume more energy for operation). Also, the automatic operation benefit not only the indoor comfort but also the cooling of the PV module in situations in which the interior ventilation was not needed, theoretically contributing to increasing the η_e of the module, once the higher the T_{pv}, the lower the η_e. In an air-based thermal system, the Q_v plays an essential role in the thermal efficiency, once the aim of the system is heating the adjacent thermal zone based on the air temperature gradient generated within the air cavity. The calculation of the energy efficiencies of the systems took into consideration the Q_v, that was calculated based on the results obtained by the experimental campaign, and the Q_{int}, directly

obtained by the measurement campaigns.

4.5.1 BIPVT energy performance and efficiencies

The efficiency of the system for heating purposes was calculated and is presented in Fig. 81, considering the same opening hours. The total efficiency of the system varies from 17% to almost 20% during the hours with high solar radiation. The slight increase in the efficiency is due to the decrease of the incident solar radiation in the vertical surface (G_V) (wall in which the BIPVT / Prototype is installed), obtained by the second pyranometer, installed in this vertical surface. Also, the η_e varies according to the T_{pv}. The η_t is nearly 4%, while η_e varies from 13% to almost 16%. The efficiencies shown are considerably low due to the factors previously mentioned. Portugal is a country with mild temperatures during the year, which means that during the year the temperatures are not very high or very low for an extended period. The case study building is considerably efficient in thermal aspects. Besides, the high temperatures that the PV module achieves during the day are also responsible for a reduction in its η_e, considering the nominal operation condition temperature of 20 ºC.

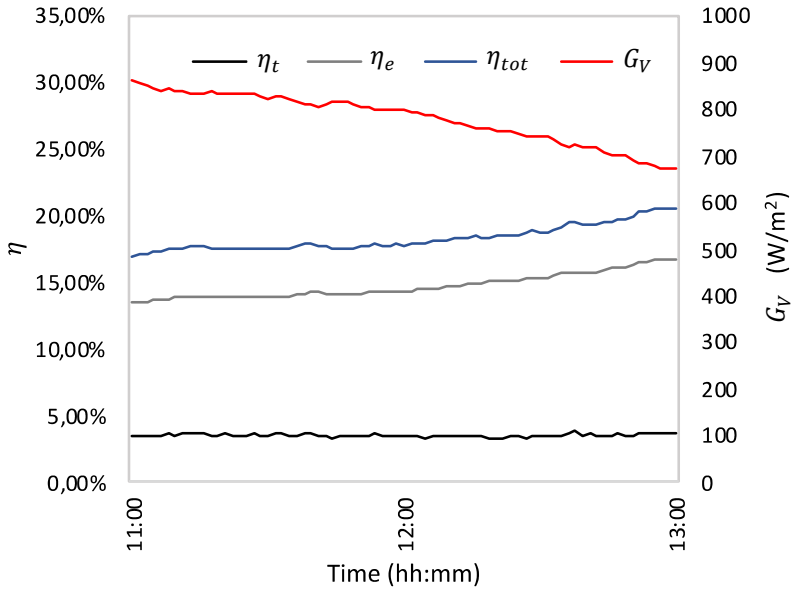

Fig. 81. (BIPVT) System efficiency profile for heating purposes.

In Fig. 82, the η_t is also presented in the function of the difference between the medium temperature (T_{ac}) and T_{amb}, divided by G_V . Most of the coordinated points are located in lower

efficiencies, related to a lower correlation of $(T_{ac}\text{-}T_{amb})/G_V$. The higher values are associated with a higher correlation of $(T_{ac}\text{-}T_{amb})/G_V$. It does not necessarily mean that the difference between the medium and T_{amb} are higher, but also can mean that the G_V is decreasing at a faster rate than the system/exterior temperature differences.

In Fig. 83, the relationship between η_t/G_V and T_{ac}/G_V is presented. It is possible to see that both η_t and T_{ac} increase with the G. For both Fig. 82 and Fig. 83, a linear approximation equation is also calculated and presented in the graph, to allow a mathematical representation of the values obtained. The dimensionless temperature in function of dimensionless height is presented in Fig. 84.

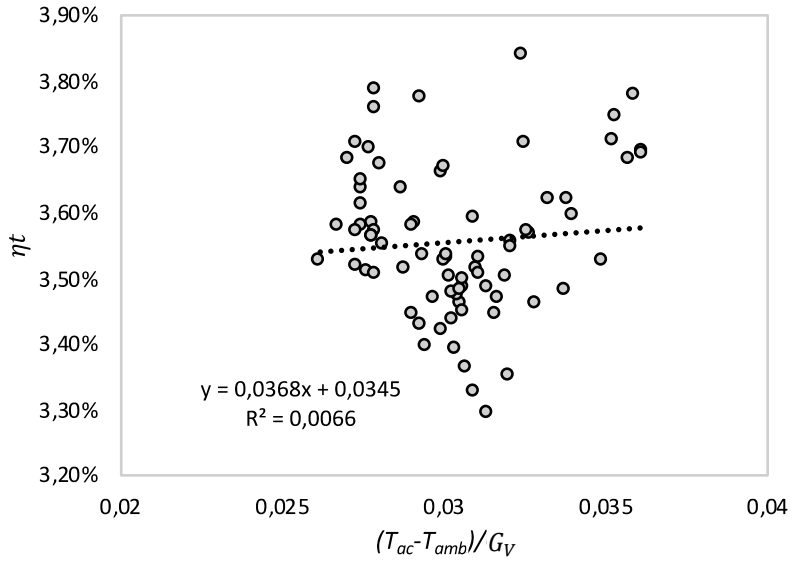

Fig. 82. (BIPVT) η_tx $(T_{ac}\text{-}T_{amb})/ G_V$.

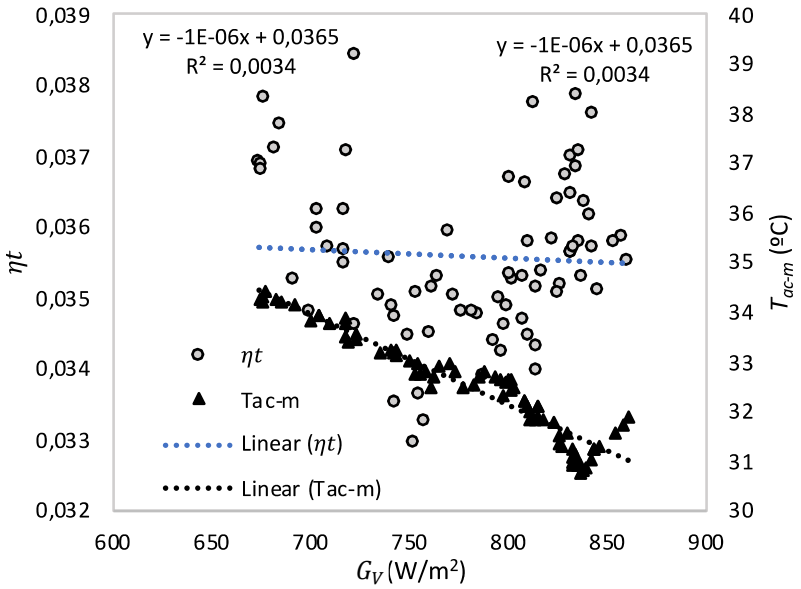

Fig. 83. (BIPVT) Relationship between η_t, G_V and T_{ac}.

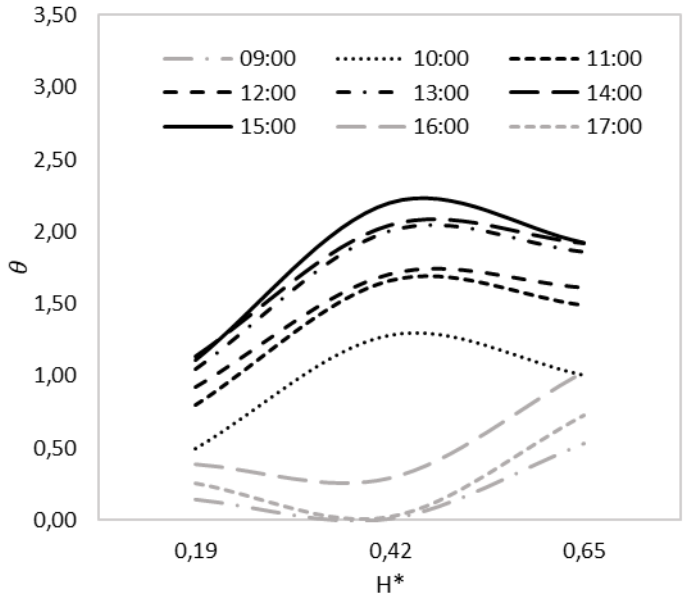

Fig. 84. (BIPVT) Dimensionless temperature and height (January 11th, 2019).

4.5.2 Prototype (a, b) energy performance and efficiencies

After the analysis of the experimental results of the BIPVT system, the new BI-SES prototype is evaluated in similarity. The calculated efficiency of the system (P1a – manual mode) is presented in Fig. 85, that shows the η_t, η_e and η_{tot} of the system in time during an opening period of the interior vents (from 09:00 h to 11:00 h). The G_V is also presented in this graph. The η_{tot} of the system for the period in consideration may be assumed as nearly 20%, once in the initial period the G_V was lower and still increasing, resulting in correlation in a higher efficiency that may not correspond to the efficiency that will represent the system in most of the time. The η_t of the system is varies between 3,5% and 4,5% within the assessed period, while the calculated η_e is nearly 16%. For the P1a in automatic mode, the η_t remains nearly 4% near 10:30 h, the η_e assumes a value of 12%, account to a η_{tot} of 16%. In this first two graphs, in inverse relationship is noted in both modes of operation, in which the η_e is further reduced due to the high G_V value and increased due to the low G_V value peaks.

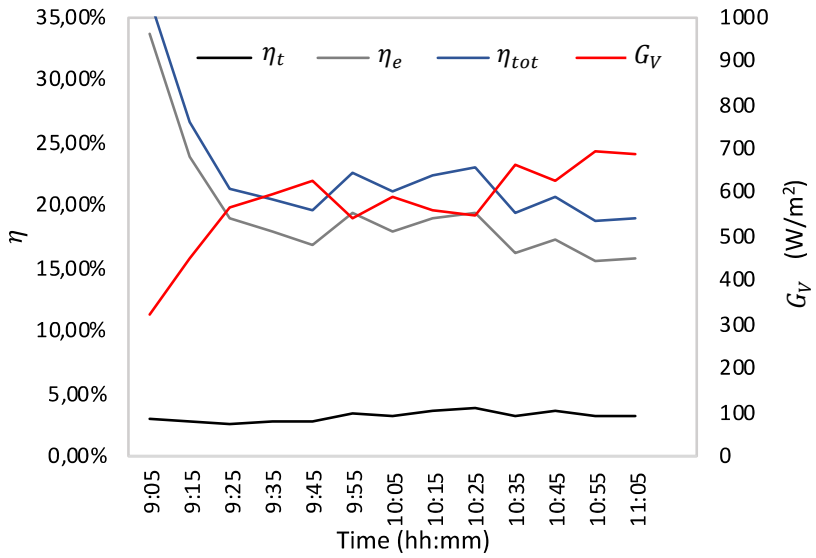

Fig. 85. (P1a) System efficiency profile – manual operation mode on February 13.

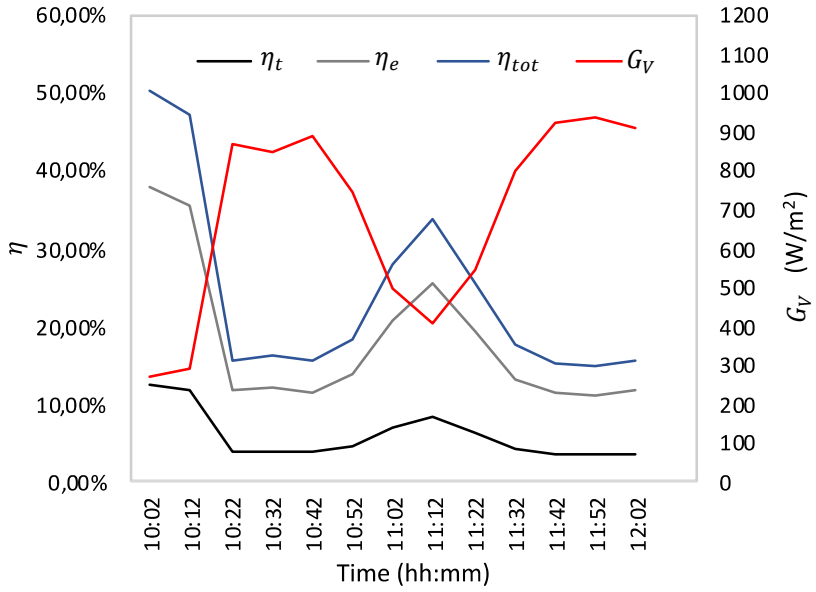

Fig. 86. (P1a) System efficiency profile – automatic operation mode on March 21.

In P1b, considering both the automatic and manual mode of operation between 10:00 h and 12:00 h, the G does not presents considerable fluctuations. In automatic operation (Fig. 87), η_t hits 4,8% and η_e varies between 15,1% and 14,5%, being the η_{tot} between 18% and 20%. In the manual mode (Fig. 88), the highest value for η_t is 2,5% in the mentioned period. Still considering the manual mode, the η_e varies between 17% and 15%, while the η_{tot} assumes a value near 18%.

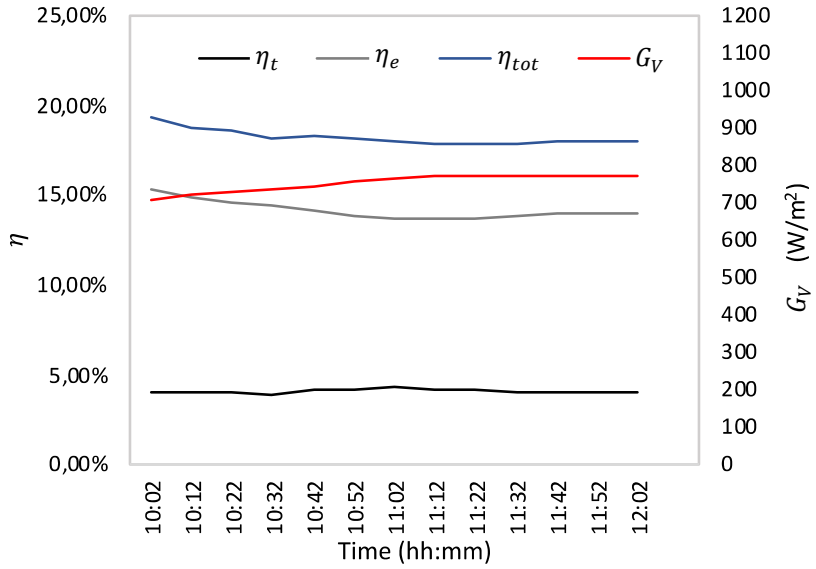

Fig. 87. (P1b) System efficiency profile – automatic operation mode on March 22nd.

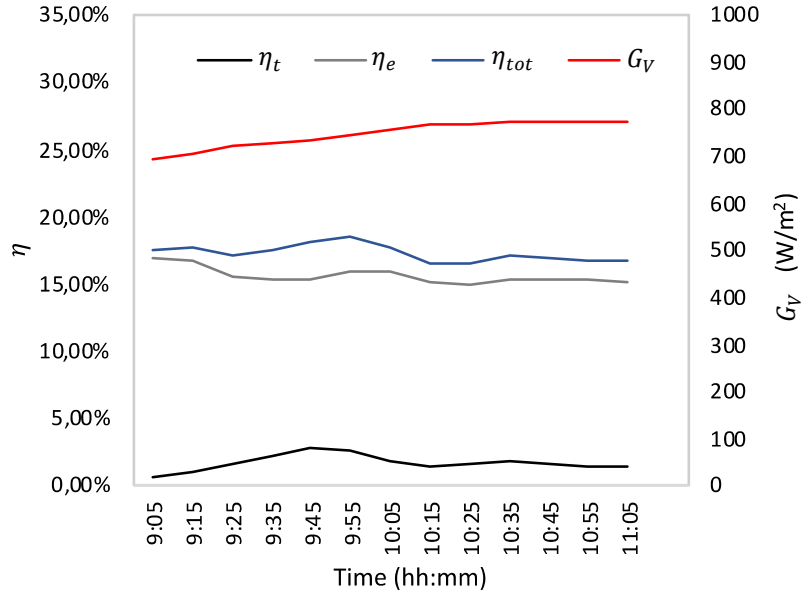

Fig. 88. (P1b) System efficiency profile – manual operation mode on April 19th.

For the period used for the calculation of the efficiency previously presented for P1a, Fig. 89 and Fig. 90 present the relationship between η_t and $(T_{ac}\text{-}T_{amb})/G_V$. Fig. 91 and Fig. 92 presents the same relationship for the P1b in both modes of operation.

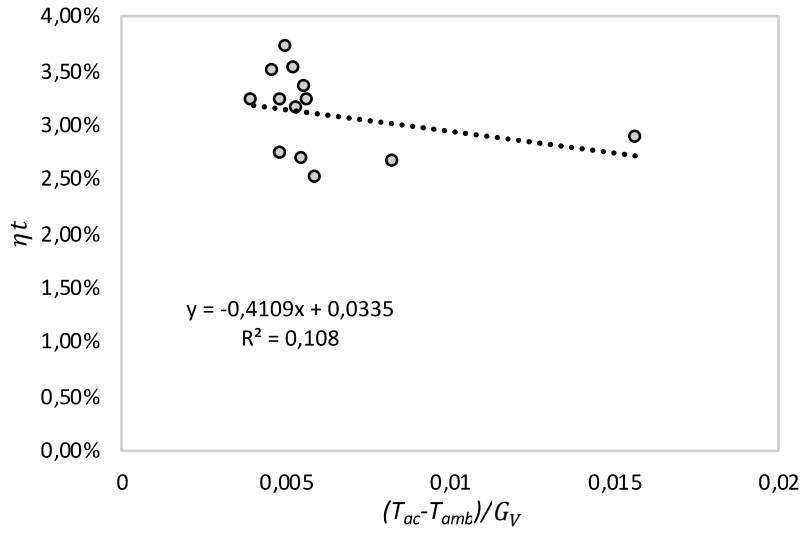

Fig. 89. (P1a) η_t x $(T_{ac}\text{-}T_{amb})/G_V$ for February 13.

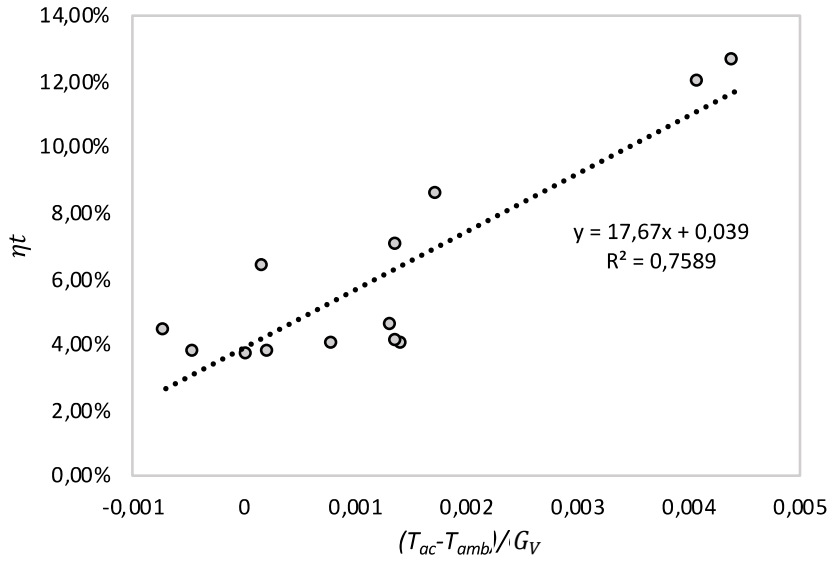

Fig. 90. (P1a) η_t x $(T_{ac}\text{-}T_{amb})/G_V$ for March 21.

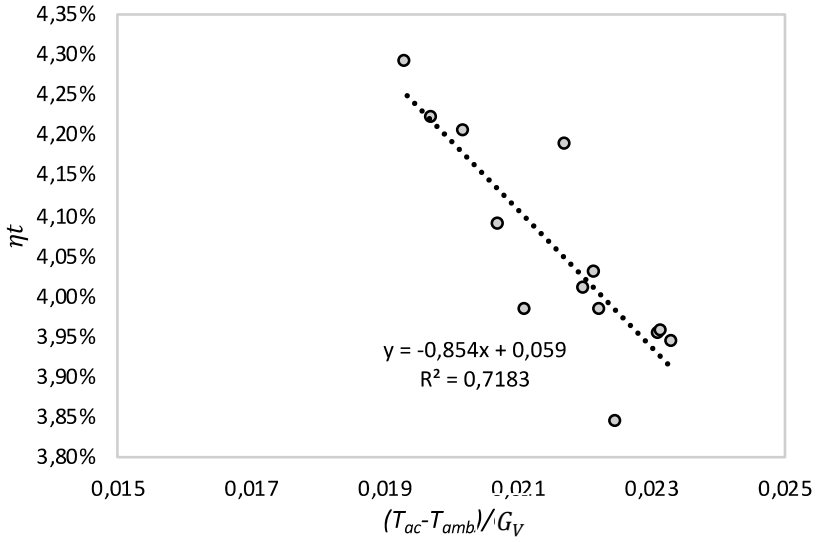

Fig. 91. (P1b) η_t x $(T_{ac}\text{-}T_{amb})/G_V$ for March 22nd.

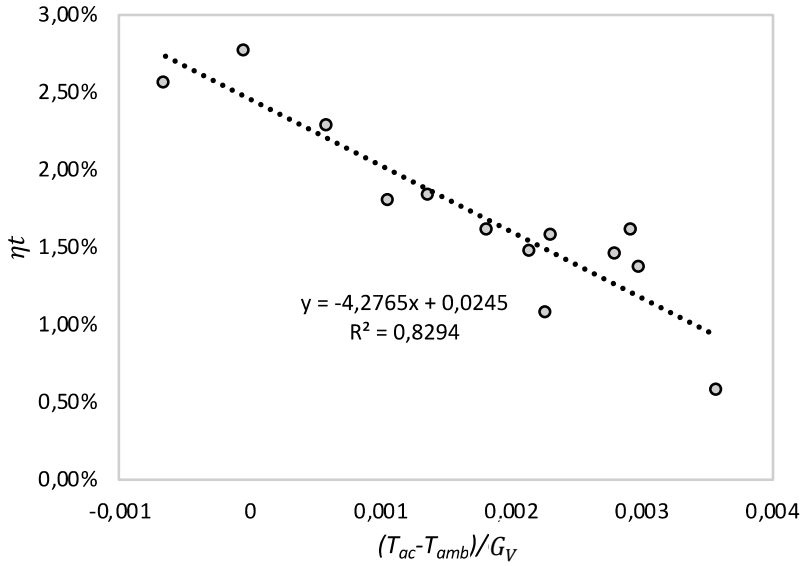

Fig. 92. (P1b) η_t x (T_{ac}-T_{amb})/ G_V for April 19th.

Also, in similarity to the BIPVT analysis previously presented, Fig. 93 presents the relationship between η_t and G_V, and T_{ac} and G_V , with the correspondent linear equations that approximate the behaviour for the boundary conditions existent in the date of record for P1a in a manual mode of operation. The height of the system has an influence in the thermal behaviour; once in high G_V conditions, the system tends to reduce the temperature gradient between the inlet and outlet, impacting on the equation. Fig. 94 presents the same for the P1a in automatic operation mode, Fig. 95 presents for the P1b in automatic mode and Fig. 96 for P1b in manual operation mode.

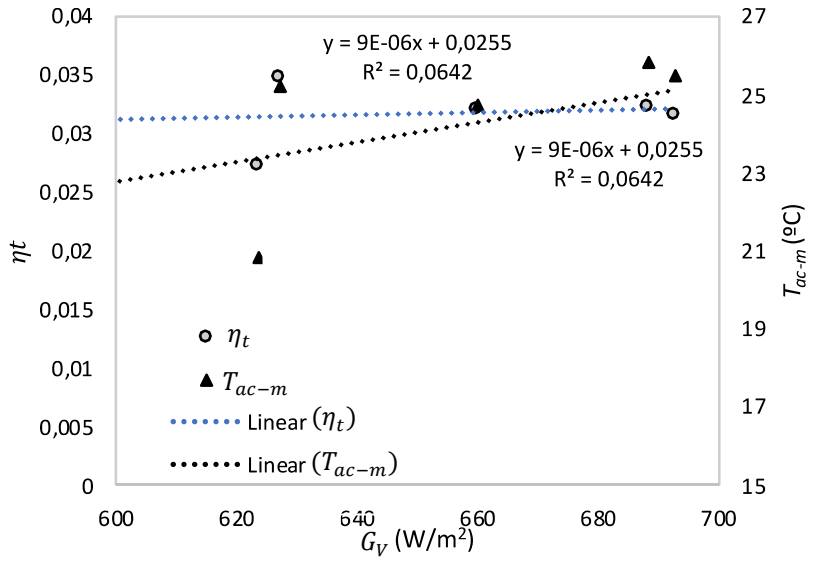

Fig. 93. (P1a) Relationship between η_t, G_V and T_{ac} – manual operation mode for February 13.

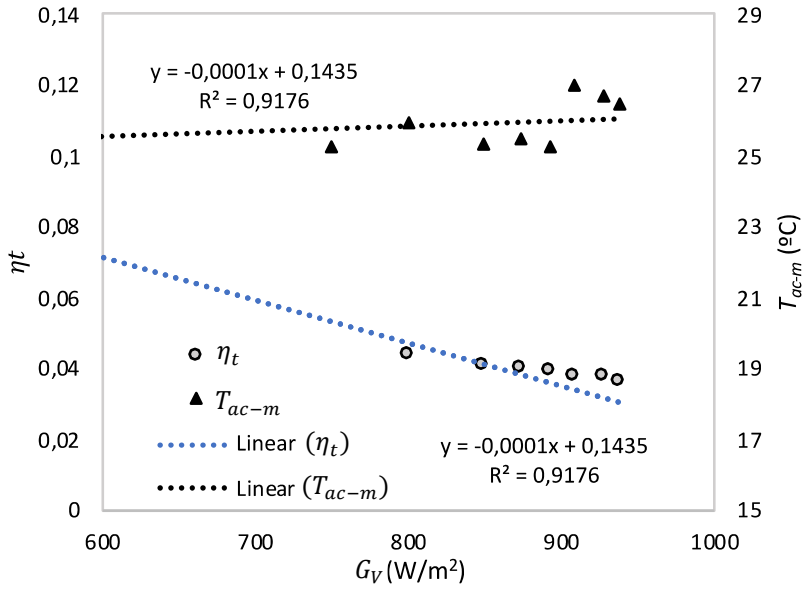

Fig. 94. (P1a) Relationship between η_t, G_V and T_{ac} – automatic operation mode for March 21.

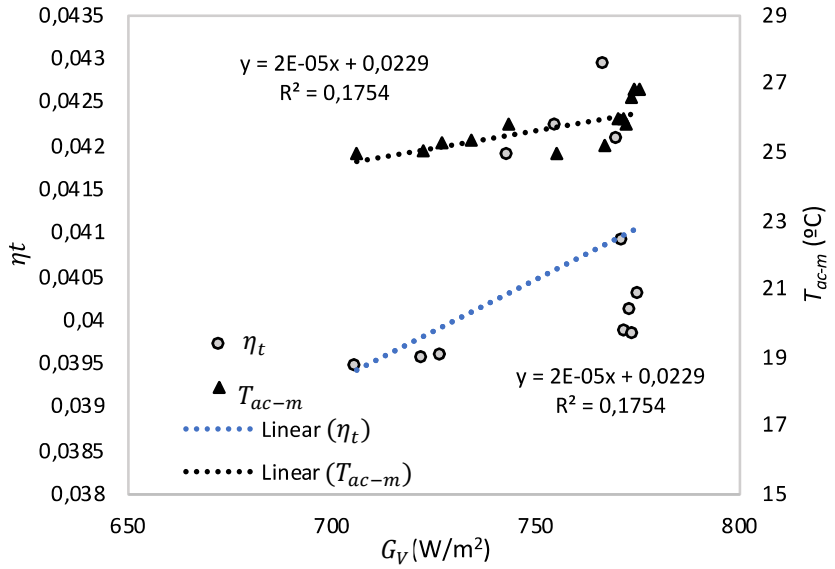

Fig. 95. (P1b) Relationship between η_t,G_V and T_{ac} – automatic operation mode for March 22nd.

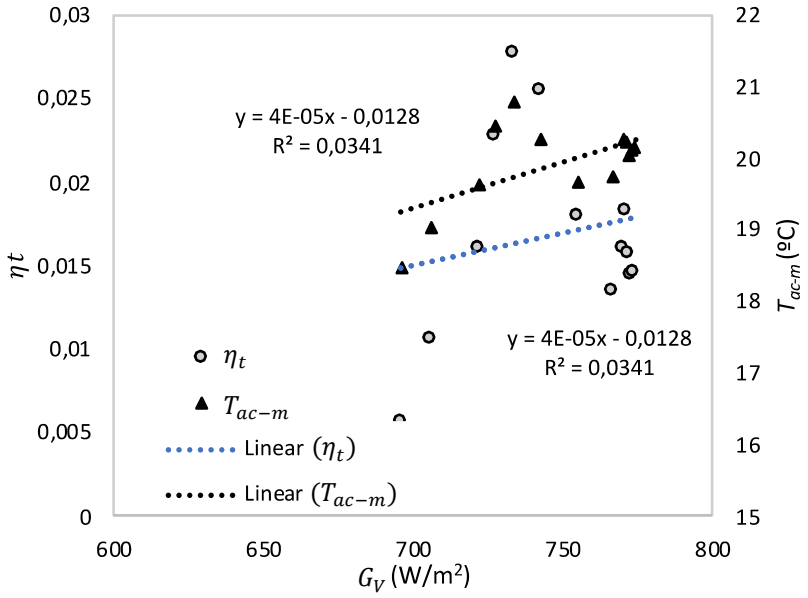

Fig. 96. (P1b) Relationship between η_t, G_V and T_{ac} – manual operation mode for April 19th.

For the new Prototype, it was performed an additional analysis considering the convection coefficients, calculated based on the acquired experimental data of the system. Moreover, as so, the values used for the calculations are the ones previously presented in experimental campaign results for the mentioned days/hours. The coefficients studied in the scope of this thesis are the Gr number (Eq. 5), Ra (Eq. 7), h (in W/(m^2.K)) and Nu (Eq. 4). The temperature of the PV module, interior module and air were considered as measured in the experimental campaign for the days into the analysis (55 ºC), whereas the equations used are presented in Chapter 2.

Fig. 97 presents these coefficients for the prototype P1a in manual mode, while Fig. 98 presents them for P1a in automatic mode. The following figures, Fig. 99 and Fig. 100, present these coefficients for the prototype P1b in automatic and manual mode, respectively.

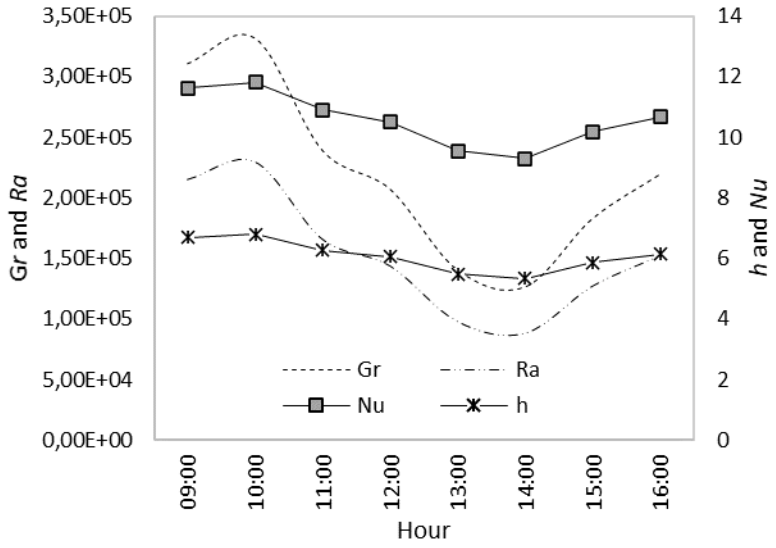

Fig. 97. (P1a) Convection coefficients February 13.

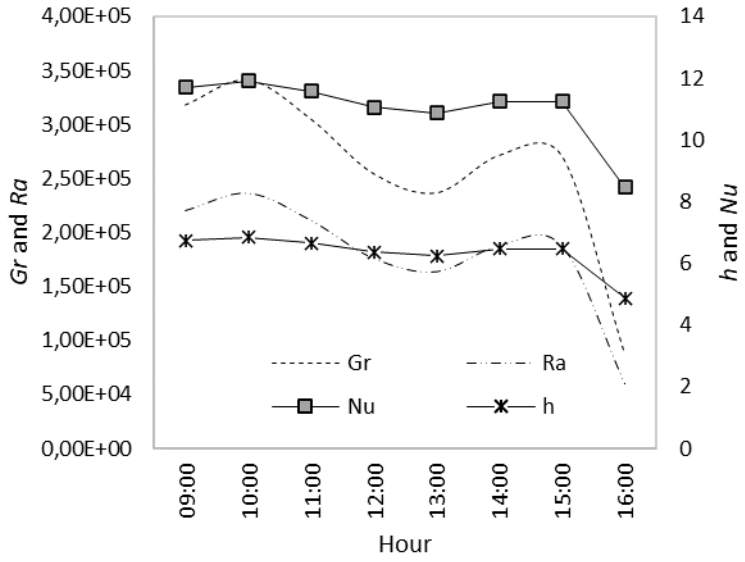

Fig. 98. (P1a) Convection coefficients March 21 automatic mode.

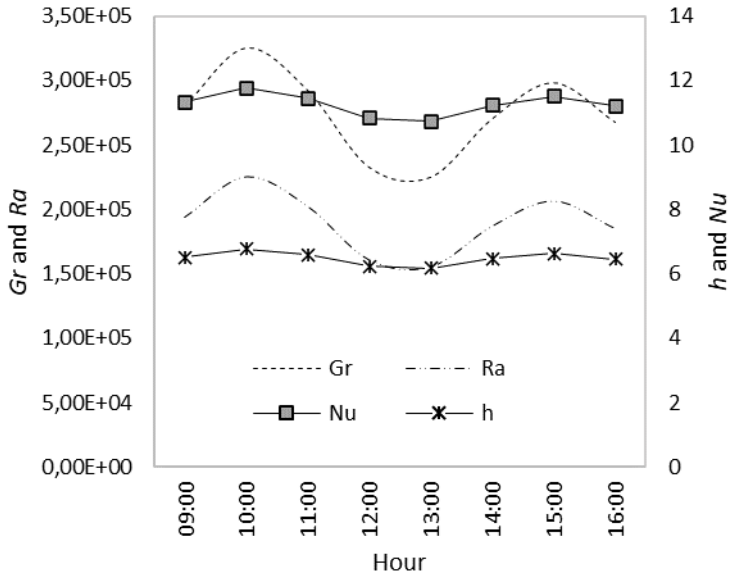

Fig. 99. (P1b) Convection coefficients March 22nd.

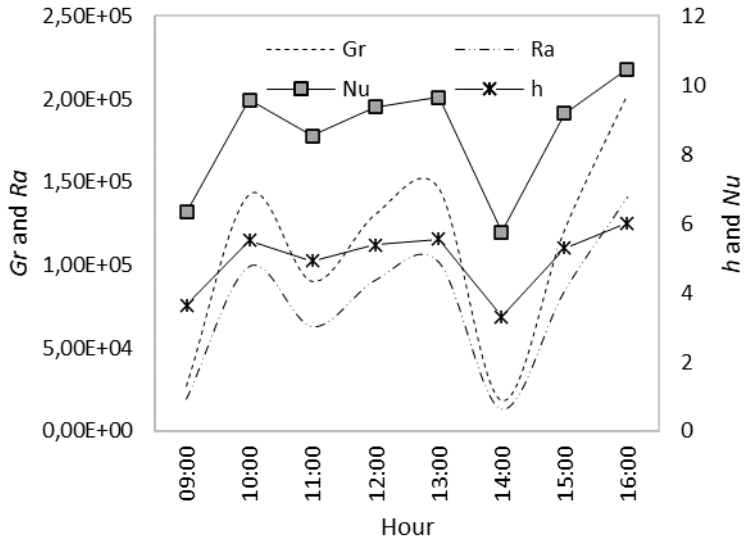

Fig. 100. (P1b) Convection coefficients April 19th.

The relationship between dimensionless temperature and dimensionless height is presented for the four versions of the prototype, for daily hours (from 09:00h to 17:00h). Fig. 101 presents the values for the prototype P1a in manual mode and Fig. 102 for the P1a in automatic mode. Fig. 103 presents them for the prototype P1b in automatic mode, whereas Fig. 104 presents if for the P1b in manual mode.

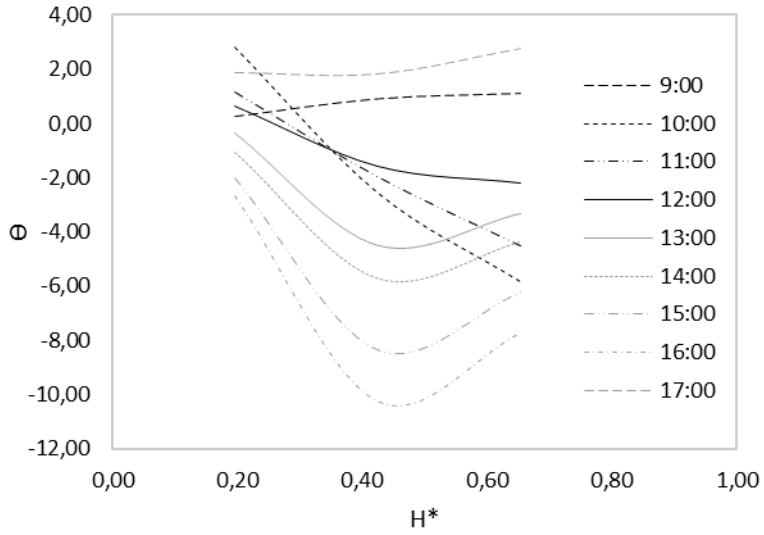

Fig. 101. (P1a) Dimensionless temperature and height (the manual mode - February 13rd, 2019).

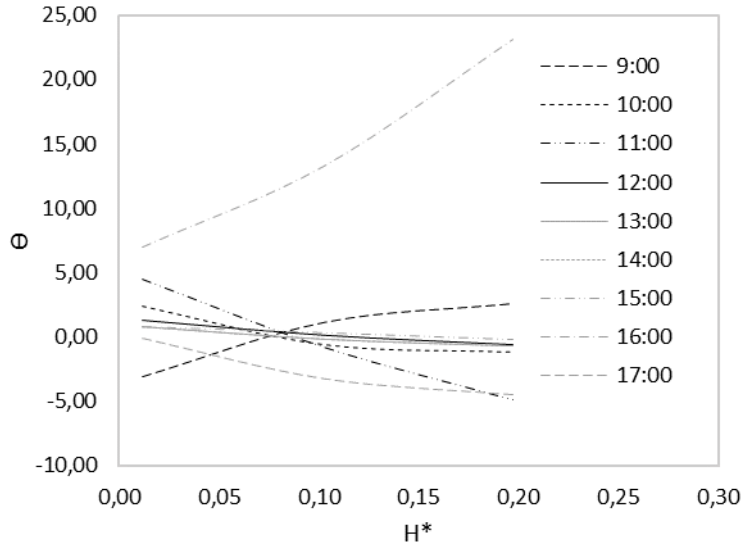

Fig. 102. (P1a) Dimensionless temperature and height (automatic mode - March 21st, 2019).

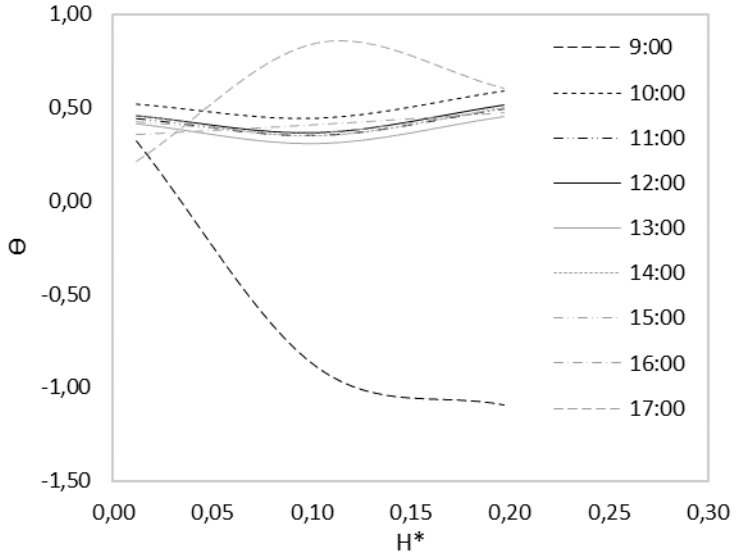

Fig. 103. (P1b) Dimensionless temperature and height (the automatic mode - March 22nd, 2019).

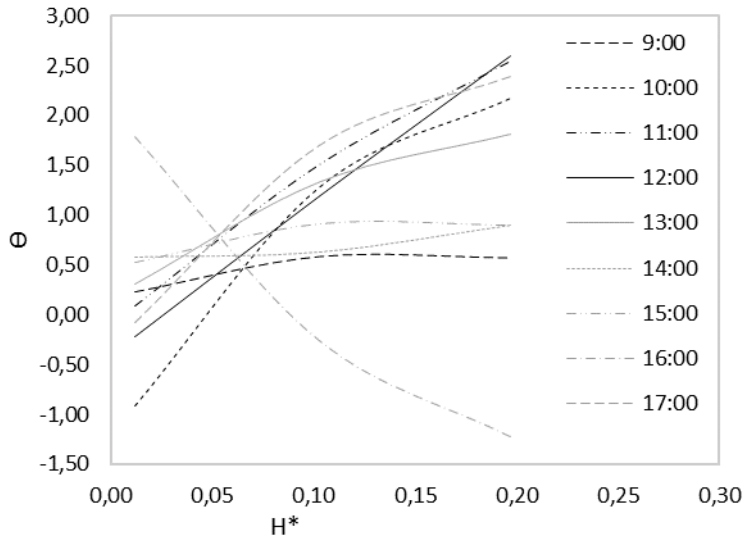

Fig. 104. (P1a) Dimensionless temperature and height (the manual mode - April 19th, 2019).

After the presentation and analysis of the results of the experimental campaign, the next chapter of this work presents the numerical analysis.

4.6. Experimental analysis main remarks

This study performed an experimental analysis concerning the registers of weather (solar radiation, ambient temperature), room temperature and usage pattern, and system's characteristics. This subsection

aims to briefly list the main remarks of the experimental analysis developed in the scope of this thesis, concerning the characterization of the BIPVT systems. They are:

- Thermal efficiencies calculated varied from 2,5% to 4,8%;
- Theoretical electrical efficiencies calculated varied from 12% to 17%;
- Total efficiencies calculated within the testing period – nearly 20%;
- Higher R^2 values were obtained for manual operation, and lower R^2 values for automatic operation;
- The short period of monitoring for the Prototype in its two interior modules and operation modes may be a limitation of the study.

Chapter 5. Numerical analysis

In Chapter 5 the numerical analysis is performed, both specifically for the BIPVTs systems, and for the integration of the BIPVTs with the room. The numerical analysis is segmented in three parts. The first part is the BI-SES fluid thermal behaviour analysis through the CFD technique. The second part develops the dynamic simulation of the systems in real conditions, while the third part develops a parametric analysis of the interaction between the system and the room, considering different parameters.

5.1. Elements numerical analysis

The numerical characterization of the façade elements is developed using the computational fluid dynamics (CFD) approach, with the software Ansys Fluent. It aims to characterize the thermal behaviour of the system in its fluid and solid parts, through the analysis of temperature profile, air velocity and turbulence, having into consideration the cross-section of the element in a bi-dimensional analysis in steady state conditions. Despite all three heat transfer modes are present in or around the multi-element façade systems, which forms the object of the present study, this work will put the emphasis namely on the conductive and convective heat transfer mechanism.

The equations that govern the fluid flow and heat transfer processes inside the air gap formed between the vertical façade solid elements are the equations of mass, momentum and energy conservation. The conservation of mass states that the mass of the system must remain constant over time for all closed system to all transfer of matter and energy (mass is not created nor destroyed - quantity of mass is conserved over time) (Lax and Wendroff, 1960). The equation of the conservation of mass applied to a fluid is known as the continuity equation. Eq. 12 gives the generalist form of the mass conservation equation.

$$\frac{\partial \rho}{\partial t} + \nabla . (\rho \vec{v}) = S_m \qquad \text{Eq. (12)}$$

In a closed system, the total moment is constant. The equation of the conservation of momentum (Eq.13) is known as Newton's second law applied to fluid flow. It is quite general and applicable to both continuum and non-continuum flows and loses its generality when shear stress tensors are applied.

$$\frac{\partial}{\partial t}(\rho \vec{v}) + \nabla .(\rho \vec{v}\vec{v}) = -\nabla p + \nabla .(\tau) + \rho \vec{g} + \vec{F} \qquad \text{Eq. (13)}$$

The total energy in a closed system remains constant (Noether's theorem). Conjugate heat transfer is also important with regards to the heat transfer in façade elements. It refers to the computation of conductions of heat through solids, coupled with convective heat transfer in a fluid. The conjugate heat transfer is applicable whenever there are two adjacent domains, and the objective is to analyse the heat transfer between these spheres – either solid or fluid.

The fundamentals of the CFD technique are widely discussed in the literature and will not be further described here, besides the basics concerning the simulation set-up used. However, a detailed description of the computational fluid dynamics method may be found in (Versteeg and Malalasekara 2007; Ansys 2018). For this kind of calculations, it is critical to select appropriate boundary conditions that best represent the system.

The general scheme of analysis is shown in Fig. 105. It starts by designing the systems' geometry using the Ansys Design Modeler, according to the data provided in the case study description. Next step was to determine the mesh to be used in the fluid and solid parts, followed by the setup of the simulation.

The setup of the simulation is done through the consideration of general features (as equations, steady-state mode, among others), model definition, boundary conditions of the system, reference values, solution and initialization configurations. In the solution tab, is possible to set the methods, monitors to be displayed, variables to be calculated, and reporting variables. The model results are observed through the selected plots and graphs.

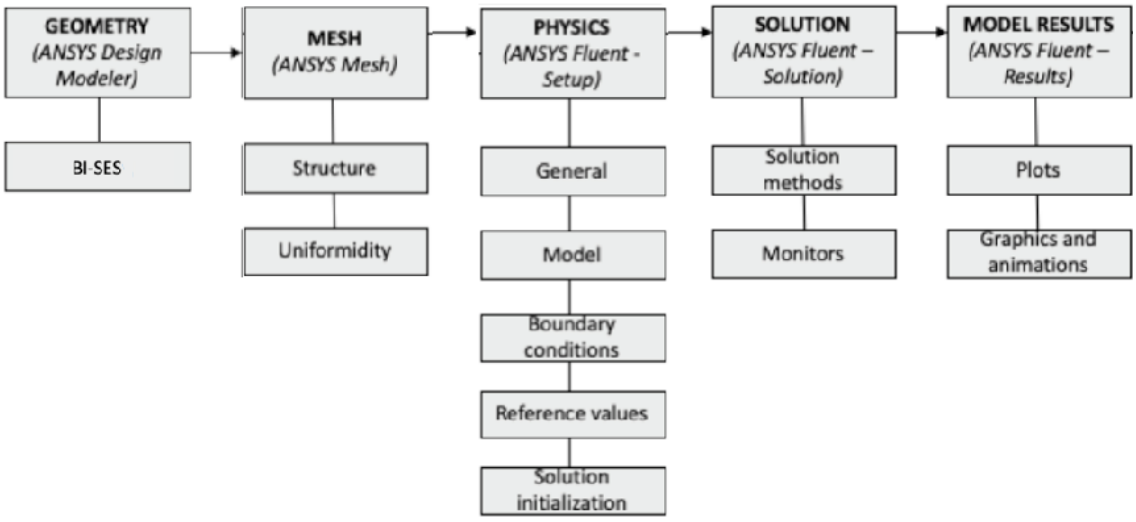

Fig. 105. Scheme of the CFD analysis.

In the scope of this thesis, the thermal behaviour of the system is studied in steady-state simulation. The simulation setup is briefly described here. The turbulent motion, described by the Navier-Stokes equations and characterised as an irregular condition of the flow with random variation with time and space coordinates, has been considered using the k-ε model with standard wall functions. These equations are solved using SIMPLE algorithm. The acronym SIMPLE stands for Semi-Implicit Method for Pressure-Linked Equations. and is essentially a guess-and-correct procedure for the calculation of pressure on the staggered grid arrangement introduced above. The method is illustrated by considering the two-dimensional laminar steady flow equations in Cartesian coordinates.

The energy model is considered activated. The turbulent viscosity is computed by combining k and ε, while the constants assume the default values of $C1\varepsilon = 1.44$; $C2\varepsilon = 1.92$; $C3\varepsilon = 0.09$; $\sigma k = 1.0$; $\sigma\varepsilon = 1.3$. The standard k-ε model is used to perform the calculations in the software. The simplest "complete models" of turbulence are the two-equation models in which the solution of two separate transport equations allows the turbulent velocity and length scales to be independently determined. The pressure-velocity coupling uses the coupled mode, whereas the influence of buoyancy force caused by the difference of densities due to the heating process was considered by inducting the Boussinesq approximation model (Boussinesq hypothesis). This method uses a starting guess for pressure and velocity to solve the corresponding velocities via momentum equations, followed by introduced correction factors until convergence (Versteeg and Malalasekara 2007).

The standard k-ε model is a semi-empirical model based on model transport equations for the

turbulence kinetic energy (k) and its dissipation rate (ε). The model transport equation for k is derived from the exact equation, while the model transport equation for ε was obtained using physical reasoning and bears little resemblance to its mathematically exact counterpart, according to the software theory guide. The Boussinesq hypothesis is based on the assumption that the components of the Re stress tensor are proportional to the mean velocity gradients, assuming that eddies behave like molecules, that turbulence is isotropic and that there exists local equilibrium between stress and strain.

Thus, default residuals are used for continuity, x-momentum, y-momentum, energy, turbulence kinetic energy and turbulence kinetic energy dissipation rate for checking convergence of the solution. The more detailed numerical formulation may be found in the software theory reference guide, as well as details on time discretization equations (Ansys 2018; Yee, Sweby, and Griffiths 1991; Ansys 2011) .

The mentioned approach was used to describe in two-dimension thermal terms for both the BIPVT system and the new prototype (P1a and P1b) proposed in this work.

All CFD problems are defined in terms of initial and boundary conditions, as is deep explored in Versteed and Malalasekera (2007). Flows inside a CFD solution domain are driven by the boundary conditions and the most common cause of rapid divergence of CFD simulations is an inappropriate selection of boundary conditions. It is important that the user specifies these correctly and understands their role in the numerical algorithm. In transient problems the initial values of all the flow variables need to be specified at all solution points in the flow domain, however this work assumes steady-state conditions. The boundary conditions considered in the scope of the CFD simulation of this work is the inlet, outlet, solid surfaces, prescribed pressure. The most accurate simulations can only be achieved by supplying measured inlet values of turbulent kinetic energy k and dissipation rate ε. However, in most cases such data are often not available and default values are adopted.

In this CFD analysis, the PV module was considered a heat source surface for both the BIPVT and Prototype systems, with a temperature associated. The temperature assumed (Fig. 101) for the PV surface (T_{pv}) at a given moment (steady state condition) are based on the experimental campaign previously developed, as well as the interior module/wall temperature. The interior module/wall is assumed being the same as the T_i at the initial boundary condition, whereas the inlet velocity is assumed as being the same as the registered in the experimental campaign for

the BIPVT system (instant observation through the use of an anemometer), corresponding to 0,0098 m/s normal to boundary. It is necessary to highlight, as previously explained, that the obtained values for the registered period in the Prototype are not useful and are constituted by the noise of the system. The inlet turbulent intensity fraction is considered to be 0.5 and the turbulent viscosity ratio 10. The outlet has a backflow direction specification method as normal to boundary, while the backflow pressure specification is the total pressure. Moreover, the T_{bf} is assumed as being the same as the T_i at a given moment.

All the elements were simulated under the same conditions of heat source and inlet velocity, in order to obtain comparable values – contrary to the experimental campaign in which each one of the elements were evaluated at a different time-period with different boundary conditions. The PV surface is considered at 55 ºC (based on the experimental data for the detailed day of the BIPVT system). The T_{inl} is also the same as experimental campaign for the given day. Outlet boundary conditions may be used in conjunction with the inlet boundary conditions. Air properties are sourced from the software database. Same was done for the water properties, sourced from the software database. The solid properties were the mentioned in the case study description, and no slip and no permeability hydrodynamic condition along X and Y directions are considered.

It is important to highlight that the real system presents more heat losses, once in the CFD simulation, the upper and bottom surface of the air cavity is considered adiabatic due to the lack of control in experimental campaign to determine the heat fluxes through these surfaces. Fig. 106 presents the boundary conditions and the domains of the systems, used both for the pre-existing BIPVT system and the new prototype.

The impact of the mesh sizing in the accuracy of the simulation is recognizable (Sande and Ray 2014). The mesh resolution is inversely proportionate to cell area. However, it is to highlight that the impact of mesh sizing is not object of this work, despite the author recognizing the importance of this step in a computational fluid dynamic analysis. Due to computational resources available (and taking into consideration that CFD analysis and high resolution mesh sizing implicates a good computational power) and due to software academic license limitations, for all the models, the mesh was considered uniform and in its maximum possible resolution considering these mentioned constrains. Considering these remarks, the results obtained for each simulation are presented in the following subsections.

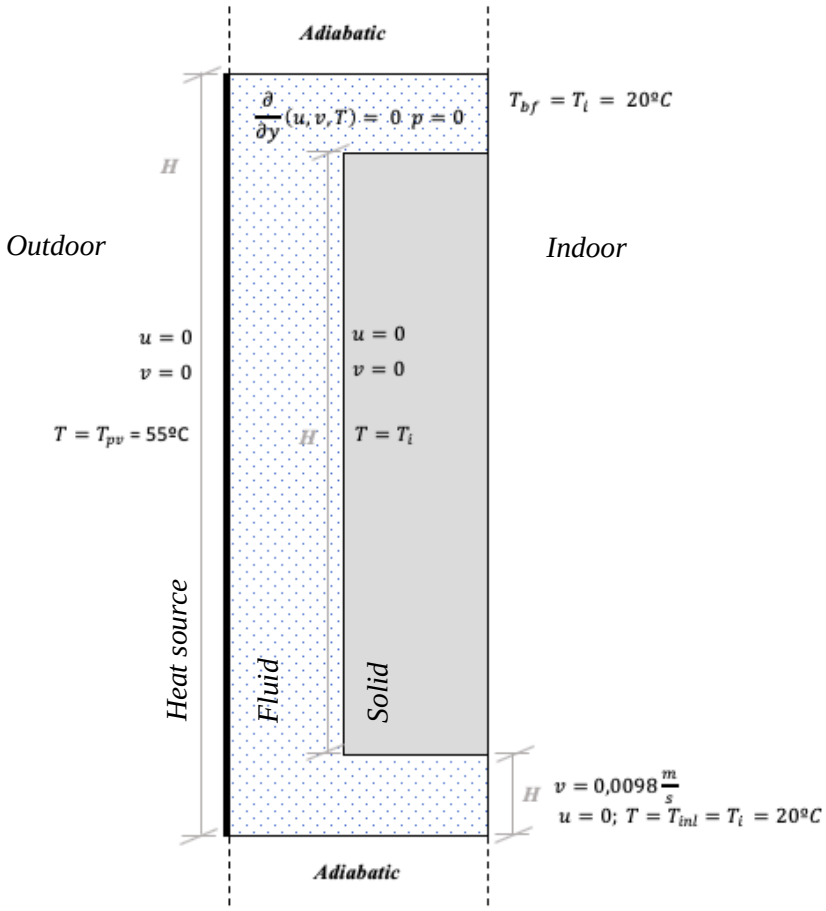

Fig. 106. Boundary conditions of the BIPVT systems in the CFD analysis.

5.1.1. BIPVT CDF results

The BIPVT analysis used a mesh size of 0.005m, and prototype P1a and P1b analysis used a mesh size of 0.002, chosen due to the computational capabilities to process the mesh given the area of the geometry, and the results are presented for temperature distribution in the air cavity and interior wall, velocity of air inside the cavity, and turbulence. The results for the temperature contour of the cross-section is presented in Fig. 107. Fig. 108-a presents the velocity contour of the cross section, with a detail on the outlet vectors of velocity (Fig. 108-b). Turbulence is presented in Fig. 109.

Considering the BIPVT system (Fig. 107), the temperature increases due to the source of heat

from the PV module, entering the cavity in the inlet at a defined temperature of 20 ºC and leaving the air cavity at an T_{out} of near 35 ºC. The solid temperature presents a gradient that varies from 20 ºC to 31 ºC, in similarity to the air cavity, achieving higher temperatures in the upper part of its geometry. The temperature is higher near to the PV module surface, due to this being the heat source of the simulation. The air cavity velocity reaches a value to 0,017 m/s in some points, showing an increase of 0,007 m/s in relation to the inlet velocity.

In the BIPVT case, there was only one sensor to represent the air cavity results in terms of air temperature. The position of the sensor (installed in a period previously than the thesis development), impacts the results not only in vertical axis terms, but also in the distance from the heat source surface (PV module) or the interior part of the system. Considering the middle height of the system, in horizontal axis terms, the temperature may vary from 23 ºC (near to the interior part surface) to 55 ºC (value of the heat source surface temperature).

The air velocity is also shown to increase inside the air cavity, due to the buoyancy effects of the natural convection. It is higher for the BIPVT system and the P1a system (shown below), once there is lower heat loss to the interior elements, that are composed by an insulation layer.

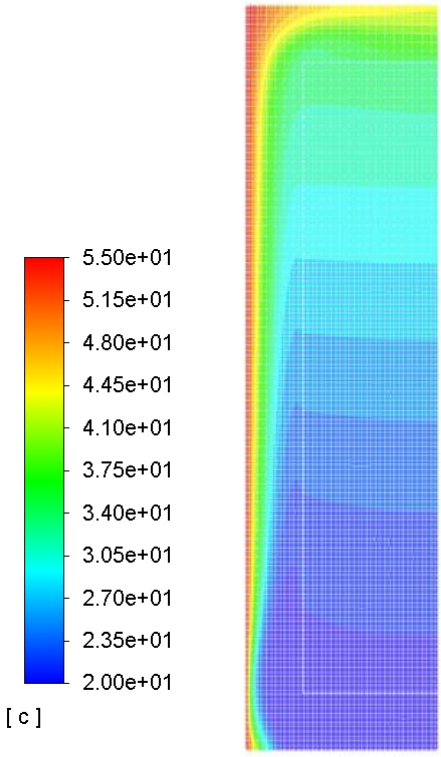

Fig. 107. BIPVT temperature contour (ºC).

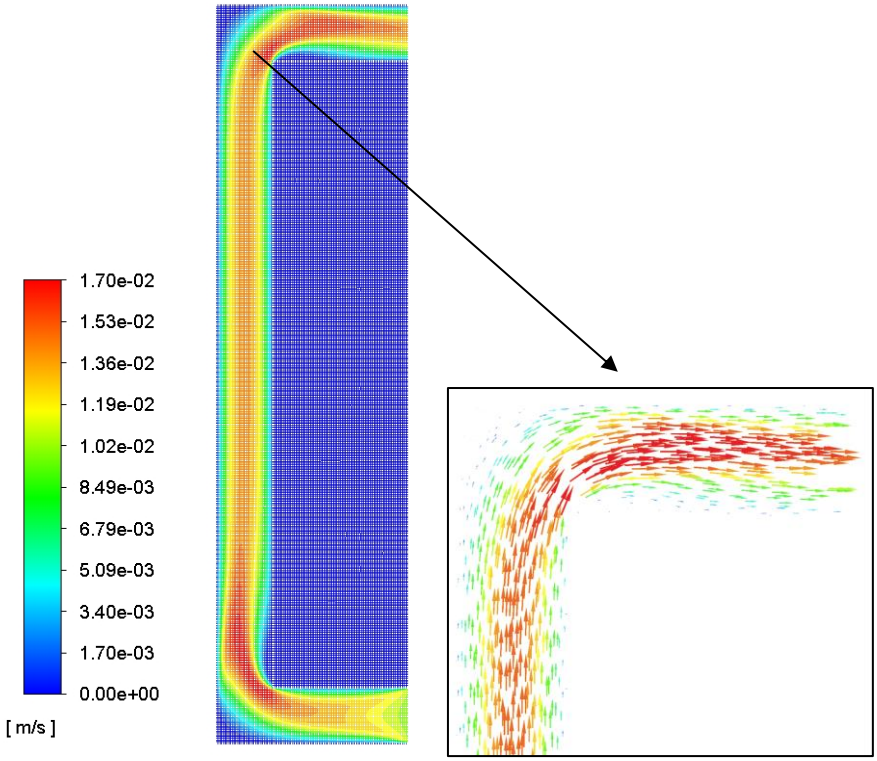

(a) (b)

Fig. 108. (a) BIPVT velocity contour (m/s); (b) vectors details.

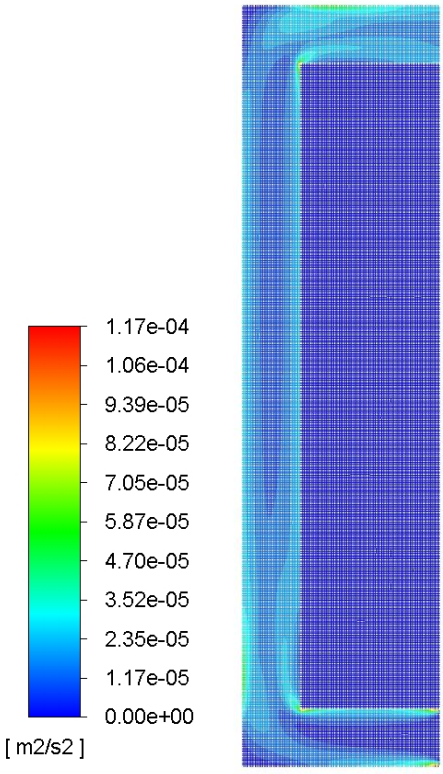

Fig. 109. BIPVT turbulence contour (m^2/s^2).

5.1.2. Prototype CFD results

The P1a and P1b analysis used a mesh size of 0.002m, chosen due to the computational capabilities to process the mesh given the area of the geometry, and the results are presented for temperature contour in the air cavity and interior wall, velocity of air inside the cavity, and turbulence for both P1a and P1b. As previously mentioned, as an attempt to represent the real conditions of the module position during the prototype experimental campaign, the P1b has nearly 1cm more of the air cavity thickness than the P1a. The water interior module has higher temperatures than the EPS insulation interior module. In fact, and as it was possible to see in the experimental campaign, the water module presented an increased heat transfer through the interior module, as was possible to see in the experimental campaign that the water module presented heat flux in both directions – from room to air cavity and from air cavity to the room, according to the temperature difference.

In contrast with the BIPVT system, the prototype in versions P1a and P1b have more sensors to acquire data concerning the system thermal behaviour than the BIPVT system. As it was possible to see in the experimental analysis, the prototype had three air temperature sensors in the air duct, in the inlet and in the outlet, representing in a more accurate form the results for the cross-section. It makes the calculation of the thermal efficiencies more reliable, and all the further analysis done with the acquired data from the sensors. Considering that the air cavity of the P1b is slightly thicker than the P1a, the velocity of the air in the air duct shown to be reduced, even if the obtained results for velocity in all the simulated BI-SES elements are overall very low. The turbulence of the air in the duct is also very low, but higher in the BIPVT system than in the prototype, especially due to the increased height of the system.

Results for P1a are presented in Fig. 110, Fig. 111 and Fig. 112. As is known, the temperature increases due to the source of heat from the PV module. The air enters the cavity in the inlet at a defined temperature of 20 ºC and leaving the air cavity at an T_{out} of near 37,5 ºC (2,5ºC higher than the BIPVT system). The solid temperature presents a gradient that varies from 20 ºC to 30 ºC, and in similarity to the air cavity it achieves higher temperatures in the upper part of its geometry. The temperature is higher near to the PV module surface, due to this being the heat source of the simulation. The air cavity velocity reaches a value to 0,017 m/s in some points (similar to the BIPVT system), showing an increase of 0,008 m/s in relation to the inlet velocity.

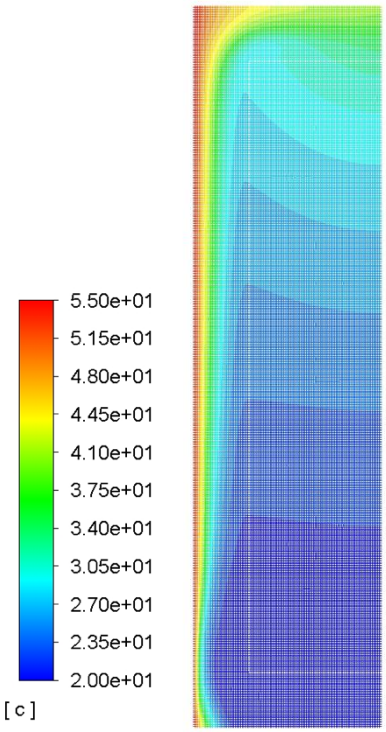

Fig. 110. P1a temperature contour (ºC).

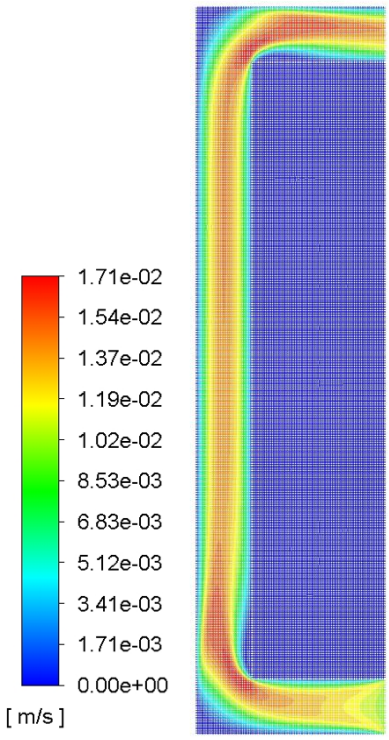

Fig. 111. P1a velocity contour (m/s).

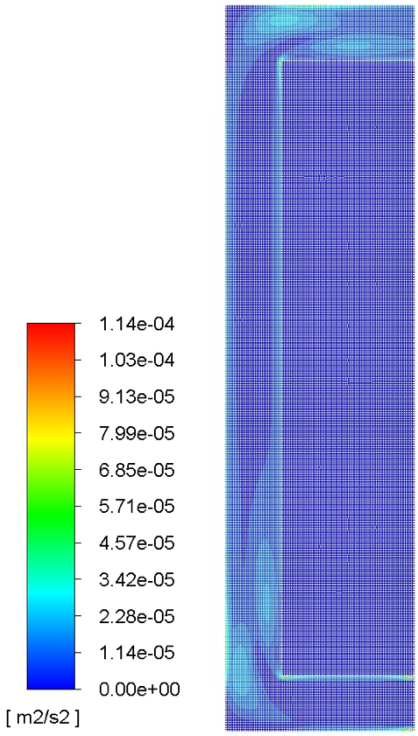

Fig. 112. P1a turbulence contour (m^2/s^2).

The temperature contour results for the P1b is shown in Fig. 113, the velocity contour in Fig. 114, and the turbulence contour in Fig. 115. As was previously seem in the other two systems, the temperature increases due to the source of heat from the PV module, entering the cavity in the inlet at a defined temperature of 20 ºC and leaving the air cavity at an T_{out} of near 40 ºC (achieving higher values than both of the other systems). The solid temperature presents a gradient that varies from 20 ºC to 28 ºC, in similarity to the air cavity, achieving higher temperatures in the upper part of its geometry. The temperature is higher near to the heat source and decreases in the X-direction in the approximation with the interior module that separates the air cavity from the test room. The air cavity velocity reaches a value to 0,015 m/s in some points. The results for the air velocity in P1b are lower than for P1a, due to the larger geometry in the X-direction (also reducing the turbulence regions in the system).

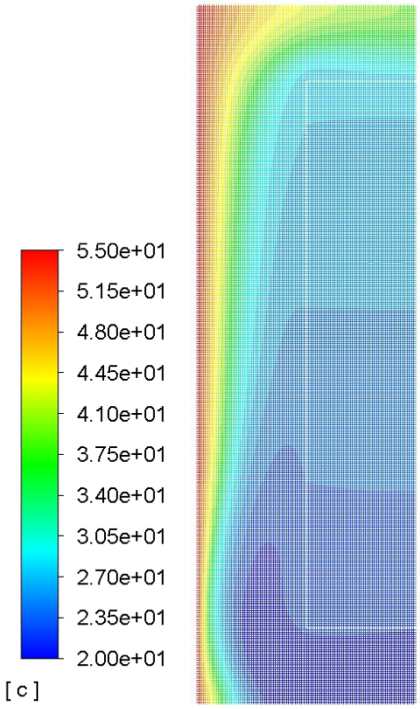

Fig. 113. P1b temperature contour (ºC).

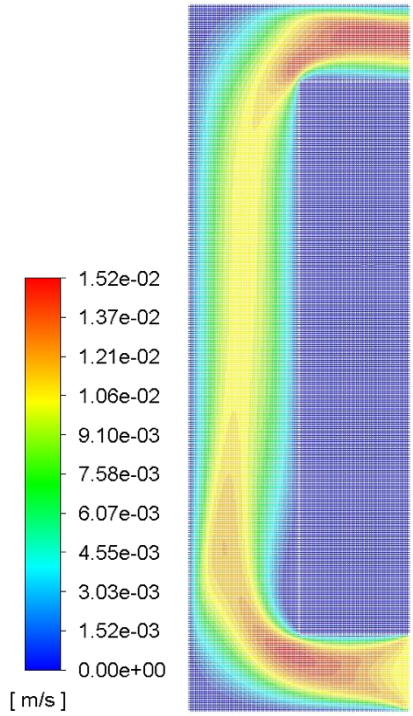

Fig. 114. P1b velocity contour (m/s).

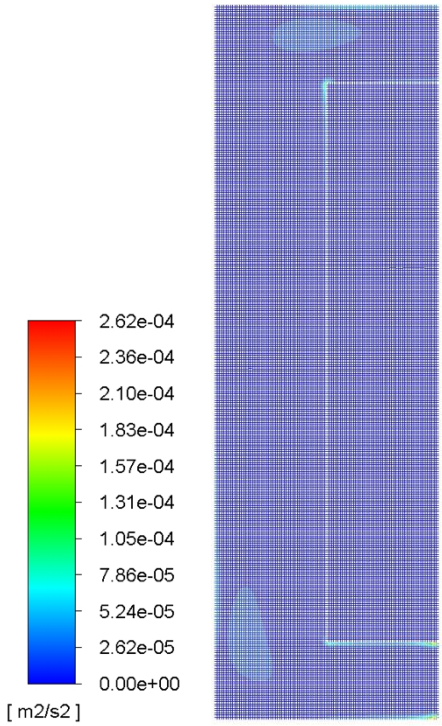

Fig. 115. P1b turbulence contour (m^2/s^2).

The data were considered validated by means of temperature comparison with the experimental data concerning detailed day of each BIPVT and prototype. This analysis through the CFD software, even not being extensive, is fundamental in different ways. First, the detailed profile of the cross-section modelling results is useful due to the impacts of the sensor location have on the results of the experimental analysis. For example, and taking into consideration the results obtained and shown, when the results obtained from a sensor located in the lower part of the air cavity closer to the interior module, and from another sensor located in the upper part of the air cavity closer to the PV module, it would result in a higher temperature gradient within the air duct, reflecting in a higher efficiency value than the actual efficiency of the system (keeping the other parameters constant).

It highlights the importance of the accurate experimental setup disposition within the system, to obtain more accurate results. Moreover, it enhances the importance of having more than one sensor to characterize the temperature profile, in experimental campaign terms, the air cavity. Furthermore, it highlights the importance of having more than one sensor to characterize the temperature profile, in experimental campaign terms, the air cavity.

However, it is important to refer to that the elements are very dynamic in terms of heat transfer, and the CFD analysis performed in the scope of this work is a steady-state simulation, representing the results of the calculation (until reaching convergence) for a certain set of inputs, that in other words represent a specific hour of the day and room condition in terms of the T_{inl}, interior wall/module temperature and backflow in the outlet. For further representation during the year, the BI-SES systems should be tested in a CFD analysis for more than one condition, in different hours of the day, and preferably in different weather stations. The CFD analysis is also shown very useful in preliminary analysis, pre-manufacturing of the final prototype design, to access the better materials and geometry in a more cost-effective way before production.

The next and last step in this work is the development of the dynamic simulation analysis.

5.2. Dynamic simulation in real conditions

Most studies on building heating and cooling load calculations are strongly based on computer simulations, due to the challenges posed by the many aspects involved in modeling the entire building. To evaluate the interaction between the system and the room, EnergyPlus software (EnergyPlus 2018) is used, in the version 8.6.0. EnergyPlus was developed by the US Department of Energy, with the primary purpose of estimating thermal changes, lighting levels, heating and cooling, natural ventilation, water uses, photovoltaic systems, thermal comfort indices, and other variables. It can be adapted to different climates from weather archives with hourly data. As a result, a wide range of calculated data, such as interior temperatures, surface temperatures, heat flow through building components, interior heat gains, air exchange, energy use and others, are obtained.

The real conditions dynamic simulation is focused on the Solar XXI NZEB test room and energy systems tested as integrated façade solutions. Overall, the main façade is south oriented, as it was possible to see on the case study section. The time step set for the simulation is 20 time steps per hours, beginning in 1st January and ending in 31st of December, accounting for 8760 hours simulated for each case in same boundary conditions regarding weather conditions

for the parametric analysis (based on the original weather file for Lisbon) and modified weather file for the model under validation process. The daylight-saving period was set from 30th March to 30th October. The HVAC template used for nominal energy needs calculation is 20 ºC for constant heating setpoint and 25 ºC for constant cooling setpoint, which results were obtained through the utilization of an ideal loads system (described in detailed parameters in Fig. 116). Detailed information is given in the next sub-section.

Field	Units	Obj1
Zone Name		Gabinete Thermal Zone
Template Thermostat Name		Termostato
System Availability Schedule Name		Always On
Maximum Heating Supply Air Temperature	C	50
Minimum Cooling Supply Air Temperature	C	13
Maximum Heating Supply Air Humidity Ratio	kgWater/kgDryA	0.0156
Minimum Cooling Supply Air Humidity Ratio	kgWater/kgDryA	0.0077
Heating Limit		NoLimit
Maximum Heating Air Flow Rate	m3/s	
Maximum Sensible Heating Capacity	W	
Cooling Limit		NoLimit
Maximum Cooling Air Flow Rate	m3/s	
Maximum Total Cooling Capacity	W	
Heating Availability Schedule Name		
Cooling Availability Schedule Name		
Dehumidification Control Type		ConstantSensibleHeatRatio
Cooling Sensible Heat Ratio	dimensionless	0.7
Dehumidification Setpoint	percent	60
Humidification Control Type		None
Humidification Setpoint	percent	30
Outdoor Air Method		None
Outdoor Air Flow Rate per Person	m3/s	
Outdoor Air Flow Rate per Zone Floor Area	m3/s-m2	
Outdoor Air Flow Rate per Zone	m3/s	
Design Specification Outdoor Air Object Name		
Demand Controlled Ventilation Type		None
Outdoor Air Economizer Type		NoEconomizer
Heat Recovery Type		None
Sensible Heat Recovery Effectiveness	dimensionless	0.7
Latent Heat Recovery Effectiveness	dimensionless	0.65

Fig. 116. EnergyPlus interface example and the Ideal Loads object.

5.2.1. Model validation

First, the model for experimental validation was developed (M1). This model was elaborated in order to compare its results with the data recorded by the experimental campaign carried out at the test room site, to validate the inputs inserted in the program. To ensure that the results obtained by computer modeling effectively represent the thermal behaviour of the building, it is essential that the simulation model is properly calibrated (Nannei and Schenone 1999). The usage pattern (occupancy, lighting and equipment) registered in the building for the considered days was inserted in the validation model, from data in Chapter 3. Moreover, observational

measurements were done to confirm the infiltration calculations.

The weather file containing the TRY values (reference year) of the city of Lisbon was modified, with radiation, temperature data and relative humidity recorded by the experimental campaign. The modification of the weather file may be a tricky process, and the steps were used and are described in detail in (J. Pereira 2015). The weather file was modified using the experimental data from January and February of 2018, and the remaining of the file was kept as the original. After the modification of the weather file, this study followed to the simulation of the validation model. The procedure to modify the EPW file is described (J. Pereira 2015).

The simulation parameters used for the validation model are described in this sub-section and are kept for all the models developed in EnergyPlus in the scope of this work. The main simulation parameters and objects, and is value/option are:

- Simulation control - "run simulation for Weather file run periods";
- Building – south oriented, solar exposed, wind exposed, city, convergence criteria for thermal loads of 0,04 and for temperature 0,4 ºC, solar distribution full interior and exterior, and 25 days of convergence;
- Shadow calculation – 20 days (standard value);
- Surface convection algorithm – inside and outside; DOE2 and TARP;
- Timestep – 20 timesteps per hour;
- Site location – Lisbon;
- Run period – whole year;
- Schedules compact – based on the previously described occupation pattern during a typical week of work;
- Surface elements – as previously described in the case study section;
- Surfaces and thermal zones – as previously described in the case study section;
- Interior loads – people, lights and equipment as previously described in the case study section;
- Infiltration flow rates – as previously described in the case study section;
- Output reporting – variable dictionary, variables (zone temperature and ideal loads) and diagnostics, with display of extra warnings.

The results obtained for the model using EnergyPlus software were compared with temperature measurements made within the thermal zones in which the case study was performed.

The root mean square error (RMSE) (Eq. 14) and mean bias error (MBE) were calculated and compared with the maximum allowable values for validation (Nannei and Schenone 1999; ASHRAE Guideline 2002; 2014). To have a more accurate validation of the model, two periods were used (from 22/01/2018 to 28/01/2018 and from 15/02/2018 to 22/02/2018). To demonstrate the comparison between the fluctuations of temperature in experimental results and simulation results, Fig. 117 presents three days of the second validation period, for the room and the BIPVT.

$$RMSE = \sqrt{\frac{1}{n}\sum(y_t - \hat{y}_t)^2} \quad \text{Eq. (14)}$$

Taking into consideration the parameters of Coefficient of Variation of Root-Mean Squared Error(cv(RMSE)) (Eq. 15) and of the mean bias error (MBE) (Eq. 16), the model was considered validated due to the parameters' result being within the limits suggested by the references, as shown in Table 15.

$$MBE = \frac{1}{n}\sum(y_t - \hat{y}_t) \quad \text{Eq. (15)}$$

$$cv(RMSE) = \frac{\sqrt{\frac{1}{n}\sum(y_t - \hat{y}_t)^2}}{\bar{y}} \quad \text{Eq. (16)}$$

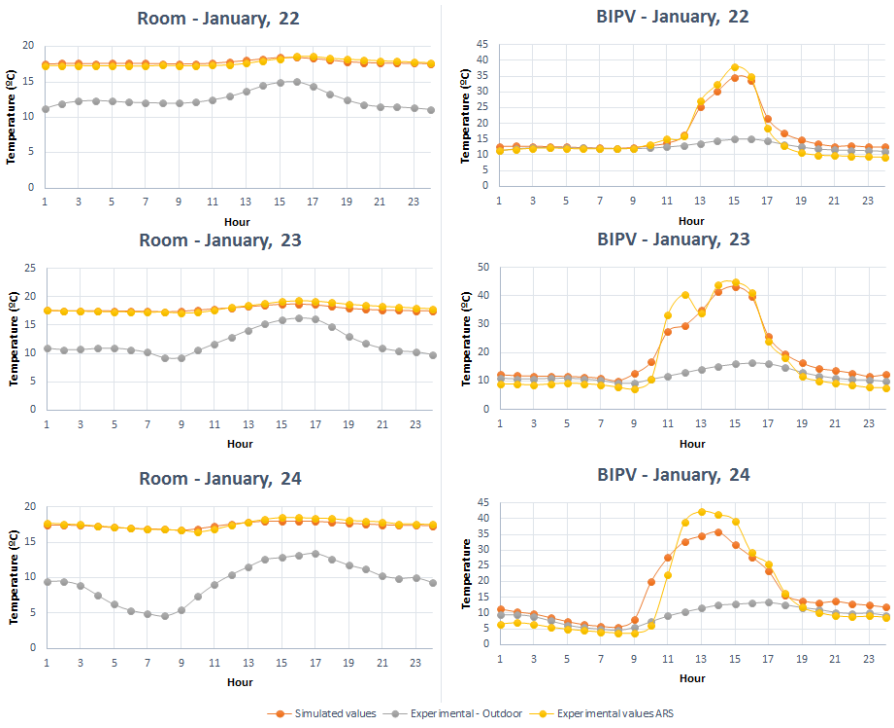

(a)

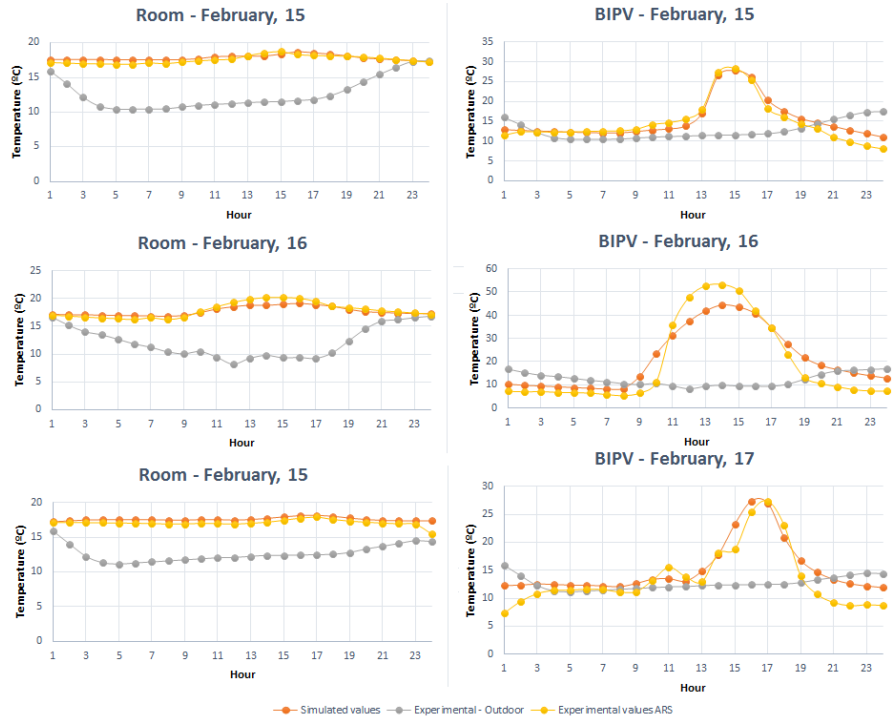

(b)

Fig. 117. Validation model results and experimental results comparison (2018).

Table 15. Calculation of the validation parameters and their limits – Period 1.

From 22/01/2018 to 28/01/2018		
RMSE	***cv(RMSE)***	***MBE***
	Room	
0.341	0.019	0.004
	BIPVT	
4.103	0.248	-0.078
From 15/02/2018 to 22/02/2018		
RMSE	***cv(RMSE)***	***MBE***
	Room	
0.550	0.031	-0.011
	BIPVT	
4.229	0.260	-0.081
Limits	*0.3*	*0.1*

5.2.2. Parametric analysis

The parametric analysis aims to recognize the impact of different parameters in the overall building performance. After validating the model, the scenarios for the parametric analysis were set and the reference models were developed. The reference model is the model that effectively represents the building with one or other system, used for comparison with other models in which different strategies are inserted, and is different for each system under consideration, as explained in the next sub-sections.

To simulate these models, all the inputs needed are added into the model on EnergyPlus and the weather file that contains the values of TRY (Test Reference Year - climatic reference year) of the city of Lisbon was used, without any kind of modification (and thus, different from what was previously used in the validation model).

A utilization pattern was also established, for occupation, and equipment – for working hours from Monday to Friday, from 08:00h to 12:00h and from 13:00h to 17:00h. Lighting was not considered due to the good solar light exposition of the room. Total thermal gains are convective, radiant and latent gain results in various proportions. Convective gains are instantaneous additions of heat to the thermal zone, since the radiant gains are distributed on the surfaces of the zones where they are first absorbed and then released. Latent gains, in turn, need to be handled through ventilation and air conditioning (DOE, 2017).

The established BIPVT and prototype infiltration was 0,01 m^3/s whereas for the room was 1,32 air change per hour, and considered constant along the simulation period. It is important to highlight that the prototype is equipped with vents that increase the air flow of the natural convection through forced convection, and despite not being tested in the experimental campaign, they are considered in the numerical analysis through the assumption of different air flow rates. The window is closed all the time.

5.2.2.1. Geometries of the systems in the façade

The parametric analysis accounts with different geometries, not only one for all the models. The three geometries were developed, through the OpenStudio plug-in in SketchUp, for the test room with the BI-SES elements. The figures (Fig. 118, Fig. 119 and Fig. 120) present the geometry normal (a), and the same geometry renderized (b) to segment the thermal zones by color. The test room with the BIPVT element is presented in Fig. 118. The test room with the P1a and P1b (once both have same geometry, despite varying in interior component construction) is shown in Fig. 119. The geometry of the simulations with both BI-SES systems – BIPVT and prototype – is shown in Fig. 120.

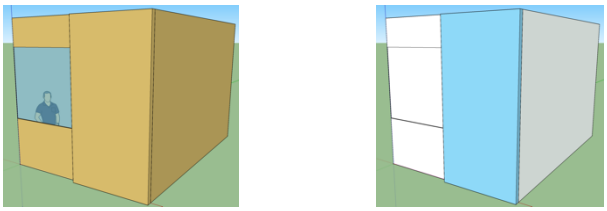

(a) (b)

Fig. 118. Test room and BIPVT SketchUp geometry: a) normal render, and b) render based on thermal zones.

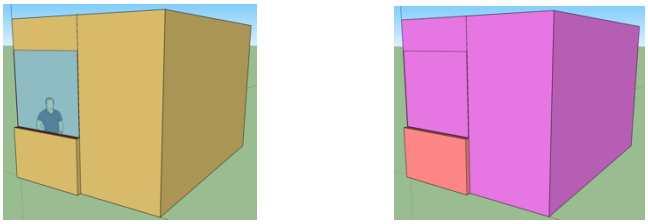

(a) (b)

Fig. 119. Test room and Prototype SketchUp geometry: a) normal render, and b) render based on thermal zones.

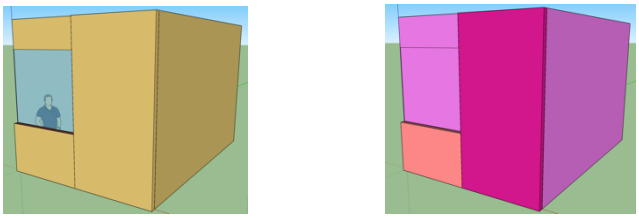

(a) (b)

Fig. 120. Test room, Prototype and BIPVT SketchUp geometry: a) normal render, and b) render based on thermal zones.

5.2.2.2. Simulation scenarios

The scenarios simulated in the parametric analysis have been studied in terms of five groups of parameters:

- Window blind position (Open or closed);
- Air gap thickness (0.5, 0.1, 0.16, 0.20 m);
- Zone mixing air flow (0.01, 0.02, 0.03 m^3/s);
- Number of PV panels (4, 3, 2, 1 panel);
- Zone mixing setpoint for operation (detailed in Table 16).

Table 16 presents the scenarios with blinds open, and accounts for 41 scenarios. The study in the scope of this thesis is, however, composed by 82 scenarios (second set is composed by Table 16 scenarios except the window blinds are always closed). It is important to highlight that in a real-life situation, there would be needed to account with lighting system to provide adequate visual comfort. However, for providing equal conditions of internal gains for comparison purposes, the lights were not considered.

Table 16. Parametric analysis scenarios.

Group	***Room and system***			***Air cavity thickness (m)***				***Zone mixing air flow (m3/s)***			***Nº of PV panels***				***Zone mixing setpoint***				
Value	***BIPVT***	***P1a***	***P1b***	***0,05***	***0,1***	***0,16***	***0,20***	***0,01***	***0,02***	***0,03***	***4***	***3***	***2***	***1***	***Dec-Feb from 10h to 16h***	***Nov-Mar from 10h to 16h***	***Always on, Source >18 ºC and Gab <24 ºC***	***Always on, Source >20 ºC and Gab <24 ºC***	***Dec-Feb from 10h to 16h and Gab < 24 ºC***
M1	x					x		x			x				(opening of the vents according to experimental campaign)				
M2	x					x					x						(vents always closed)		
M3[1]	x					x		x			x				x				
M4	x					x		x			x					x			
M5	x					x		x			x						x		
M6	x					x		x			x							x	
M7	x					x			x		x				x				
M8	x					x			x		x					x			
M9	x					x			x		x						x		
M10	x					x			x		x							x	
M11	x					x		x				x			x				
M12	x					x		x					x		x				
M13	x					x		x						x	x				
M14	x				x			x			x				x				
M15	x						x	x			x				x				
M16		x			x												(vents always closed)		
M17[2]		x			x			x							x				
M18		x			x			x						x		x			
M19		x			x			x						x			x		
M20		x			x			x						x				x	
M21		x			x				x					x	x				
M22		x			x					x				x	x				
M23		x			x				x					x			x		

M24		x			x					x		x					x					
M25		x		x				x				x	x									
M26		x					x	x				x	x									
M27			x		x										(vents always closed)							
M28[3]			x		x			x					x									
M29			x		x			x				x			x							
M30			x		x			x				x					x					
M31			x		x			x				x							x			
M32			x		x				x			x	x									
M33			x		x					x		x	x									
M34			x		x				x			x					x					
M35			x		x					x		x					x					
M36			x	x								x	x									
M37			x				x	x				x	x									
M38	x	x		x				x				x	x									
M39	x	x		x				x				x										x
M40	x		x	x				x				x	x									
M41	x		x	x				x				x										x

[0]Validation model [1] Reference model for the BIPVT set; [2] Reference model for P1a set; [3] Reference model for P1b

5.2.2.3. Reference cases

For the BIPVT, the reference case is considered as being the M3. For the P1a, the reference case is considered as being the M17. For the P1b, the reference case is considered as being the M28. Moreover, four scenarios are simulated considering both systems. The characteristics of the reference cases, for each system, are presented below:

- **M3 (BIPVT)**: is represented by an air cavity thickness of 0,16 m, with zone mixing air flow of 0,01 m^3/s, 4 PV modules, zone mixing fixed scheduled from December to February.

- **M17 (P1a)**: is represented by an air cavity of 0,10 m, with zone mixing air flow of 0,01 m^3/s, 1 PV module, zone mixing fixed scheduled from December to February.

- **M28 (P1b)**: is represented by an air cavity of 0,10 m, with zone mixing air flow of 0,01 m^3/s, 1 PV module, zone mixing fixed scheduled from December to February.

5.2.2.4. Simulation results

The obtained results are fully presented here in terms of nominal energy needs for heating and cooling of the building, taking into consideration a setpoint of T_{comf} with lower limit at $T_{comf}^{min} = 18$ ºC (under which the building will be thermal conditioned) and upper limit at $T_{comf}^{max} = 25$ ºC (above which the building will be thermal conditioned). As the description of each scenario were given in Table 16, Table 17 presents the results for all the scenarios under consideration in this parametric analysis.

Table 17. Nominal energy needs results for the parametric analysis.

Model	Simulation with windows without blind				Simulation without window blind			
	Heating	Cooling	Total	%	Heating	Cooling	Total	%
M1[(0)]	(model developed for validation in free-floating mode)							
M2	0,02	36,4	36,42	-3,60%	19,98	1,16	21,15	25,59%
M3[(1)]	0	37,78	37,78	*	15,27	1,57	16,84	*
M4	0	39,99	39,99	5,85%	13,71	1,16	14,87	-11,70%
M5	0	36,34	36,34	-3,81%	11,42	0,86	12,29	-27,02%
M6	0	36,49	36,49	-3,41%	11,19	1,23	12,43	-26,19%
M7	0	40,44	40,44	7,04%	13,5	1,16	14,65	-13,00%
M8	0	44,98	44,98	19,06%	9,65	1,35	11	-34,68%
M9	0	36,05	36,05	-4,58%	8,1	0,54	8,64	-48,69%
M10	0	36,32	36,32	-3,86%	7,73	1,09	8,82	-47,62%
M11	0	38,99	38,99	3,20%	15,34	1,13	16,47	-2,20%
M12	0	39,98	39,98	5,82%	15,27	1,14	16,41	-2,55%
M13	0	40,48	40,48	7,15%	15,26	1,15	16,42	-2,49%
M14	0	42,39	42,39	12,20%	13,87	2,02	15,88	-5,70%
M15	0	38,56	38,56	2,06%	14,57	1,83	16,39	-2,67%
M16	0	37,77	37,77	-2,73%	18,93	0,96	19,89	-22,49%
M17[(2)]	1,24	37,59	38,83	*	24,71	0,95	25,66	*
M18	0	39,53	39,53	1,80%	15,6	0,95	16,55	-35,50%
M19	2,68	34,82	37,5	-3,43%	31,42	0,17	31,59	23,11%
M20	2,19	34,82	37,01	-4,69%	26,5	0,17	26,67	3,94%
M21	4,95	37,52	42,47	9,37%	30,11	0,95	31,06	21,04%
M22	9,91	37,48	47,39	22,04%	35,54	0,95	36,49	42,21%
M23	0	37,81	37,81	-2,63%	10,3	1,03	11,33	-55,85%
M24	0	37,81	37,81	-2,63%	7,99	0,95	8,94	-65,16%
M25	0,91	37,6	38,51	-0,82%	23,52	0,95	24,47	-4,64%
M26	0,88	37,48	38,36	-1,21%	23,62	0,92	24,54	-4,36%
M27	0,08	37,26	37,34	-3,44%	19,76	1,85	21,61	-18,30%
M28[(3)]	1,47	37,2	38,67	*	24,62	1,83	26,45	*
M29	0,07	38,07	38,14	-1,37%	17,45	1,83	19,28	-27,11%
M30	2,84	35,31	38,16	-1,32%	30,58	0,98	31,57	19,36%
M31	2,29	35,31	37,61	-2,74%	26,51	0,98	27,49	3,93%
M32	4,57	37,16	41,73	7,91%	29,24	1,83	31,07	17,47%
M33	8,59	37,13	45,73	18,26%	33,89	1,83	35,72	35,05%
M34	0,04	37,26	37,3	-3,54%	13,49	1,85	15,33	-42,04%
M35	0,03	37,24	37,27	-3,62%	11,52	1,78	13,3	-49,72%
M36	0,03	37,24	37,27	-3,62%	21,2	1,78	22,99	-13,08%
M37	0,68	36,53	37,2	-3,80%	22,15	1,66	23,8	-10,02%
M38	0	45,18	45,18	19,59%	12,57	3,21	15,78	-6,29%
M39	0	38,29	38,3	1,38%	12,79	1,44	14,23	-15,50%
M40	0,05	43,15	43,2	14,35%	14,34	3,95	18,29	8,61%
M41	0,08	37,86	37,94	0,42%	14,34	2,37	16,71	-0,77%

[(0)]Validation model [(1)] Reference model for the BIPVT set; [(2)] Reference model for P1a set; [(3)] Reference model for P1b

To evaluate the effect of the strategies (presented in Table 16) on energy use while reducing the uncertainty brought by the direct heat gain through the window, two sets of scenarios were simulated. In the first set, the blinds were considered open all the time. In the second set, the blinds were considered totally closed all the year.

Fig. 121 presents the simulation results from M2 to M41 (without window blinds), showing the heating, cooling and total energy needs. It is possible to see that the cooling energy needs are predominant and may constitute the total of the energy needs for the building to reach comfortable temperatures. Fig. 122 presents the simulation results from M2 to M41 with window blinds always closed, showing the heating, cooling and total energy needs.

It is possible to see that there is a shift in the energy needs, from cooling to heating, point to the huge role the direct heat gains play in the thermal behaviour of the building. In most cases, the total energy needs dropped by almost half of its value. The models growth in complexity, and for this reason, M2 shows the results for the room with windows closed and without any air mixing between the zones. From M3 onwards, the models beginning to present air mixing between zones.

As described in Table 16, from model 3 to model 16, the simulations concern about the use of BIPVT element. Model 3 to model 6 present the room with the BIPVT with 0,16m of air cavity thickness, varying the zone air mixing parameter, from two fixed schedules of operation to two smart operations (0,01 m^3/s). Among these models, the fixed operation schedule (presented in the simulation scenarios) resulted in higher values of the nominal energy needs, whereas the smart operation (with very similar results between them) presented a decrease in the nominal energy needs, in comparison with fixed schedule. From model 7 to model 10, the schedule of operation of the air mixing are also evaluated, however with an increased flow of 0,02 m^3/s. In this group, the smart operation schedule shows similar results than the previous ones with reduced air flow, however the energy needs for the fixed schedule increased.

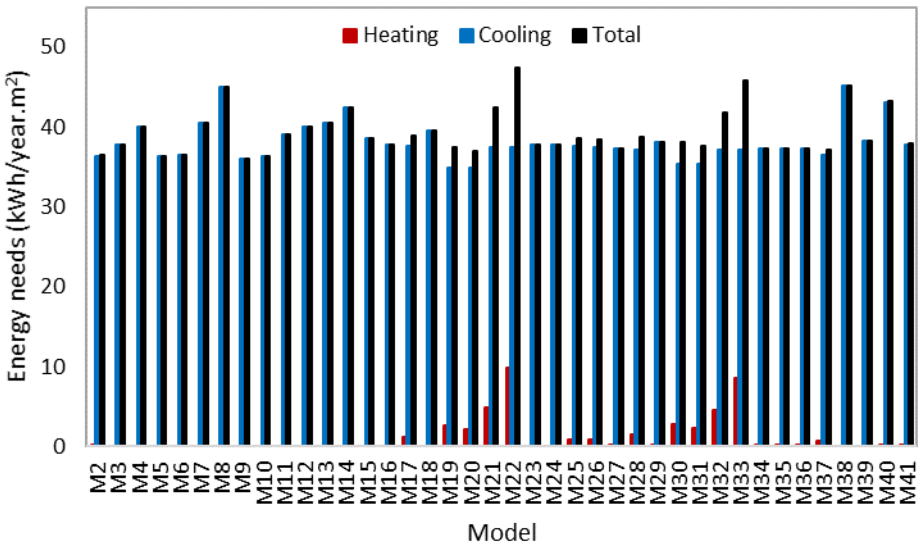

Fig. 121. Simulation results for the scenarios with window blinds always open.

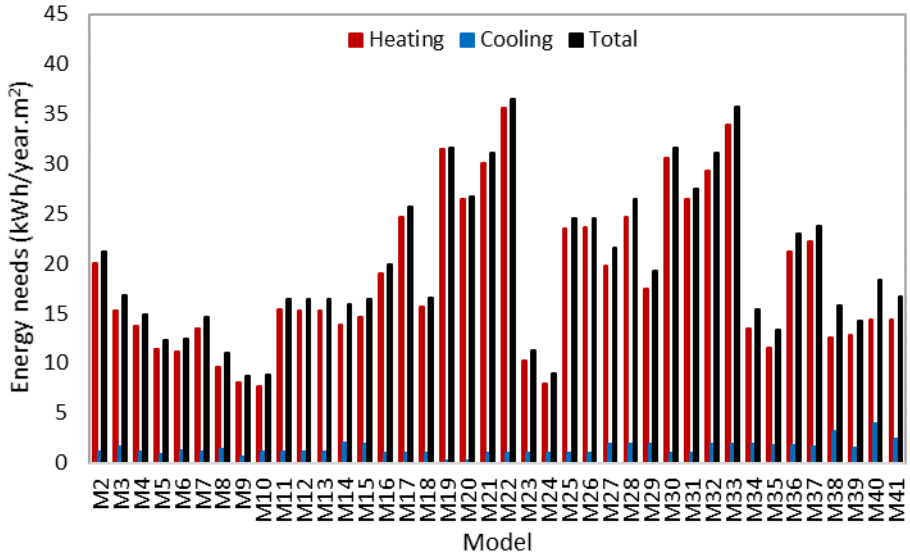

Fig. 122. Simulation results for the scenarios with window blinds always closed.

As described in Table 16, from model 11 to model 13 (and model 6, same configuration but with 4 panels), the number of PV modules vary (while the air mixing are maintained with fixed schedule). For this group, it is possible to notice that the energy needs are inversely proportional to the number of panels - as the number of PV modules decrease, the energy needs increase. Model 14 and model 15 vary the thickness of the air cavity to 0,10 m and 0,30 m, respectively. The needs are higher for the lower values of the air cavity thickness.

Concerning the segmented results for each kind of system, Fig. 123 presents the same obtained results, but only for the BIPVT system. The system with higher energy needs are the M8 (0,02 m^3/s in zone mixing system and setpoint of operation from Nov-Mar from 10h to 16h) the variations among models reach 10 kWh/year.m^2. For most of the models, the results vary slightly. Considering the simulations with the blinds always closed, it is possible to notice, however, that the M9 is one of the models with the lower total energy needs results (Fig. 124).

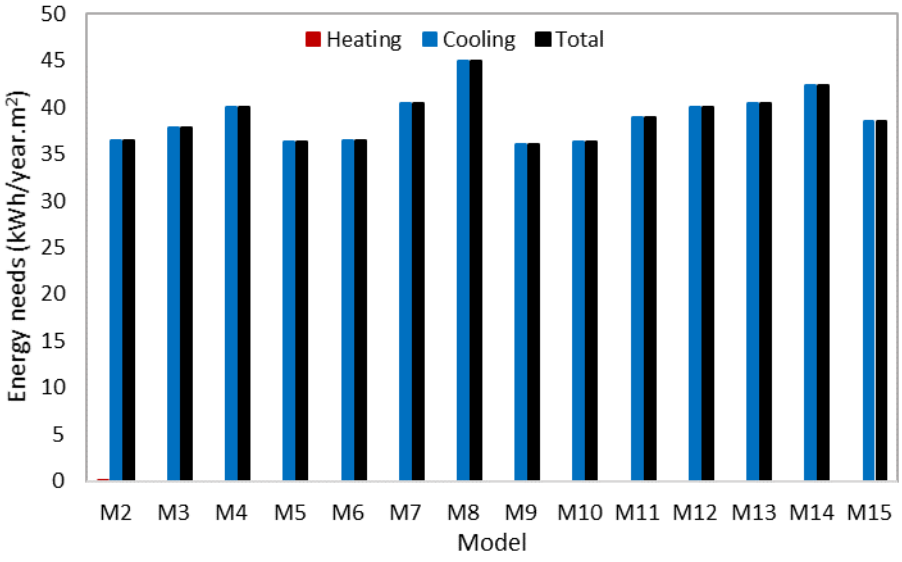

Fig. 123. BIPVT simulation results with window blinds always open.

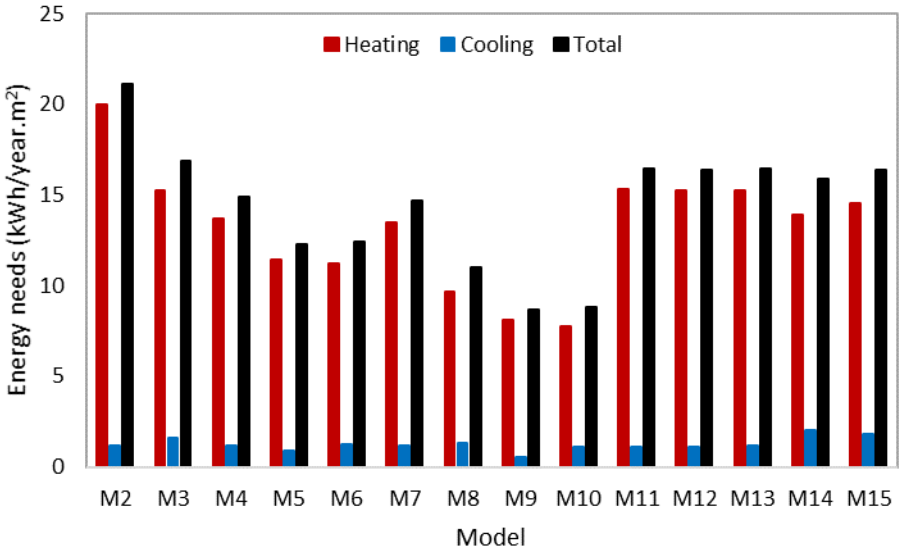

Fig. 124. BIPVT simulation results with window blinds always closed.

Results for P1a are presented in Fig. 125 and Fig. 126 (for window without blind and with blind, respectively). From model 16 to model 26, the results refer to the P1a, varying the same

parameters, except with different air cavity thicknesses. The results with the window glazing opened are shown from model 17 onwards, once model 16 correspond to the model without air changes between zones, and results with air mixing between zones are shown from model 17 to model 26. The results, for the P1a and considering the window blind open, are very similar, with exception to model 22, in which the air cavity thickness was increased to 0,3 m. The simulation results for the model with smart operation schedule are lower than the ones with fixed schedule of operation. Very similar results may be seen for P1b, in Fig. 127 (window blind open) and Fig. 128 (window blind closed).

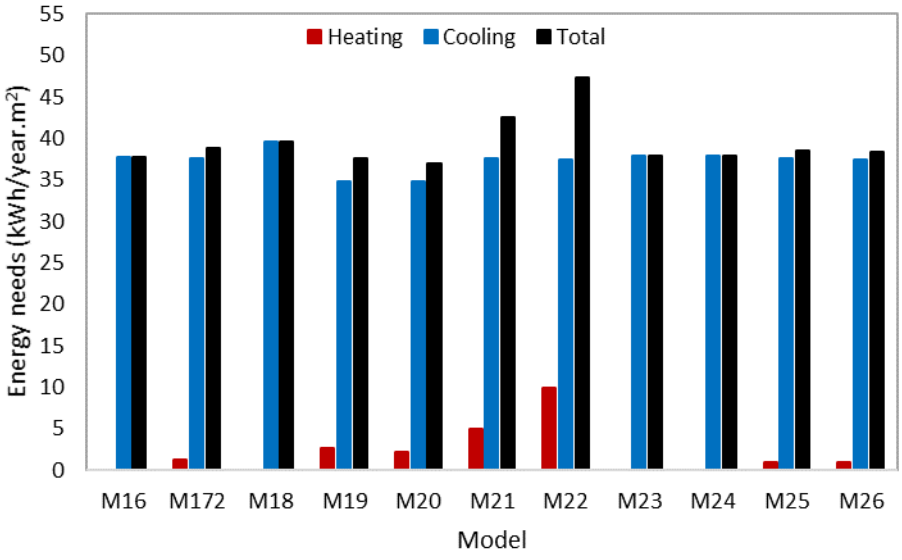

Fig. 125. P1a simulation results with window blinds always open.

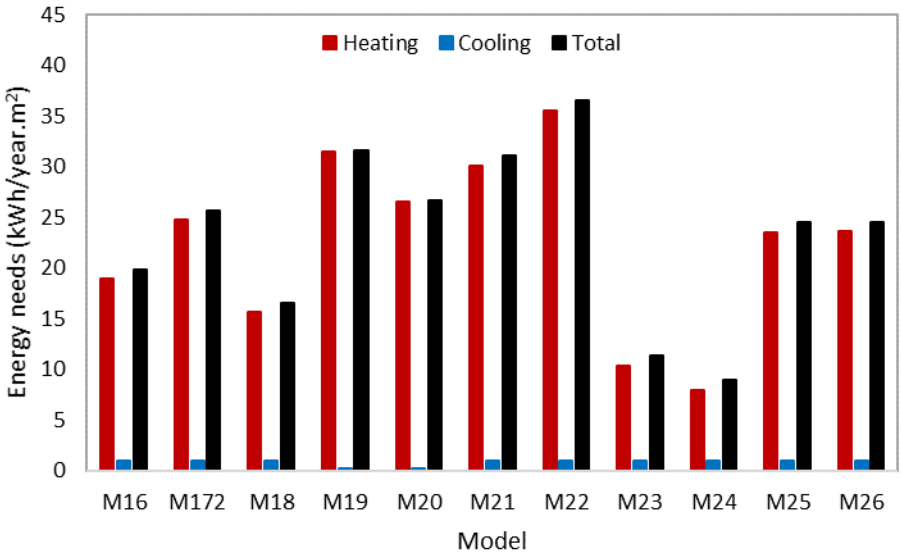

Fig. 126. P1a simulation results with window blinds always closed.

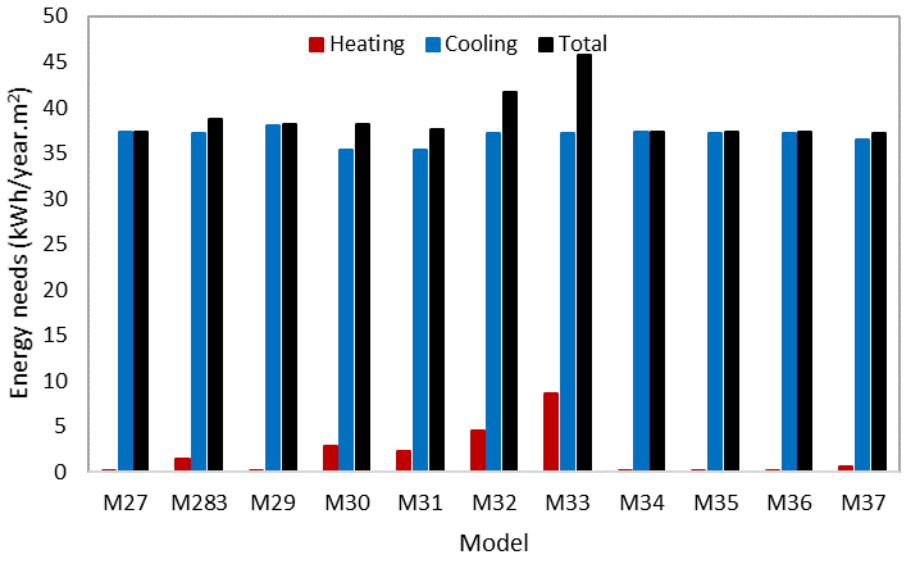

Fig. 127. P1b simulation results with the window blinds always open.

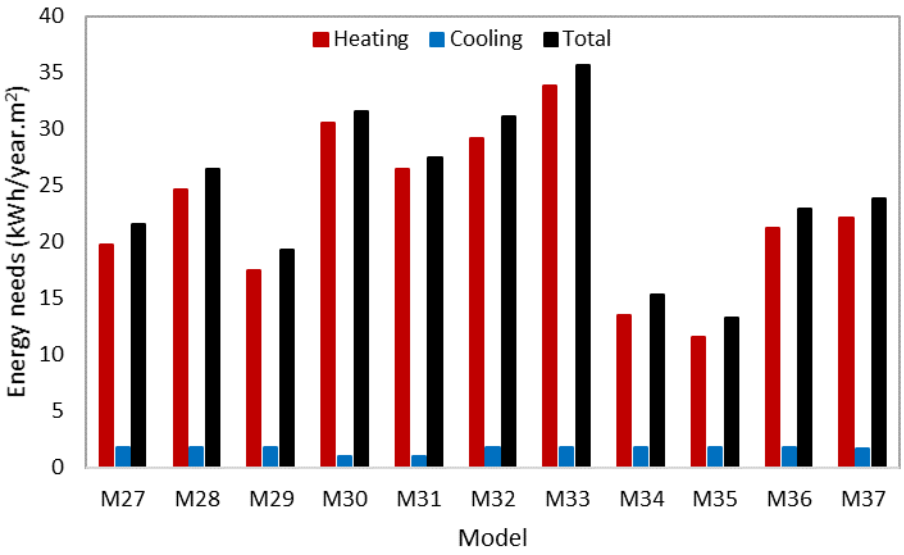

Fig. 128. P1b simulation results for the window blinds always closed.

From model 38 to model 41, the results refer to both the systems - BIPVT and prototype (P1a and P1b). They present the association of the system, operating at the same control logic of air mixing between zones (one smart and one fixed for P1a and BIPVT; one smart and one fixed for P1b and BIPVT). The percentual impact of these models are in relation to the reference model of the BIPVT set of models (M3).

The percentual results in relation to the reference models results are presented in Fig. 129 for the simulations without window blinds and in Fig. 130 for the simulations with window blinds closed. For the first set, the higher percentual impact was an increase of 22,04%, namely in

model M24. Higher reduction was near 5% in model M22. For the second set (with blinds closed, Fig. 123) model 22 also presented the higher impacts in increasing, whereas M24 presented the higher impacts in decreasing the energy needs.

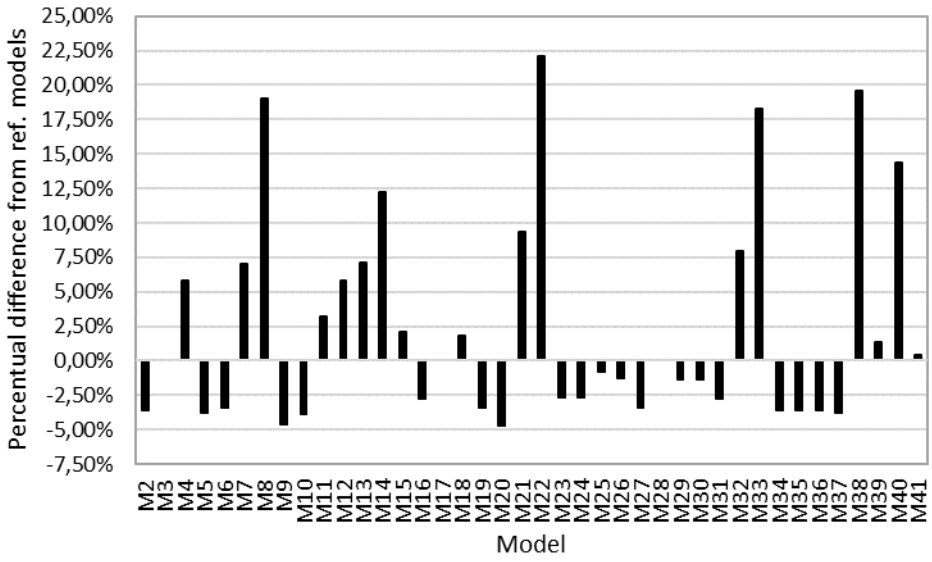

Fig. 129. Percentual difference from the reference cases – simulation with window blinds open.

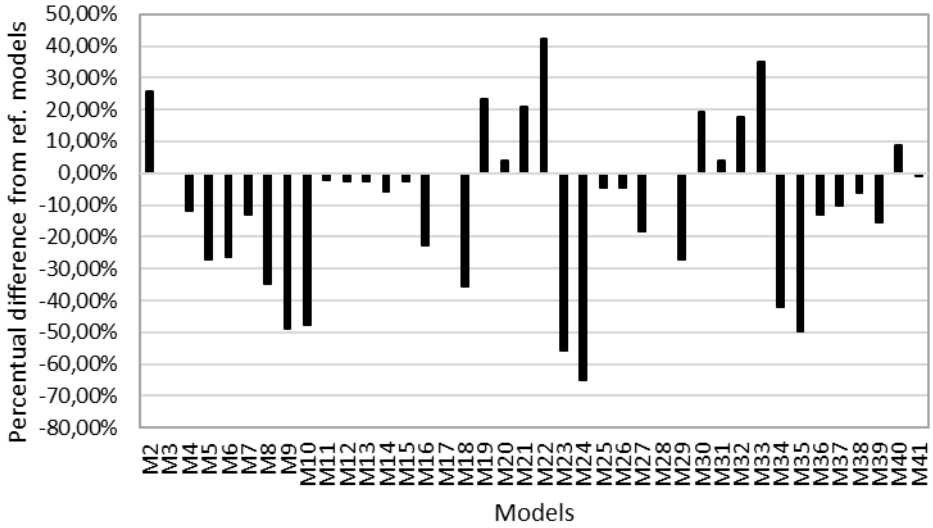

Fig. 130. Percentual difference from the reference cases - simulation with window blinds closed.

Overall, as it is possible to see in the results shown, for the cases in which the room does not have the blind closed, the BIPVT is the system with the higher number of scenarios in which the nominal energy needs increase compared to the reference model, reaching a percentual increase of nearly 20%. The higher percentual increase may be found, however, in the P1a group, namely for the model 22 – with fixed schedule of operation and 0,02m^3/s of air flow.

P1b also presents the most critical value for the same configuration of P1a, with exception of having a different interior module (M33). Still considering the blinds opened, for the best situation in each one of the systems, concerning the BIPVT system the model 5 and model 6 (smart operation of the air mixing between zones), model 9 and model 10 presented improvements in comparison to its reference model (flow increased to 0,02 m^3/s and also smart operation). For the P1a, model 19 and model 20 (smart operation), model 23 and model 24 (smart operation with increased air mixing flow), and model 25 and model 26 (0,05m of air cavity thickness and 0,2m of air cavity thickness, even presented improvements in comparison to its reference case.

For the P1b (in the set with blinds opened), model 29, model 30 and model 31 presented reductions in comparison with the reference case. In these models, the schedule of air mixing operation is varied from different fixed-time of operation and also smart operation. Also, model 34 and model 35 presented improvements, considering smart operation and increased air flow in the air mixing between zones.

Moreover, model 36 and model 37 presented improvements in comparison to its reference case, having them different air cavity thicknesses and maintaining the fixed schedule of operation used in the reference model. For the conjugation of both of the systems, with blinds opened, the only situations in which the energy needs decrease is in the smart operation of the air mixing between zones, showing the effective work of the controlling system adopted.

When the simulation set is changed to the direct solar gains avoided with the use of a blind on the window, as was previously seem, the situation is inverse. The overall energy needs reduce considerably in comparison to the reference case, despite some of the models still reach critical raise on the needs compared to the reference case, as is the case of model 19 to model 23 (P1a). In this situation of avoidance of the direct solar gains, all the models contribute to reducing the energy needs compared to model M2, where only the BIPVT system exists but no air change is done between the room and the system.

When the window blind is open, the smart operation of the air mixing is the main contributor to reducing the energy needs of the buildings, showing that a totally passive operation is not the best choice when comparing to operation focusing on meeting temperature requirements. The air flow of the air mixing between the systems and the room do also have positive impact for the prototype, but may have reverse effect on the BIPVT, due to the bigger area of the heat

source surface (four PV modules instead of one).

5.3. Numerical analysis main remarks

This study developed a numerical analysis segmented in two parts: system simulation (through the use of CFD method) and dynamic simulation of the interaction of the system and the adjacent thermal zone (through the use of the software EnergyPlus). The main remarks of the CFD numerical analysis are here presented.

- The CFD simulation was a cross-section analysis (2D) of the systems;
- The mesh was set uniform and with size of 0,005 and 0,002m due to computational capabilities, in steady-state simulation;
- It is recognized that the results may be limited, and in the future the analysis should have non-uniform mesh with higher resolution in the contour parts and inlet and outlet;
- A 3D analysis would benefit the analysis, in which the system horizontal length is also assessed.

Concerning the dynamic simulation analysis, the main remarks are here briefly presented:

- When the window blind is open, the smart operation of the air mixing is the main contributor to reducing the energy needs of the buildings, showing that a totally passive operation is not always the best choice;
- The air flow rate of the air mixing between the systems and the room do also have positive impact for the prototype, but may have reverse effect on the BIPVT, due to the bigger area of the heat source surface;
- In buildings as Solar XXI, can benefit from the amount of data the monitoring systems can supply, and from the awareness of the building occupants about the controlled ambient that is desired to generate in the test rooms (as the need to avoiding opening doors and windows without the need of it). However, it is also necessary to recognize that the existence of different systems in the same ambient (as earth pipes, blinds and BIPVT wall) can increase the uncertainty applied to the results;
- It was important to complement the experimental analysis with the numerical analysis, in order

to validate de data and access the thermal behaviour of the systems through simulation, in which the different systems could be brought to the same basis of weather conditions and room usage operation.

Chapter 6. Conclusions

6.1. Main findings

In this work, the design and thermal behaviour of the BI-SES elements and its integration with the test room has been studied by means of design, experimental and numerical analysis. In the last years, there has been a growing focus on the strategic development of building façades, in order to make the elements to meet engineering requirements while contributing to improve the sustainability of the building, in terms of reducing the energy demand and contributing to the energy supply. This strategic development brings new experiments, innovative systems and technology to the formal functions of the envelope. Given this context and the flexibility the façade elements can offer in terms of design and materials, innovative façade elements based on solar energy systems can introduce significant benefits.

The main aim of the present study is to propose the design of new concepts of BIPVT systems, to assess their performance through the use of solid experimental investigation, to develop a numerical analysis to assess the systems through the use of CFD analysis, and to develop a parametric analysis based on validated models of dynamic simulation of the integration between the systems and the test room, aiming to improve the system design.

The building in which the case study is based is the Solar XXI building from the National Laboratory for Energy and Geology, Lisbon, Portugal, which is recognized for having implemented a wide range of strategies to reduce the cooling and heating loads through solar control strategies and passive systems as buried pipes. The main building façade is composed by building integrated photovoltaic thermal systems (BIPVT), that aim not only to generate electrical energy but also act as a heat recovery system. In the whole building, these systems consist of 76 photovoltaic multi-crystalline silicon modules and have an area of about 96 m^2 and 12 kW peak power installed.

The findings of this work indicated that the existent (BIPVT) and the proposed (P1a and P1b) façade BIPVT prototype have a good potential to improve the sustainability of the building by reducing the nominal energy needs for achieving thermal comfort. Their operation mode must,

however, be adequate to the other strategies' existent in the room, as the presence of windows and blinds for the allowance or avoidance of direct solar gains.

State of the art

In this work, an extensive review of the state of the art of the Building Integrated Solar Energy Systems (BI-SES) studies being published in the recent years was presented. More than 100 papers were reviewed in this section, in order to elaborate a broad panorama of the current BI-SES being developed (segmented in photovoltaic, thermal and hybrid systems), and design and optimisation practices concerning the engineering point of view. It was found out that the BIPV is still the system with more studies being published in the recent year, however other innovative designs concerning thermal and hybrid system are emerging, focused mainly in the use of innovative materials and in the use of solar energy elements as shading devices.

New BIPVT prototype

The need of the design of new building integrated solar energy systems to continually improve the integration of renewable energy in the urban context was addressed in this thesis. The proposition of the new system prototype was based on the use of engineering concepts, methods and techniques in order to provide a solution that contributes to meet the needs identified. The objective of this work was to develop an innovative BIPVT that promoted the reduction of both heating and cooling energy needs while generating electricity, being also modular and able to work through passive techniques, either operated manually or automatically. The prototype required an area compatible with the area of the lower glazing surface of the test room. It consists of a frame, a built-in photovoltaic panel module, inverter and other accessories, adjustable air cavity, P1a) an isolation built-in module and P1b) a storage built-in module (water tank), and then substitution between them in the construction solution is possible. The automatic operation is based on the sensors installed on the prototype.

Experimental analysis

The experimental analysis was developed to obtain a detailed characterization of the systems in real use conditions in the building. Three main aspects were studied in this thesis, concerning the experimental analysis. They were the weather parameters, the BI-SES parameters, and the room parameters.

The weather parameters were observed and registered during the whole year of 2018 and first semester of 2019. The campaign was based on the register of ambient temperature, global horizontal radiation, diffuse horizontal radiation and normal direct radiation components. A comparison with the TRY weather file was developed. The indoor room temperatures also monitored during the whole period of analysis, to calculate the efficiencies and determine the boundary conditions to be used in the numerical analysis and model validation. It was concluded that the building already has an efficient thermal performance, once the Solar XXI was projected to meet NZEB requirements, and for so, the needs for cooling and heating are also reduced, in comparison to the traditional constructive solutions being used in Portugal.

Concerning the BI-SES elements, the BIPVT system was the BI-SES system with a bigger period of analysis (from Jan/2018 to Feb/2019), having a huge number of registers associated to it. It presented the data concerning the T_{ac}, inlet and T_{out} in the air cavity, T_{pv}, and heat flux through the interior wall. During the day studied in detail, the system presented a total efficiency between17% and 20% for heating purposes. The prototype in versions P1a and P1b had less time of data acquirement, once manufactured and installed in a later phase. The prototype has a complex system of sensors installed, to allow the operation of the vents both in manual and automated ways. For the period under study, the P1a presented, for heating purposes, a total efficiency of near 20% for the manual mode of operation, and near 15% for the automatic operation was determined. For the P1b, an efficiency near 17% was determined for the manual operation mode, and 18% for the automatic mode of operation. It is necessary to highlight, however, that these efficiencies are values that represent the behaviour of the system for the boundary conditions existent in the time period considered for the calculation. In another words, the results may vary according to factors as the solar radiation availability and T_i. The differences between the calculated efficiencies in automatic and manual modes of operation was impacted by the weather conditions surrounding the systems, and the calculation of

efficiencies were purely based on these experimental campaign results.

Considering the previously described prototypes, more varied data were acquired in comparison to the BIPVT existent system, and it accounts for superficial temperature sensors in different heights, anemometers and also a complex automation system. The total efficiency reached in those systems, during the days studied in detail, varied from 15% to 20%. Dimensionless analysis was also developed based on the obtained results, as well as the calculation of the convection coefficients.

Numerical analysis

The numerical analysis was developed with the objective to evaluate the impact of the systems in the nominal energy needs of the adjacent thermal zone, namely for heating and cooling. The numerical analysis was segmented in two parts: i) component assessment through CFD analysis in steady-state mode through the use of ANSYS Fluent; and ii) dynamic simulation of building in real condition through the use of the EnergyPlus. The CFD analysis focused in obtaining the stratification of the temperatures, velocities and turbulence within the air gap, as well as the impact of the air cavity and T_i in the interior wall (BIPVT) or interior module (P1a and P1b). The element analysis used as boundary conditions the parameter values observed in the experimental campaign, aiming to describe the air behaviour of the system in its current state (no parametric analysis was developed through the use of CFD software).

The dynamic simulation parametric analysis elaborated on the base of 81 scenarios and described the room nominal energy needs for cooling and heating (given a determined setpoint), with the association of the BI-SES elements. Half of the scenarios accounted for the room with the window blind always open and half with the window blind always closed to reduce the uncertainty. The most noticeable result was the shift between cooling need and heating needs concerning the blind position to control the direct solar gains.

The numerical analysis of systems installed in buildings as Solar XXI, from the National Laboratory for Energy and Geology, can benefit from the amount of data the monitoring systems can supply, and from the awareness of the building occupants about the controlled ambient that is desired to generate in the test rooms (as the need to avoiding opening doors and

windows without the need of it). However, it is also necessary to recognize that the existence of different systems in the same ambient (as earth pipes, blinds and BIPVT wall) can increase the uncertainty applied to the results, and it is not easy to isolate the results in terms of which heat exchange was consequence of one or another. For this reason, it was important to complement the experimental analysis with the numerical analysis, in order to validate de data and access the thermal behaviour of the systems through simulation, in which the different systems could be brought to the same basis of weather conditions and room usage operation.

Concluding remarks of the BIPVT analysis

It was found out that the energy needs of the test room can effectively be reduced by the use of the BI-SES elements, however careful analysis must be done concerning the configuration of the system in use - operation mode, zone air mixing flow between zones, and also the thickness of the air cavity – due to the integration with other passive systems in the test room, as is the case of the window that allows the direct solar gain. It was perceived that not all the configurations brought benefits to the test room in thermal terms. Some of the configurations raised the nominal energy needs and overheated the room, and they are mainly the ones with fixed setpoint of the prototype operation.

The automated operation of the vents of the prototype – allowing either exterior ventilation or interior ventilation – was the parameter with highest impact on the reduction of the energy needs for cooling and heating. Following, the obtained results shown that the increase of the air flow in the zone mixing can be beneficial in some cases, namely when coupled with smart operation. These results strongly highlight the importance of the smart operation due to the automation in the BI-SES systems, in particular for mild climates as is the case of Portugal. In mild climates, the daily temperature in a thermal zone can range from below T_{comf}^{min} to above the T_{comf}^{max}. In this case, the purely passive operation of the explored BI-SES systems can go from contributing to achieving thermal comfort to increasing the thermal discomfort due to overheating or excessive cooling. In this scenario, the flexibility of the smart systems are fundamental in order to adapt to the different thermal conditions during the day, and during the different seasons of the year. Also, the occupants may interact with the BI-SES systems HMI

to set the band of temperatures of their preference, once the thermal comfort preferences may change from one building user to another.

This work contributes to the advancement of the BI-SES in the façades, and more specifically generates, through the extensive experimental campaign, detailed data of the behaviour of these systems in Portugal. Not only to the city in which the case study is located, the remarks concluded by this work may be applied to other locations with similar climate. It also contributed to the modular design of the BI-SES, showing that the operation mode of systems as BIPVT wall can also be applied to small areas of the façade, as was the case of the prototypes developed in the scope of the NZEB_LAB project and this thesis.

6.2. Suggestions for future works

Some recommendations for future works in related topics are made based on the development of the present thesis:

- As it was noticed, there is a huge impact of the direct solar gains in the obtained results. More precise results to alleviate the uncertainty caused by the presence of the window would be obtained by means of a near adiabatic room for the experimental campaigns;
- The development of optimisation would be indicated via the use of grey-box models or black-box models, with few parameters being tested in a broad range of values. Not only for the isolated systems but also considering the integration between them (including the automation of the other systems present in the test room, as the buried pipes and blind);
- The association of the visual comfort analysis would be valuable, given the fact that an always closed window, despite improving thermal comfort in this building's case, is not feasible due to the need of daylight to achieve visual comfort and general satisfaction;
- The association of automated smart blinds to the test room simulation, in order to try to complement the systems' collaboration to meet both heating and cooling needs;

- The analysis of the daylight use impact on the thermal behaviour of the building and also automatic control of the lighting system based on setpoints;
- A longer period of observation of the experimental analysis of the prototypes would also be advisable, to reduce the specific weather condition impacts on the results of the thermal characterization;
- In the future, the modularity of the system should be further explored in terms on experimental analysis;
- The use of mesh sensitivity analysis is very important in the scope of a CFD simulation. It was not performed in the scope of this work due to the constrains related to the free software version and also computational capabilities. It is, however, recommended that in future works this aspect should be taken into consideration.
- The sustainability of the solution and its cost benefit analysis should be also object of study, as well as embodied energy of the materials.

References

Abu Bakar, Nur Najihah, Mohammad Yusri Hassan, Hayati Abdullah, Hasimah Abdul Rahman, Md Pauzi Abdullah, Faridah Hussin, and Masilah Bandi. 2015. "Energy Efficiency Index as an Indicator for Measuring Building Energy Performance: A Review." *Renewable and Sustainable Energy Reviews* 44: 1–11. https://doi.org/10.1016/j.rser.2014.12.018.

Aelenei, Laura Elena. 2006. "Thermal Performance of a Naturally Ventilated Cavity Wall." Instituto Superior Técnico.

———. 2016. "Sistemas Prefabricados Para Edifícios de Baixo Consumo: Design; Modulação; Prototipagem e Testes." Lisbon: III Jornadas Técncas da Primavera da EFRIARC; Tektonica.

Aelenei, Laura, Antonio Frattari, Laurent Riscala, Haşim Altan, Arman Hashemi, Kheira Anissa Tabet Aoul, and Masa Noguchi. 2016. "Zero Energy Homes." In *ZEMCH: Toward the Delivery of Zero Energy Mass Custom Homes*, 275–309. Springer.

Aelenei, Laura, R Pereira, and Helder Gonçalves. 2013. "BIPV/T versus BIPV/T-PCM: A Numerical Investigation of Advanced System Integrated into Solar XXI Building Façade." In *2nd International Conference on Sustainable Energy Storage*.

Agathokleous, R, G Barone, A Buonomano, C Forzano, S A Kalogirou, and A Palombo. 2019. "Building Facade Integrated Solar Thermal Collectors for Air Heating: Experimentation, Modelling and Applications." *APPLIED ENERGY* 239 (April): 658–79. https://doi.org/10.1016/j.apenergy.2019.01.020.

Agathokleous, Rafaela A, and Soteris A Kalogirou. 2016. "Double Skin Facades (DSF) and Building Integrated Photovoltaics (BIPV): A Review of Configurations and Heat Transfer Characteristics." *Renewable Energy* 89: 743–56.

———. 2018. "Part II: Thermal Analysis of Naturally Ventilated BIPV System: Modeling and Simulation." *Solar Energy* 169: 682–91.

Aguacil, Sergi, Sophie Lufkin, and Emmanuel Rey. 2019. "Active Surfaces Selection Method

for Building-Integrated Photovoltaics (BIPV) in Renovation Projects Based on Self-Consumption and Self-Sufficiency." *ENERGY AND BUILDINGS* 193 (June): 15–28. https://doi.org/10.1016/j.enbuild.2019.03.035.

Ahmed-Dahmane, Mohamed, Ali Malek, and Tahar Zitoun. 2018. "Design and Analysis of a BIPV/T System with Two Applications Controlled by an Air Handling Unit." *Energy Conversion and Management* 175: 49–66.

Ansys. 2018. "ANSYS." 2018. https://www.ansys.com/products/fluids/ansys-fluent.

Ansys, Inc. 2011. "ANSYS FLUENT Theory Guide." *Canonsburg, Pa*, 794.

Antoniadou, Panagiota, and Agis M Papadopoulos. 2017. "Occupants' Thermal Comfort: State of the Art and the Prospects of Personalized Assessment in Office Buildings." *Energy and Buildings*.

Ascione, Fabrizio, Nicola Bianco, Claudio De Stasio, Gerardo Maria Mauro, and Giuseppe Peter Vanoli. 2015. "A New Methodology for Cost-Optimal Analysis by Means of the Multi-Objective Optimization of Building Energy Performance." *Energy and Buildings* 88: 78–90.

Asfour, Omar S. 2018. "Solar and Shading Potential of Different Configurations of Building Integrated Photovoltaics Used as Shading Devices Considering Hot Climatic Conditions." *SUSTAINABILITY* 10 (12). https://doi.org/10.3390/su10124373.

ASHRAE Guideline. 2002. "Guideline 14-2002." *Measurement of Energy and Demand Savings*, 4. https://www.techstreet.com/ashrae/standards/guideline-14-2002-measurement-of-energy-and-demand-savings?gateway_code=ashrae&product_id=1645226.

———. 2014. "Guideline 14-2014." *Measurement of Energy, Demand, and Water Savings*.

Banos, Raul, Francisco Manzano-Agugliaro, F G Montoya, Consolacion Gil, Alfredo Alcayde, and Julio Gómez. 2011. "Optimization Methods Applied to Renewable and Sustainable Energy: A Review." *Renewable and Sustainable Energy Reviews* 15 (4): 1753–66.

Barman, Sankar, Amartya Chowdhury, Sanjay Mathur, and Jyotirmay Mathur. 2018.

"Assessment of the Efficiency of Window Integrated CdTe Based Semi-Transparent Photovoltaic Module." *SUSTAINABLE CITIES AND SOCIETY* 37 (February): 250–62. https://doi.org/10.1016/j.scs.2017.09.036.

Bazilian, Morgan D, Harry Kamalanathan, and D K Prasad. 2002. "Thermographic Analysis of a Building Integrated Photovoltaic System." *Renewable Energy* 26 (3): 449–61.

Beaudin, Marc, and Hamidreza Zareipour. 2015. "Home Energy Management Systems: A Review of Modelling and Complexity." *Renewable and Sustainable Energy Reviews* 45: 318–35.

Biyik, Emrah, Mustafa Araz, Arif Hepbasli, Mehdi Shahrestani, Runming Yao, Li Shao, Emmanuel Essah, Armando C Oliveira, Teodosio del Caño, and Elena Rico. 2017. "A Key Review of Building Integrated Photovoltaic (BIPV) Systems." *Engineering Science and Technology, an International Journal* 20 (3): 833–58.

Borggaard, Jeff, John A. Burns, Amit Surana, and Lizette Zietsman. 2009. "Control, Estimation and Optimization of Energy Efficient Buildings." *Proceedings of the American Control Conference*, 837–41. https://doi.org/10.1109/ACC.2009.5160552.

bp solar. 2003. "BP 3160 Photovoltaic Module."

Bunthof, L A A, F P M Kreuwel, A Kaldenhoven, S Kin, W H M Corbeek, G J Bauhuis, E Vlieg, and J J Schermer. 2016. "Impact of Shading on a Flat CPV System for Facade Integration." *SOLAR ENERGY* 140 (December): 162–70. https://doi.org/10.1016/j.solener.2016.11.001.

Buonomano, Annamaria, Francesco Calise, Adolfo Palombo, and Maria Vicidomini. 2016. "BIPVT Systems for Residential Applications: An Energy and Economic Analysis for European Climates." *Applied Energy* 184: 1411–31. https://doi.org/10.1016/j.apenergy.2016.02.145.

Buonomano, Annamaria, Cesare Forzano, Soteris A Kalogirou, and Adolfo Palombo. 2018. "Building-Façade Integrated Solar Thermal Collectors: Energy-Economic Performance and Indoor Comfort Simulation Model of a Water Based Prototype for Heating, Cooling, and DHW Production." *Renewable Energy*.

Burman, Esfand, Dejan Mumovic, and Judit Kimpian. 2014. “Towards Measurement and Verification of Energy Performance under the Framework of the European Directive for Energy Performance of Buildings.” *Energy* 77: 153–63. https://doi.org/10.1016/j.energy.2014.05.102.

Chen, Xi, Hongxing Yang, and Jinqing Peng. 2019. “Energy Optimization of High-Rise Commercial Buildings Integrated with Photovoltaic Facades in Urban Context.” *ENERGY* 172 (April): 1–17. https://doi.org/10.1016/j.energy.2019.01.112.

Cheng, Yuanda, Min Gao, Jie Jia, Yanyi Sun, Yi Fan, and Min Yu. 2019. “An Optimal and Comparison Study on Daylight and Overall Energy Performance of Double-Glazed Photovoltaics Windows in Cold Region of China.” *ENERGY* 170 (March): 356–66. https://doi.org/10.1016/j.energy.2018.12.097.

Chialastri, A, and M Isaacson. 2017. “Performance and Optimization of a BIPV/T Solar Air Collector for Building Fenestration Applications.” *ENERGY AND BUILDINGS* 150 (September): 200–210. https://doi.org/10.1016/j.enbuild.2017.05.064.

Cho, Heejin, Weimin Wang, Atefe Makhmalbaf, Kyung Tae Yun, Jason Glazer, Larry Scheier, Viraj Srivastava, and Krishnan Gowri. 2011. “Extend EnergyPlus to Support Evaluation, Design, and Operation of Low Energy Buildings.” Pacific Northwest National Lab.(PNNL), Richland, WA (United States).

Cipriano, J, G Houzeaux, G Mor, U Eicker, J Carbonell, and S Danov. 2016. “Development of a Dynamic Model for Natural Ventilated Photovoltaic Components and of a Data Driven Approach to Validate and Identify the Model Parameters.” *SOLAR ENERGY* 129 (May): 310–31. https://doi.org/10.1016/j.solener.2016.01.039.

Connelly, Karen, Yupeng Wu, Jun Chen, and Yu Lei. 2016. “Design and Development of a Reflective Membrane for a Novel Building Integrated Concentrating Photovoltaic (BICPV) `Smart Window’ System.” *APPLIED ENERGY* 182 (November): 331–39. https://doi.org/10.1016/j.apenergy.2016.07.125.

Correia, Sandra F H, Patricia P Lima, Edison Pecoraro, Sidney J L Ribeiro, Paulo S Andre, Rute A S Ferreira, and Luis D Carlos. 2016. “Scale up the Collection Area of Luminescent Solar Concentrators towards Metre-Length Flexible Waveguiding Photovoltaics.” *PROGRESS IN PHOTOVOLTAICS* 24 (9): 1178–93.

https://doi.org/10.1002/pip.2772.

Crawley, Drury B, Jon W Hand, Michaël Kummert, and Brent T Griffith. 2008. “Contrasting the Capabilities of Building Energy Performance Simulation Programs.” *Building and Environment* 43 (4): 661–73.

Dear, Richard J De, and Gail S Brager. 2002. “Thermal Comfort in Naturally Ventilated Buildings: Revisions to ASHRAE Standard 55.” *Energy and Buildings* 34 (6): 549–61.

Debbarma, Mary, K. Sudhakar, and Prashant Baredar. 2017. “Thermal Modeling, Exergy Analysis, Performance of BIPV and BIPVT: A Review.” *Renewable and Sustainable Energy Reviews* 73 (August 2015): 1276–88. https://doi.org/10.1016/j.rser.2017.02.035.

Dehra, Himanshu. 2017. “An Investigation on Energy Performance Assessment of a Photovoltaic Solar Wall under Buoyancy-Induced and Fan-Assisted Ventilation System.” *APPLIED ENERGY* 191 (April): 55–74. https://doi.org/10.1016/j.apenergy.2017.01.038.

Deng, S, R Z Wang, and Y J Dai. 2014. “How to Evaluate Performance of Net Zero Energy Building–A Literature Research.” *Energy* 71: 1–16.

Diário da República n.º 159/2013. 2013. *Decreto-Lei 118/2013*. Lisbon: Ministério da Economia e do Emprego.

Diário da República n.º 234/2013. 2013. “Despacho 15793-F/2013.”

DoE, U S. 2010. *Energyplus Engineering Reference*. *The Reference to Energyplus Calculations*. Washington: U.S. Department of Energy.

Dounis, Anastasios I, and Christos Caraiscos. 2009. “Advanced Control Systems Engineering for Energy and Comfort Management in a Building Environment—A Review.” *Renewable and Sustainable Energy Reviews* 13 (6–7): 1246–61.

EnergyPlus. 2018. “EnergyPlus.” 2018. https://energyplus.net.

European Comission. 2002. “Directive 2002/91/EC of the European Parliament and of the Council of 16 December 2002 on the Energy Performance of Buildings.” *Official Journal L 001, 04/01/2003*, 65–71.

———. 2010. “Directive 2010/31/EU of the European Parliament and of the Council of 19

May 2010 on the Energy Performance of Buildings (Recast)." *Official Journal of the European Union* 18 (06): 2010.

European Commission. 2000. *Energy Audit Guide - Part A: Methodology and Technics*. Athens, Greece: European Commission.

European Parliament. 2010. "Directive 2010/31/EU of the European Parliament and of the Council of 19 May 2010 on the Energy Performance of Buildings (Recast)." *Official Journal of the European Union* 18 (06): 2010.

———. 2018. "Directive 2018/844/EU of the European Parliament and of the Council of 19 June 2018 on the Energy Performance of Buildings (Recast)." *Official Journal of the European Communities* 61 (156): 75–91.

Evins, Ralph. 2013. "A Review of Computational Optimisation Methods Applied to Sustainable Building Design." *Renewable and Sustainable Energy Reviews* 22: 230–45.

Favoino, Fabio, Francesco Fiorito, Alessandro Cannavale, Gianluca Ranzi, and Mauro Overend. 2016. "Optimal Control and Performance of Photovoltachromic Switchable Glazing for Building Integration in Temperate Climates." *APPLIED ENERGY* 178 (September): 943–61. https://doi.org/10.1016/j.apenergy.2016.06.107.

Formentini, Marco, and Stefano Lenci. 2018. "An Innovative Building Envelope (Kinetic Façade) with Shape Memory Alloys Used as Actuators and Sensors." *Automation in Construction* 85: 220–31.

Foucquier, Aurélie, Sylvain Robert, Frédéric Suard, Louis Stéphan, and Arnaud Jay. 2013. "State of the Art in Building Modelling and Energy Performances Prediction: A Review." *Renewable and Sustainable Energy Reviews* 23: 272–88.

Garde, Françios, Joseph Ayoub, Laura Aelenei, Daniel Aelenei, and Alessandra Scognamiglio. 2017. *Solution Sets for Net Zero Energy Buildings: Feedback from 30 Buildings Worldwide*. John Wiley & Sons.

Garnier, Celine, Tariq Muneer, and John Currie. 2018. "Numerical and Empirical Evaluation of a Novel Building Integrated Collector Storage Solar Water Heater." *RENEWABLE ENERGY* 126 (October): 281–95. https://doi.org/10.1016/j.renene.2018.03.041.

Gaur, Ankita, and G N Tiwari. 2015. “Analytical Expressions for Temperature Dependent Electrical Efficiencies of Thin Film BIOPVT Systems.” *APPLIED ENERGY* 146 (May): 442–52. https://doi.org/10.1016/j.apenergy.2015.01.106.

Georgescu, Michael, and Igor Mezić. 2015. “Building Energy Modeling: A Systematic Approach to Zoning and Model Reduction Using Koopman Mode Analysis.” *Energy and Buildings* 86: 794–802.

Ghasempourabadi, Mohammadhossein, Kostas Sinapis, Roel C.G.M. Loonen, Roland M.E. Valckenborg, Jan L.M. Hensen, and Wiep Folkerts. 2016. “Towards Simulation-Assisted Performance Monitoring of BIPV Systems Considering Shading Effects.” *Conference Record of the IEEE Photovoltaic Specialists Conference* 2016-Novem: 3123–28. https://doi.org/10.1109/PVSC.2016.7750241.

Giovanardi, A, A Passera, F Zottele, and R Lollini. 2015. “Integrated Solar Thermal Facade System for Building Retrofit.” *SOLAR ENERGY* 122 (December): 1100–1116. https://doi.org/10.1016/j.solener.2015.10.034.

Goldberg, David E, and John H Holland. 1988. “Genetic Algorithms and Machine Learning.” *Machine Learning* 3 (2): 95–99.

Gonçalves, Helder, Laura Aelenei, and Carlos Rodrigues. 2012. “Solar XXI: A Portuguese Office Building towards Net Zero-Energy Building.” *The REHVA European HVAC Journal*, 34–40.

Guarino, Francesco, Andreas Athienitis, Maurizio Cellura, and Diane Bastien. 2017. “PCM Thermal Storage Design in Buildings: Experimental Studies and Applications to Solaria in Cold Climates.” *APPLIED ENERGY* 185 (1): 95–106. https://doi.org/10.1016/j.apenergy.2016.10.046.

Halawa, Edward, Amirhosein Ghaffarianhoseini, Ali Ghaffarianhoseini, Jeremy Trombley, Norhaslina Hassan, Mirza Baig, Safiah Yusmah Yusoff, and Muhammad Azzam Ismail. 2018. “A Review on Energy Conscious Designs of Building Façades in Hot and Humid Climates: Lessons for (and from) Kuala Lumpur and Darwin.” *Renewable and Sustainable Energy Reviews* 82: 2147–61.

Hamdy, Mohamed, Ala Hasan, and Kai Siren. 2013. “A Multi-Stage Optimization Method for

Cost-Optimal and Nearly-Zero-Energy Building Solutions in Line with the EPBD-Recast 2010." *Energy and Buildings* 56: 189–203.

Harish, V S K V, and Arun Kumar. 2016. "A Review on Modeling and Simulation of Building Energy Systems." *Renewable and Sustainable Energy Reviews* 56: 1272–92. https://doi.org/10.1016/j.rser.2015.12.040.

He, Wei, Xiaoqiang Hong, Bingqing Luo, Hongbing Chen, and Jie Ji. 2016. "CFD and Comparative Study on the Dual-Function Solar Collectors with and without Tile-Shaped Covers in Water Heating Mode." *RENEWABLE ENERGY* 86 (February): 1205–14. https://doi.org/10.1016/j.renene.2015.09.053.

He, Wei, Xiaoqiang Hong, Xudong Zhao, Xingxing Zhang, Jinchun Shen, and Jie Ji. 2015. "Operational Performance of a Novel Heat Pump Assisted Solar Facade Loop-Heat-Pipe Water Heating System." *APPLIED ENERGY* 146 (May): 371–82. https://doi.org/10.1016/j.apenergy.2015.01.096.

Hengstberger, Florian, Christoph Zauner, Katharina Resch, Stefan Holper, and Michael Grobbauer. 2016. "High Temperature Phase Change Materials for the Overheating Protection of Facade Integrated Solar Thermal Collectors." *ENERGY AND BUILDINGS* 124 (July): 1–6. https://doi.org/10.1016/j.enbuild.2016.04.020.

Hensen, Jan L M, and Roberto Lamberts. 2012. *Building Performance Simulation for Design and Operation*. Routledge.

Hermelink, A, S Schimschar, T Boermans, L Pagliano, P Zangheri, R Armani, K Voss, and E Musall. 2012. "Towards Nearly Zero-Energy Buildings—Definition of Common Principles under the EPBD—Final Report"." Ecofys.

Hoes, P, J L M Hensen, MGLC Loomans, B De Vries, and D Bourgeois. 2009. "User Behavior in Whole Building Simulation." *Energy and Buildings* 41 (3): 295–302.

Hofer, Johannes, Abel Groenewolt, Prageeth Jayathissa, Zoltan Nagy, and Arno Schlueter. 2016. "Parametric Analysis and Systems Design of Dynamic Photovoltaic Shading Modules." *ENERGY SCIENCE & ENGINEERING* 4 (2): 134–52. https://doi.org/10.1002/ese3.115.

Huang, Junchao, Xi Chen, Hongxing Yang, and Weilong Zhang. 2018. “Numerical Investigation of a Novel Vacuum Photovoltaic Curtain Wall and Integrated Optimization of Photovoltaic Envelope Systems.” *APPLIED ENERGY* 229 (November): 1048–60. https://doi.org/10.1016/j.apenergy.2018.08.095.

Ibanez-Puy, Maria, Cesar Martin-Gomez, Javier Bermejo-Busto, Jose Antonio Sacristan, and Elia Ibanez-Puy. 2018. “Ventilated Active Thermoelectric Envelope (VATE): Analysis of Its Energy Performance When Integrated in a Building.” *ENERGY AND BUILDINGS* 158 (January): 1586–92. https://doi.org/10.1016/j.enbuild.2017.11.037.

Jaluria, Yogesh. 2007. *Design and Optimization of Thermal Systems*. CRC press.

Junker, Rune Grønborg, Armin Ghasem Azar, Rui Amaral Lopes, Karen Byskov Lindberg, Glenn Reynders, Rishi Relan, and Henrik Madsen. 2018. “Characterizing the Energy Flexibility of Buildings and Districts.” *Applied Energy* 225: 175–82.

Kang, Juhoon, Changsoon Cho, and Jung-Yong Lee. 2015. “Design of Asymmetrically Textured Structure for Efficient Light Trapping in Building-Integrated Photovoltaics.” *ORGANIC ELECTRONICS* 26 (November): 61–65. https://doi.org/10.1016/j.orgel.2015.07.021.

Kaplani, E, and S Kaplanis. 2014. “Thermal Modelling and Experimental Assessment of the Dependence of PV Module Temperature on Wind Velocity and Direction, Module Orientation and Inclination.” *Solar Energy* 107: 443–60.

Karthick, A, K Kalidasa Murugavel, L Kalaivani, and U Saravana Babu. 2018. “Performance Study of Building Integrated Photovoltaic Modules.” *ADVANCES IN BUILDING ENERGY RESEARCH* 12 (2): 178–94. https://doi.org/10.1080/17512549.2016.1275982.

Killian, M, and M Kozek. 2016. “Ten Questions Concerning Model Predictive Control for Energy Efficient Buildings.” *Building and Environment* 105: 403–12.

Krarti, Moncef. 2016. *Energy Audit of Building Systems: An Engineering Approach*. CRC press.

Kusuda, Tamami, and T A Ta. 1977. “Fundamentals of Building Heat Transfer” 82 (2): 97–106.

Lai, Chi-ming, and Shuichi Hokoi. 2017. “Experimental and Numerical Studies on the Thermal Performance of Ventilated BIPV Curtain Walls.” *INDOOR AND BUILT ENVIRONMENT* 26 (9): 1243–56. https://doi.org/10.1177/1420326X15611194.

Lai, Chi-Ming, and Shuichi Hokoi. 2015. “Solar Facades: A Review.” *BUILDING AND ENVIRONMENT* 91 (SI): 152–65. https://doi.org/10.1016/j.buildenv.2015.01.007.

Lamberts, Roberto, Enedir Ghisi, and Ana L Papst. 2000. “Desempenho Térmico de Edificações.” *Universidade Federal de Santa Catarina*.

Lamnatou, Chr, J. D. Mondol, D. Chemisana, and C. Maurer. 2015. “Modelling and Simulation of Building-Integrated Solar Thermal Systems: Behaviour of the System.” *Renewable and Sustainable Energy Reviews* 45: 36–51. https://doi.org/10.1016/j.rser.2015.01.024.

Lee, Jaewook, Jeongsu Park, Hyung-Jo Jung, and Jiyoung Park. 2017. “Renewable Energy Potential by the Application of a Building Integrated Photovoltaic and Wind Turbine System in Global Urban Areas.” *ENERGIES* 10 (12). https://doi.org/10.3390/en10122158.

Li, Kai, and Tao Zhang. 2018. “Forecasting Electricity Consumption Using an Improved Grey Prediction Model.” *Information* 9 (8): 204.

Li, Li, Ming Qu, and Steve Peng. 2016. “Performance Evaluation of Building Integrated Solar Thermal Shading System: Building Energy Consumption and Daylight Provision.” *ENERGY AND BUILDINGS* 113 (February): 189–201. https://doi.org/10.1016/j.enbuild.2015.12.040.

Liu, Huei-Mei, Chin-Huai Young, Der-Juinn Horng, Yih-Chearng Shiue, and Shin-Ku Lee. 2016. “Improving the Performance of a Semitransparent BIPV by Using High-Reflectivity Heat Insulation Film.” *INTERNATIONAL JOURNAL OF PHOTOENERGY*. https://doi.org/10.1155/2016/4174216.

Loonen, Roel C G M, Fabio Favoino, Jan L M Hensen, and Mauro Overend. 2017. “Review of Current Status, Requirements and Opportunities for Building Performance Simulation of Adaptive Facades.” *Journal of Building Performance Simulation* 10 (2): 205–23.

Luo, Yongqiang, Ling Zhang, Zhongbing Liu, Xiaosong Su, Jinbu Lian, and Yongwei Luo. 2018. “Coupled Thermal-Electrical-Optical Analysis of a Photovoltaic-Blind Integrated Glazing Facade.” *APPLIED ENERGY* 228 (October): 1870–86. https://doi.org/10.1016/j.apenergy.2018.07.052.

Luo, Yongqiang, Ling Zhang, Zhongbing Liu, Jing Wu, Yelin Zhang, and Zhenghong Wu. 2018. “Numerical Evaluation on Energy Saving Potential of a Solar Photovoltaic Thermoelectric Radiant Wall System in Cooling Dominant Climates.” *ENERGY* 142 (January): 384–99. https://doi.org/10.1016/j.energy.2017.10.050.

Marszal, Anna Joanna, Julien S Bourrelle, Eike Musall, Per Heiselberg, Arild Gustavsen, and Karsten Voss. 2010. “Net Zero Energy Buildings-Calculation Methodologies versus National Building Codes.” *The Proceedings of EuroSun*.

Martinaitis, Vytautas, Edmundas Kazimieras Zavadskas, Violeta Motuzienė, and Tatjana Vilutienė. 2015. “Importance of Occupancy Information When Simulating Energy Demand of Energy Efficient House: A Case Study.” *Energy and Buildings* 101: 64–75.

Maurer, Christoph, Christoph Cappel, and Tilmann E Kuhn. 2017. “Progress in Building-Integrated Solar Thermal Systems.” *SOLAR ENERGY* 154 (SI): 158–86. https://doi.org/10.1016/j.solener.2017.05.065.

Mendes, Rui Alexandre Dias. 2011. “Estudo Experimental Do Comportamento Térmico de Uma Parede Ventilada Com Um Sistema PV Integrado.”

Miranda, P, F E S Coelho, António Rodrigues Tomé, Maria Antónia Valente, Anabela Carvalho, Carlos Pires, Henrique Oliveira Pires, Vanda Cabrinha Pires, and Carlos Ramalho. 2002. “20th Century Portuguese Climate and Climate Scenarios.” *Climate Change in Portugal. Scenarios, Impacts and Adaptation Measures—SIAM Project (Santos FD, Forbes K, Moita R, Eds). Lisbon: Gradiva Publishers*, 23–83.

Mosavi, Amir, Mohsen Salimi, Sina Faizollahzadeh Ardabili, Timon Rabczuk, Shahaboddin Shamshirband, and Annamaria R Varkonyi-Koczy. 2019. “State of the Art of Machine Learning Models in Energy Systems, a Systematic Review.” *Energies* 12 (7): 1301.

Nagy, Zoltan, Bratislav Svetozarevic, Prageeth Jayathissa, Moritz Begle, Johannes Hofer, Gearoid Lydon, Anja Willmann, and Arno Schlueter. 2016. “The Adaptive Solar Facade:

From Concept to Prototypes.” *Frontiers of Architectural Research* 5 (2): 143–56.

Nannei, E., and C. Schenone. 1999. “Thermal Transients in Buildings: Development and Validation of a Numerical Model.” *Energy and Buildings* 29 (3): 209–15. https://doi.org/10.1016/S0378-7788(98)00060-7.

Navarro, Lidia, Alvaro de Gracia, Albert Castell, and Luisa F Cabeza. 2016. “Experimental Study of an Active Slab with PCM Coupled to a Solar Air Collector for Heating Purposes.” *ENERGY AND BUILDINGS* 128 (September): 12–21. https://doi.org/10.1016/j.enbuild.2016.06.069.

Neves, Diana, and Carlos A Silva. 2014. “Modeling the Impact of Integrating Solar Thermal Systems and Heat Pumps for Domestic Hot Water in Electric Systems–The Case Study of Corvo Island.” *Renewable Energy* 72: 113–24.

Nguyen, Tuan Anh, and Marco Aiello. 2013. “Energy Intelligent Buildings Based on User Activity: A Survey.” *Energy and Buildings* 56: 244–57.

O’Hegarty, Richard, Oliver Kinnane, and Sarah J McCormack. 2016. “Review and Analysis of Solar Thermal Facades.” *SOLAR ENERGY* 135 (October): 408–22. https://doi.org/10.1016/j.solener.2016.06.006.

Ogunsola, Oluwaseyi T, and Li Song. 2015. “Application of a Simplified Thermal Network Model for Real-Time Thermal Load Estimation.” *Energy and Buildings* 96: 309–18.

Oh, Jeongyoon, Choongwan Koo, Taehoon Hong, and Seung Hyun Cha. 2018. “An Integrated Model for Estimating the Techno-Economic Performance of the Distributed Solar Generation System on Building Façades: Focused on Energy Demand and Supply.” *Applied Energy* 228: 1071–90.

Olesen, Bjarne W, and K C Parsons. 2002. “Introduction to Thermal Comfort Standards and to the Proposed New Version of EN ISO 7730.” *Energy and Buildings* 34 (6): 537–48.

Palacios-Jaimes, Gloria Y, Pablo Martin-Ramos, Francisco J Rey-Martinez, and Ignacio A Fernandez-Coppel. 2017. “Transformation of a University Lecture Hall in Valladolid (Spain) into a NZEB: LCA of a BIPV System Integrated in Its Facade.” *INTERNATIONAL JOURNAL OF PHOTOENERGY*.

https://doi.org/10.1155/2017/2478761.

Pantic, Lana S, Tomislav M Pavlovic, Dragana D Milosavljevic, Dragoljub Lj. Mirjanic, Ivana S Radonjic, and Miodrag K Radovic. 2016. “ELECTRICAL ENERGY GENERATION WITH DIFFERENTLY ORIENTED PHOTOVOLTAIC MODULES AS FACADE ELEMENTS.” *THERMAL SCIENCE* 20 (4): 1377–86. https://doi.org/10.2298/TSCI150123157P.

Peng, Jinqing, Dragan C Curcija, Lin Lu, Stephen E Selkowitz, Hongxing Yang, and Weilong Zhang. 2016. “Numerical Investigation of the Energy Saving Potential of a Semi-Transparent Photovoltaic Double-Skin Facade in a Cool-Summer Mediterranean Climate.” *APPLIED ENERGY* 165 (March): 345–56. https://doi.org/10.1016/j.apenergy.2015.12.074.

Peng, Jinqing, Lin Lu, Hongxing Yang, and Tao Ma. 2015. “Comparative Study of the Thermal and Power Performances of a Semi-Transparent Photovoltaic Facade under Different Ventilation Modes.” *APPLIED ENERGY* 138 (January): 572–83. https://doi.org/10.1016/j.apenergy.2014.10.003.

Pereira, J. 2015. “Simulação Energética de Películas Em Envidraçados.” Instituto Superior Técnico.

Pereira, R.J. 2015. “Design and Optimization of Building Integration PV/T Systems (BIPV/T).” Universidade de Évora.

Platzer, Werner, Hans Simmler, and Ida Bryn. 2005. “ENERGY PERFORMANCE OF FACADES AND BUILDINGS–IEA AS SUPPORT FOR THE EUROPEAN DIRECTIVE?” *Tampere, Finland*, 578–82.

Pomponi, Francesco, Poorang A E Piroozfar, Ryan Southall, Philip Ashton, and Eric R P Farr. 2016. “Energy Performance of Double-Skin Façades in Temperate Climates: A Systematic Review and Meta-Analysis.” *Renewable and Sustainable Energy Reviews* 54: 1525–36.

Prieto, Alejandro, Ulrich Knaack, Thomas Auer, and Tillmann Klein. 2018. “Feasibility Study of Self-Sufficient Solar Cooling Facade Applications in Different Warm Regions.” *ENERGIES* 11 (6). https://doi.org/10.3390/en11061475.

Qiu, Changyu, Hongxing Yang, and Weilong Zhang. 2019. “Investigation on the Energy Performance of a Novel Semi-Transparent BIPV System Integrated with Vacuum Glazing.” *BUILDING SIMULATION* 12 (1): 29–39. https://doi.org/10.1007/s12273-018-0464-6.

Resch-Fauster, Katharina, Florian Hengstberger, Christoph Zauner, and Stefan Holper. 2018. “Overheating Protection of Solar Thermal Facades with Latent Heat Storages Based on Paraffin-Polymer Compounds.” *ENERGY AND BUILDINGS* 169 (June): 254–59. https://doi.org/10.1016/j.enbuild.2018.03.068.

Sabry, Mohamed. 2016. “Prismatic TIR (Total Internal Reflection) Low-Concentration PV (Photovoltaics)-Integrated Facade for Low Latitudes.” *ENERGY* 107 (July): 473–81. https://doi.org/10.1016/j.energy.2016.04.057.

Sadineni, Suresh B, Srikanth Madala, and Robert F Boehm. 2011. “Passive Building Energy Savings: A Review of Building Envelope Components.” *Renewable and Sustainable Energy Reviews* 15 (8): 3617–31.

Sande, P C, and S Ray. 2014. “Mesh Size Effect on CFD Simulation of Gas-Fluidized Geldart A Particles.” *Powder Technology* 264: 43–53.

Sartori, Igor, Assunta Napolitano, and Karsten Voss. 2012. “Net Zero Energy Buildings: A Consistent Definition Framework.” *Energy and Buildings* 48: 220–32.

Schwingshackl, Clemens, Marcello Petitta, Jochen Ernst Wagner, Giorgio Belluardo, David Moser, Mariapina Castelli, Marc Zebisch, and Anke Tetzlaff. 2013. “Wind Effect on PV Module Temperature: Analysis of Different Techniques for an Accurate Estimation.” *Energy Procedia* 40: 77–86.

Shaikh, Pervez Hameed, Nursyarizal Bin Mohd Nor, Perumal Nallagownden, Irraivan Elamvazuthi, and Taib Ibrahim. 2014. “A Review on Optimized Control Systems for Building Energy and Comfort Management of Smart Sustainable Buildings.” *Renewable and Sustainable Energy Reviews* 34: 409–29.

———. 2016. “Intelligent Multi-Objective Control and Management for Smart Energy Efficient Buildings.” *International Journal of Electrical Power & Energy Systems* 74: 403–9.

Shen, Hui, Athanasios Tzempelikos, Anna Maria Atzeri, Andrea Gasparella, and Francesca Cappelletti. 2015. “Dynamic Commercial Facades versus Traditional Construction: Energy Performance and Comparative Analysis.” *JOURNAL OF ENERGY ENGINEERING* 141 (4). https://doi.org/10.1061/(ASCE)EY.1943-7897.0000225.

Shen, Jingchun, Xingxing Zhang, Tong Yang, Llewellyn Tang, Ali Cheshmehzangi, Yupeng Wu, Guiqin Huang, Dan Zhong, Peng Xu, and Shengchun Liu. 2016. “Characteristic Study of a Novel Compact Solar Thermal Facade (STF) with Internally Extruded Pin-Fin Flow Channel for Building Integration.” *APPLIED ENERGY* 168 (April): 48–64. https://doi.org/10.1016/j.apenergy.2016.01.021.

Shukla, Akash Kumar, K. Sudhakar, and Prashant Baredar. 2017. “Recent Advancement in BIPV Product Technologies: A Review.” *Energy and Buildings* 140: 188–95. https://doi.org/10.1016/j.enbuild.2017.02.015.

Shukla, Akash Kumar, K Sudhakar, and Prashant Baredar. 2016. “A Comprehensive Review on Design of Building Integrated Photovoltaic System.” *ENERGY AND BUILDINGS* 128 (September): 99–110. https://doi.org/10.1016/j.enbuild.2016.06.077.

Silva, C.A.S., and P. Carreira. 2014. “Green Sustainable Data Centres.” In *Greening by IT*. Open University Netherlands.

Smyth, M, A Pugsley, G Hanna, A Zacharopoulos, J Mondol, A Besheer, and A Savvides. 2019. “Experimental Performance Characterisation of a Hybrid Photovoltaic/Solar Thermal Facade Module Compared to a Flat Integrated Collector Storage Solar Water Heater Module.” *RENEWABLE ENERGY* 137 (SI): 137–43. https://doi.org/10.1016/j.renene.2018.04.017.

Sornek, Krzysztof, Mariusz Filipowicz, and Jakub Jasek. 2018. “The Use of Fresnel Lenses to Improve the Efficiency of Photovoltaic Modules for Building-Integrated Concentrating Photovoltaic Systems.” *JOURNAL OF SUSTAINABLE DEVELOPMENT OF ENERGY WATER AND ENVIRONMENT SYSTEMS-JSDEWES* 6 (3): 415–26. https://doi.org/10.13044/j.sdewes.d6.0204.

Sun, Yanyi, Katie Shanks, Hasan Baig, Wei Zhang, Xia Hao, Yongxue Li, Bo He, et al. 2018. “Integrated Semi-Transparent Cadmium Telluride Photovoltaic Glazing into Windows: Energy and Daylight Performance for Different Architecture Designs.” *APPLIED*

ENERGY 231 (December): 972–84. https://doi.org/10.1016/j.apenergy.2018.09.133.

Sun, Yanyi, Yupeng Wu, Robin Wilson, and Shuyue Sun. 2016. “Thermal Evaluation of a Double Glazing Facade System with Integrated Parallel Slat Transparent Insulation Material (PS-TIM).” *BUILDING AND ENVIRONMENT* 105 (August): 69–81. https://doi.org/10.1016/j.buildenv.2016.05.004.

Tablada, Abel, Vesna Kosoric, Huajing Huang, Ian Kevin Chaplin, Siu-Kit Lau, Chao Yuan, and Stephen Siu-Yu Lau. 2018. “Design Optimization of Productive Facades: Integrating Photovoltaic and Farming Systems at the Tropical Technologies Laboratory.” *SUSTAINABILITY* 10 (10). https://doi.org/10.3390/su10103762.

Tak, Sehyun, Soomin Woo, Jiyoung Park, and Sungjin Park. 2017. “Effect of the Changeable Organic Semi-Transparent Solar Cell Window on Building Energy Efficiency and User Comfort.” *SUSTAINABILITY* 9 (6). https://doi.org/10.3390/su9060950.

Taleghani, Mohammad, Martin Tenpierik, Stanley Kurvers, and Andy Van Den Dobbelsteen. 2013. “A Review into Thermal Comfort in Buildings.” *Renewable and Sustainable Energy Reviews* 26: 201–15.

Tripathy, M, P K Sadhu, and S K Panda. 2016. “A Critical Review on Building Integrated Photovoltaic Products and Their Applications.” *RENEWABLE & SUSTAINABLE ENERGY REVIEWS* 61 (August): 451–65. https://doi.org/10.1016/j.rser.2016.04.008.

Tsanakas, John A, Long Ha, and Claudia Buerhop. 2016. “Faults and Infrared Thermographic Diagnosis in Operating C-Si Photovoltaic Modules: A Review of Research and Future Challenges.” *Renewable and Sustainable Energy Reviews* 62: 695–709.

Valladares-Rendon, L G, Gerd Schmid, and Shang-Lien Lo. 2017. “Review on Energy Savings by Solar Control Techniques and Optimal Building Orientation for the Strategic Placement of Facade Shading Systems.” *ENERGY AND BUILDINGS* 140 (April): 458–79. https://doi.org/10.1016/j.enbuild.2016.12.073.

Vega, A M, F Santamaria, and E Rivas. 2015. “Modeling for Home Electric Energy Management: A Review.” *Renewable and Sustainable Energy Reviews* 52: 948–59.

Velasco, Abel, Sergi Jimenez Garcia, Alfredo Guardo, Alfred Fontanals, and Monica

Egusquiza. 2017. “Assessment of the Use of Venetian Blinds as Solar Thermal Collectors in Double Skin Facades in Mediterranean Climates.” *ENERGIES* 10 (11). https://doi.org/10.3390/en10111825.

Ventura, J.M.G.B. 2014. “Estudo Experimental de Um Sistema BIPV/T-PCM.” Universidade de Lisboa.

Verbeke, Stijn, and Amaryllis Audenaert. 2018. “Thermal Inertia in Buildings: A Review of Impacts across Climate and Building Use.” *Renewable and Sustainable Energy Reviews* 82: 2300–2318.

Versteeg, H. K., and W. Malalasekara. 2007. *An Introduction to Computational Fluid Dynamics - The Finite Volume Method*. Pearson Education Limited.

Wang, Jiang-Jiang, You-Yin Jing, Chun-Fa Zhang, and Jun-Hong Zhao. 2009. “Review on Multi-Criteria Decision Analysis Aid in Sustainable Energy Decision-Making.” *Renewable and Sustainable Energy Reviews* 13 (9): 2263–78.

Wang, Meng, Jinqing Peng, Nianping Li, Lin Lu, Tao Ma, and Hongxing Yang. 2016. “Assessment of Energy Performance of Semi-Transparent PV Insulating Glass Units Using a Validated Simulation Model.” *ENERGY* 112 (October): 538–48. https://doi.org/10.1016/j.energy.2016.06.120.

Wang, Meng, Jinqing Peng, Nianping Li, Hongxing Yang, Chunlei Wang, Xue Li, and Tao Lu. 2017. “Comparison of Energy Performance between PV Double Skin Facades and PV Insulating Glass Units.” *APPLIED ENERGY* 194 (May): 148–60. https://doi.org/10.1016/j.apenergy.2017.03.019.

Wang, Zeyu, and Ravi S Srinivasan. 2015. “A Review of Artificial Intelligence Based Building Energy Prediction with a Focus on Ensemble Prediction Models.” In *2015 Winter Simulation Conference (WSC)*, 3438–48. IEEE.

———. 2017. “A Review of Arti Fi Cial Intelligence Based Building Energy Use Prediction : Contrasting the Capabilities of Single and Ensemble Prediction Models.” *Renewable and Sustainable Energy Reviews* 75 (October 2016): 796–808. https://doi.org/10.1016/j.rser.2016.10.079.

Wu, Yupeng, Karen Connelly, Yuzhe Liu, Xiaowen Gu, Yanfeng Gao, and George Z Chen. 2016. “Smart Solar Concentrators for Building Integrated Photovoltaic Facades.” *SOLAR ENERGY* 133 (August): 111–18. https://doi.org/10.1016/j.solener.2016.03.046.

Yang, Rebecca Jing. 2015. “Overcoming Technical Barriers and Risks in the Application of Building Integrated Photovoltaics (BIPV): Hardware and Software Strategies.” *AUTOMATION IN CONSTRUCTION* 51 (March): 92–102. https://doi.org/10.1016/j.autcon.2014.12.005.

Yee, Helen C, Peter K Sweby, and David Francis Griffiths. 1991. “Dynamical Approach Study of Spurious Steady-State Numerical Solutions of Nonlinear Differential Equations. I. The Dynamics of Time Discretization and Its Implications for Algorithm Development in Computational Fluid Dynamics.” *Journal of Computational Physics* 97 (2): 249–310.

Zhang, Weilong, Lin Lu, and Jinqing Peng. 2017. “Evaluation of Potential Benefits of Solar Photovoltaic Shadings in Hong Kong.” *ENERGY* 137 (October): 1152–58. https://doi.org/10.1016/j.energy.2017.04.166.

Zhang, Xingxing, Jingchun Shen, Yan Lu, Wei He, Peng Xu, Xudong Zhao, Zhongzhu Qiu, Zishang Zhu, Jinzhi Zhou, and Xiaoqiang Dong. 2015. “Active Solar Thermal Facades (ASTFs): From Concept, Application to Research Questions.” *RENEWABLE & SUSTAINABLE ENERGY REVIEWS* 50 (October): 32–63. https://doi.org/10.1016/j.rser.2015.04.108.

Zhao, Hai-xiang, and Frédéric Magoulès. 2012. “A Review on the Prediction of Building Energy Consumption.” *Renewable and Sustainable Energy Reviews* 16 (6): 3586–92.